

3208

DEFECT-INDUCED TRANSPORT STUDIES OF SEMICONDUCTING POLYMERS

A Thesis

Submitted for the Degree of
Doctor of Philosophy

By

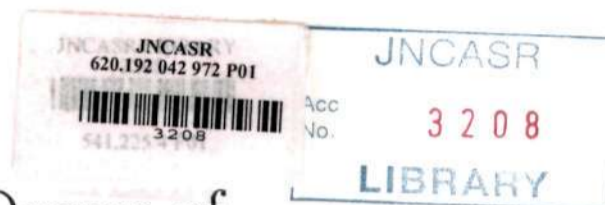
A. A. Alagiriswamy



TO

MANIPAL ACADEMY OF HIGHER EDUCATION
THROUGH
JAWAHARLAL NEHRU CENTER FOR ADVANCED
SCIENTIFIC RESEARCH
BANGALORE - 560064, INDIA

APRIL 2001



JNCASR Library



3208

To my parents

&

my family members

620 192 042 972
POI

DECLARATION

This is to certify that this thesis entitled "DEFECT-INDUCED TRANSPORT STUDIES OF SEMICONDUCTING POLYMERS" is a research work done by A. A. ALAGIRISWAMY, which is confined and constrained, under the guidance of Prof. K. S. Narayan and has not previously formed the basis for the award of any Degree, Diploma, Associateship or Fellowship or other similar titles, and that the thesis as a whole in its approach to the subject, in its organization of the material and in its critical evaluation represents independent work on the part of the candidate.



A. A. ALAGIRISWAMY

Email: alagiri@jncasr.ac.in

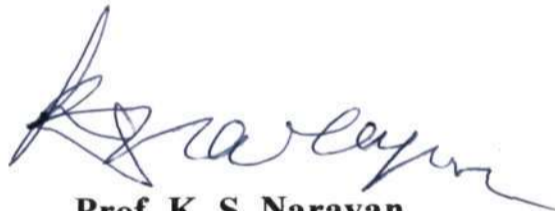


Chemistry & Physics of Materials Unit
JAWAHARLAL NEHRU CENTRE FOR ADVANCED SCIENTIFIC RESEARCH
Jakkur P.O., Bangalore - 560 064. India

25, April 2001

CERTIFICATE

Certified that the work described in the "**DEFECT-INDUCED TRANSPORT STUDIES OF SEMICONDUCTING POLYMERS**" is the result of investigations carried out by Mr. A. A. Alagiriswamy in the Chemistry and Physics of Materials Unit, Jawaharlal Nehru Center for Advanced Scientific Research, Jakkur, Bangalore - 560064 under my supervision and the results presented in the thesis have not previously formed the basis for the award of any other diploma, degree, degree or fellowship.



Prof. K. S. Narayan

ACKNOWLEDGMENTS

I register my deep sense of gratitude to Prof. K. S. Narayan (Molecular Electronics Lab), for his guidance, advise, encouragement, invaluable suggestions and for supporting me throughout my graduate study towards a Ph. D. research career. I thank Prof. C. N. R. Rao, chairman of CPMU, for providing all the relevant facilities and for developing our institute as one of the esteemed research institutes. I am greatly indebted to Prof. V. Krishnan, president of JNCASR, for having encouraged me to embark on this research project under the guidance of Prof. K. S. Narayan who offered me the right kind of motivation and enabled me to proceed on proper lines.

I acknowledge Dr. Bob Spry, Polymer Branch, AFRL for providing the polymer samples. I thank Prof. R. Govindaraju (University of Windsor, Canada) for providing the samples polyimide Kapton, Tefzel etc., and for enlightening discussions during his stay with us. I also thank Dr. K. L. Narasimhan (TIFR. Mumbai) for the Photothermal deflection spectroscopy measurements.

My sincere thanks are to Prof. M. K. Chandrasekaran, Drs. V. K. Sharma, Raju, Natarajan, Kulkarni, Chandrabhas and Umesh Waghmare for their scholarly suggestions and words of encouragement. Especially I am thankful to Dr Kulkarni and Dr. Bala Subramaniam for providing not only the computer facilities, but also for supporting me in other aspects. I record my deep sense of gratitude to the Administrative Officer (Mr. Nagaraja Rao) and all the staff of JNC, Bangalore for having extended all possible help during the course of my research endeavor. Especially I would like to acknowledge Administrative officer (Mr. N. Nagaraja Rao), who has helped me in various aspects. I thank Dr. Madhusudan who helped me and providing the library facilities. I extend my thanks to our library staff. I acknowledge Basavaraj, Keshav and Harish who have supported me with their assistance and friendship. Thanks are especially due to Basavaraj for Xeroxing the relevant items in earlier days.

I thank my lab mates Th. Birendra Singh and A. G. Manoj for the preparation of my thesis. My special thanks to Dr. Geetha K. Varrier and N. Kumar for providing great company in the lab and prompting my research carrier. I also thank my JNC colleagues Anil Kumar, Vasudeva, Basavaraj and Srinath for their help and moral support. Apart from them I would like to acknowledge all of my IISc friends Dr. A. Navaraj, M. Raja (no more), Mr. Murali Krishnan, Mr. R. Illango, Dr. K. Raghavan, Mr. Rajesh, Dr. J. Jayasekaran, Dr. N. Kannan, Dr. V. Vijaya Kumar, Dr. P. Pitchumani, Dr. Venkat Pratab, Dr. J. Victor Meyer, Mr. P. Raja, Dr. Venkata Subramaniam, Mr. Balamurugan, Dr. R. Sankaran (The Madurai group) and many, many more kind people whom I can't mention their names all in this short space. I extend my thanks to other IISc friends Dr. N. Thirupathi Natesan, Dr. N. Shiva Shankar, Dr. Murugavel (JNC), I. V. R. Sivakumar (JNC), Dr. Govindaraj (JNC), N. Mohan, K. Raja, K. Prasad, S. Arunachalam, L. Peter, P. Johnny, T. Francis, T. Kumar, K. Jacob and A. Madhavan from various departments. Their help and encouragement will not be forgotten.

In particular, I thank my JNC friends Praveen Bhat, Dr. Kumaradhas, C. P. Vinod, Gautam, P. John Thomas, Pattnaik, M. Krishnan, Jamal, Sujay and R. Gopalan. I extend my thanks to Rajesh for supporting me to work in computer lab other than office hours.

I owe special thanks to Ms. V. Sheeba (JNC) and Mrs. S. T. Aruna (Israel) for their invaluable and never-ending sequences of moral support, whenever I was stymied. I also would like to be grateful to Ms. Kavitha Siva (JNC) and Mrs. T. Sudha (California), particularly no order, for their "pretty hard up" encouragement and help. I acknowledge Mrs. Priya Rao (Bangalore) to have valuable suggestions and her encouragement.

PREFACE

Defects play an important factor in electronic and opto-electronic properties of semiconducting polymers. The importance of defects is highlighted in certain ladder and non-ladder type conjugated polymers. Poly (benzimidazobenzophenanthroline), BBL, a high temperature ladder type polymer with predominant n -type carriers was studied in detail. The electrical conductivity $\sigma(T)$ of BBL at room temperature increases substantially, $T > 600$ K), by more than six orders in magnitude. The thermal hysteresis of $\sigma(T)$ and its anisotropic features were observed. The variation in the thermally induced dc conductivity with respect to ambient conditions was studied.

The photocurrent and photothermal deflection measurements of BBL exhibit a long tail (0.5 eV) well below the absorption edge at 1.7 eV. The origin of the defects, which manifest as localized states for the electronic transport can be probed by thermally stimulated current relaxation techniques, TSC, and zero bias light-induced current (ZBPIC) decay profiles. These methods were also applied to variety of conjugated systems such as poly (3-octyl thiophene) P3OT, poly (9-vinylcarbazole) PVK, poly (2-methoxy-5-(2'-ethyl-hexoxy)-1, 4 paraphenylenevinylene) MEHPPV and non-conjugated polymer systems such as poly (4, 4'-oxydiphenylene-pyromellitimide) Kapton.

Systematic TSC in these systems was studied with varying initial conditions and also as a function of thickness and different electrode materials. The various physical parameters for BBL, such as density of defect states ($N_t \simeq 10^{14}$ to 10^{18} cm^{-3}), activation energy for the traps or defects ($E_t \simeq \text{few meV to } 0.7 \text{ eV}$), trapping cross sections ($S_n \simeq 10^{-20}$ to 10^{-18} cm^2) were obtained from the results. Defect parameters were also quantified in MEHPPV, P3OT light emitting diode devices and for Kapton. The utility of this technique was also explored to investigate the nature of the states present at the p polymer - n polymer interfaces, such as bilayered BBL/PVK and BBL/P3OT systems.

DEDICATION	ii
DECLARATION	iii
Certificate	iv
ACKNOWLEDGMENTS	v
PREFACE	vii
Table of contents	viii
Chapter	1
Introduction	1
1.1 Electronic states of non-conjugated and conjugated systems	2
1.1.1 Conjugated polymers	4
1.2 Quasiparticles in conjugated polymers	12
1.2.1 Solitons	12
1.2.2 Polarons	16
1.2.3 Bipolarons	16
1.2.4 Excitons	16
1.3 Doping of conjugated polymers	17
1.4 Su Schreiffer Heeger (SSH) model	21
1.5 Origin of conduction mechanism	29
1.6 Electroluminescence and Photovoltaic effects	30
Chapter 2	34
Transport Mechanisms in Conducting Polymers	34
Theoretical background	34
2.1 Localization	34
2.2 Conduction in disordered materials	39
2.3 Conduction in localized states	41
2.4 Conduction in band tails	42
2.5 Conductivity mechanism model for conjugated polymers	46
2.5.1 Sheng's model	48
2.5.2 Charge Energy Limited Transport (CELT) model	48

2.5.3 Poole-Frenkel effect	49
2.5.4 Intersoliton hopping conduction	50
2.5.5 Tunneling conduction in Composite Materials	50
2.5.6 Thermal Fluctuation modified tunneling	51
2.6 Transport properties of quasi-1d disordered systems	52
Chapter 3	56
Thermally Stimulated Relaxation Processes	
Background	56
3.1 Theory of thermally stimulated relaxation processes	
3.2 The OTOR model (Shockley-Read statistics)	59
3.3 Concept of Quasi-Fermi levels	63
3.4 Experimental procedure for TSC	69
3.5 Classification of Trapping States	74
3.5.1 Shallow traps	75
3.5.2 Deep traps	75
3.5.3 Intermediate traps	76
3.6 Determination of kinetic parameters from experimental results	76
3.6.1 Urbach's method	76
3.6.2 The initial rise method	76
3.6.3 Ilich's method (Modified form of initial rise method)	78
3.6.4 Heating rate method	79
3.6.5 Bube's method	80
3.6.6 Peak shape methods	80
3.6.7 Chen's method	83
3.6.8 Grosswiener's method	84
3.6.9 Lushchik's method	84
3.6.10 Halperin and Braner's method	85
3.6.11 Area Measurement method	85
3.6.12 Chen's additional formula	85

3.6.13 Keating method	85
3.6.13 The curve fitting method	
Chapter 4	88
Ladder polymers	88
4.1 Processing of thin BBL films	93
4.2 BBL characterization	93
4.2.1 UV-VIS absorption spectra	94
4.2.2 Thermogravimetric analysis (TGA)	95
4.2.3 X-ray analysis (X-ray)	95
4.2.4 Photoluminescence Spectra (PL)	96
4.2.5 Photo thermal spectroscopy (PDS)	97
(i) Basic Processes in Photo thermal Spectroscopy	98
(ii) Theoretical and experimental aspects	100
4.3 Essentials of polymer stability	100
Chapter 5	102
Experimental Techniques	102
5.1 Basics of DC conductivity measurements	102
5.2 Four-point probe technique	103
5.3 Two-point probe technique	105
5.4 Photoconduction mechanism	110
5.4.1 Monomolecular recombination	113
5.4.2 Bimolecular recombination	114
5.4.3 Higher order kinetics	115
5.4.4 Role of traps	116
5.5 Steady State photocurrent Measurements	117
5.5 Transient photocurrent measurements	118
Chapter 6	120
Experimental results: DC conductivity of BBL	120
6.1 RESULTS AND DISCUSSION	122

6.2 Summary	133
Chapter 7	134
Results and Analysis: Active defects in BBL	134
7.1 TSC Procedure	136
7.2 Results and Discussions	136
7.3 Photo-Induced Current Measurements	146
7.4 Transient photoconductivity measurements	148
Chapter 8	156
8.1 Light emitting, electro luminescent materials	156
8.2 Role of traps in EL devices	159
8.3 Experiments and Results	161
8.3.1 Introduction	161
8.3.2 Experimental	161
8.4 Results and Discussion	163
Chapter 9	167
Interfacial effects in bilayer devices	167
9.1 Introduction	167
9.2 Bilayer structure	171
9.3 Results and Discussions	172
9.3.1 Short circuit photocurrent measurements	172
9.3.2 Thermally stimulated current (TSC) measurements	176
Chapter 10	182
10.1 I-V Characteristics and Relaxation processes in Kapton	182
10.2 I-V Characteristics	185
10.3 Procedures for studying Electric Relaxation currents in insulators	186
10.4 Relaxation mechanisms in Kapton	189
10.4.1 Dipolar orientation	190
10.4.2 Space charge or interfacial mechanism	191
10.5 Theory of thermally stimulated relaxation processes for	

insulating systems	192
10.6 Isothermal transient current measurements (ITC)	194
10.7 Summary	207
Chapter 11	209
Summary and Future Directions	209
References	212

Chapter 1

Introduction

A polymer is a long chain macromolecule that is made up of repeating monomer units. Polymers can be visualized as long-chain macromolecules in which hundreds or thousands of atoms or molecules are linked together in various ways, resulting in a range of what we call microstructures (e.g., linear chains, branched chains, densely interconnected networks, and so on) to form a one-dimensional network [1-5,7,8]. The long molecular chains are characterized by strong chemical bonding within the chain and much weaker interchain bonding [1]. In this sense, a polymer solid can be considered to be an assembly of individual chains. Each chain consists of a very large number (10^5 or even more) of identical subunits bonded together. Each subunit can be viewed as a separate molecule with electronic states consisting molecular orbitals of the molecule. In describing the electronic states of polymers, especially the class of conjugated polymers (described later in this section) the degenerate molecular orbitals that overlap in a periodic fashion lift their degeneracy by forming extended, that is band of electronic states [1]. Thus, bonding and antibonding molecular orbitals lead to polymer valence and conduction bands, respectively. To this degree, polymers can be viewed as organic semiconductors and by analogy with the more familiar conventional inorganic crystalline semiconductors such as silicon, germanium, gallium arsenide etc., the concepts of energy band theory can be used to characterize their electronic states and their related properties [1].

Polymer based materials have been studied extensively in the last couple of decades from the perspective of their utility as active media in electrical, optical and opto-electronic applications [1]. Conventional polymer based solids are known to be insulators at room temperatures. The origin of these properties in these polymer materials, which are apparently similar to conventional inorganic semiconductors, has been intensively studied during this

period. Based on the tremendous progress of the field and "for the discovery and development of electrically conductive polymers", The Royal Swedish Academy of Sciences decided to award the Nobel Prize in Chemistry for 2000 for revolutionizing the development of electrically conductive polymers, to Professor Alan J. Heeger, Professor Alan G. MacDiarmid and Professor Hideki Shirakawa [2]. According to the citation "The choice was motivated by the important scientific position that the field has achieved and the consequences in terms of practical applications and of interdisciplinary development between chemistry and physics". However, a clear understanding of the various phenomena in these systems is yet to emerge. This section of the thesis-report briefly traces the important results and concepts, which have evolved in the process of studies of these materials. Due to the inter-disciplinary nature of the subject, a tremendous volume of work, spanning many issues is present in the literature. This report focuses on work-related to characterization of the defects or traps in the conjugated and conducting semiconducting polymers, their role in the charge transport mechanism and its impact on their electrical and optical properties.

Polymer based solids consist of both crystalline and amorphous regions [1]. The molecular weight of polymers are normally so high ($>10^5$) and are different from the other materials because of the long-chain characters and thus give rise to the solid-state materials properties such as excellent tensile strength, elasticity, fiber or film forming properties, that may not be found in other organic compounds.

1.1 Electronic states of non-conjugated and conjugated systems

One can classify polymers in the following structural terms. The first kind consists of polymers with the bonds saturated (i.e., complete bond satisfaction, e.g.; polyethylene PE) or polymers with saturated backbones but with appended aromatic chromophores that normally project out of the chain. A pendant group can be considered as a molecular unit attached to the polymer backbone at an angle to the chain direction. Non-conjugated

Polystyrene (PS) and poly (N-vinyl carbazole) (PVK or PVCA) are the representative examples of this class [1]. Fig. 1.1 schematically represents examples of these two polymer classes together with the appropriate electronic energy level picture.

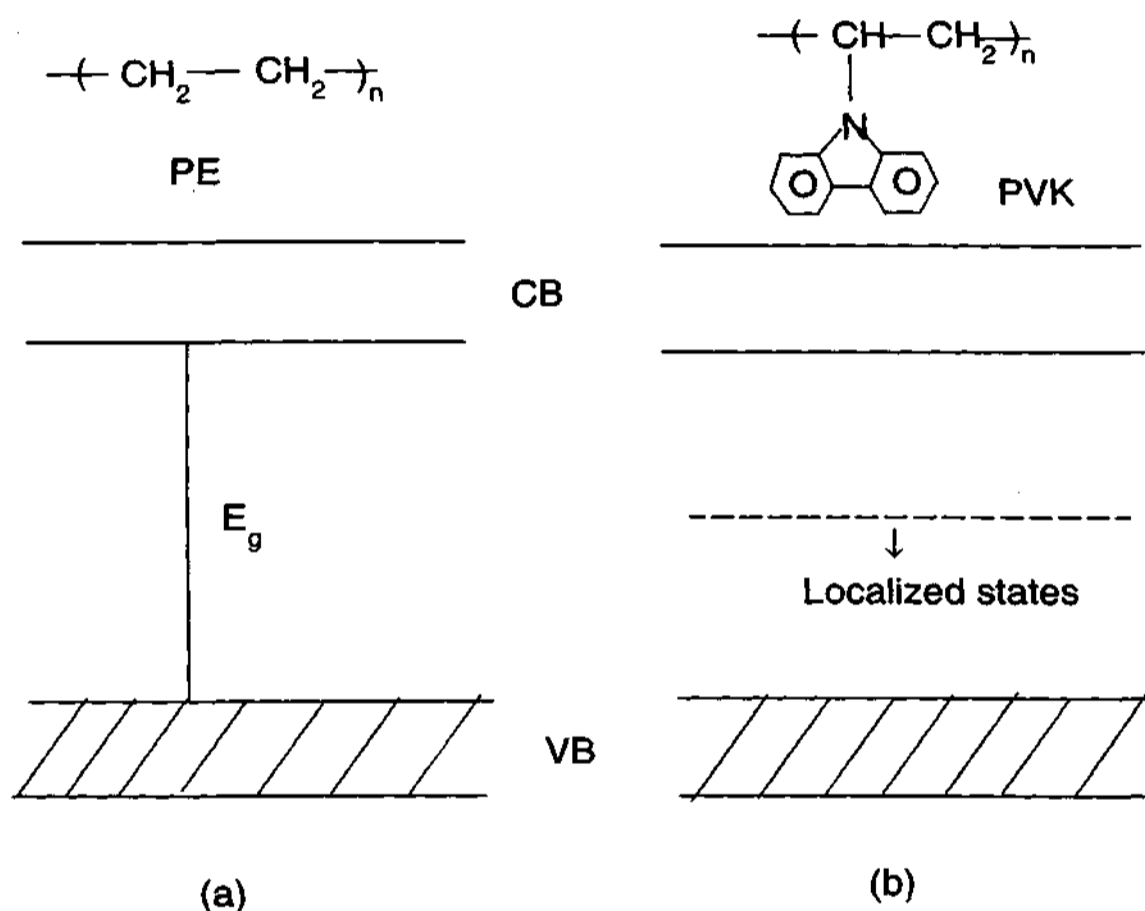


Fig. 1.1: Examples of a saturated polymer (a) without pendant groups, polyethylene PE and (b) with a pendant group, poly (N-vinyl carbazole) PVK and associated energy level picture.

The strong intrachain covalent bonding leads to wide band of states with an energy gap, E_g between the last filled and first unfilled band. This approach is conceptually applicable even for amorphous polymers because of the maintenance of periodicity in the chain direction. An important requirement for the applicability of band theory relates the strength

of any electron-phonon coupling with the width W of the energy band. In order for a carrier to remain within an energy band of width W after a phonon scattering event, the Heisenberg uncertainty principle states that $W\tau > \hbar$, where τ is the electron-phonon scattering time. Since $\mu = \frac{e\tau}{m^*}$, where m^* is the effective mass of the carrier, then it must satisfy the condition such that $\mu > \frac{\hbar e}{m^* \tau}$. A minimum value of mobility of $\mu_{min} \simeq 0.2 \text{ cm}^2 \text{ V}^{-1} \text{ sec}^{-1}$ is required for the validity of band theory¹. In contrast, the theoretical calculations for PE and PA predict mobilities higher than the minimum value and suggests that the concepts of band theory may have applicable to this systems. In reality, all polymeric materials are not ordered as in single crystals. Any variation in the energy of a molecular orbital due to disorder (compositional, translational or rotational) can impede band formation by the disruption of the required periodicity [1]. However the low mobility materials have the consequences of strong electron-phonon interactions relative to band-widths together with substantial effects of disorder. The concept of localization due to disorder and electron-electrons are discussed in the next chapter.

The pendant perpendicular to the chain direction and its planar character can lead to very little overlap and therefore interaction even between adjacent pendant groups [1]. Aromatic pendant group polymers give rise to electronic states in the gap between VB and CB and play a dominant role in the static and dynamic electric and optical properties. Most of the amorphous pendant group polymers are therefore similar to a random assembly of isolated pendant molecules. A significant application of this system as electronic materials in electrophotography as organic photoreceptors and photorefractive materials. Polymers such as PVK can be used for their hole transporting and injection properties [1]. This feature of PVK is demonstrated and reviewed in detail in the chapter 8. The second class comprises of unsaturated, conjugated polymers and is discussed in the following section [5-14,198-203,97,23,?].

1.1.1 Conjugated polymers

In this case of polymers without pendant groups, the electronic properties are deter-

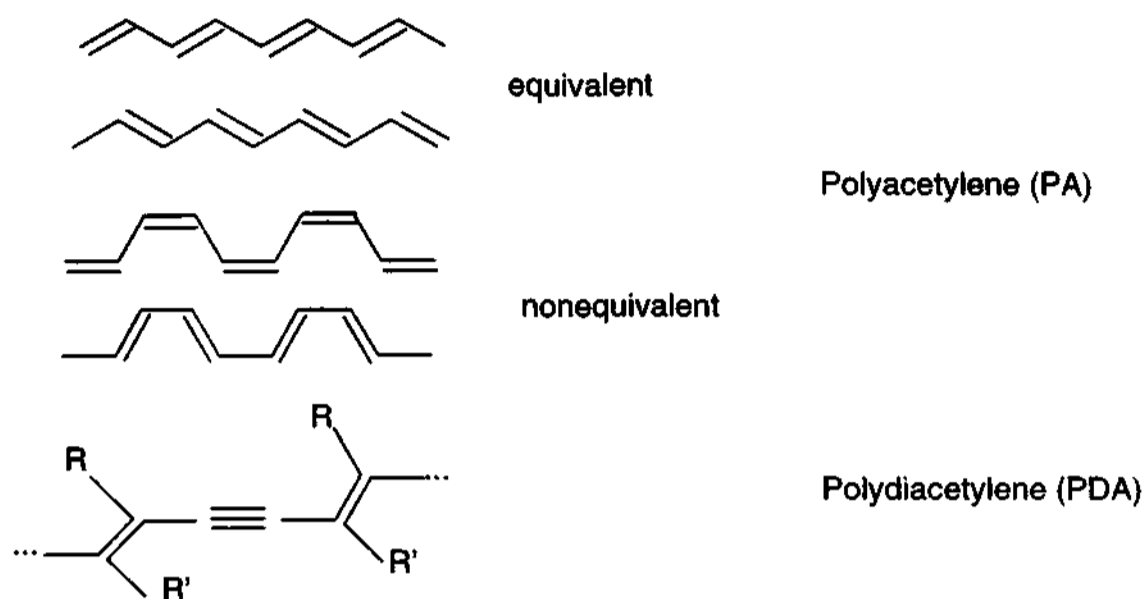
mined by the states which are associated with the strong covalent bonding between the atomic building blocks within the chain. Conjugated polymers consist of infinitely long chains, in which the backbones are mainly comprised of carbon atoms linked together or separated by heteroatoms such as O, N, P, S etc., rather than C and H atoms [6,7,9,11,14,8]. If a heteroatom is involved in chemical bonding, one or more "extra" electrons usually do not participate in chemical bonding process. These electrons are called n -bonding or also called non-bonding electrons and play an important role in chemical reactivity [1]. The side groups attached to the main skeleton of the polymers improves the processibility and modifies the interchain interactions. These heteroatoms also take part in conjugation and play an important role in determining the electronic properties of this system [1].

The existence of π -electron conjugation in a molecule produces a kind of "propagation" of electronic influences along the corresponding carbon chain. The electronic transition energy, often follow, in a series of oligomers empirical laws of the form $E(N) = A + BN^{-1}$, where A represents the value corresponding to the infinite perfect conjugated polymer [6]. Beyond a certain values of N, changes in E can be negligible. Conjugated polymers can be considered as a set of materials, which are derivatives of polyenes; i.e., of compounds with extended systems of conjugated bonds [11,24-32]. They are linear and unbranched chains having an extra orbital overlap of p_z electrons. Physical or chemical defects will hinder or interrupt the conjugation. In such a model the polymer can be considered and characterized by a distribution of several box lengths(i.e conjugation lengths) with orbital overlap.

In many materials, such as crystals, stretched polymers or liquid crystals, macroscopic properties such as strength and optical electrical properties generally depend on direction. They are said to be anisotropic. Similarly, the material's electrical conductivity may depend on direction and be anisotropic [2].

Graphite and polyacetylene both have mobile π electrons and are, when doped, highly anisotropic metallic conductors.

1. Linear carbon chains



2. Linear chains of conjugated rings

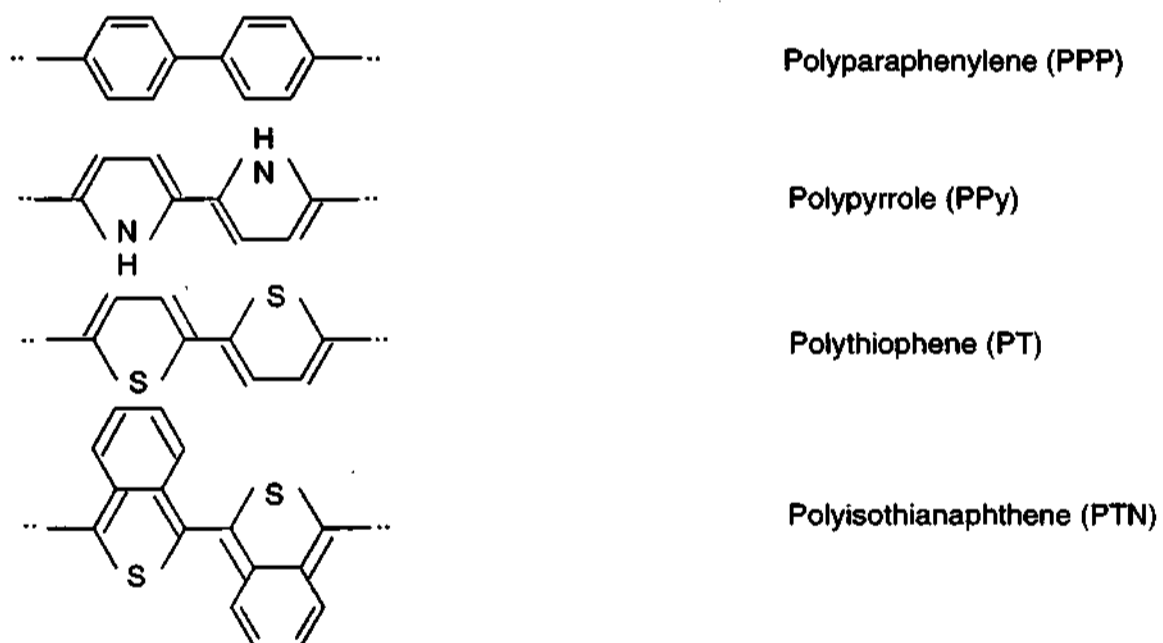


Fig. 1.2: Chemical structures of conjugated polymers with linear carbon chains and of conjugated rings

The conductivity is about one million times greater in the plane of the graphite rings than at right angles to this plane [2]:

$$\frac{\sigma_{\parallel}}{\sigma_{\perp}} = 10^6 \quad (1)$$

Correspondingly, the stretched oriented polyacetylene is some 100 times higher in the stretch direction than perpendicular to it. The smaller anisotropy compared to graphite, i.e., non-vanishing σ_{\perp} , could suggest "short-circuiting" across the chains [2]. Since the polyacetylene chains are not infinite, contacts between them are important if the material is to be macroscopically conductive. This could thus explain the lower conduction anisotropy compared to graphite [2].

The band gap of pristine conjugated polymers typically lies in the range of 1.5 eV (near IR) to 3 eV, resulting in semiconductor properties. In contrast, the bandgap for the simplest σ -bonded non-conjugated polymer, polyethylene or $(\text{CH}_2)_x$ is about 9 eV [1]. A few examples of π -bonded conjugated compounds are polyacetylene (PA), polythiophene (PT), polydiacetylene (PDA), polyparaphenylene (PPP), polypyrrole (PPy), polyisothianaphthene (PN), polyphenylenevinylene (PPV), polythienylenevinylene (PTV), polyphenylenesulfide (PPS), polyaniline (PANi) etc. Variations of these model polymers are formed with introduction of functional or non-functional side groups.

These polymers can also be treated as organic semiconductors [198] and their chemical structures of common conjugated polymers are shown in the Fig. 1.2 and Fig. 1.4. One of the classical distinctions between the π -conjugated and σ -bonded non-conjugated polymers such as PE, PS etc., is that they have relatively large electron affinities, small ionization potentials and low bandgaps, which would correspond to the low energy excitations [1].

As the π system is made longer, then the electronic properties will vary, e.g., the electronic transition energies decrease. Conjugated polymers are often treated as ideal one-dimensional systems: infinite perfect ordered isolated linear chains regularly built from repeat units containing π electrons [10,11]. The π electron system is extended infinitely

along the chain without interruption of the conjugation.

Fig. 1.3 shows the conjugated chain of *trans*-polyacetylene. A special class of polymers with thermal stability at elevated temperatures are ladder-type polymers (reviewed in the chapter 5) and few examples of this type are also shown in the Fig. 1.5 [12,13,33–38]. Real systems differ from the idealization in a number of ways; the system is disordered, the chains are

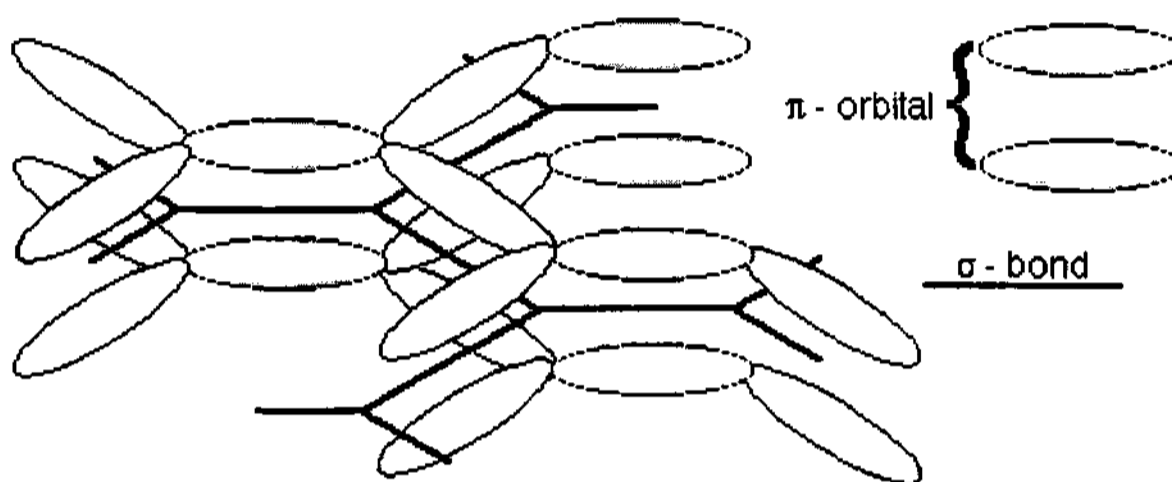
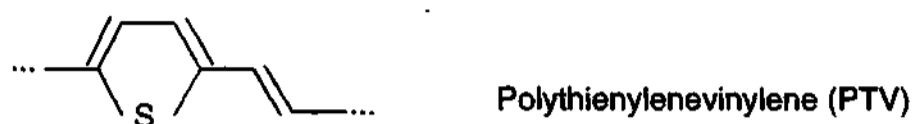
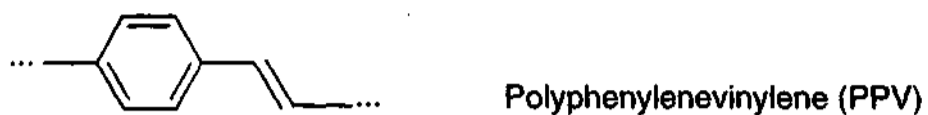


Fig. 1.3 Orbital picture of *trans*-polyacetylene with π and σ bonds

distorted, the chains are not isolated but in most of the cases they are three-dimensionally coupled together, and so on. Therefore, these effects must be taken in to account in studying electronic and optical properties of the real conjugated systems.

The origin of the band gap ($\pi - \pi^*$ transition energy) is mainly due to the average interaction between single carbon atoms and the bond alternation effects with an additional contribution due to Coulombic repulsion between electrons. Certain cases nitrogen p_z and C_6 orbitals also take part in conjugation and play an important role in determining the charge transport mechanism. All states below the gap are occupied form the highest occupied molecular orbitals (HOMO) and the states above are empty form the lowest unoccupied molecular orbitals (LUMO) which is analogous to the valence and conduction bands in conventional inorganic semiconductors.

3. Chains of alternating rings and C = C bonds



4. Chains of alternating rings and heteroatoms

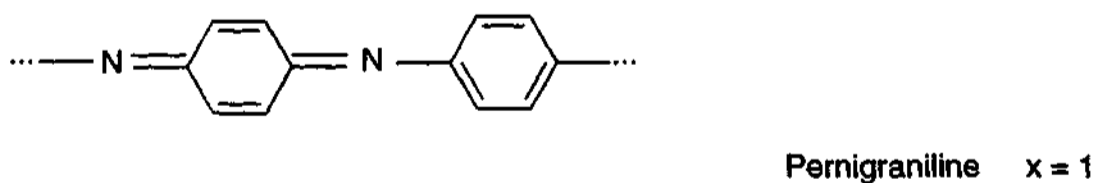
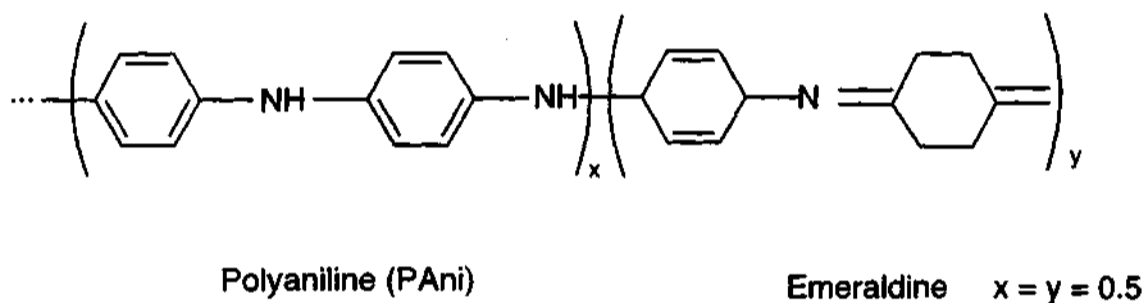


Fig. 1.4: Chemical structures of conjugated polymers with chains of alternating rings with double bonds ($C = C$) and heteroatoms

Chemical structure of ladder-type polymers

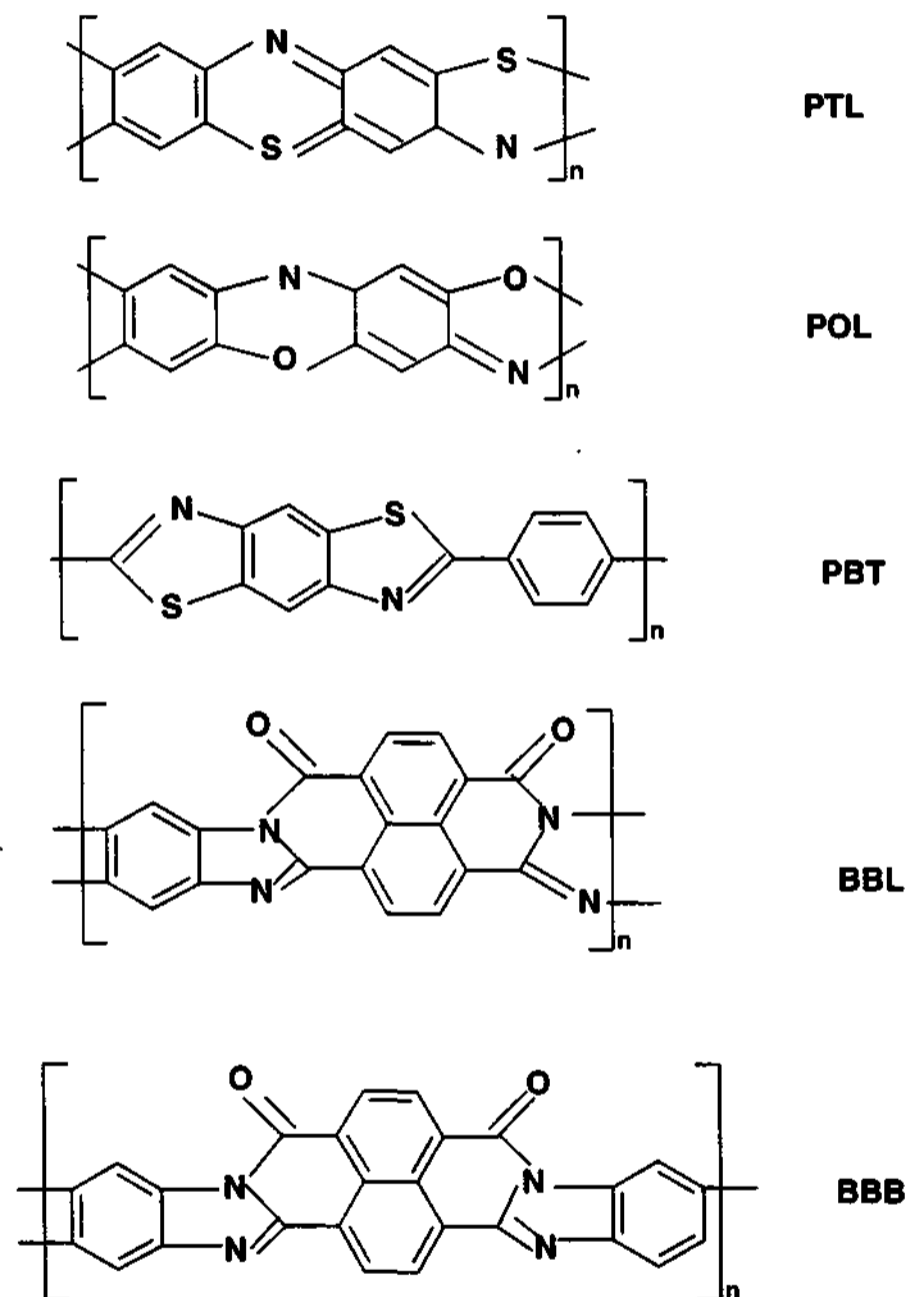


Fig. 1.5 Examples of ladder-type polymers with heteroatoms (N, O and S)

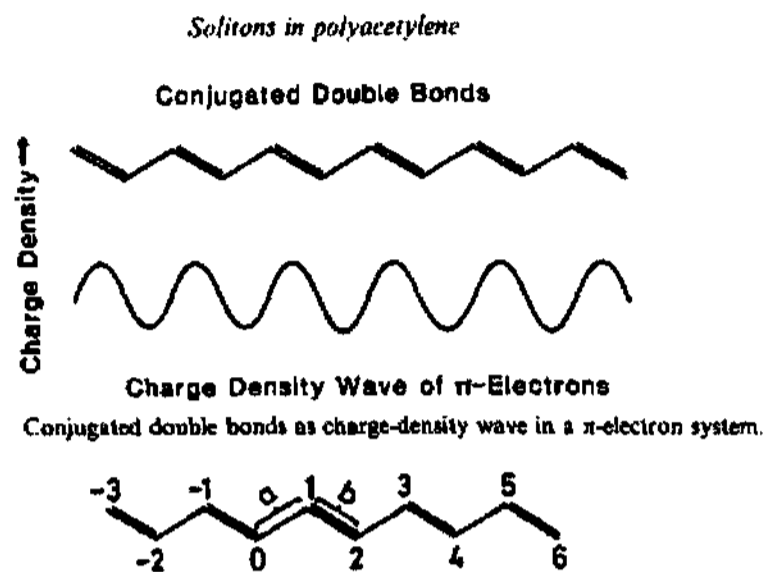


Fig. 1.6 Conjugated double bonds as charge density wave (CDW) in a π -electron system

In the polymeric chains s (σ -electrons) form σ bonds and p (π electrons) form π bonds. The splitting of π and π^* orbitals through the interaction between carbon pairs will give rise to bands and the differences in energy is normally called as transition energy or band gap. The σ electrons have very little role in the electrical and optical properties to provide the basic binding to give structural stability, while the mobile π electrons are characterized by low-lying excited states, which dominate the electrical and optical properties [6,198].

The double bond should not be considered as an individual character but as part of a collective system and in addition to that the conjugation leads to the interesting symmetry properties. Due to the single and double bonds, the charge density oscillates periodically if one moves along the chain. This phenomenon is termed as a bond order wave, because the electron density is not modulated at the lattice sites but rather between the lattice sites [16]. It is important to note that the double bond has a higher electron density than the single bond. The charge density wave of the electrons modifies the lattice of the "positive ions" (CH groups). The ions will move towards of higher electron density, i.e. into the double to maintain the local charge neutrality. This makes the double bond shorter than the single

bond. This feature significantly indicate there is a bond alternation due to shortened and lengthened bonds.

1.2 Quasiparticles in conjugated polymers

Due to the alternation in the bond lengths and the lattice distortion sometimes called as dimerization, the system opens up the gap called as Peierls distortion [39–44]. This distortion is characterized by the bond alternation parameter p , which is given by the relative difference between the long and short bond lengths and it is designated as $p = 2(a - b)/(a + b)$, where a and b are the bond lengths of the long and short bonds [42]. Experimental values on polyacetylene suggests a value of the differences between the short and long bonds is approximately given by 0.3 to 0.4 nm [43,45,46]. The bond alternation parameters of *trans*-polyacetylene are shown in the Fig. 1.6. Due to the bond alternation there is a periodic modulation of the π electron density. At that misfit the charge density wave has a 180° phase slip. In addition to the electron-lattice coupling there are further, equally important interactions, often referred to correlation effects. To take these into account the parameter p can be generalized as "bond order parameter" and the charge density wave as "bond order wave" [9,42]. The two-fold coordination associated with linear conjugated polymers and the proportionality of bond length to bond strength (or bond order) in conjugated systems, leads to a deep interconnection between their electronic and chemical structures. As a result of this interconnection, the elementary excitations in semiconducting polymers (electrons and holes in classic inorganic semiconductors) involve lattice (geometrical) relaxation around the electrons and holes. The lattice relaxation in the excited state leads to self-localization and the formation of solitons, polarons and bipolarons [11,41,46].

1.2.1 Solitons

Solitons are quasi-particles corresponding to solitary waves, similar to phonons corresponding to sound waves and photons to electromagnetic waves [11]. Speaking in terms of step functions particles and antiparticles are easily identified as up-steps and down-steps as illustrated in the Fig. 1.7. In charge density waves they correspond to phase-slip centers of

created by doping, either as carbonium ions or carbanions [11]. From a chemical point of view in pairs creation is evident, since it involves the breaking of a bond, which leaves two dangling bonds (or the splitting of an electron pair which leaves two radicals).

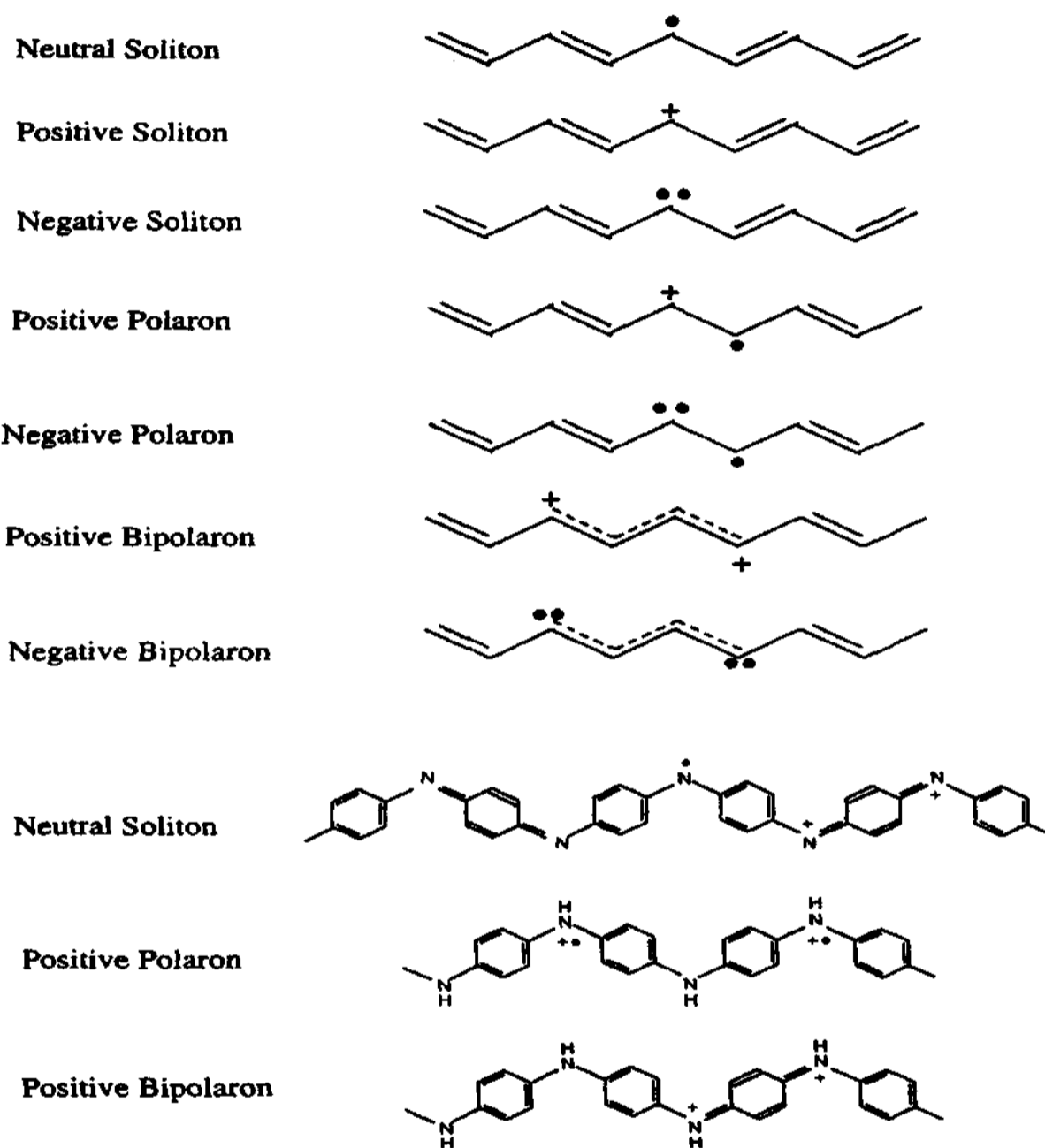


Fig. 1.8 Schematic illustrations of solitons, polarons, and bipolarons in trans-polyacetylene and polyaniline

Evidently an odd-numbered chain must have an unpaired electron, i.e., there must be a soliton in the ground state. A soliton moves by pairing to an adjacent electron and leaving its previous partner unbound. The soliton always occupies odd numbered sites and the even-numbered sites are reserved for antisolitons [2,11]. A soliton is free to move, because the total energy of the system does not depend on the position of the soliton. It can move only along the chain; there is no tunnel effect between the chains. Because of this anisotropic feature, doped polymers (and conducting low mass organic molecules) are called low-dimensional conductors, synthetic metals or organic metals. If the chain is long enough, the short chain end effects will push the solitons to the center [6,11].

A soliton has to overcome an energy barrier when moving from one site to the next. The existence of this kind of barrier leads to "self trapping" of the soliton in the chain. Free soliton motion is possible only in pA. It is not the electron that is moving the defect is moving and this means that the electrons change their partners not their position. Of course this requires a slight displacement to determine the effective mass of the soliton. Within this model, Su, Schrieffer and Heeger estimated the effective mass of a polyacetylene soliton to amount to about six free electron masses [41]. There are neutral as well as positively and negatively charged solitons. The dangling bond consists of an electron sitting on a lattice site, which is also occupied by a positively charged ion. Electronic and ionic charges compensate for the defect as they do in the undisturbed part of the chain. However in redox reactions, the defect is more sensitive than the rest of the chain.

A soliton is a domain wall separating two isoenergetic regions with an opposite sense of bond alternation. In the neutral, uncharged chain, the excitation is a spin 1/2 and charge 0 state. In chemical language, it is a free radical and can be thought as a non bonding orbital occupied by a single electron given by the $2p_z$ orbital of the C atom without distortion. It has been known in the conjugated polymer literature as a soliton, although two such defects do not cross each other without distortion. By symmetry, the energy level of a soliton lies in the middle of the forbidden gap. It may contain $n = 0, 1$ or 2 electrons ($n = 1$ for neutral

solitons). If an electron is removed or added to a neutral, then a charged soliton is created, which has a positive charge or a negative charge respectively. The existence of the solitons requires the degeneracy of the ground state as in the case of polyacetylene.

1.2.2 Polarons

The polaron is defined as the electron that is dressed up by the lattice distortion [32,47]. In the language of conducting polymers, the term polaron refers a localized state, which is always accompanied by a lattice distortion. Unlike solitons, polarons can exist in both degenerate and non-degenerate ground state conducting polymers. The polaron has the spin $1/2$ and charge $\pm e$. The polaron has either smaller radius or larger radius depending upon the strength of the electron phonon coupling. In the case of conventional inorganic semiconductors, the polaronic radius is smaller and larger for conjugated polymers. The polaron binding energies will be the order of 10 to 30 meV, and effective masses is few times of free electron masses.

1.2.3 Bipolarons

The spinless conductivities have been observed in doped polymers with a nondegenerate ground state in many cases [48]. This suggests that the polarons are not the appropriate excitations in these cases. Charged solitons have no spin, but polymers with a non-degenerate ground state cannot support solitons. These new species are bipolarons. The bipolaron is defined as the pairing of polarons with charge $2e$ and spin zero. The energy gained by the bipolaron must be large enough to overcome the Coulombic repulsion between two nearby charges of the same sign and the entropic term. Fig. 1.8 shows the bond alternation mobile species of conjugated polymers. A bipolaron can be viewed as a doubly ionized soliton-antisoliton pair-two nearby solitons sandwiching a short segment of a high energy geometry. Thus the bipolarons can exist in both degenerate and nondegenerate ground state polymers.

1.2.4 Excitons

Another type of quasiparticle is the exciton, a neutral excitation well known in inorganic semiconductors where it often dominates the onset of electronic optical absorption.

An exciton is defined as a pair of an electron and a hole bound by Coulomb interaction. A molecule with an electron in an unoccupied, high energy orbital and a hole in an occupied, low energy orbital is in an excited state. Since the excitation consists of an electron and a hole, it is charge neutral.

Different types of exciton in crystals are the Frankel exciton, the Mott-Wannier exciton and the charge-transfer exciton. A short description is as follows:

- Frenkel exciton - electron and hole on the same molecule/atom,
- Mott-Wannier exciton - large distance between electron and hole.
- Charge transfer exciton - hole on one molecule, electron on another.

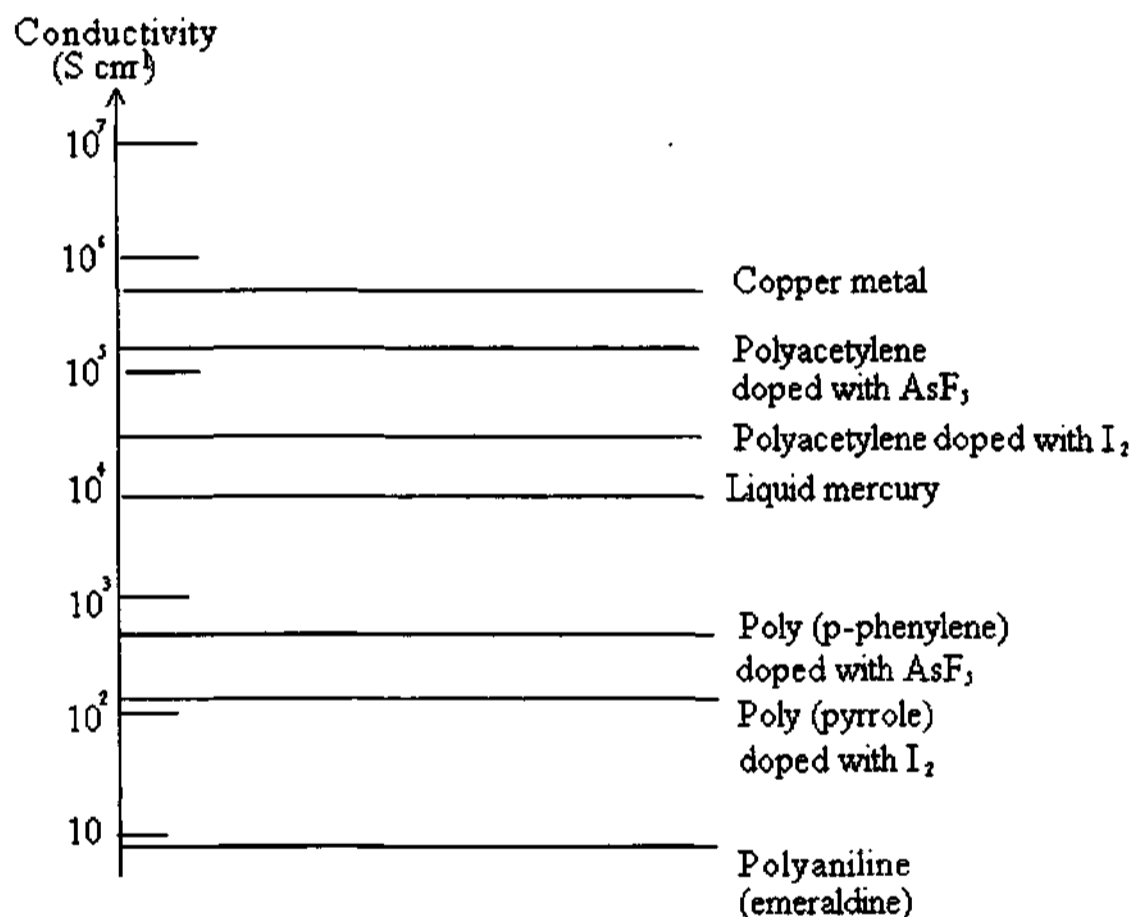
Excitons in inorganic semiconductors are mostly Mott-Wannier excitons. They have a small binding energy, E_b , typically less than 0.1 eV (e.g. 1 - 2 meV for Ge), and a large radius (e.g. 5×10^{-7} cm for Ge). Frenkel excitons are observed in molecular, ionic and noble-gas crystals and E_b is usually high, in the order of 1 eV. The typical values of binding energies for inorganic semiconductors, E_b : From: 4.9 meV, 5.1 meV (GaAs, InP) To: 29 meV, 59 meV (Zns, ZnO) and for organic semiconductors E_b : From: 0.1 eV To 1 eV [49,50]. Most of the cases the value will be typically around 0.3 eV in organic semiconductors. Frenkel excitons either singlet (spin 0) or triplet (spin 1), are in fact the most important excitations for understanding the electronic properties, the visible and near UV absorption to begin with, of crystals of small conjugated molecules, such as naphthalene. Solitons, polarons, and bipolarons have been extensively used to account the charge transport properties in doped conducting polymers, while excitons have been proposed to explain the luminescent properties of undoped conjugated polymers.

1.3 Doping of conjugated polymers

Polymers with conjugated chains are, for these reasons, merely semiconductors and insulators, even if the chains are planar. These low conductivities can be substantially

increased, however, if the polymers are doped with substances such as I_2 , AsF_5 , BF_3 , etc.: doping with AsF_5 raises the specific electrical conductivity of *trans*-poly (acetylene) from 10^{-9} to 1200 S/cm and of poly (*p*-phenylene) from 10^{-15} to 500 S/cm [51–55]. Such doped polymers can be processed like thermoplastics to any desired shape, which together with their light weight, makes them attractive for many applications.

The action of these dopants is quite different from those of small amounts of dopants in conventional inorganic semiconductors. The doping of inorganic semiconductors such



Logarithmic conductivity ladder locating some metals and conducting polymers

Fig. 1.9 Comparison of conductivity of some doped polymers with metals

as Si, GaAs, GaP, InSb or Ge generates quasi-free electrons (*n*-carriers) or defect electrons (*p*-carriers), whereas the doping of suitable organic polymers leads to oxidation (*p*-doping)

or reduction (*n*-doping) reactions. The role of the dopant is either to remove or to add electrons to the polymer. For example, iodine (I_2) will abstract an electron under formation of an I_3^- ion. Sizable effects in organics are thus only achieved if large amounts of dopants are used, often up to 1:1 molar ratios of dopants to repeating units.

Doped polymers exhibit neither Curie paramagnetism (localized charge carriers) nor Pauli paramagnetism (electrons delocalized over the entire system). Thus the electrical conductivity of such systems is assumed to be due to solitons or polarons. If an electron is removed from the top of the valence band of a semiconductive polymer, such as polyacetylene or polypyrrole, the vacancy (hole) so created does not delocalize completely, as would be expected from classical band theory. If one imagines that an electron is removed locally from one carbon atom, a radical cation would be obtained. The radical cation (also called a "polaron") is localized, partly because of Coulomb attraction to its counterion (I_3^{-1}), which has normally a very low mobility, partly because of a local change in the equilibrium geometry of the radical cation relative to the neutral molecule. The mobility of a polaron along the polyacetylene chain can be high and charge is carried along as shown in Fig. 1.7. However, since the counterion (I_3^{-1}) to the positive charge is not very mobile, a high concentration of counterions is required so that the polaron can move in the field of close counterions and explains the need for large dopant content. If a second electron is removed from an already-oxidized section of the polymer, either a second independent polaron may be created or, if it is the unpaired electron of the first polaron that is removed, a bipolaron is formed. The two positive charges of the bipolaron are not independent, but move as a pair. While a polaron, being a radical cation, has a spin of $1/2$, the spins of the bipolarons sum to $S = 0$. Other animals in the zoo of polymer chain defects important for conductivity in polyacetylene are solitary wave defects, "solitons". The understanding of the bulk conductivity gets further complicated due to interchain effects and the large disorder in the solid state of these macromolecular systems. The disorder causes localization of electronic states, band tailing, and broadening of the optical transitions. This 1-D band description ignores the attractive Coulomb interaction between electrons in the π^* band and holes in the

π band. This attraction causes the formation of excitons; i.e. neutral electron-hole bound states. One of the fundamental unresolved issues of the physics of semiconducting polymers is the magnitude of the exciton binding energy.

The doping of these polymers essentially increases the number of charge carriers by a large amount and give rise to increase in conductivity [202,56–59]. There are two types of charge transfer to the π conjugated polymers: one is to encounter the counterions, in order to maintain the neutrality condition and other is without involving counterions. The former process leads to a permanent doping level, while the latter only temporarily oxidizes or reduces the polymer. Doping process in conducting polymers is different from that of conventional semiconductor in that the counterions in between the polymer chains can freely move. Doping is a continuous process or a stoichiometric reaction and whether there is a phase segregation between doped and undoped regions and whether the doped material dissolves in the host. It could be chemical, electrochemical and protonic acid doping. Chemical doping involves the charge transfer mechanism between the polymer and the counterions, which become the dopants. The small amount of voltage is applied to the samples to make oxidation or reduction states in the case of electrochemical doping. Without increasing the number of electrons, by adding the protons to the intrinsic samples lead to the protonic acid doping. All the three processes mentioned above are reversible.

The conductivity of undoped polyacetylene is in the order of 10^{-5} S/cm and the value of 10^5 S/cm has been obtained for I_2 doped polyacetylene. The most important condition for the existence of electrical conductivity of this polymer seems to be the ability to form overlapping molecular orbitals. The planar structure of *trans*-poly (acetylene) promotes the overlapping of its π and p orbitals. In poly (*p*-phenylene sulfide) PPS, $\sim [S-(p-C_6HT_4)]_n \sim$, p and d orbitals of sulfur atoms promote overlap with the π systems of phenylene groups; PPS-AsF₅ shows an electrical conductivity of 10 S/cm, although the chain is not planar and the phenylene residues are ranged at angles 45° to the planar zigzag chain of the sulfur atoms. The possibilities of dedoping and redoping are some of the novel doping features in

conducting polymers.

Another method, which has been attempted in these polymers to enhance the conduction in these materials, is by ion implantation. This process involves the bombardment of inert gas ions like Argon, Krypton etc. when the high energy ions are bombarded to the polymer and loses energy to the polymer provide electronic collisions. These collisions will be able to break the bonds depending upon the energy of the incident beam and temperature. This process not only removes the heteroatoms selectively, but also it can completely remove the extra atoms attached to the backbone of the carbon skeleton, which are strongly linked by higher dosage and forming a complex network. This process is often referred as graphitization or carbonization, while these polymers resemble the graphite like structure and it is completely irreversible process. This kind of mechanism may impart the surface damage if the dose concentration is high. The bombardment process results in generation of more free carriers and hence the increase in conductivity.

1.4 Su Schreiffer Heeger (SSH) model)

A one-dimensional metal is highly unstable against a periodic lattice distortion was

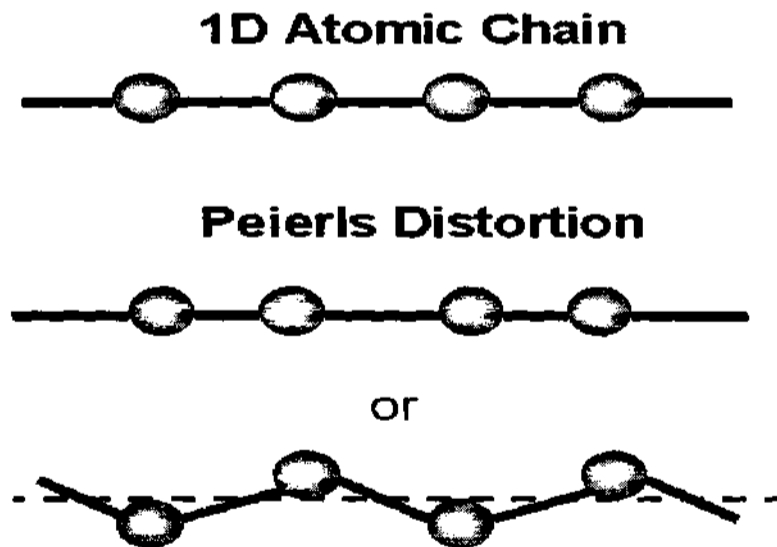


Fig. 1.10 (a) Peierls distortion in simple monoatomic chains.

shown by Peierls in 1950 [39]. For the physicist, the conjugation arises from symmetry breaking. Fig. 1.10 a shows the Peierls distortion of monoatomic chains. Fig. 1.10 b and c show the Peierls effect in polyacetylene chains. For an infinitely long chain of CH units, where the sp^2 orbitals have already established σ bonds to the neighbors, but where the remaining π -electron

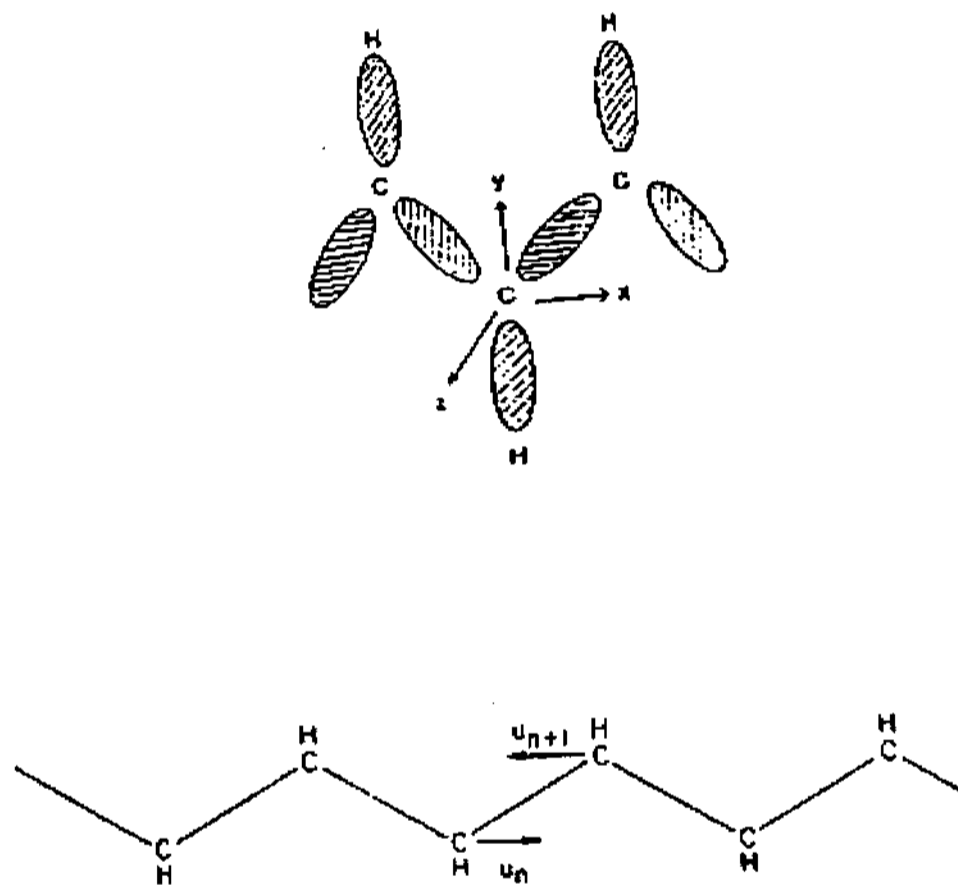


Fig. 1.10 (b) Sp^2 hybridized σ bonds in the molecular plane, (c) structure of $(CH)_x$ backbone

has not yet decided whether it should bind to the left or to the right. This hypothetical state would be stable in polyacetylene at temperatures above 10000 K [11,41]. It would be a one-dimensional metal with a half-filled energy band: the π electrons are completely delocalized, metallic, and are now called π electrons. If the metal is cooled down, a charge

density wave and a corresponding deformation of the lattice of the CH group will form Peierls distortion. In the energy band of the π electrons a gap will form at the Fermi level (i.e. in the middle of the band in the case of half filling). The formation of the gap allows the system to lower its electronic energy. Part of the energy gained is used as elastic energy in the Peierls distortion of the lattice, but it can be shown that at low temperatures the energy balance is positive. This transforms the metal to semiconductor or insulator, due to the opening of the gap. Such metal-to-semiconductor transitions are well known in one-dimensional systems. The change in the band structure arising from the Peierls distortion is shown in the figure. According to the conventional semiconductor physics, the lower (and filled) sub-band is called the "valence band"; the upper (empty band) sub-band, the "conduction band". In the chemistry language, π and π^* bands are analogous to the valence and conduction bands. The former contains bonding and latter the antibonding states: the HOMO (highest occupied molecular orbitals) is at the edge of the valence band and at the edge of the conduction band is the LUMO (lowest unoccupied molecular orbitals). The difference between the two levels is the band gap and it is influenced the charge transport of the conjugated polymers.

The simple prototype conjugated molecule is polyacetylene. It consists of three unsaturated sp^2 hybridized σ bonds, whereas the conjugation is by π electrons which are perpendicular to the molecular plane as shown in the Fig. 1.11. Bond alternation defects in polyenes have been thoroughly studied using the Huckel molecular orbital (HMO) [60,61]. The first step in this procedure is the separation of σ and π electron systems. Because of the orthogonality of σ ($2sp^2$) and π ($2p_x$) orbitals and usually the interaction between them is neglected in many cases. The total energy of a chain has two main components: Hence the σ molecular backbone and the π electron system can be treated independently. These orbitals are built up as the linear combinations of $2p_x$ like atomic orbitals (LCAO). The respective coefficients for the atomic orbitals are gained via the variational principle, i.e., minimizing the energy of each π MO. The total π system energy is simply the sum of all π electron

energies. The ground state of π system is obtained by filling up the energetically favored lowest MO's with electrons of antiparallel spins. Su, Schrieffer and Heeger have applied the Huckel model to prototype polyacetylene in 1979 [41]. The following approximations are made to construct this model (SSH) Hamiltonian:

- ¶ The Born-Oppenheimer (adiabatic approximation), the nuclear motion is considered to be stationary when compared to the electronic motion.

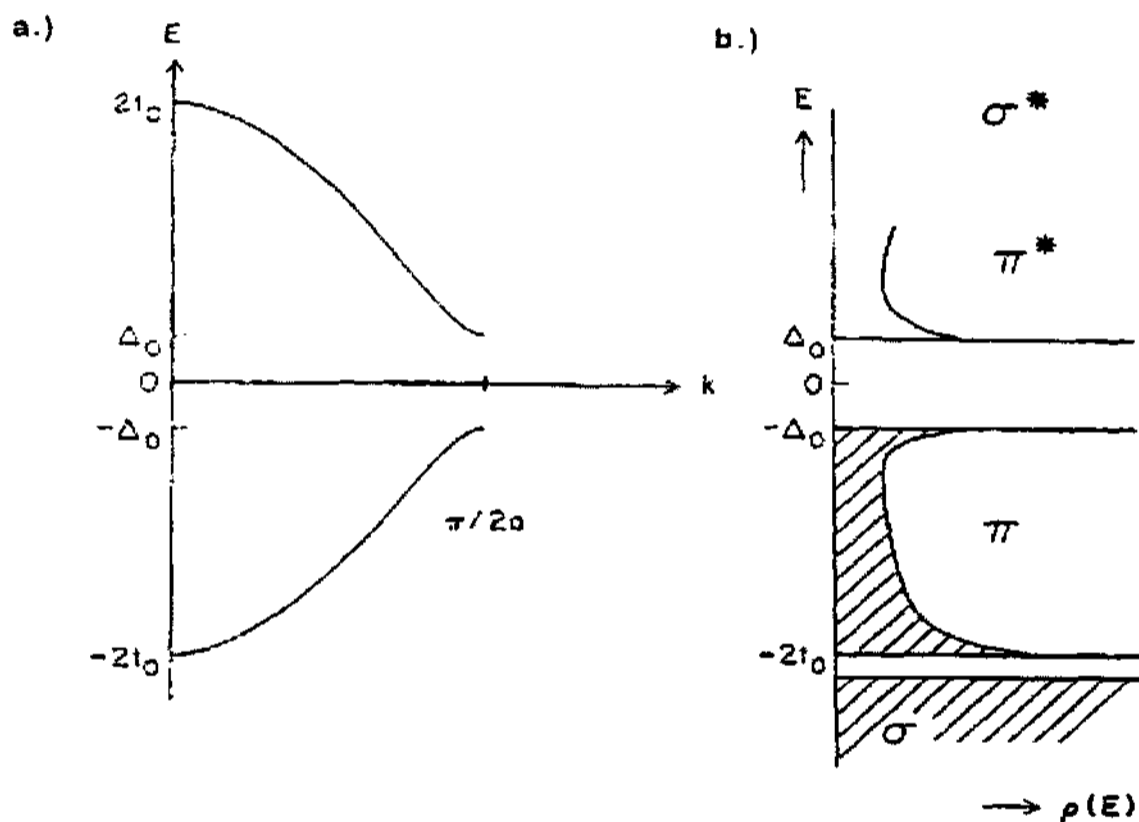


Fig. 1.11 Band structure (a) and density of states (b) for $\text{trans}-(\text{CH})_x$

- ¶ π electrons can be treated independently of s and other p electrons (Huckel method). The mutual interaction between p electrons is accounted only and correlation effects are ignored.

¶ Translation groups of CH units (whole) are considered only in the chain direction and the interchain interactions are neglected by introducing the concept of one-dimensional semiconductors.

For constructing a π MO only the next carbon neighbors' atomic orbitals are used in the LCAO method (tight binding method). Within the theory of second quantization, the SSH Hamiltonian reads:

$$H = \frac{M}{2} \sum u_n^2 + \frac{K}{2} \sum (u_n - u_{n+1})^2 - \sum [t_0 + \alpha(u_n - u_{n+1})] \times [c_{n+1,s}^+ c_{n,s} + c_{n,s}^+ c_{n+1,s}] \quad (2)$$

where u_n is the deviation of the equilibrium position of CH group n , t_0 the hopping integral between nearest neighbors for an undimerized chain, α the electron phonon coupling constant (electron lattice displacement), $c_{n,s}^+$ the (creation/annihilation) operator of π electrons on group n with spin $s = \pm 1/2$, M the mass of CH group and K the σ spring constant between two CH groups. The first and second terms represent the kinetic and bonding (elastic) energies and the third term represents the electron-phonon coupling, which is the standard form used for metals. The nuclear kinetic energy is also taken into account for the total energy of the system. It is noted that the bonding term increases the energy of the system, while the electronic term decreases the energy. The system must be in a state, which has the minimum energy.

For a half filled band system such as polyacetylene, $K_F = \pi/2a$, so that the distortion has a wavevector of π/a corresponding to a real space dimerization of the lattice. This amount of bonding or elastic energy will distort the lattice, due to the dimerization and finally it turns out the decrease of electronic energy. Suppose the polyacetylene chain is dimerized with the lattice displacement

$$u_n = (-1)^n u = \exp[\pm 2K_F n a u] \quad (3)$$

The electrons in states near K_F are scattered into a state near $-K_F$ and vice versa. The eigen states are superposition of the right-going and left-going states. This opens

up the energy gap at the Fermi energy therefore lowering the energy of the occupied states is shown in the Fig. 1.12

To determine the electronic spectrum of the dimerized lattice, let $t_d = t_0 - 2\alpha u$ and $t_s = t_0 + 2\alpha u$, where t_s and t_d are the hopping integrals for the single and double bonds. Upon solving the Schrodinger equation yields Bloch-type wave functions made up of Wannier atomic wave functions²⁵ in the tight binding approximation.

$$E\phi(2n) = -t_d\phi(2n+1) - t_s\phi(2n-1) \quad (4)$$

$$E\phi(2n-1) = -t_d\phi(2n) - t_s\phi(2n+2) \quad (5)$$

Applying it twice, one obtains E

$$E^2\phi(2n) = -(t_d^2 - t_s^2)\phi(2n) + t_s t_d [\phi(2n+2) + \phi(2n-2)] \quad (6)$$

If we assume that $\phi(n)$ is a Bloch function with momentum k so that

$$\phi(2n+2) = \phi(2n)\exp[2ika] \quad (7)$$

One can get the dispersion relation as

$$E_K^2 = 4t_0^2 \cos^2 ka + 16\alpha^2 u^2 \sin^2 ka \quad (8)$$

The total electronic energy of the system is obtained by integrating E_k over the first Brillouin zone. The total energy $E_0(u)$ as a function of u is given by

$$E_0(u) = -\frac{4t_0}{\pi} E(1-\eta^2) + K \frac{t_0^2 \eta^2}{2\alpha^2} \quad (9)$$

where $E(1-\eta^2)$ is the elliptic integral and $\eta = 2\alpha u/t_0$, and therefore for smaller values of η ,

$$E(1-\eta^2) \simeq 1 + \frac{1}{2} \left[\ln\left(\frac{4}{\eta}\right) - \frac{1}{2} \right] \eta^2 + \dots \quad (10)$$

Therefore the decrease in π energy is always more greater than the increase in σ energy for smaller values of u . Fig. 1.12 shows the total energy E_0 as a function of

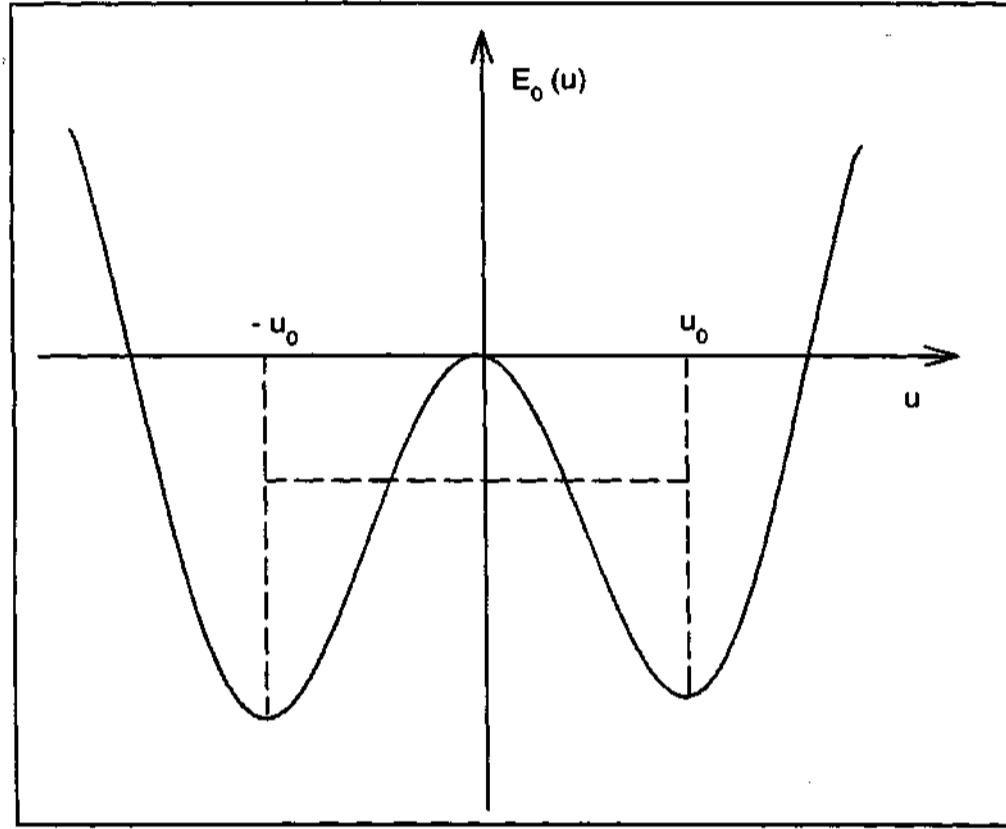


Fig.1.12 Total energy (electronic plus lattice distortion) as a function of u

dimerization parameter u . It is assumed that $E_0(u) = E_0(-u)$ is symmetrical about the origin, corresponds to the bandgap of

$$2\Delta_0 = E_g = 16t_0 \exp\left[-1 - \frac{1}{2\lambda}\right] \quad (11)$$

where $\lambda = 2\alpha^2/\pi t_0 K$ and the values of $K = 21 \text{ eV/\AA}^2$, $\alpha = 4.1 \text{ eV/\AA}$, $t_0 = 2.5 \text{ eV}$, leads to a gap $E_g = 2\Delta_0 = 1.4 \text{ eV}$ and a lattice distortion $u_n = 0.04 \text{ \AA}$.

$E = E_\pi + E_s$, where E_s is a classical energy treats all the C-C bonds as springs with a common force constant K ,

$$E_s = \sum_n \frac{k}{2} (d_{i,i+1} - a)^2 \quad (12)$$

This term approximates the changes in energy due to non- π electrons that occur when a C-C bond changes to length $d_{i,i+1}$ from some average value "a". E_π is the total energy of π electrons and is the sum of the occupied single particle energies ϵ_k .

$$E_\pi = 2 \sum_k \epsilon_k \quad (13)$$

The ϵ_k are the eigen values of a tight binding Hamiltonian:

$$H = - \sum_i \sum_j |i\rangle t_{ij} \langle j| = \delta_{ij} \quad (14)$$

t_{ij} is not zero only when i and j are nearest neighbors and $j = i \pm 1$. The value of $t_{i,i-1}$ depends on bond length $d_{i,i-1}$. All the isomers of polyacetylene have dimerized ground states in which the molecules retain distinct single and double bonds with different length.

In an undimerized chains, all C-C bond lengths have the same length a , the system energy E_s is zero, all $t_{i,i-1} = t_0$. In both isomers, under uniform dimerization, every atom site is displaced by a distance "u" in a direction at an angle of 30° to both of the neighboring bonds, in away which creates alternate short (double) and long (single) bonds, shortened and lengthened by the factor by $2\cos 30$. These bonds will have π electron coupling strengths of t_d and t_s respectively. Here $t_d = t_0 + 2\alpha u$; $t_s = t_0 - 2\alpha u$. Every bond will have spring energy of $2k'u^2 = 2ku^2 \cos^2 30$, giving total spring energy of $E_s = 2(N-1)K'u^2$. This model describes only nearest-neighbors coupling and makes no distinction between *cis* and *trans*-isomer. *Cis* has a wider band gap and lower cohesive energy which has no internal degeneracy for the actual ground state [41]. the *trans*-cisoid has much cohesive energy and lower band gap than that of *cis*-transoid. In this model, the band gap of *trans*-polyacetylene is dependent directly upon the difference in neighboring bond lengths. That is, a polymer chain that consists

of identical aromatic bonds has a band gap of zero. Besides this description of the ground state *trans*-polyacetylene, SSH also directly models conformational excitations in the polymer such as solitons and polarons. Further, extending the range of tight binding (TB) Hamiltonian, this model is able to distinguish between the isomers of PA with regard to the ordering of the total energies, band gaps and alternate excitations such as bipolarons in the *cis*-isomer. The major drawback of this model is selectively works for PA, and it is not easily extended to more complex systems [41].

1.5 Origin of conduction mechanism

Fig. 1.13 shows the schematic fibrillar structure of polymeric fibers. The conduction mechanism is mainly due to the components such as

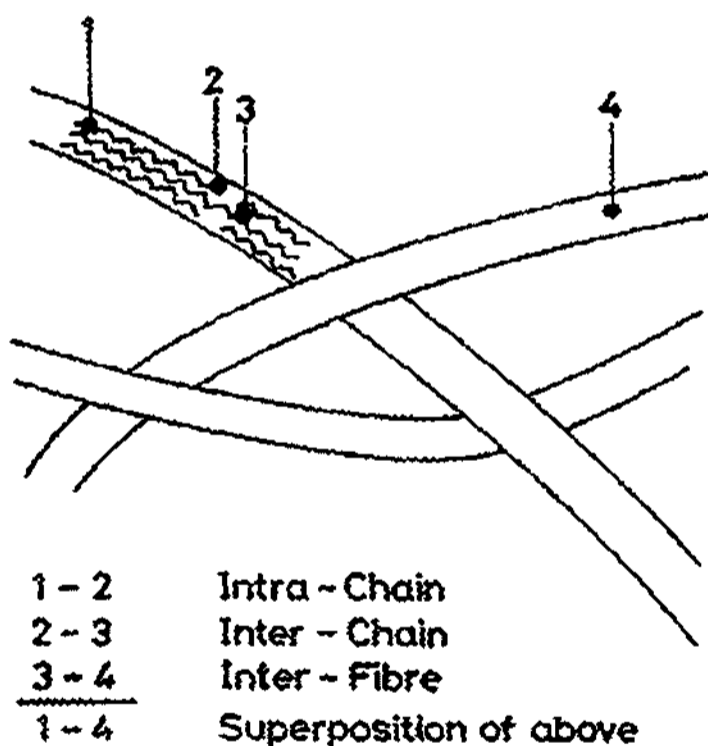


Fig. 1.13 Schematic view of the fibrillar structure of polyacetylene. The fibers are bundles of chains containing some 100 or 1000 polymer chains. [62.63]

¶ Intra-chain interactions: Isotropic, three-dimensional jump between localized

620.192 042 972
 P01

JNCASR	
Acc No	3208
LIBRARY	

states, along and between polymeric chains

- ¶ Inter-chain interactions: thermally activated tunneling between extended conducting zones
- ¶ Inter-fiber interactions: tunneling between the fibers, induced by fluctuations and
- ¶ Superposition of above

Small crystalline domains are discernible within the fibers in which the chains are well-ordered. A crystalline domain, however, is not perfectly ordered; there are point defects, chain ends, cross-links, etc. The overall electrical conductivity will be a superposition of interchain, interchain, and interfiber charge transport mechanisms. If the film is stretched, then the fibers are aligned and the crystallinity within the fibers can be improved further [62].

1.6 Electroluminescence and Photovoltaic effects.

A big impetus in this field was provided with the observation of electroluminescence and photovoltaic properties in these conjugated polymers in the early 1990's [168-172,69-74,171,172,75-78]. Electroluminescence is the process of generation of light, other than blackbody radiation by electrical excitation. This is a phenomenon that has been seen in a wide range of semiconductors, and for organic semiconductors was first reported for anthracene single crystals in the 1960s. These early studies established that the process responsible for electroluminescence requires injection of electrons from one electrode and holes from the other, the capture of oppositely charged carriers (so-called recombination), and the radiative decay of the excited electron-hole state (exciton) produced by this recombination process. The development of organic thin-film electroluminescence was spurred on in the 1980s through the work of Tang and Van Slyke, who demonstrated efficient electroluminescence in two-layer sublimed molecular film devices. These devices consisted of a hole-transporting layer of an aromatic diamine and an emissive layer of 8-hydroxy quinoline aluminium (Alq3), the

structures. Electroluminescence from conjugated polymers was first reported in 1990, using poly(p-phenylene vinylene), PPV films, sandwiched between two electrodes [168]. These polymers which can be used as active opto-electronic materials can be classified as second-generation electronic polymers. In these LED's, the Indium tin oxide, ITO layer functions as a transparent electrode, and allows the light generated within the diode to leave the device. The top electrode is conveniently formed by thermal evaporation of a metal. LED operation is achieved when the diode is biased sufficiently to achieve injection of positive and negative charge carriers from opposite electrodes. Capture of oppositely charged carriers within the region of the polymer layer can then result in photon emission. It is therefore necessary to have good balancing of electron and hole currents, efficient capture of electrons and holes within the emissive layer, strong radiative transitions for singlet excitons, and efficient coupling of these excitons to photon states allowed in the device structure.

There has been considerable progress made recently in resolving some of those issues, which determine the limits to LED device performance. Exposure to air results in the formation of carbonyl, hydroxyl and epoxide groups, which lead to the destruction of the conjugated structure.

There are two distinct types of stability. Extrinsic stability is related to vulnerability to external environmental agent such as oxygen, water, peroxides and epoxide groups. This is determined by the polymers susceptibility of charged sites to attack by nucleophiles, electrophiles and free radicals. If a conducting polymer is extrinsically unstable then it must be protected by a stable coating.

Many conducting polymers, however, degrade over time even in dry, oxygen free environment. This intrinsic instability is thermodynamic in origin. It is likely to be caused by irreversible chemical reaction between charged sites of polymer and either the dopant counter ion or the p-system of an adjacent neutral chain, which produces

an sp^3 carbon, breaking the conjugation. Intrinsic instability can also come from a thermally driven mechanism which causes the polymer to lose its dopant. This happens when the charge sites become unstable due to conformational changes in the polymer backbone. In some cases, these polymer-based devices have reached performance levels comparable to their inorganic counterparts. Some of these crucial factors leading to efficient device performance are the following:

§ Electrode Interfaces

§ Electron-Hole Recombination and Light Emission

§ External Enhancement factors

§ Efficiency and Stability

These properties relate to the intrinsic electronic structure of the polymers (for example, the energetics of triplet excitons, and the engineering of high luminescence efficiency in the presence of strong intermolecular interactions), and also to the scope for 'optical engineering' of the devices to achieve effective coupling between electronic excitations in the polymer and the generated photons.

A basic understanding of the photoexcitation and charge-transport processes in these systems is extremely important to develop efficient solar cells and photodetectors [75–79]. The excitonic (strong electron correlations) models in the last few years have been used more successfully to explain several subtle and detailed features in the optical properties of PPV, PDA, and PTH systems. The general picture out here is that photoexcitation produces a singlet exciton of mixed Frenkel and Wannier like character that is localized to a conjugated segment. The secondary processes can include interchain transfer, or migration to the lowest-energy segments of the chain. The 'apparent' Stokes shift is then largely due to spectral diffusion of photoexcited state to lower energy segments presumably with longer effective conjugation lengths. The complete knowledge of the different length scales and the time scales of

the different excitations finally culminating as free carries is required to fully exploit the potential and obtain highly efficient photo-active materials [?,81].

The presence of trap/defect states in these pristine semiconducting polymers are major factors, which affect the EL and PC properties. Understanding the role of defects and quantifying their densities, energetics is a crucial step to raise the performance levels of these devices and prevent the aging/degradation processes.

Chapter 2

Transport Mechanisms in Conducting Polymers

Theoretical background

A background in terms of the transport mechanisms in amorphous semiconductors is instructive in the context of transport studies of conducting polymer, CP films. CPs have a lot in common with amorphous materials due to its feasibility of different conformations, dangling bonds, although a certain amount of crystalline material also exists for some polymers [82]. Recent advances in the understanding of the effects of disorder to electronic and transport in amorphous semiconductors have provided some deep insights into the problem of transport in doped and undoped polymers.

2.1 Localization

The concept of localization was introduced by P. W. Anderson to explain the metal insulator transition of the non-crystalline or amorphous solids [83]. In this case, electrons wavefunction tend to form Bloch type waves which are considered to be extended states through out the sample. However, if the impurities are introduced to the system, the Bloch type waves are scattered by the impurities. Even if the small amount of disorder present in the system, the electrons are strongly localized in a regime in 1-D systems and the localization centers are normally referred as traps. Similarly the scattering centers are considered to be anti-traps which will be discussed in detail in the chapter 3. If the impurity levels are so high, that the scattering waves start interfere destructively with one another producing standing waves are formed. If by constructive interference, then the electrons will be delocalized. The disorder has to be strong enough to localize the electron wavefunction in a 3-D system for the localization to occur.

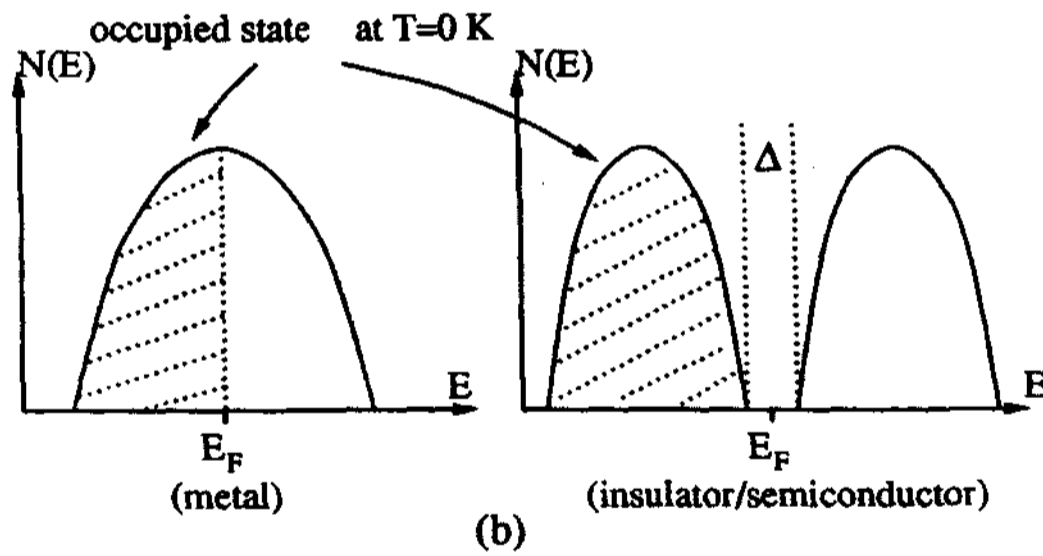
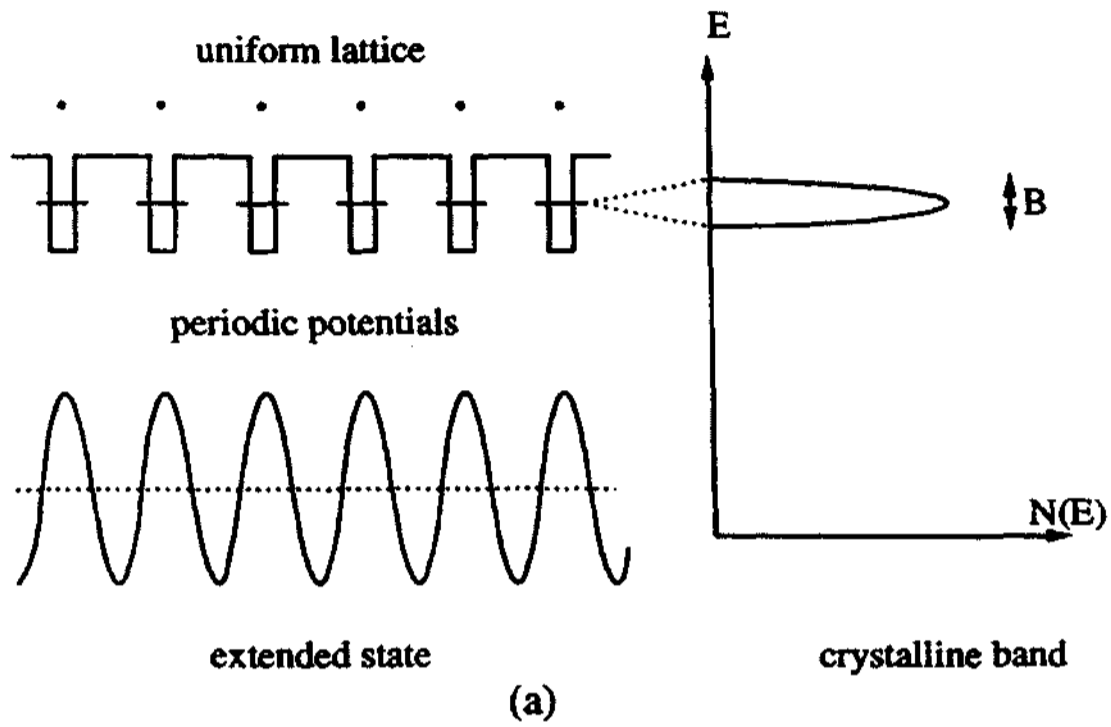


Fig. 2.1: (a) Extended electronic state and energy band (band width B) of a 1d uniform lattice. (b) Energy band structure of a metal and an insulator (or semiconductor) with a gap Δ . E_F is the Fermi energy.

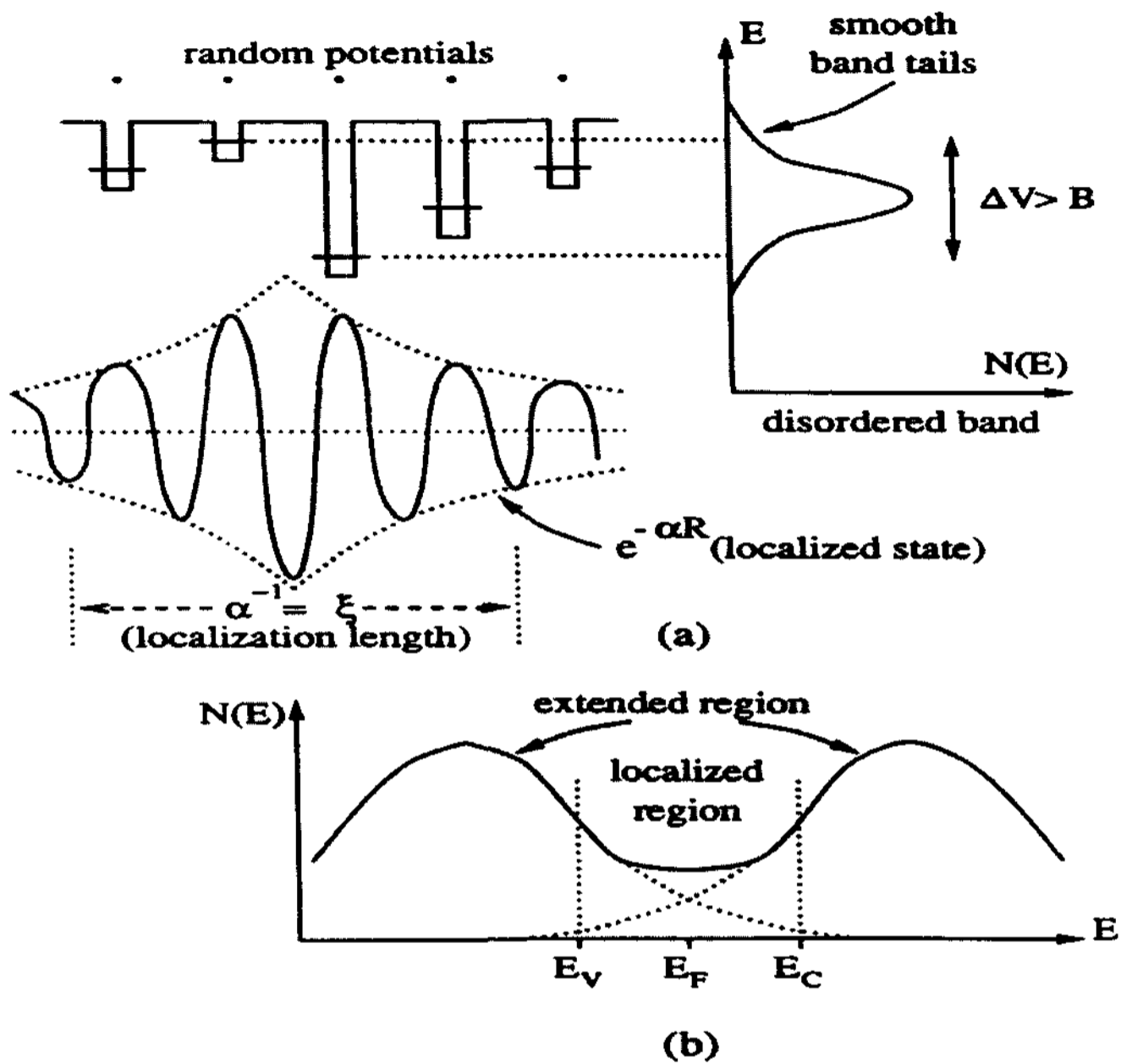


Fig. 2.2: (a) A localized wavefunction [envelope in $\exp(-\alpha R)$] in a random potential array with energy fluctuation ΔV and the broad energy band showing smooth tails. (b) A Fermi glass E_F lying between E_V and E_C , the mobility edges in valence and conduction bands, respectively. The original energy gap is smeared out.

The physical reason for the localization is that the backward scattered electron waves interfere with the forward electron wavefunctions forms standing waves and hence localize the electron states.

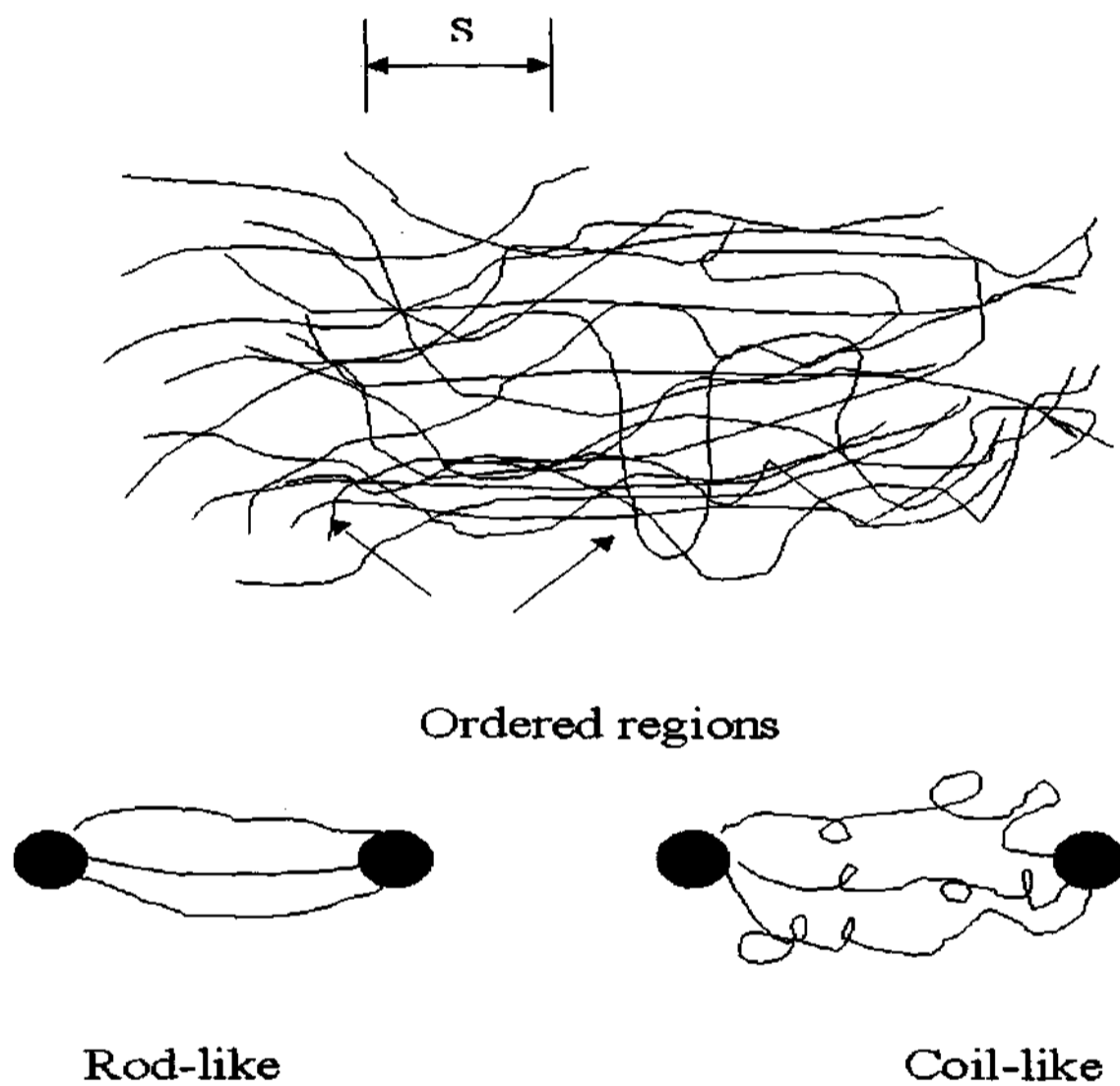


Fig. 2.3: (a) Schematic picture of the inhomogeneously disordered state of the metallic and insulating conducting polymers. (b) Schematic picture of rodlike and coil-like morphology of disordered regions.

It is well known that electron states in a strictly 1d-disordered system is localized with any weak disorder [85,84,91,195]. A localized state does not diffuse away from its site even in infinite time. More precisely, if at $t = 0$, the particle has an exponential envelope to its wavefunction with a maximum amplitude at R_0 , then at absolute zero there is a finite probability of finding the particle at R_0 even at $t \rightarrow \infty$ in an infinite system. If the localized state has energy, E , its contribution to $\sigma(E)$ is zero for $t = 0$ and zero frequency. The exponential fall-off of the wavefunction ψ and the vanishing diffusion and conductivity are the alternative definitions of localized states. Similarly an extended state may be defined as one that is not localized; potentially it is a current-carrying state. The concept of localization arising from the configurational disorder in amorphous solids leading to a localized tail, in the density of states above and below the normal band. There exists a limited energy called mobility edge, E_c or E_v , below the states are localized states and above the states are de localized. A system with its E_F lying in a localized regime is often referred to as a Fermi glass [84]. This model helps us to understand the origin of the carriers are localized within a range and it can be considered as non-periodic potential, V_0 , acting as a perturbation. It could be strong or weak depending on the magnitude of the potential. The localization is due to competition between the electrostatic potential and the kinetic energy of the carriers. At very low temperatures, kinetic energy decreases, the carriers are localized indicating the electrostatic potential dominates. This model neglects the correlation effects of electron interactions. This discrepancy was explained by the Mott's model in which the electron correlation effects are included only for nearest neighbor interactions. Davis and Mott's model for the band structure of amorphous materials are the existence of narrow band tails of localized states at the extremities of the valence and conduction band edges near the middle of the gap. If the Fermi level is at an energy such that the electronic states are extended, then finite conductivity at zero temperature is expected. This model assumes that the substantial disorder is homogeneous through the isotropic three-dimensional sample. Other external parameters

such as magnetic field or pressure can affect the localization /delocalization transition and the localization lengths. This model has received much experimental attention for doped and ion implanted polymers, although more recent studies of ion-implanted rigid rod and ladder polymers reveals a three-dimensional semimetallic conductor with weak localization effects.

2.2 Conduction in disordered materials

Electronic conduction processes in amorphous semiconducting materials can be classified into three types:

- ¶ Transport in delocalized or extended electronic states for which the carrier has a mean free path long compared to the average interatomic spacing
- ¶ Transport in delocalized states for which the mean free path is of the same order as the interatomic spacing
- ¶ Transport by thermally activated hopping between localized electronic states

The phenomenon of localization can occur for several reasons. Strong interaction between a carrier and a polar lattice can lead to localization by polaron formation. In molecular solids, a similar type of localization can be achieved by distortion of a molecule. Localization due to electron correlation is considered in the Mott transition, which describes the metal-insulator transition in several systems. The Hubbard gap is an alternative description of the insulating state produced by correlation. A third cause for localization is disorder, the effects of which on the electronic states have been discussed.

The restriction to zero temperature and small external fields allows us to classify the two basic categories of insulators namely;

- ¶ Insulators due to the electron-ion interaction,
- ¶ Insulators due to the electron-electron interaction,

¶ The localization arises mainly due to the electron-electron correlation effects.

Since the electrons try to avoid to meet each other to minimize their Coulomb repulsion and led to the definition: For a Mott insulator the electron-electron interaction leads to the occurrence of (relative) local moments. The gap in the excitation spectrum for charge excitations may arise either from the long-range order of the pre-formed moments(Mott-Heisenberg insulator) or by a quantum phase transition induced by charge and/or spin correlations (Mott-Hubbard insulator) [84]. The absence of diffusion in certain random lattices' has had a profound effect on understanding of the behavior of electrons in non-crystalline solids. The tight binding approximation can be used; that is to say, that overlap between wavefunctions is considered negligible except nearest neighbors. The approximate solutions ψ of the Schrodinger equation are

$$\psi = \sum_n \exp[ika_n] \psi|r - a_n| \quad (15)$$

where k is a wavevector, a_n are the lattice points, and $\psi(r)$ is the wavefunction for an electron in any of the wells, supposed spherically symmetrical (s-like). The states then lie in a band width $B = 2zI$, where z is the coordination number and I is the transfer integral

$$I = \int \psi|r - a_n| H \psi(|r - a_{n+1}|) d^3x \quad (16)$$

Practically all the states within one-dimensional band are thus localized. It is to be noted that in higher dimensions the disorder might not be strong enough to localize all states. In the presence of disorder the electrons in the lower-band tail of the resulting density of states are bound to deep impurity potentials and thus are localized. This argument naturally extends to the anti(-bound)(hole) states in the upper -band tail. Between two "mobility edges" for electrons (E_m^e) and holes (E_m^h), with extended states, which contribute to the electron transport at $\omega \rightarrow 0$ if E_F lies in this region. These states are also influenced by inelastic scattering length due to the electron-phonon

interaction by the presence of impurities. The Anderson transition is evidently a quantum phase transition: the electrons' kinetic energy prefers a delocalized metallic state, and the local energetic disorder favors electron localization on those impurity sites that have the lowest energy levels. In fact the quantum interference effects inherently underlie the Anderson transition. The gap is defined as the energy separation between the Fermi energy and the mobility edge beyond which excitations actually transport charge over several macroscopic distances, $\Delta_{QPT} = E_m^{e,h} - E_F$. The above considerations led to the definition of an Anderson insulator: For an Anderson insulator the disorder-induced localization of electrons leads to the occurrence of mobility edges that separate localized and de localized states in a band. If the Fermi energy lies between a band edge and its corresponding mobility edge the single-electron states around the Fermi energy are localized.

2.3 Conduction in localized states

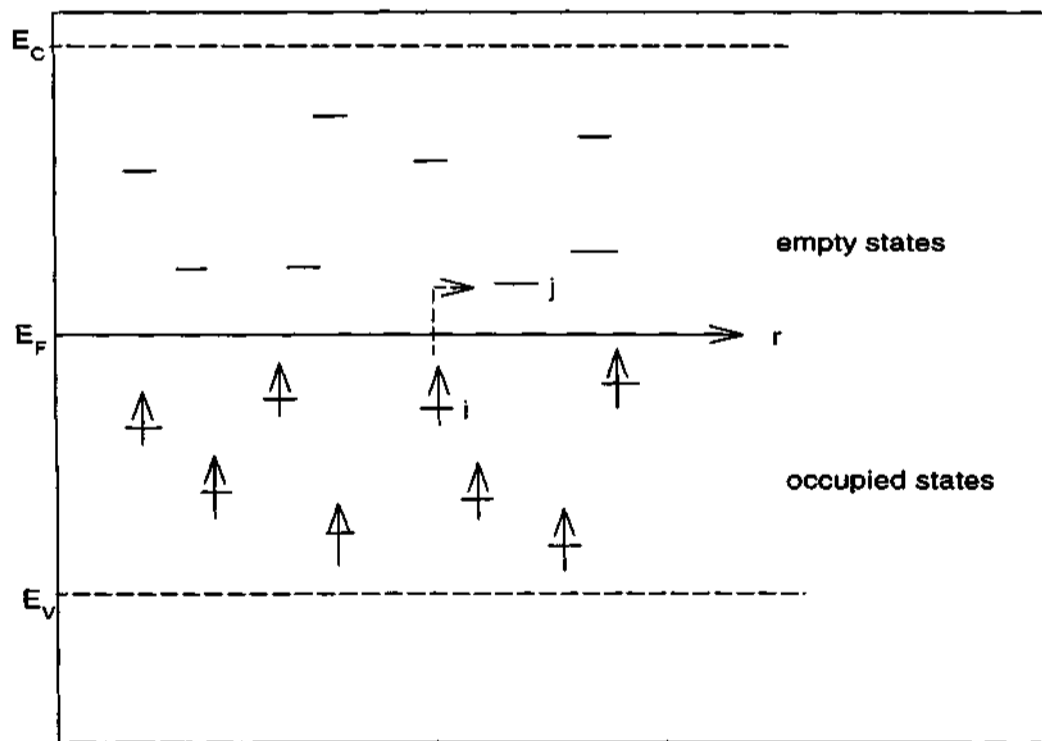


Fig. 2.4 Schematic illustration of Mott's variable range hopping model

Due to these band tails, the original band gap between the conduction and the valence bands of a semiconductor may be closed. The ramifications, including a finite density of states $N(E_F)$ produced at the Fermi level E_F between the mobility edges, were discussed [84]. Fig. 2.4 explains the Mott VRH model for nearest neighbors interactions. When the Fermi level lies in the localized region, the conductivity at zero temperature is zero even for a system with a finite density of states. The Mott variable range hopping (VRH) model is applicable to systems with strong disorder such that the disorder energy is much greater than the band width. The general form of the temperature dependent conductivity $\sigma(T)$ of Mott's model is described as

$$\sigma = \sigma_0 \exp\left[-\left(\frac{T_0}{T}\right)^{\frac{1}{d+1}}\right] \quad (17)$$

where d is the dimensionality and, for three-dimensional systems,

$$\sigma = \sigma_0^{3d} \exp\left[-\left(\frac{T_0^{3d}}{T}\right)^{\frac{1}{4}}\right] \quad (18)$$

where $T^{3d} = c/k_B N(E_F) L^3$ with a corresponding $T_0^{Q1D-VRH} = \frac{16}{k_B N(E_F) L z}$. Here L is the one-dimensional localization length and z the number of nearest neighbor chains. For an isolated one-dimensional chain the above equation does not apply, and the temperature dependence of the conductivity is thermally activated reflecting the energy ΔE_B for excitation over the largest barrier encountered during charge transport along the chain.,

$$\sigma^{1D} = \sigma_0^{1D} \exp\left[-\frac{\Delta_B}{k_B T}\right] \quad (19)$$

2.4 Conduction in band tails.

Conduction can occur through hopping between localized sites and the carriers can exchange the energy with phonon energy $W(E)$, and mobility will be thermally activated

$$\mu_{hop} = \mu_0 \exp\left[-\frac{W(E)}{kT}\right] \quad (20)$$

and

$$\sigma = \sigma_0 \frac{kT}{\Delta E} \exp\left[-\frac{-E_c - E_F + W}{kT}\right] \quad (21)$$

In the case of phonon-assisted model, in which the phonon-assisted electron hopping probability between localized states separated R and differing in energy by ΔE is given by

$$p(R, \Delta E) = \nu_{ph} \exp\left[-2\alpha R - \frac{\Delta E}{kT}\right] \quad (22)$$

where $\alpha = L^{-1}$ is the localization length. In this model, the electron is supposed to hop to a nearest neighbor. The carrier is always try to hop to a farther site to minimize ΔE . The number of states in an energy range ΔE near the Fermi level E_F is given by

$$N(R) = \frac{4\pi}{3} R^3 N(E_F) \Delta E \quad (23)$$

where $N(E_F)$ is the density of states at the Fermi level. The minimum activation energy needed for the hopping process through the probable hopping distance R is given by

$$\Delta E = \left[\frac{4\pi}{3R^3 N(E_F)}\right]^{-1} \quad (24)$$

If the Fermi energy lies in a band of localized states as predicted by Davis and Mott's model the carriers can move between the states via a phonon assisted tunneling process. The carriers acquire energy from the phonons and hop between the sites. The probability of finding of an electron will jump from one state to another is determined by three factors.

- ¶ The probability of finding a phonon with excitation energy equal to N , given by the Boltzmann distribution.
- ¶ The attempt-to-escape frequency, ν_{ph} which cannot be greater than the maximum phonon frequency.

¶ The probability of an electron from one state to another and this factor depends on the overlapping of wavefunctions.

This probability is proportional to the factor $\exp(-2\alpha R)$ where R is the average hopping distance which is the temperature dependent term. approaches the value of inter site spacing at higher temperatures, α the transfer integral between the two sites, which is representative for the rate of fall-off of a wavefunction of a site. If the overlapping is so large, then the factor $\exp(-2\alpha R)$ of the order of 1. The number and energy of the phonons decrease as temperature decreases and the energetic phonon assisted tunneling nearest hopping will become less favorable. Therefore the carriers tend to hop to a larger distances in order to find sites which lie energetically closer than the nearest neighbors. Hence the name variable range hopping (VRH). Most of the hops will be upward in energy. There are many phonons available for the electrons to assist hopping normally at higher temperatures. The phonons lose energy at low temperatures, electrons have to stay in a favored and energetically accessible state at lower temperature. But hopping over a large distance involves tunneling and therefore tunneling probability decreases exponentially with the hopping distance. The two factors compete with each other such that there will be an optimum distance R for which $p(R, \alpha E)$ is a maximum:

$$p(R, \Delta E) = \nu_{ph} \exp\left[-2\alpha R - \frac{3}{4\pi R^3 N(E_F) kT}\right] \quad (25)$$

$$\frac{dp}{dR} = 0 = \nu_{ph} \exp\left[-2\alpha R - \frac{3}{4\pi R^3 N(E_F) kT}\right] \left[-2\alpha + \frac{9}{4\pi R^4 N(E_F) kT}\right], \quad R = \left[\frac{8\pi\alpha N(E_F) kT}{9}\right]^{-\frac{1}{4}} \quad (26)$$

. On substituting this equation in the above equation, one gets the hopping probability and hence the conductivity of the Mott form $\sigma \propto \exp\left[-\frac{T_0}{T}\right]^{\frac{1}{4}}$. For more general form of the Mott VRH conduction give

$$\sigma(T) = \sigma_0 T^m \exp\left[-\left(\frac{T_0}{T}\right)^{\frac{1}{d+1}}\right] \quad (27)$$

where d is the dimensionality of the hopping system.

$$T_0 = \frac{8^3 \alpha^3}{9\pi \alpha N(E_F) kT} \quad (28)$$

$$\sigma_0(T) = \frac{e^2 \nu_{ph}}{2(8\pi)^{\frac{1}{2}}} \left[\frac{N(E_F)}{\alpha kT} \right]^{\frac{1}{2}} \quad (29)$$

It leads to a soft exponential equation where depends on the dimensionality of the hopping distance. This model assumes that a slowly varying density of states in the vicinity of the Fermi level and neglects the electron-electron correlation effects. Efros and Shklovskii considered the electron-electron interactions and showed that the density of states vanishes at the Fermi level, resulting in the so called "Coulomb gap in the form

$$N(E) \propto \frac{(E - E_F)^2 \epsilon^3}{e^6} \quad (30)$$

in three dimensional space [87]. The characteristic temperature for the Efros and Shklovskii type VRH is given by

$$T_0' \simeq \frac{2.8e^2}{k\epsilon L} \quad (31)$$

It clearly states that the temperature required to observe the Efros and Shklovskii type VRH is usually much lower than that required to observe Mott type VRH. The cross-over behavior from the Mott 3D VRH to Efros-Shklovskii type VRH in conducting polymers such as CSA doped polyaniline has been observed recently.

Due to the long chain character of conducting polymers, the charge transport occurs mainly along the polymer chains. Due to finite chain lengths and large intra-chain potential barriers, the observed macroscopic conductivity is dominated by inter-chain hopping. Considering the nearest neighbor chain hopping, the temperature dependent inter-chain conductivity is expressed as

$$\sigma_{interchain} = \sigma_0 \exp\left[-\left(\frac{T_0}{T}\right)^{\frac{1}{2}}\right] \quad (32)$$

where $T_0 = 16/kN(E_F)L_{\parallel}L_{\perp}^2$, L_{\parallel} and L_{\perp} are the localization lengths of parallel and perpendicular directions respectively [84,88].

2.5 Conductivity mechanism model for conjugated polymers

For an isolated one-dimensional metallic chain localization of charge carriers arises for even weak disorder because of quantum interference due to static back-scattering of electrons [84]. This contrasts to the strong disorder required for localization in three-dimensional systems. The localization effects in the inhomogeneously disordered (partially crystalline) conducting polymers are proposed to originate from one-dimensional localization in the disordered regions. The inhomogeneous disorder model [96,97] represents the doped polymer as relatively ordered regions (or "crystalline islands") interconnected through polymer chains traversing disordered regions is shown in the Fig. 2.3. The individual polymer chains often are longer than the island and inter-island length scales. Within this model, conduction electrons are three-dimensionally delocalized in the crystalline ordered regions (though the effects of paracrystalline disorder may limit delocalization within these regions). In order to transit between ordered regions, the conduction electrons must diffuse along electronically isolated chains through the disordered regions where the electrons readily become localized. The localization length of these electrons depends the details of the disorder (e.g., electrons traveling along tightly coiled chains are expected to have much shorter localization lengths than electrons traveling along expanded coil or relatively straight chains). Phonon-induced increases in the localization length increases the conductivity with increasing temperature. This model accounts for localized behavior at low temperature despite conductivities at room temperature in excess of the Mott minimum conductivity.

Three-dimensional crystalline order facilitates delocalization. It has been shown that nematic-like order can also increase delocalization, though less effectively. If the

localization length for some conduction electrons exceeds the separation between the ordered regions then the total delocalization will be substantially enhanced. Other approaches have emphasized the homogeneous disorder limit, assuming that the localization length is larger than the structural coherence length and that the electrons respond to an average structure. For the fully doped conducting polymers which are disordered and poorly conducting, the conduction path may be treated a charge motion on an anisotropic fractal network whose dimensionality is close to one. For this case the dc and ac conductivities are determined to follow the expectations of the quasi-one-dimensional Mott variable range hopping law for fractal systems of dimensionality close to one. As the dimensionality increases, it is predicted that both the ac conductivity and the dielectric constant would have stronger temperature dependence than for the quasi-one-dimensional or three-dimensional variable range hopping cases. Other researchers have considered the behavior of models of metallic strands interrupted by barriers. A.B. Kaiser has applied a modification this model to include charge carriers either being thermally activated over thin barriers (dominating at high temperatures) or tunneling through the barriers (dominating at low temperatures).

In the case of highly doped samples with metallic behaviour, the conduction is described either by VRH with smaller T_0 (weaker localization due to enhanced intra-chain and interchain interactions or by fluctuation-induced tunneling Sheng's model [90]. In the latter case, the conductivity is represented in the form:

$$\sigma = \sigma_0 \exp\left[-\frac{T_1}{T + T_0}\right] \quad (33)$$

and the corresponding TEP is dominated by the diffusion mechanism as

$$S(T) = -\frac{\pi^2 k^2 T}{3e} \left[\frac{d \ln \sigma(E)}{dE} \right]_{E=E_F} \quad (34)$$

This equation shows that the TEP has a linear relation with temperature, this behavior

has been observed in highly doped Poly acetylene[2-4] and in some cases for PANi [5].

2.5.1 Sheng's model

In this model, Sheng considered a heterogeneously conducting system consisting of large conducting regions separated by potential barriers [89]. Contrary to the model of granular metals, however the charging effects of the conducting regions do not have a significant influence on the charge transport due to their larger size. In the case of Poly acetylene, highly conducting regions separated by less doped or undoped regions or they might finally be crystalline regions separated by amorphous regions or vice versa. the basic picture of fluctuation assisted tunnelling is simple. In this model, at low temperatures, a crossing of potential barriers is possible only due to quantum mechanical tunnelling, leading to a finite value of the electrical conductivity.

2.5.2 Charge Energy Limited Transport (CELT) model

In the high field non-Ohmic regime, the CELT model predicts that $\sigma = \sigma'_0 \exp[-\frac{E_0}{E}]$, where E is the electric field [90]. Here σ'_0 and E_0 are the constants involved and weakly temperature dependent on T and E. The most probable separation between the centers of two metallic grains Ω is given by $\Omega = \frac{k_B D}{4eE_0}$ or $\Omega = \frac{k_B T}{4eE_t}$ where d is a constant and E_t is the threshold electric field above which Ω increases rapidly according to the above equation.

It can be considered as the capacitors are connected in series and parallel between the two grains. The capacitors can be charged by the process of the transferring of electrons from one to the other. such a process requires a certain amount of charging energy E_c has to be in the form of

$$E_c = \frac{e^2 d}{F} \left(\frac{s}{d} \right) \quad (35)$$

where e is the electronic charge, d is the grain size, s is the separation between the grains, and F is the function whose depends on the shape and arrangement of the grains

and on the interaction between the grains. The existence of E_c directly implies that the thermal equilibrium density of charge carriers, whose generation requires charging energy E_c and should be proportional to Boltzmann factor $\exp[-\frac{E_c}{2k_B T}]$. Based on the assumption that the ratio $\frac{\sigma}{s}$ is a constant whose value depends on x , where x is the concentration of the mixing. One can write the expression for the conductivity as

$$\sigma \propto \exp[-\frac{E_c}{2k_B T} - 2\xi s] = \exp[-\frac{E_c}{2k_B T} - \frac{2C}{E_c}] \quad (36)$$

It is found that σ is a peaked function of E_c with maximum occurring at $E_c = [4Ck_B T]^{\frac{1}{2}}$. On substituting this equation to the above equation, then we have

$$\sigma = \sigma_0 \exp[-(\frac{4C}{k_B T})^{\frac{1}{2}}] \quad (37)$$

The charge carriers can be generated from the thermally activated process or by an external applied field. When the voltage difference between two neighboring grains is larger than $\frac{E_c}{e}$, a pair of positive and negative charged grains can be generated. In the high field limit where $e\Delta V \gg k_B T$, the generation rate would only depend on the tunneling rate $\exp[-2\xi s]$. The dominant contribution arising from the grains within the smallest separation. Based on the assumption, one can write $2\xi s E_c = \text{constant}(C)$. From this expression, we have

$$\sigma \propto \exp[-\frac{2\xi}{s}] = \exp[-2\xi \frac{C}{2\xi e \Delta V}] = \exp[-\frac{E_0}{E}] \quad (38)$$

where $E_0 = \frac{C}{e w}$. The value of the grain size, w , can be found out by knowing T_0 from DC conductivity data $w = \frac{k_B T_0}{4e E_0}$.

2.5.3 Poole-Frenkel effect.

The Poole-Frenkel effect is the field-assisted thermal ionization occurring in insulators and semiconductors [91]. This can be treated as a system consisting of neutral atoms and not as a system of electrons moving in a self-consistent periodic potential. After ionization of impurity atom, the electron moves in the medium of a polarizable

atom and in the field of a positive ion. If the electrons are localized in an effective potential $V(r)$ centered at $r = 0$, when an electric field E is applied. $V(r)$ is given by

$$V(r) = -\frac{e^2}{4\pi\epsilon_0\epsilon r} - erE, \quad (39)$$

where ϵ_0 is the permittivity of free space and ϵ is the relative permittivity of the material. Hence the maximum height V_{max} between adjacent sites will be lowered by

$$\delta V = \left(\frac{e^3}{\pi\epsilon_0\epsilon}\right)^{\frac{1}{2}} E^{\frac{1}{2}} \quad (40)$$

leads to

$$\ln(\sigma) \propto \frac{1}{4V} \left(\frac{T_0}{T}\right)^{\frac{1}{2}} \left(\frac{\epsilon^3}{\pi\epsilon\epsilon_0}\right)^{\frac{1}{2}} E^{\frac{1}{2}} \quad (41)$$

Therefore σ varies as $E^{\frac{1}{2}}$.

2.5.4 Intersoliton hopping conduction

Kivelson et. al. proposed the model intersoliton hopping conduction and plays the important role in the charge conduction process in the case of lightly doped polyacetylene. The theory is applicable to both the neutral and charged solitons, both of which are located near the dopant ions. The energy transfer of electron from one site to the other in order to minimize the the energy. The expression for this model is

$$\sigma = \frac{Ae^2\gamma(T)}{k_B T} \frac{\xi}{R_0^2} \frac{y^0 y^+}{(y^0 + y^+)^2} \exp\left[-\frac{2BR_0}{\xi}\right] \quad (42)$$

The predictions of this model are $i\sigma\alpha T^{x+1}$ which is a slowly varying function than $\exp[-\frac{E_b}{k_B T}]$ and The dopant concentration weakly dependent on σ (T). where A and B are the dimensional constants, y^0 and y^+ are the fractions of occupied neutral and charged soliton sites respectively, R_0 is the average separation between the dopant ions and ξ is the three dimensional electronic decay length, Γ (T) is the electron-phonon coupling constant.

2.5.5 Tunneling conduction in Composite Materials

There are two types of transport mechanisms have been developed by Sheng et al

[?]. One is called Charging energy limited tunneling for smaller metallic particles. The other is by a thermally modulated tunneling between large metallic particles. However the conduction mechanisms are different from the other modes, which apply to composite materials such as conducting particles embedded in insulating matrix [92]. In these systems the charge carriers are delocalized over the large scales compared to the atomic dimensions. The electrical conduction of these media is dominated by carrier transfer between conducting segments rather than between localized states. The localized states either may be solitons, polarons or bipolarons.

2.5.6 Thermal Fluctuation modified tunneling

This model can be applied to the system where the charge density fluctuation is negligible with large metallic islands ($d \simeq \mu\text{m}$) [90]. A direct consequence of large size of conducting regions is that the charging energy required to remove an electron from a neutral aggregate is completely negligible, in sharp contrast to the conduction in granular metals where the charging energy plays an important role. Therefore, charge transfers in this case can be regarded as tunnelling between two bulk conductors. Assuming the tunnel barrier is in the form of a plane parallel junction of area A and separation w , and the barrier potential in the form of $V(x) = V_0 - \frac{4V_0}{w^2}x^2$, where x is defined as the center of the junction. tunneling current density can be calculated using WKB method as

$$j(E) = j_0 \exp\left[-\frac{\pi\xi w}{2} \left(\frac{|E|}{E_0}\right)^2\right] \quad (43)$$

where $E_0 = \frac{4V_0}{ew}$ and $(\xi = 2mV_0/\hbar^2)^{\frac{1}{2}}$. There are two possible sources for the electric field. One is the applied electric field E_A , the other possibility is that there is a thermal fluctuation voltage given by $(\frac{k_B T}{C})^{\frac{1}{2}}$ with $C = \frac{A}{4\pi w}$ the capacitance of the junction. the total electric field across the junction is the sum of the two. since the thermal electric field can be in both the directions, at a fixed and small applied electric field, $E_A < |E_T|$, the net forward current is given by

$$\Delta j = j(E_A + E_T) - j(E_A - E_T) \quad (44)$$

with the thermal average, one can get the dominant conductivity as

$$\sigma = \sigma_0 \exp\left[-\frac{T_1}{T + T_0}\right] \quad (45)$$

with $T_1 = \frac{wAE_0^2}{8\pi k_B}$ and $T_0 = \frac{AE_0^2}{4\pi^2 \chi k_B}$, here T_1 is a measure of the energy required to move an electron across the insulating gap and T_0 is the temperature much below which the conductivity reduces to a temperature-independent tunneling. The high electric field behavior can be similarly obtained as

$$j(E) = j_0 \exp\left[-a(T)\left(\frac{E_A}{E_0} - 1\right)^2\right] \quad (46)$$

where $a(T) = \frac{T_1}{T + T_0}$ is a constant depends on temperature

2.6 Transport properties of quasi-1d disordered systems

In the 1d localized states, e.g., $w < w_c$, charge transport is dominated by quasi-1d VRH at low temperatures [84,93]. For a strict 1d - disordered systems, VRH conductivity varies as $\ln \sigma \simeq T^{-1}$. But for a quasi 1d - disordered systems near the metal-insulator ($w \simeq w_c$) where the electron wavefunctions are extended over several chains, there exists a fairly high temperatures, below which the quasi-1d VRH conductivity along the chains is given by [93,95].

$$\sigma = \sigma_0 \exp\left[-\left(\frac{T_0}{T}\right)^{\frac{1}{2}}\right] \quad (47)$$

and

$$\sigma = \frac{e^2 \nu_{ph}}{A \alpha k_B T}, \quad T_0 = \frac{8\alpha}{g(E_F) k_B} \quad (48)$$

where e is the electron charge, ν_{ph} is the attempt-to-escape frequency, k_B is the Boltzmann constant, $g(E_F)$ is the density of states with one sign of spin (since phonons are

spinless so that electron spins are approximately conserved during hopping process, a is the average cross sectional area of each chain. Here ν_{ph} is a function of temperature, but Mott took it as a constant. Nakhmedov expressed $\nu_{ph} \propto T^p$ and $p \geq 1$. The pre-exponential factor can be in principle, from the resistor network model which was proposed by Miller and Abrahams for single phonon assisted hopping processes [94]. This model gives an upper limit of ν_{ph} on the order of the phonon frequency, but ν_{ph} decreases rapidly with increasing hopping energies or temperatures [84,87]. Therefore at elevated temperatures the contribution to the conductivity from single acoustic hopping processes may be smaller than that of multi-phonon hopping processes [84,47]. The latter may be important in many non-crystalline materials where hopping energy is in the range of $10^{-2} - 10^0$ eV.

For weak interchain coupling, i.e., $w \ll w_c$ or $\tau_i \ll \hbar$, it is shown that longitudinal localization length $\alpha^{-1} = 4l$, and transverse localization length $\beta^{-1} = b$ where l_i is longitudinal mean free path and b is the interchain separation [93]. Since the probability of a charge hopping beyond the nearest neighboring chains is very small in the case of the weak interchain coupling (though there is "variable range hopping" along the chain direction), we can consider the VRH between the nearest neighboring chains only. Interchain hopping conductivity hopping perpendicularly to the chains is [93]

$$\sigma_{\perp} = \frac{2e^2 g(E_F) b^2 \nu_{ph}}{A} \left(\frac{t_{\perp}}{\tau_i \hbar} \right)^2 \exp\left[-\left(\frac{T_0}{T}\right)^{\frac{1}{2}}\right] \quad (49)$$

where $T_0 = \frac{8\alpha}{g(E_F)} z k_B$ where z is the number of nearest neighboring chains. the most probable hopping distance (R_{opt}) and hopping energy (W) are

$$R_{opt} = \frac{\alpha^{-1}}{4} \left(\frac{T_0}{T}\right)^{\frac{1}{2}}, \quad W = \frac{k_B}{2} (T_0 T)^{\frac{1}{2}} \quad (50)$$

For the component of interchain hopping conductivity parallel to chain direction, the interchain hopping distance $\simeq R_{opt}$ is used instead of b and we obtain

$$\sigma_{\parallel} = \frac{e^2 \nu_{ph}}{A \alpha k_B T z} \left(\frac{t_{\perp} \tau_i}{\hbar} \right)^2 \exp\left[-\left(\frac{T_0}{T}\right)^{\frac{1}{2}}\right] \quad (51)$$

The above equation is in contrast with the intrachain VRH conductivity [38](without any interchain motion allowed) is the same as that of a strict 1d-DS. i.e.,

$$\sigma_{intrachain} = \frac{2e^2 g(E_F) \nu_{ph}}{A \alpha^2} \left(\frac{z T_0}{16T} \right) \exp\left[-\frac{z T_0}{16T}\right] \quad (52)$$

The hopping energy is given by $W \simeq \frac{z k_B T_0}{16}$.

For the case of weak interchain coupling, $\frac{t_{\perp} \tau_i}{\hbar} \ll 1$, interchain σ_{\perp} and σ_{\parallel} are much smaller than intrachain σ_{intra} . Due to finite chain lengths and occasional large intrachain barriers, it is expected that the observed temperature dependence of the conductivity for an experiment is determined by interchain hopping. The hopping conductivity is expected to depend on electric field F. At moderate electric field $eRF \simeq k_B T$ [19], we have

$$\sigma(F) \propto \exp\left[\frac{eRF}{k_B T}\right] \quad (53)$$

where R is the hopping distance. For the interchain hopping, if F is in the chain direction, r is the most probable hopping distance [30] $R_{\parallel} = \frac{L_{\parallel} T_0}{4}^{\frac{1}{2}}$. If F is perpendicular to the chain direction $R = a$ for the hopping to the nearest neighboring chains or $R = L_{\perp}$ for nearest inter-bundle hopping. At higher F ($eRF \gg k_B T$), the electrical field dependence of $\sigma(F)$ is not thermally activated and $\sigma \propto \exp\left[-\left(\frac{F_0}{F}\right)^{\frac{1}{2}}\right]$ for quasi-1d-VRH.

The general equations of dc conductivity for different models at low temperatures can be expressed in the form of

- ¶ $\sigma(T) = \sigma_0 \exp\left[-\frac{T_0}{T}\right]^{\beta}$, $\beta = 1$ for thermally activated process.
- ¶ $\beta = \frac{1}{\beta+1}$, Mott relation characterizes VRH of localized carriers [84].
- ¶ $\beta = \frac{\xi}{\beta+\xi}$, VRH of carriers between localized and super-localized regimes [84].
- ¶ $\beta = \frac{1}{2}$, Coulombic interaction between the electrons is strong. [87]

It is difficult to exactly determine the microscopic mechanism of electronic conductivity in these systems by bulk measurements alone due to variety of other transport limiting factors present at different length scales. The $\sigma(T)$ dependence alone cannot provide the mechanism as shown by the expressions from the different models. However, systematic measurements on a particular system done as a function of various degree of order, crystallinity along with a quantification of the defects can shed light on the charge transport mechanism in these materials.

Chapter 3

Thermally Stimulated Relaxation Processes: Background

The present section deals with models for characterizing the traps, specifically to be used in tandem with the experimental results, related to thermally stimulated currents (TSC) and transient photocurrent measurements (I_{tr}) which are discussed in chapter 6 [99–127, 138, 139, 128–137, 140, 141] and [142, 143]. In this chapter the theory of TSC and its corresponding models used are reported in detail. The initial part deals with the system consists of only one trap and one recombination center and is then extended for several trap models with interactive and non interactive systems. The solution for a single type trap model itself is difficult to obtain exactly and it gets more complicated when multi-trap levels are introduced.

One important class of semiconductors are those presenting a continuous distribution of localized states in the band gap of the material [114–120, 134]. Examples of amorphous semiconductors such as amorphous silicon and chalcogenide glasses, microcrystalline semiconductors. Because of these gap states, the trapping, detrapping, and recombination processes in these materials under steady-state external excitation or perturbation. We present a simple model which provides better guidance and insights, numerical calculations which take into account more complexities but often is less transparent in physics.

3.1 Theory of thermally stimulated relaxation processes

The basic theory of the thermally stimulated relaxation processes in a model is based upon certain number of carriers in discrete trapping levels which may be thermally excited into the conduction band; recombination of free electrons takes place

at deep centers. The analysis of thermally stimulated luminescence, TL and thermally stimulated current or conductivity (TSC) are based on the description of these processes developed by researchers over the last five decades. The simplest model consists of a single localized state for electrons and one for holes. Charges getting released thermally are freed and eventually undergo recombination. While in the delocalized bands, the free carriers give rise to transient conductivity (TSC) and during recombination they may yield luminescence (TL). The various models of an insulator or semiconductor have been used in the theoretical treatments of TL and TSC. These models are of two distinct types, clearly differentiated by the behavior of the free carrier lifetime:

§ A constant recombination-limited lifetime, used by Randall and Wilkins (1945) in the first order case and extended to cover retrapping by Haering and Adams (1960) and Dussel and Bube (1966)

§ A rapidly varying recombination-limited lifetime, introduced by Garlick and Gibson (1948), developed by (amongst others) Schon (1958), Boer et al (1958), and Braunlich (1963).

The theory presented here is applicable to both of these extreme cases, and to the intermediate ones where the recombination lifetime varies more slowly than in the theory of Garlick and Gibson. The degree of retrapping is arbitrary and thus the cases of 'fast' and 'slow' retrapping are also unified in a single expression. Of all the parameters which control the shape and position of a TSL or TSC peak, only the heating rate and the initial filling conditions are under experimental control. The assumptions based on the model for insulator and semiconductor are listed and discussed below [113].

¶ The problem is symmetrical with regard to the polarity of the charged carriers.

It will be assumed that the hole traps act only as potential recombination centers

resembling small perturbations. Appropriate modifications to the definitions lead easily to the opposite case.

- ¶ It will be assumed that there are no free holes, and accordingly no transitions involving the valence band, thus excluding the complex cases which result from the simultaneous presence of free holes and electrons.
- ¶ The conductivity or current and the luminescence with intensity I will be taken to arise solely from thermal stimulation, and no consideration will be given to carrier injection into the semiconductor or to photo excitation. The process of initial excitation will not be discussed. Reabsorption of TSL or TSC is ignored in many cases.
- ¶ Transitions between localized trapping levels will be neglected in view of the low cross sections for such transitions compared with those involving free states in a band.
- ¶ The temperature T of the insulator is restricted to a range in which one of the trapping levels is emptying by thermal stimulation such that peaks in TSL and TSC are observed at temperatures T_L and T_c respectively. This particular level will be referred to as the active level, with a density of centers N_t and containing a density of trapped electrons n_t . It will be taken into account that initial excitation at a temperature T_0 below the range under consideration has introduced a density n_0 into the active level, and that subsequently T has been increasing monotonically at a known rate.
- ¶ Other trapping levels will be taken to fall into two groups. The first group comprises the shallow levels which have low populations in the temperature.
- ¶ The recombination will be taken to proceed via a set of recombination centers with a single value of electron capture cross section S_e , which may be a suitable average over all the available recombination centers, but must not then be a rapidly varying function of temperature in the range considered. It will be assumed

that the recombination process involves the release of a photon, so that TSL is produced, and that a sufficient number of recombination centers is available so that saturation is not achieved.

- ¶ The activation energy E_t from the active level to the conduction band and the capture cross section S of the trap in the active level will be taken to be single-valued, and thus results a re applicable only to discrete levels, but can in principle be extended to the case of distributed levels by the introduction of suitable integrals and average values.
- ¶ It will be assumed that the electrons are in a state of quasi-equilibrium, i.e. the density n of free electrons in the conduction band and the density n_t of electrons trapped in the active level change by only negligible amounts within a single recombination-limited lifetime τ . This assumption is applicable to all theories of TSL and TSC.
- ¶ It will be assumed that the temperature dependence of the free electron mobility μ , the capture cross sections S and R , the density N_c of states in the conduction band and the mean velocity v of a free electron can be approximated by taking the variables to be proportional to certain arbitrary powers of the temperature, so that $N_c R v \propto T^a$, $N_c S v \propto T^b$ and $N \mu \propto T^c$. Such 'slow' temperature variations will be explicitly included in the solutions.
- ¶ It will be assumed that the relationship between temperature T and time t is governed by a heating rate β such that $T = T_0 + \beta t$. The heating rate β is allowed to vary such that it proportional to an arbitrary power of the temperature; we take $\beta \propto T^{b-y}$, so that $\frac{NSv}{\beta} \propto T^y$.

3.2 The OTOR model (Shockley-Read statistics)

There are six variables in the model which determine the characteristics of the TL or TSC peak [111,137,?]. These are

- ¶ the activation energy of the traps or defect levels,
- ¶ the attempt-to-escape frequency s ,
- ¶ the total concentration of the traps N_t ,
- ¶ the initial filled concentration of the traps n_0 ,
- ¶ the capture cross section S_t of the traps,
- ¶ the capture cross section S_r of the recombination centers (RC).

When a thermally disconnected deep trap (TDDT) is added to the energy level scheme to make it more realistic, the set of variable parameters increases by another two if the system is non-interactive and by three if it is interactive [137].

Consider first a single non-degenerate trap level of density N_t at energy E_t (Fig. 3.1) as a special case of an arbitrary trap distribution with conduction electrons density n_c . The model assumes that

- the concentrations of filled trap and recombination center RC are equal.
- recombination process occurs through via a delocalized bands.

According to Shockley and Read, the rate of capture of electrons, r_3 in the conduction band by the trap is

$$r_3 = \beta n_c N_t [1 - f(E)], \quad \beta = \langle v_n \rangle S_n \quad (54)$$

where $\langle v_n \rangle$ is the average thermal velocity of the electrons, S_n the capture cross section of electrons, $f(E)$ the occupancy function or probability that the trap level is occupied by an electron, and β the capture coefficient of an electron. At thermal equilibrium conditions, the occupancy function $f(E)$ can be expressed as

$$f(E) = \frac{1}{\exp\left[\frac{E_t - E_F}{kT} + 1\right]} \quad (55)$$

The knowledge of this function at any time during the thermally stimulated relaxation processes with the information of the respective capture and thermal emission rates,

completely determines the statistics of the system, that could lead to non-equilibrium steady state situation. In this the equilibrium Fermi level E_F is replaced by a quasi Fermi level E_{Fn} . The rate of thermal release of trapped electrons from the trap or localized states is

$$r_\alpha = \alpha N_c f(E), \text{ where } \alpha = \beta N_c \exp\left[-\frac{E_c - E_t}{kT}\right] \quad (56)$$

α is the coefficient for thermal emission of electrons from the traps into the conduction band.

One trap one recombination model (OTOR)

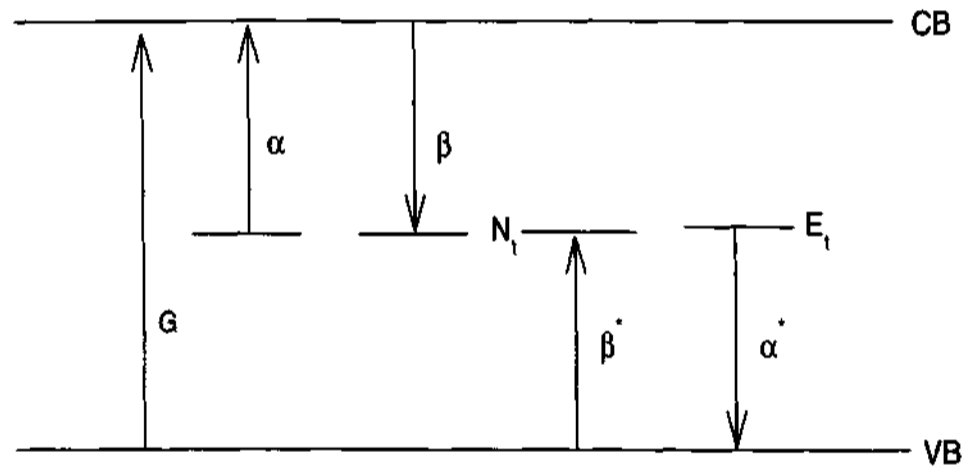


Fig. 3.1 Energy levels and allowed transitions in the model insulator or semiconductor.

Similarly, the capture rate for holes from the valence band is

$$r_\beta^* = 3^* p N_t f(E), \beta^* = \langle v_p \rangle S_p \quad (57)$$

where p is the hole density in the valence band, $\langle v_p \rangle$ is the average thermal velocity

for holes, S_p is the hole capture cross section and β^* is the capture coefficient of holes. The releasing probability of holes into the valence band from the trap levels is

$$r_\alpha^* = \alpha^* N_c f(E) \quad \text{and} \quad \alpha^* = \beta^* N_v \exp\left[-\frac{E_t - E_v}{kT}\right] \quad (58)$$

α^* are the releasing probability of holes from the trap levels into the valence band. In thermal equilibrium, the net rate of capture and emission of electrons and holes must be zero (principle of detailed balance). It is therefore $r_\beta = r_\alpha$ and $r_{\beta^*} = r_{\alpha^*}$, which yields

$$\alpha = \langle v_n \rangle S_n N_c \exp\left[-\frac{E_c - E_t}{kT}\right] \quad \text{and} \quad \alpha^* = \langle v_p \rangle S_p N_v \exp\left[-\frac{E_t - E_v}{kT}\right] \quad (59)$$

In most of the cases, the non-equilibrium steady-state situation exists, for example, during exposure of sufficient quanta of light energy is enough to create electron-hole pairs. When the sample is uniformly illuminated, a steady state is established such that creation of electrons and holes is balanced by the capture and releasing probabilities correspondingly at the trapping levels [?]. In any kind of arbitrary distribution $N(E)$ of non-degenerate trapping states per unit energy and volume, this may be expressed as

$$\frac{dn_c}{dt} = G - \int_{E_v}^{E_c} c_n N(E) [1 - f(E)] dE + \int_{E_v}^{E_c} \alpha N(E) f(E) dE \quad (60)$$

$$\frac{dp}{dt} = G - \int_{E_v}^{E_c} c_p N(E) f(E) dE + \int_{E_v}^{E_c} \alpha^* N(E) [1 - f(E)] dE \quad (61)$$

where $c_n \equiv \langle v_n \rangle S_n n_c$ and $c_p \equiv \langle v_p \rangle S_p p$. Here G is the net generation rate of electron-hole pairs. In the steady-state equilibrium $dn_c = dp = 0$ and

$$\int_{E_v}^{E_c} N(E) [-c_n(1 - f) + \alpha f + c_p f - \alpha^*(1 - f)] dE = 0 \quad (62)$$

This condition is valid for any kind of distribution of trapping states $N(E) \neq 0$, so that the term in the bracket must be equal to zero and

$$f(E) = \frac{c_n + \alpha^*}{\alpha + \alpha^* + c_n + c_p} \quad (63)$$

The probability of occupation in thermal equilibrium is replaced by this new distribution function that characterizes the non-equilibrium steady state during the ongoing stimulation (perturbation). The occupation function $f(E)$ independent of any kind of perturbation, and the stimulation does not alter $N(E)$, i.e., there are no new defect levels are created in this stimulation process. In this model, the occupation function $f(E)$ is assumed to be independent of the external perturbation and does not alter $N(E)$, i.e., no new defects are created in the stimulation process. The situation becomes more complex when $f(E)$ depends on external perturbation and practically difficult to attain the steady-state situation.

3.3 Concept of Quasi-Fermi levels

It is based on the assumption that in the non-equilibrium steady-state situation the relative populations of electrons over certain available levels are indeed, in close approximation, determined by a thermal equilibrium between these levels [105]. For an example, the populations of electrons in the conduction band and electron traps can be characterized by an occupational function $f(E) = \frac{1}{\exp[\frac{E-E_F}{kT} + 1]}$ and a quasi-Fermi level E_f such that

$$n_c = N_c \exp\left[-\frac{E_c - E_f}{kT}\right] \quad (64)$$

Similarly, the quasi-Fermi level for holes in the valence band is E_p and

$$p = N_v \exp\left[-\frac{E_p - E_v}{kT}\right] \quad (65)$$

It is assumed that the thermal release of electrons from the trap states, recombination of electrons do not significantly disturb the quasi-equilibrium between free and trapped electrons, which are maintained by recapture of thermally released electrons. The introduction of quasi-Fermi levels does not give enough information about the electron

or hole densities as a function of energies and temperature in the various levels. However they provide the information of new Fermi levels through the measurement of occupation densities.

The concept of two additional quasi-Fermi levels, E_f^n and E_f^p for trapped electrons and holes respectively which allows to express the occupational function $f(E)$ of traps in a Fermi-Dirac form. If the large number of traps is involved then characterizing the statistical properties of these traps via individual quasi-Fermi levels is impractical and it becomes more convenient to use which provides a single occupational function for the system. If an arbitrary distribution $N(E)$ of traps each set of traps with unique of capture cross sections S_n for electrons and S_p for holes will be characterized by its own distribution function and set of values for E_f^n and E_f^p . Both S_n and S_p may depend on E as well as on T [116–119,123–130,132,141]. It is possible to neglect α^* in the above equation 1.23 at all energies above the equilibrium Fermi level E_F and conversely, α at $E < E_F$:

$$f(E) = \frac{c_n}{\alpha + c_n + c_p}; \quad \alpha^* \ll c_n, c_p, \alpha; \quad (66)$$

$$f(E) = \frac{c_n + \alpha^*}{\alpha^* + c_n + c_p}; \quad \alpha \ll c_n, c_p, \alpha^*; \quad (67)$$

However these occupational functions can be modified and rewritten in the form of

$$c_n N_c \exp\left[-\frac{E_c - E_f^n}{kT}\right] = n_c (c_n + c_p) \quad (68)$$

and a quasi-Fermi level E_f^p via

$$c_p N_v \exp\left[-\frac{E_f^p - E_v}{kT}\right] = p (c_n + c_p) \quad (69)$$

Using these expressions, the occupational function $f(E)$ can be written as

$$f(E) = \left(\frac{c_n}{c_n + c_p}\right) \frac{1}{\exp\left[\frac{E_t - E_f^n}{kT}\right] + 1} \quad (70)$$

$$1 - f(E) = \left(\frac{c_p}{c_n + c_p} \right) \frac{1}{\exp\left\{\frac{E_f^p - E_t}{kT}\right\} + 1} \quad (71)$$

These expressions are clearly recognized as those for electrons and holes and E_f^n and E_f^p as quasi-Fermi levels for trapped electrons and holes. Under non-equilibrium steady-state conditions $E_f^n > E_f$ and $E_f^p < E_f$. At thermal equilibrium, all quasi-Fermi levels coincide with the equilibrium Fermi level E_F . This type of condition can be never met even in simple systems. This feature makes the analysis more difficult.

A qualitative description of thermally stimulated luminescence (TL) and thermally stimulated conductivity is presented within the kinetic-order approximations. This model consists of a single active trap in the presence of a large concentrations of deep, thermally disconnected traps and recombination centers [111,?]. The model explains the trap filling and emptying processes depending upon the initial conditions. The usual analysis of thermally stimulated luminescence (or thermoluminescence, TL) and thermally stimulated conductivity (TSC) are based on the models developed by Randall and Wilkins and Garlick and Gibson. The simplest model consists of a single localized state both for electrons and holes. The trapped carriers are getting released from the trap levels and recombine with the holes. The thermally freed carriers which are in the delocalized bands give rise to transient conductivity (TSC) and during recombination give rise to luminescence (TL). The thermally freed electrons will eventually recombine with the trapped holes in a Shockley-Read process, although the concept of free holes recombining with trapped electrons [111,?].

¶ The model: The simple model consists of a single electron (or hole) and a single recombination center with kinetics parameters based on certain approximations. This model does not give valuable information about the rich variety of experimentally observed TL and TSC phenomena.

¶ The inability of obtaining exact solutions.

The exact analytical solutions have not been possible for even the simplest models.

The quasi-equilibrium conditions has been to the system and rigorous calculations have been never

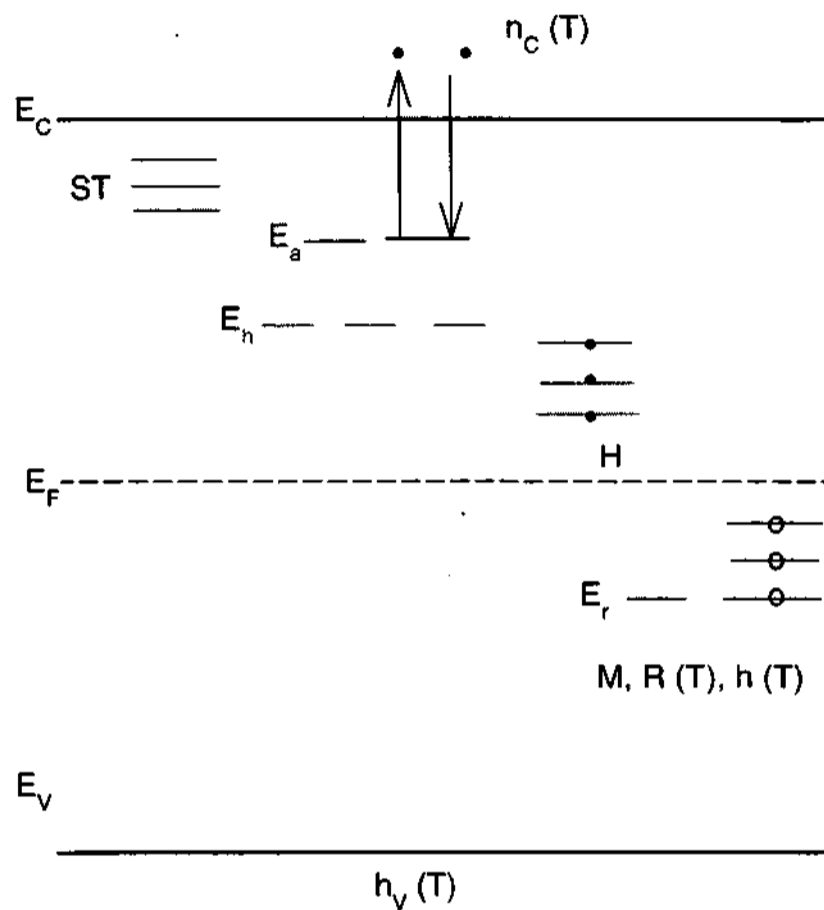


Fig. 3.2 Energy level diagram of the model under consideration. The model consists of a distribution of shallow levels (ST's), the active level (AT) at energy E_a , a distribution of deep thermally disconnected electron traps (DET's) from energies E_F to E_h and a distribution of thermally disconnected hole traps (DHT's) from energies E_r to E_F .

applied to the system. In addition to this approximation, traditional equations have been developed into very specific cases in which one expresses the degree by which the recombination processes dominate over retrapping (or vice versa) and in this way

introduce the concept of kinetic order (K.O). It must be true that for a particular TL or TSC peak that recombination or retrapping dominates over certain temperature ranges, this condition cannot be made a priori. Attempts have been made to generalize the concept of kinetic order by the introduction of a kinetic-order parameter. or by the introduction of mixed-order solutions that contain parameters to be adjusted so as to achieve an optimal fit of experimental data.

The model chosen here closely resembles one first considered by Dussel and Bube and later by Saunders is shown in the figure. The model consists of the following types of levels:

- § the active electron traps (AT's),
- § a distribution of shallow electron traps (ST's),
- § a distribution of deep, thermally disconnected electron traps (DET's).
- § a distribution of deep, thermally disconnected hole traps (DHT's).

The top of the valence band is denoted E_v , the concentration of free holes is $h_v(T)$, the bottom of the conduction band is denoted E_c , and the concentration of free electrons is $n_c(T)$ [111,?]. The Fermi energy, E_F , is located schematically in the center of the band gap. The active electron traps are assumed to be of one defect type. They exist in concentration N and are located at energy E_a , thus having activation energy E , where $E = E_c - E_a$. In this case both the quantities E and N are assumed to be singular and temperature independent. The active temperature range ($T_0 - T_f$) is defined as the temperature range over which these traps are thermally active, meaning that thermally induced transitions out of these traps are highly probable. Transitions taking place over the active temperature range will be further characterized by the temperature -dependent functions $n(T)$ and $S(T)$, where the former represents the concentration of full traps and the latter represents the electron-capture cross section at any temperature T .

Shallow electron traps may exist as several defect types, but since the activation energies of these levels are less than E_t , these traps are empty over the active temperature range and do not constitute stable retrapping centers. For this reason they play a minor role in the latter thermally induced redistribution of charge. The traps do not contribute TSC are considered as a thermally disconnected deep traps, over the active temperature range in which the probability of the carriers getting release from these trap levels is negligible. Those levels having energies less than some energy E_h , where $E_h < E_a$, but greater than E_F , form a distribution of levels labeled as the deep thermally disconnected electron traps. H characterizes the total concentration of these levels and is defined by

$$H = \int_{E_F}^{E_h} G(E)dE, \quad (72)$$

where $G(E)$ is the density of states function. Those levels with energy less than E_F but greater than some energy E_r form a distribution of levels collectively labeled as the deep thermally disconnected hole traps. M is the total concentration of these levels and is defined by the relation

$$M = \int_{E_r}^{E_F} G(E)dE \quad (73)$$

It will be assumed that $E_c - E_a$ is less than $E_r - E_v$ so that over the active temperature range little or no simultaneous hole release is possible. By excluding the direct band-to-band recombination as well. these hole traps function as the recombination centers for the system during the trap emptying process. these centers further characterized by the temperature-dependent functions $h(T)$, the total concentration of full hole traps and $R(T)$, the average capture cross section for electrons(i.e., the recombination cross section). Formally $R(T)$ is given by

$$R(T) = \frac{1}{M} \sum_i M_i r_i(T), \quad (74)$$

where M is the concentration of hole traps of defect type i and $r_i(T)$ is the capture cross section for electrons of a hole trap of defect type i . The sum is over all defect types that lead to energy levels less than E_F . Finally, this model requires that the concentration of trapped holes be somewhat greater than the concentration of trapped electrons so that over the active temperature range the deep electron traps remain full and therefore do not constitute retrapping centers for free electrons. This configuration means that the existence of deep electrons traps enters the formalism only through the neutrality condition. The theory of TSL and TSC is essentially symmetric with respect to carrier type, and one could therefore define an analogous model making holes the freed carrier type during trap emptying.

3.4 Experimental procedure for TSC

The system is held at a constant temperature lower than T_0 , is subjected to an external perturbation either illumination or radiation of energy greater than the band gap of the material. The excitation induces the transitions across the band gap creating a large concentration of free electrons and holes, which then relax into the various traps. Trap filling is continued in this way until equilibrium is achieved (this ensures complete filling of the deep electron traps). The excitation is then removed and the system is heated according to a linear heating profile, $dT/dt \equiv \beta$, in the dark conditions. During heating the trap emptying process begins as electrons are thermally freed out of the shallow levels. however, the active temperature range, the allowed transitions is shown in the Fig. 3.1 and Fig. 3.2 show that the electrons are excited into the conduction band from the active level with free carrier removal proceeding along two possible pathways. recombination and retrapping. Since the deeper electron traps do not empty until temperatures well past the active range, these traps remain full and therefore do not constitute potential trapping sites. Hence, transitions into these traps are forbidden. The thermal release probability function per unit time,

$P(T)$ is given by [111,?]

$$P(T) = s(T) \exp\left[-\frac{E}{k_B T}\right] \quad (75)$$

where $s(T)$ is the frequency factor, E_t is the previously defined trap depth, T the absolute temperature, and k_B is the Boltzmann constant. In the case of charge neutrality conditions the concentration of the free and trapped holes are assumed to be equal for any temperature range. The condition is expressed for the temperatures greater than T_0

$$n_c + n + H = h + h_v \quad (76)$$

where h and h_v are the hole concentrations in the recombination centers and in the valence band. All terms except h are temperature dependent. The final assumption can be made based on the active traps would contribute the TSR process, such that

$$n + H \gg n_c - h_v \quad (77)$$

since in the active temperature range $h_v = 0$, this approximation consists of trapped electrons is always much greater than the concentration of free electrons. This approximation does not severely limit the applicability of this model, since in most physical systems the concentration of traps actually at any temperature is small compared with the concentration of deeper inactive traps. within this approximation, the eqn becomes $h \simeq n + H$, meaning that the concentration of available hole centers must at least be equal to $N + H$. The recombination lifetime, τ , is given by

$$\frac{1}{\tau(T)} = v_e(T) h R \simeq v_e(T) R (n + H) \quad (78)$$

where v_e is the thermal velocity of an electron in the conduction band and is approximately given by

$$v_e = \left[\frac{3kT}{m^*} \right] \quad (79)$$

where m^* is the effective mass of an electron. The rate equations governing the detrapping of charge carriers over the active temperature range are [3]

$$\frac{dn}{dt} = -nN_cSv_{th}\exp\left[-\frac{E_t}{kT}\right] + n_c(N_t - n)Sv_{th} = -R_d + R_t \quad (80)$$

$$\frac{dn_c}{dt} = nN_cSv_{th}\exp\left[-\frac{E_t}{kT}\right] - n_c(N_t - n)Sv_{th} - \gamma n_c f - \nu_e n_c = R_d - R_t - R_r + R_e \quad (81)$$

where $R_d = \alpha n$, $R_t = n_c(N_t - n)Sv_{th}$, $R_r = \gamma n_c f$ and $R_e = \nu_e n_c$ represent the detrapping, the retrapping, the recombination and the exo electronic emission rates respectively. For practical purposes the exo electronic emission rate can be ignored for the case of measuring either TSL or TSC.

$$\frac{dn_c}{dt} = -\frac{n_c}{\tau} - \frac{dn}{dt} \quad (82)$$

where $N_c(T)$, is the density of states in the conduction band, $S(T)$ is the capture cross-section, $v_{th}(T)$ is the average thermal velocity of the electrons, E_t is the ionization energy or activation energy of the trapped carrier and τ is the recombination lifetime of the electrons in the conduction band. If τ is short enough such that $\frac{dn_c}{dt} \ll \frac{n_c}{\tau}$ then from equation (2) $n_c(T) \simeq -\tau \frac{dn}{dt}$. On substituting eqn. (2) in (1), $n_c(T)$ can be expressed as

$$n_c(T) = \frac{nN_cSv_{th}}{\left(\frac{1}{\tau} + (N_t - n)Sv_{th}\right)} \exp\left[-\frac{E_t}{kT}\right] \quad (83)$$

The solutions for n_c gets more complicated for realistic systems and solutions for TSC can only be obtained assuming certain assumptions [?]. For example, with the following combined assumptions:

§ $n_c \ll n$ implying that the majority of electrons are trapped,

§ $\frac{dn_c}{dt} \ll \frac{dn}{dt}$ implying a quasi-equilibrium state approximation.

Within this approximation the solutions for I_{TSC} and I_{TL} are given by

$$I_{TSC}(T) = \frac{AFe\mu\tau s T^d}{\left(\frac{1}{\tau} + (N_t - n)Sv_{th}\right)} \exp\left[-\frac{E_t}{kT}\right] \quad (84)$$

$$I_{TL}(T) = \frac{\eta n s T^d}{\tau\left(\frac{1}{\tau} + (N_t - n)Sv_{th}\right)} \exp\left[-\frac{E_t}{kT}\right] \quad (85)$$

Based on the following assumptions, there are three special cases are listed below.

¶ Slow retrapping (first order), $\tau^{-1} \gg (N_t - n)Sv_{th}$:

$$I_{TSC}(T) = \frac{dn}{dt} = AeF\mu\tau sn_0 T^d \exp\left[-\frac{E_t}{kT} - \frac{s}{\beta} \int_{T_0}^T T^d \exp\left[-\frac{E_t}{kT}\right] dT'\right] \quad (86)$$

$$I_{TL}(T) = \eta n_0 s T^d \exp\left[-\frac{E_t}{kT} - \frac{s}{\beta} \int_{T_0}^T T^d \exp\left[-\frac{E_t}{kT}\right] dT'\right] \quad (87)$$

where A is the effective area of the sample, n_0 the initial concentration of the trapped electrons depends on filling conditions, F the electric field distribution, $\mu\tau$ the mobility lifetime product which is temperature dependent, l the order of kinetics, $s'(T)$ the temperature dependent frequency factor $(N_c Sv_{th})$ and d a constant which can take a value from -2 to +2 [?].

¶ Retrapping, $\tau^{-1} \gg (N_t - n)Sv_{th}$:

$$I_{TSC} = AeF\mu\tau n_0 \frac{s T^d}{2} \exp\left[-\frac{E_t}{kT} - \frac{s}{2\beta} \int_{T_0}^T T^d \exp\left[-\frac{E_t}{kT}\right] dT'\right] \quad (88)$$

$$I_{TL} = \eta n_0 \frac{s T^d}{2} \exp\left[-\frac{E_t}{kT} - \frac{s}{2\beta} \int_{T_0}^T T^d \exp\left[-\frac{E_t}{kT}\right] dT'\right] \quad (89)$$

¶ Fast retrapping, $\tau^{-1} \ll (N_t - n)Sv_{th}$:

$$I_{TSC}(T) = \frac{dn}{dt} = AeF\mu\tau n_0 \frac{N_c}{N} \exp\left[-\frac{E_t}{kT} - \frac{1}{\beta N} \int_{T_0}^T \frac{N_c}{\tau} \exp\left[-\frac{E_t}{kT}\right] dT'\right] \quad (90)$$

$$I_{TL}(T) = \frac{dn}{dt} = \frac{\eta}{\tau} n_0 \frac{N_c}{N} \exp\left[-\frac{E_t}{kT} - \frac{1}{\beta N} \int_{T_0}^T \frac{N_c}{\tau} \exp\left[-\frac{E_t}{kT}\right] dT'\right] \quad (91)$$

An alternative, simplistic approach for analyzing the peaks in the TSC spectra, which is valid in certain cases, is in terms of the initial rise method [?]. This method is independent on the order of kinetics even if the frequency factor is temperature dependent and the TSC arising from the emptying of filled trap levels as the temperature is increased can be expressed as $I_{TSC}(T) = C \exp\left[-\frac{E_t}{kT}\right]$ for $T < T_{max}$, with $AeF\mu n_0 s T^d$ as the pre-exponential factor. Thus a plot of the logarithm of the $I_{TSC}(T)$ against $\frac{1}{kT}$ yields a straight line with a slope of E_t . The drawback of this method is apparent in systems where several activated trapping levels are present [111,?].

Several theories have been developed to correlate the experimental observable quantities with the activation energy of the traps. These theories are based on the trap-limited band transport model, where TSC is due to increased density of free carriers moving in an extended band state with a unique (microscopic) mobility [?]. The existing theories may not be valid for all cases and the theory is modified in which the analyzes of TSC in the case of disordered materials, the transport is mainly due to hopping of carriers from a localized state to other without ever moving in an extended state. It can be visualized as due to the increased mobility of all the carriers. For disordered, amorphous semiconductors where the transport in the conduction band is not a simple extended state transport, the TSC is further modified by the temperature and field dependence the mobility of the charge carriers in the polymer. In this case the increased TSC can be explained in terms of hopping transport in which the mobility can be function of electric field, E and temperature, T^{18} . The temperature dependence of mobility in hopping systems are found to be thermally activated, and can be represented by the Arrhenius relation. If the mobility μ_R at a reference temperature T_R is known, the mobility at any other temperature can be written

$$\mu(T) = \mu_R \exp\left[\frac{\Delta}{k}\left(\frac{1}{T_R} - \frac{1}{T}\right)\right] \quad (92)$$

where Δ is the activation energy of the carrier transport. It is often found that mobility is a field dependent, and the field dependence is contained in the activation energy.

The observed quantity is not the true activation energy, it is apparent one and can be found out by extrapolating to zero field. The above equations n_0 is the initial concentration of electrons trapped at the active level. For the fast retrapping cases it is modified to $\frac{n_0}{N} \ll 1$ [?]. It should be recognized that each of the above equations reduces to the final form of

$$I \simeq C \exp\left[-\frac{E_t}{kT}\right] \quad (93)$$

when $T \simeq T_0$, where I is the TL or TSC intensity during the initial rise part of the TL or TSC peak. This led to the development of the initial rise analysis and provides us an quick method of resulting to find out the value of E_t without the knowledge of kinetics orders, mobility, lifetime and frequency factors.

3.5 Classification of Trapping States

A defect state can either act as a trap or a recombination center, depending on its location and it depends on the probability of capture probability of a hole (or a free electron) and releasing probability of an electron (or hole). Since the latter is largely determined by the Boltzmann factor $\exp[-E_t/kT]$, defect states around the center of the forbidden gap tend to be recombination centers, those in the upper part electron traps and those in the lower part hole traps [134,?]. In principle, any defect state has a finite capture cross section for electrons and holes. Coulomb-attractive for free electrons may be neutral or even repulsive for holes and, thus, have a vastly smaller cross section for hole capture as compared to that for electron capture. Defect states in the forbidden gap may act as electron traps or hole traps depending on their occupancy functions. Capture of carriers in traps or recombination can be nonradiative and thermal emission of carriers from traps is a nonradiative transition. Nonradiative recombination processes are difficult to identify because their occurrence can usually only be inferred from a low luminescence emission efficiency. If the nonradiative and radiative recombination processes have lifetimes τ_r and τ_{nr} , respectively,

$$\eta = \frac{\tau_r}{\tau_{nr}} + 1^{-1} \quad (94)$$

The luminescence efficiency η can be temperature dependent, decreasing with increasing T. The introduction of their quasi-Fermi levels allows the classification of trapping states as shallow or deep traps.

3.5.1 Shallow traps

The states in which there is a high probability of the trapped carriers can be reemitted back into the band from which they came from. These states are empty and are classified as shallow traps. The occupancy of the carriers in the trapping levels can be temperature dependent and the definition of shallow traps may be "statistical" one. Shallow traps are normally characterized by a very small ionization energy which is of the order of the phonon energies ($\simeq kT$). The concentration of the shallow traps is very high, in the region of $10^{18}cm^{-3}$, and the transport of electrons occurs via hopping between the traps. As the concentration of the shallow traps is very high, and there is a frequent interaction between electrons and these traps, a thermodynamic equilibrium occupation of these traps can be assumed even immediately after the external perturbation is removed.

3.5.2 Deep traps

The states in which there is a less probability of the trapped carrier can be reemitted back into the band and it may involve multi-phonon transitions[. Naturally, at all temperatures above several kT, shallow trapping states are also ionized (empty), in which case both definitions of shallow traps are identical. On the other hand, at elevated temperatures deep trapping states may turn into "statistically" shallow traps. The definition of deep traps may be ionization energy is order of several kT and involves radiationless capture of free carriers. In contrast to this, for the deep traps that exist at a concentration of about $10^{14}cm^{-3}$ there is not necessarily an equilibrium occupation

after a change of the applied electric field. As a consequence of the relatively low concentration of free electrons, and of these deep traps too, it will take some time - which may mean hours or even days - until these traps are occupied. In other words, the current will flow for some time without taking notice of these traps, thus without being influenced by them. Depending on the concentration of the electrons hopping between the shallow traps, there will be an occupation after some time of the deep traps too, and an immobile space charge will be generated by this. The trapped space charge will last a very long time and it may be impossible to remove it totally from the polymer. A consequence of this space charge is a locally varying electric field strength that determines the current density, mainly by influencing the hopping probability of the electrons between the shallow traps.

3.5.3 Intermediate traps

The definition of intermediate traps lies in between shallow and deep ones. This can be qualitatively argued that the ionization energy lies within the range of shallow and deep levels. F-centers is one of the examples of this type.

3.6 Determination of kinetic parameters from experimental results

In this section, we present the various models to obtain the unknown trapping parameters with certain appropriate assumptions. These are the following models:

3.6.1 Urbach's method

Urbach's method was the first method to evaluate the activation energy for the traps or defect levels based on the following empirical expression:

$$E_t = \frac{T_M}{500} \text{ eV} \quad (95)$$

where T_M is the temperature maximum of the peak. This method was obtained

empirical assumption based on experimental observations and this method is not too sensitive to trapping parameters such as kinetics order, frequency factor, magnitude of TSC and heating rate.

3.6.2 The initial rise method

A slightly more realistic value for E_t is obtained using the initial rise method. This method is valid for mono-energetic traps only in the regime $T \ll T_{max}$.

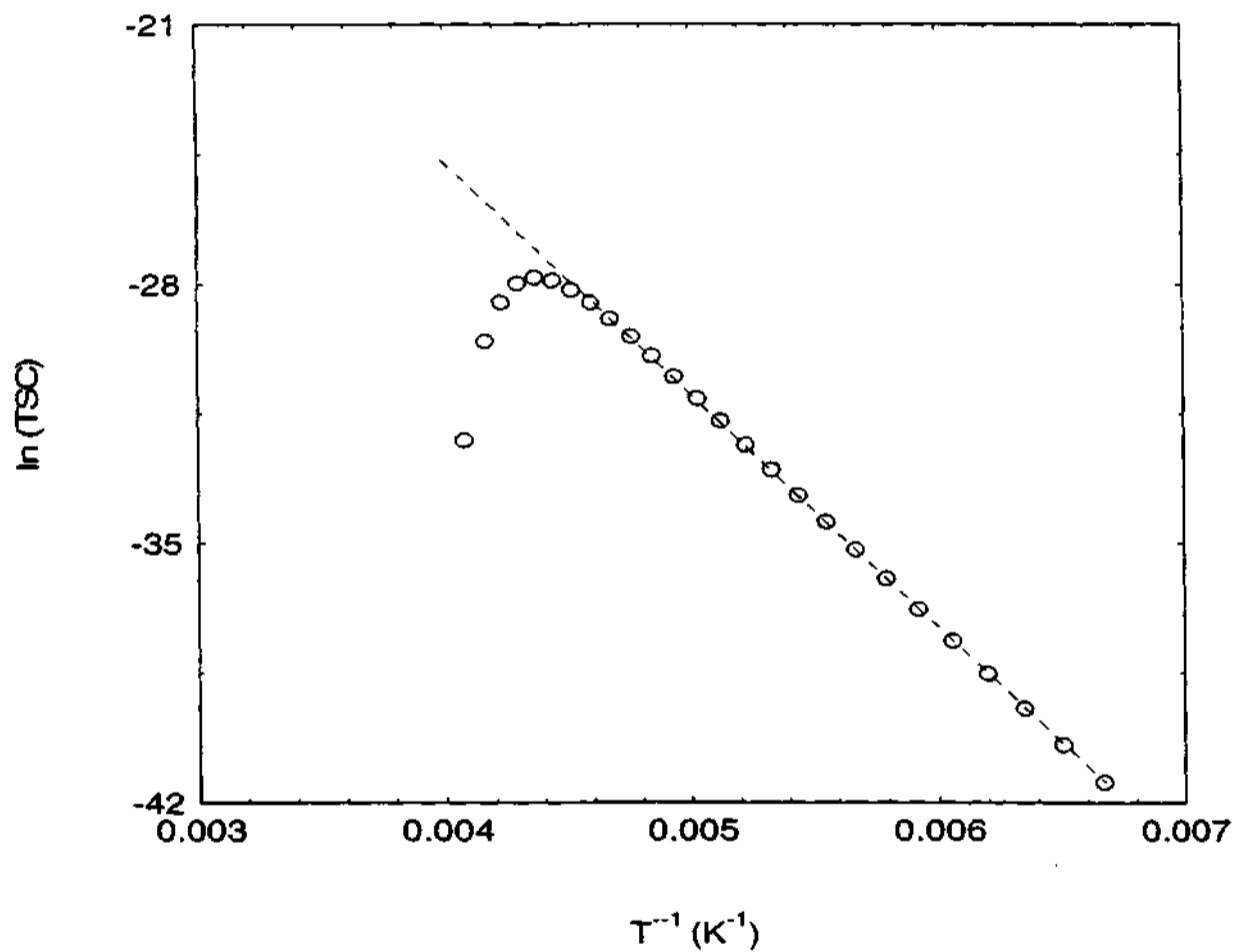


Fig. 3.3 Plot of $\ln (TSC)$ Vs $1/T$

The justification for this method is apparent when one reduces the equations for TSC as obtained from first and second order kinetics equations. The equations for the first

and second order kinetics are respectively

$$I(T) = cn_0sT^d \exp\left[-\frac{E_t}{kT} - \left(\frac{s}{\beta}\right) \int_{T_0}^T T^d \exp\left[-\frac{E}{kT'}\right] dT'\right] \quad (96)$$

and

$$I(T) = cn_0^2s'T^d \exp\left[-\frac{E_t}{kT}\right] \left[1 + \left(\frac{s}{\beta}\right) \int_{T_0}^T T^d \exp\left[-\frac{E}{kT'}\right] dT'\right]^{-1} \quad (97)$$

where I is the current intensity, s is the frequency factor (s^{-1}), n_0 the initial concentration of the trapped electrons (cm^{-3}), T_0 the initial temperature, β the linear heating rate (Ks^{-1}), $T = T_0 + \beta t$ and s' the pre-exponential factor with dimensions of cm^3s^{-1} .

The regions below [$T \ll T_M$] and above [$T \gg T_M$] are noted to be as the releasing and emptying of the trapped carriers from the trap levels. In the region where $T \ll T_M$ for all the factors other than $\exp[-\frac{E_t}{kT}]$ in both previous equations do not show an appreciable variation with T and therefore in the initial part of the peak, $I \propto \exp[-\frac{E_t}{kT}]$ for either type of kinetics. Thus, the plot of $\ln(\text{TSC})$ versus $\frac{1}{T}$ is linear in a limited temperature regime, with a slope equal to $-\frac{E_t}{k}$. Fig. shows the plot of $\ln(\text{TSC})$ Vs $\frac{1}{T}$ for $T \ll T_M$. This method validates and provides a quick analysis of the initial ascending part of the peak which allows an evaluation of E_t without any knowledge of the frequency factor. This method is more valid only for first peak and sensitive to the shape of the peak. In other words this method is not applicable to multi-trapping cases which would resemble overlapping of several peaks brings out in obtaining inaccurate results.

3.6.3 Ilich's method (Modified form of initial rise method)

Ilich's method is also based on the initial rise part of the peak. Assuming that the current intensity $I(T)$ has the form $I(T) = c \exp[-\frac{E_t}{kT}]$, its derivative $\frac{dI}{dT}$ gives the slope $(\frac{dI}{dT})_{T=T_t}$ of the tangent to the TSC peak. The final expression for E_t is given by

$$E = \frac{kT_t^2}{T - T^*} \quad (98)$$

where T^* is the intersection of the above mentioned tangent with the T axis.

3.6.4 Heating rate method

The trap energy is related to the temperature T_m corresponding to the TSC peak by

$$E_t = kT_m \ln\left(\frac{S_n \nu_n N_c k T_m^2}{\beta E_t}\right) \quad (99)$$

As shown by Hoogenstraten [?], if several heating rates are used and T_m is determined as a

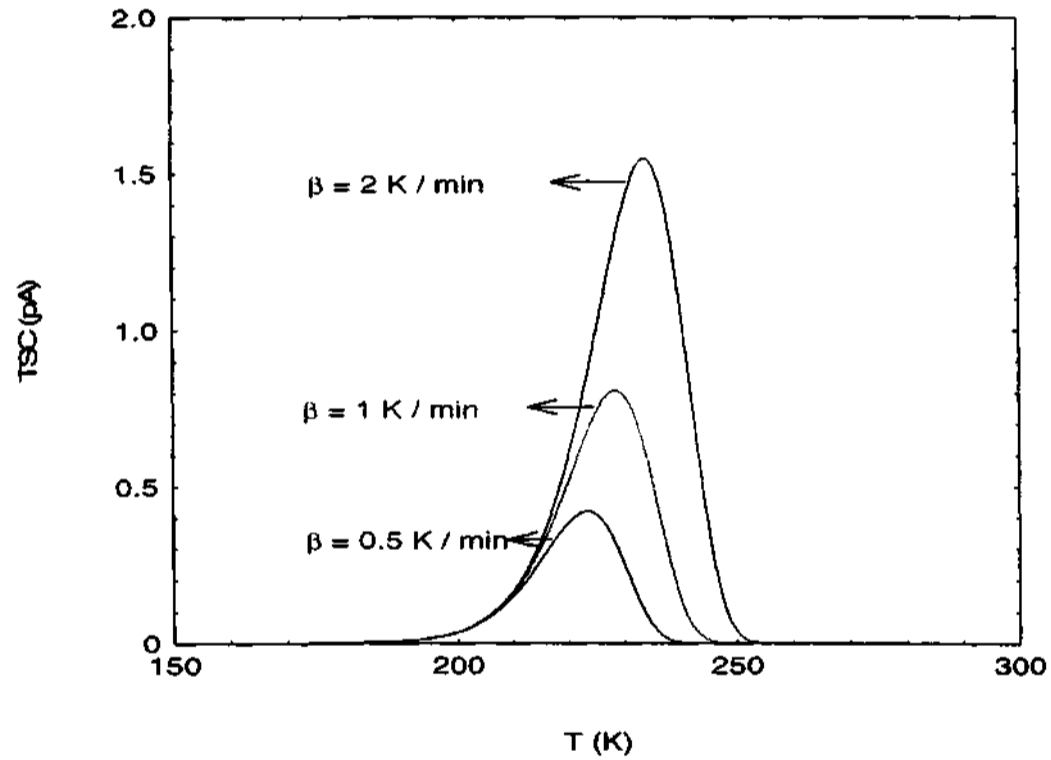


Fig. 3.4 shows an example of a TSC measurement of different heating rates with arbitrarily chosen parameters: $E/k = 6000 \text{ K}$, $d = 2$, $n_0 = 10^{-9} \text{ C}$, $s = 10^4 \text{ s}^{-1}$.

function of β , it is possible to derive E_t from the slope of the straight line which should be obtained by plotting $\ln\left(\frac{T_m^2}{\beta}\right)$ against $\frac{1}{T_m}$. Fig. 3.4 shows the plot with the parameters

chosen arbitrarily. In either case, the integrated current over time reveals the number of defects emptying their charge and this can then be related to the defect density if one knows the dimensions (depletion width W^* or charge distribution length ξ and electrode area A) of the active region [?,?]. Note that the integrated curve (over time!) is equal in all three cases ($\int I dt = \int I \frac{dT}{\beta}$). That's why the biggest curve looks larger, but it is scanned at higher speed. In most of the cases it is assumed, that all the defects in the depletion width release their charges in a TSC experiment. For more precise calculations, one should use a value of ΔW^* or $\Delta \xi$ instead of W^* or ξ , which is the part of the carriers contribute TSC.

3.6.5 Bube's method

The evaluation of E_t of the trapping center responsible for the current peak is given by the expression:

$$E_t = kT_m \ln\left(\frac{N_c}{n}\right) \quad (100)$$

where n is the electron concentration at the peak temperature.

3.6.6 Peak shape methods

On the assumption that the area is the TSC curve is comparable to the area of a triangle, several methods have been proposed which use the peak temperature T_M and two temperatures T_1 and T_2 which are respectively the temperatures on either side of T_M corresponding to half intensity. T_1 and T_2 depend on the peak shape. For a characterization of the single TSC or TL peak Halperin and Braner introduced a parameter called the symmetry factor (μ_g) which allows us to find out the order of kinetics. The trapping parameters required to apply these methods are $\delta = T_2 - T_M$, $\tau = T_M - T_1$, $\omega = T_2 - T_1$, $\mu_g = \frac{\delta}{\omega}$, where T_m (K) is the temperature corresponding to the maximum of TL glow curve or TSC thermogram, I_m of the TL or TSC; T_1 (K) and T_2 (K) are the temperatures at which the TL or TSC is equal to half of the

maximum intensity on either side of T_m ($T_2 > T_1$). The interdependence of μ_g with l is given by

$$\mu_g = \frac{1}{l^{l-1}} \left[\frac{1}{1 + \frac{(d+2)kT_m}{E_t} - \frac{(d+2)(d+3)(kT_m)^2}{E_t^2} + \dots} \right] \quad (101)$$

This factor depends on peak position and shape of the TSC or TL curve and introduce errors there is a slight deviation in finding out the exact location of the peak.

It is possible to calculate the area of a part from TSC or TL at a given temperature range.

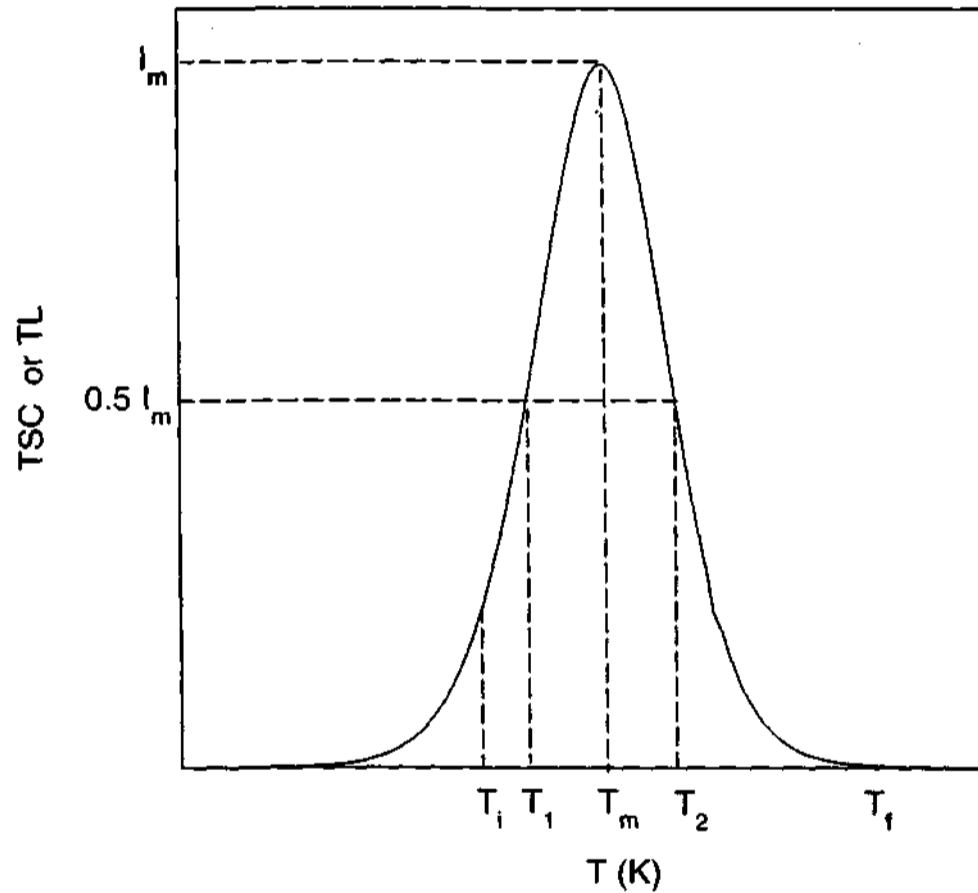


Fig. 3.5 shows an isolated peak with shape parameters

This model is more appropriate and validates that TSC or TL consists of a well-defined single peak, corresponding to the traps of only one kind. At the end of the curve all

the traps are emptied. Then the concentration of traps which are populated at the beginning of the TSC or TL curve, n_0 , is proportional to the area under the curve. Again the concentration of traps emptied up to the temperature T_i is given by the area under the TSC or TL curve up to T_f . Hence the concentration of the populated traps at temperature T_i during the TSC or TL run is proportional to the area A_i which is equal to the total area under the TSC or TL curve less than that of the area under the TSC or TL curve between the initial point and T_i . Thus the A_i is equal to the area under the TSC or TL curve between the T_i and T_f , where T_f is the temperature at which the TSC or TL intensity vanishes to zero after reaching a maximum value is shown in the fig.

Consider the maximum of the TSC or TL peak, I_m

$$I_m = (A_m)^l \frac{S}{N^{l-1}} T_m^d \exp\left[-\frac{E_t}{kT}\right] \quad (102)$$

where A_m is the area under the TSC or TL curve between T_m and T_f . Now, assuming that $I_1 = \frac{I_m}{2}$ and $I_2 = \frac{I_m}{2}$ are the half intensities of TSC or TL that occur at T_1 (K) and T_2 (K), respectively, then the following equations can be written in the form:

$$I_1 = \frac{I_m}{2} = (A_1)^l \frac{S}{N^{l-1}} T_m^d \exp\left[-\frac{E_t}{kT_1}\right] \quad (103)$$

$$I_2 = \frac{I_m}{2} = (A_2)^l \frac{S}{N^{l-1}} T_m^d \exp\left[-\frac{E_t}{kT_2}\right] \quad (104)$$

where A_1 and A_2 indicate the areas under TSC or TL curve from temperatures T_1 and T_f . From equations (44) and (45) one obtains

$$\ln(2) = \ln\left[\frac{A_m}{A_1}\right] - \frac{E_t}{k} \left[\frac{1}{T_m} - \frac{1}{T_1}\right] \quad (105)$$

and similarly from equations (44) and (46) one obtains

$$\ln(2) = \ln\left[\frac{A_m}{A_2}\right] - \frac{E_t}{k} \left[\frac{1}{T_m} - \frac{1}{T_2}\right] \quad (106)$$

Equation (47) can be rewritten as

$$E_t = \{ \ln(2) - \ln\left[\frac{A_m}{A_1}\right] \} \left[\frac{kT_1 T_m}{T_m - T_1} \right] \quad (107)$$

Equation (48) can be rewritten as

$$E_t = \{ \ln(2) - \ln\left[\frac{A_m}{A_2}\right] \} \left[\frac{kT_2 T_m}{T_m - T_2} \right] \quad (108)$$

Now equating the above equations (49) and (50) one easily obtains l in terms of the shape parameters:

$$l = \frac{T_m [T_1 - T_2] \ln(2)}{T_1 [T_m - T_2] \ln\left[\frac{A_m}{A_1}\right] - T_2 [T_m - T_1] \ln\left[\frac{A_m}{A_2}\right]} \quad (109)$$

By knowing these shape parameters one can easily obtain l . [Chen R 1969 J. Appl. Phys. 40 570]. The major drawback of this method to obtain E_t is that one has to know the knowledge of l involved in the TSC or TL process in advance. However the validity of this method can be examined for a broad range of values of kinetic order ($0.7 < l < 2.5$).

3.6.7 Chen's method

The order of the kinetics was first estimated by means of the value of the symmetry factor μ_g . Chen found that μ_g changes with the order of kinetics, l , and ranges from 0.42 to 0.52, where these two limits correspond to first and second order kinetics respectively. However, it is to be stressed that Chen's exact method is the only one that, requiring knowledge of the μ_g parameter only, is applicable even to the intermediate kinetic orders with $1 < \mu_g < 2$. The following formulae of Chen have been used in order to find E_t

$$E_\tau = [1.51 + 3(\mu_g - 0.42)] \frac{kT_M^2}{\tau} - [1.58 + 4.2(\mu_g - 0.42)] 2kT_M \quad (110)$$

$$E_\delta = [0.976 + 7.3(\mu_g - 0.42)] \frac{kT_M^2}{\delta} \quad (111)$$

$$E_{\omega} = [2.52 + 10.2(\mu_g - 0.42)] \frac{kT_M^2}{\omega} - 2kT_M \quad (112)$$

The estimate of the frequency factor s can be made using the following expressions for first and general-order kinetics peaks respectively

$$s = \frac{\beta E}{kT_M^2} \exp\left[\frac{E}{kT_M}\right] \quad (113)$$

$$s = \frac{\beta E}{kT_M^2} \exp\left[\frac{E}{kT_M}\right] \left[1 + (l-1) \frac{2kT_M}{E}\right]^{-1} \quad (114)$$

Halperin and Braner suggested that, whenever μ_g is greater than $e^{-1}[1 + (\frac{2kT_M}{E})]$, a second order kinetics can approximately be assumed.

3.6.8 Grosswiener's method

Grosswiener gave a method for finding the activation energy using the value of τ . The method is based on the approximation followed by the rising portion of the TSC peak. The expression is given by

$$E_{\tau} = a_{\tau} \frac{\tau k T_1 T_M}{\tau} \quad (115)$$

where $a_{\tau} = 1.41$ or 1.68 for first and second order kinetics respectively.

3.6.9 Lushchik's method

The expressions for first and second order kinetics are obtained on the assumption of the area of the peak towards the fall-off is equal to the area of the triangle having the same height and half width. For first and second order kinetics the formulae, modified by Chen were

$$E_{\delta} = 0.976 \frac{kT_M^2}{\delta} \quad (116)$$

$$E_{\delta} = 1.706 \frac{kT_M^2}{\delta} \quad (117)$$

3.6.10 Halperin and Braner's method

Halperin and Braner obtained the expressions for first and second order kinetics by using the parameters T_1 and T_M . Considering the low-temperature half peak and the correction performed by Chen[12], the first and second order kinetics expressions were as follows:

$$E_\tau = 1.52 \frac{kT_M^2}{\tau} - 3.16kT_M \quad \text{1st order} \quad (118)$$

$$E_\tau = 1.813 \frac{kT_M^2}{\tau} - 4kT_M \quad \text{2nd order} \quad (119)$$

3.6.11 Area Measurement method

It is possible to write the expression for activation energy E_t

$$E_t = kT_i \left[c + \ln \frac{I(T_i)}{S(T_i)^\alpha} \right] \quad (120)$$

where T_i and T_f are the setting points, $S(T_i)$ is the area obtained between T_i and T_f , α is a numerical value which linearizes the above equation. A plot of $\ln \left[\frac{I(T_i)}{S(T_i)^\alpha} \right]$ versus $\frac{1}{T_i}$ gives straight line when the appropriate value of α is chosen.

3.6.12 Chen's additional formulae

Chen proposed the new formulae based on the total half width, and for first and second order kinetics can be expressed as

$$E_\omega = 2.29 \frac{kT_M^2}{\omega} \quad (121)$$

$$E_\omega = 2kT_M \left[1.756 \frac{T_M}{\omega} - 1 \right] \quad (122)$$

3.6.13 Keating method

This method assumed that the frequency factor S , is temperature dependent. Keating considered $S = B T^d$, where B is a constant. For the first order kinetics the final expression for E_t is found to be

$$E = kT_m[(1.2\Gamma - 0.54)\left(\frac{T_2 - T_1}{T_m}\right) + 5.5e^{-3} = \left[\frac{1}{2}(\Gamma - 0.75)\right]^2] \quad (123)$$

where $\Gamma = \frac{T_2 - T_1}{T_m - T_1}$, and T_1 and T_2 being defined earlier. The formula is found to hold true for $0.75 < \Gamma < 0.9$ and $10 < E/kT_m < 35$. [122]

3.6.14 The curve fitting method

The fitting method starts from the expression for each peak [109,110]. For the numerical calculation of the TL or TSC intensity, one needs to evaluate the integral either numerically or approximated by an asymptotic series, truncated after a certain number of terms. This report presents the best fitting model for the experimental data.

$$F(T, E) = \int_{T_0}^T T^d \exp\left[-\frac{E_t}{kT}\right] dT' \quad (124)$$

This integral cannot be solved in an analytical form. However, with successive integrations by parts it is found to be

$$F(T, E) \simeq T^{d+2} \frac{\exp\left[-\frac{E_t}{kT}\right]}{\frac{E_t}{k}} \Delta \quad (125)$$

where $\Delta = 1 - (d+2)\frac{kT}{E_t} + (d+2)(d+3)\left(\frac{kT}{E_t}\right)^2 - (d+2)(d+3)(d+4)\left(\frac{kT}{E_t}\right)^3 + \dots$

¶ The function for a first order kinetics

$$I_{TSC}(T) = \frac{dn}{dt} = AeF\mu\tau sn_0 T^d \exp\left[-\frac{E_t}{kT}\right], l = 1 \quad (126)$$

$$= AeF\mu\tau sn_0 T^d \exp\left[-\frac{E_t}{kT} - \frac{s}{\beta} \int_{T_0}^T T^d \exp\left[-\frac{E_t}{kT}\right] dT'\right] \quad (127)$$

Using this approximation in equation [1], it follows that for the first kinetics order as

$$= AeF\mu\tau sn_0 T^d \exp\left[-\frac{E_t}{kT} - \frac{skT^{d+2}}{\beta E_t} \Delta\right] \quad (128)$$

By equating the derivative (1) to zero, the condition for the maximum is found to be

$$\frac{s}{\beta} = \left(\frac{E_t}{k} + dT_m\right) \frac{\exp\left[\frac{E_t}{kT_m}\right]}{T_m^{d+2}} \quad (129)$$

By inserting this equation into the above equation, the expression for $I = I_m$ ($T = T_m$) can be written at the peak maximum,

$$I_m = AeF\mu\tau\beta \left\{ \frac{E_t}{k} + dT_m \right\} \frac{n_0}{T_m^2 \exp[1 - \Delta_m] \left(1 + \frac{dkT_m}{E_t}\right)} \quad (130)$$

where $\Delta_m = 1 - (d+2)\frac{kT_m}{E_t} + (d+2)(d+3)\left(\frac{kT_m}{E_t}\right)^2 - (d+2)(d+3)(d+4)\left(\frac{kT_m}{E_t}\right)^3 + \dots$

The first order kinetics of TSC intensity can be expressed in terms of known quantities I_m and T_m , after rearrangement

$$I(T) = I_m \left(\frac{T}{T_m}\right)^{d+2} \exp\left[\frac{E}{kT_m} - \frac{E}{kT} + \left(\frac{dkT_m}{E_t} + 1\right)(1 - \Delta_m - \left(\frac{T}{T_m}\right)^{d+2} \exp\left(\frac{E}{kT_m} - \frac{E}{kT}\right))\right] \quad (131)$$

¶ The function for a general order kinetics

I_{TSC} can be expressed as follows for the general order of kinetics

$$\begin{aligned} I_{TSC}(T) &= \frac{dn}{dt} = AeF\mu\tau s' n^l \exp\left[-\frac{E_t}{kT}\right], \quad s' = sn_0^{l-1}, \quad l \neq 1 \\ &= \frac{AeF\mu\tau s' n_0 \exp\left[-\frac{E_t}{kT}\right]}{\left[(l-1) \frac{s'}{\beta} \int_{T_0}^T T^d \exp\left[-\frac{E_t}{kT}\right] dT' + 1\right]^{\frac{1}{l-1}}} \end{aligned} \quad (132)$$

The condition for maximum is

$$\frac{s}{\beta} = \left(\frac{E_t}{k} + dT_m\right) \frac{\exp\left[\frac{E_t}{kT_m}\right]}{z_m l T_m^{d+2}} \quad (133)$$

where $z_m = 1 - \frac{l-1}{l} \left(1 + \frac{dkT_m}{E_t}\right) (1 - \Delta_m)$

The peak maximum intensity I_m is

$$I_{TSC} = \frac{I_m \left(\frac{T}{T_m}\right)^{d+2} \exp\left[\frac{E}{kT_m} - \frac{E}{kT}\right]}{\left[1 - \left(\frac{l-1}{l}\right)\left(1 + \frac{dkT_m}{E_t}\right)\right] \left(1 - \Delta_m - \left(\frac{T}{T_m}\right)^{d+2} (1 - \Delta) \exp\left[\frac{E}{kT_m} - \frac{E}{kT}\right]\right)^{\frac{l}{l-1}}} \quad (134)$$

This expression is modified to second order kinetics when $l = 2$. In this section, the most of the models are applicable to the conventional inorganic semiconductors in terms of band type and hopping type of transports. Within the certain approximation, we adopt certain models based on appropriate qualitative explanations of TSC. However the models may not be completely valid, but it can give rough information about trap levels and its distribution.

Chapter 4

Ladder polymers

Heterocyclic aromatic systems have influenced the development of thermally stable organic polymers. The polymer stability depends critically on the structure, reactivity, and mutual interaction of the macromolecules. Rigid chain structures containing aromatic or heterocyclic rings together can overcome those problems and provide additional features due to their stability. Introduction of the side groups to the major group, that promote strong primary and Vander Waals bonding forces, hydrogen bonding, resonance stabilization, molecular symmetry or cross-linking have been used to achieve this combination of thermal stability and physical properties. Unfortunately these structural features, which endow the desirable physiochemical properties, in thermally stable rigid-chain polymers, also cause processing difficulties due to insolubility in organic solvents and the extremely high glass transition, softening or melting temperatures ($> 250 - 350^{\circ}$).

Ladder-type polymers, as a class, provides a new direction in research on semi-conducting and metallic polymers [?,144-146,148,149,?]. These polymers, i.e, conjugated polymers with at least two conduction paths in parallel can also be doped to achieve higher conductivity. Ladder-type polymers exhibit structurally double stranded conjugated systems, an extensive orbital overlap, stable at elevated temperatures provides a bridge between the single-stranded quasi one-dimensional conjugated polymers such as polyacetylene, polythiophenes, polyaniline and polyp-phenylene and two-dimensional graphite which is a semimetal with an extremely high-in plane conductivity. Theoretical interest in this kind of polymers has been stimulated by recent theoretical calculations of the electronic structures of ideal ordered ladder polymers, such as polyacene, polyacenacene, polyphenanthrene, polyquinoxaline

and polypyrene, which suggest the possibility of achieving intrinsic semiconductors, metals and strategy for superconductors was expected. The molecular structures of representative π conjugated ladder-type polymers are shown in the fig. Among these are the ladder and semi-ladder poly(benzimidazolebenzophenanthrolines) also known as poly (7-oxo-7, 10-benz[de]imidazo[4', 5':5, 6](BBL, BBB), aromatic heterocyclic polymers, poly(p-phenylene benzobisthiazole) (PBZT) and poly[2, 2'-(p, p'-stilbene)-6, 6'-bis(4-phenylquinoline)] (PSPQ), the heteroaromatic polyimine, poly(1, 4-phenylenemethyldynenitrilo-1, 4-phenylenenitrilomethyldyne) (PPI), and its derivatives have excellent thermal stability, mechanical and good optical properties.

Synthesis of ladder-type polymer (BBL)

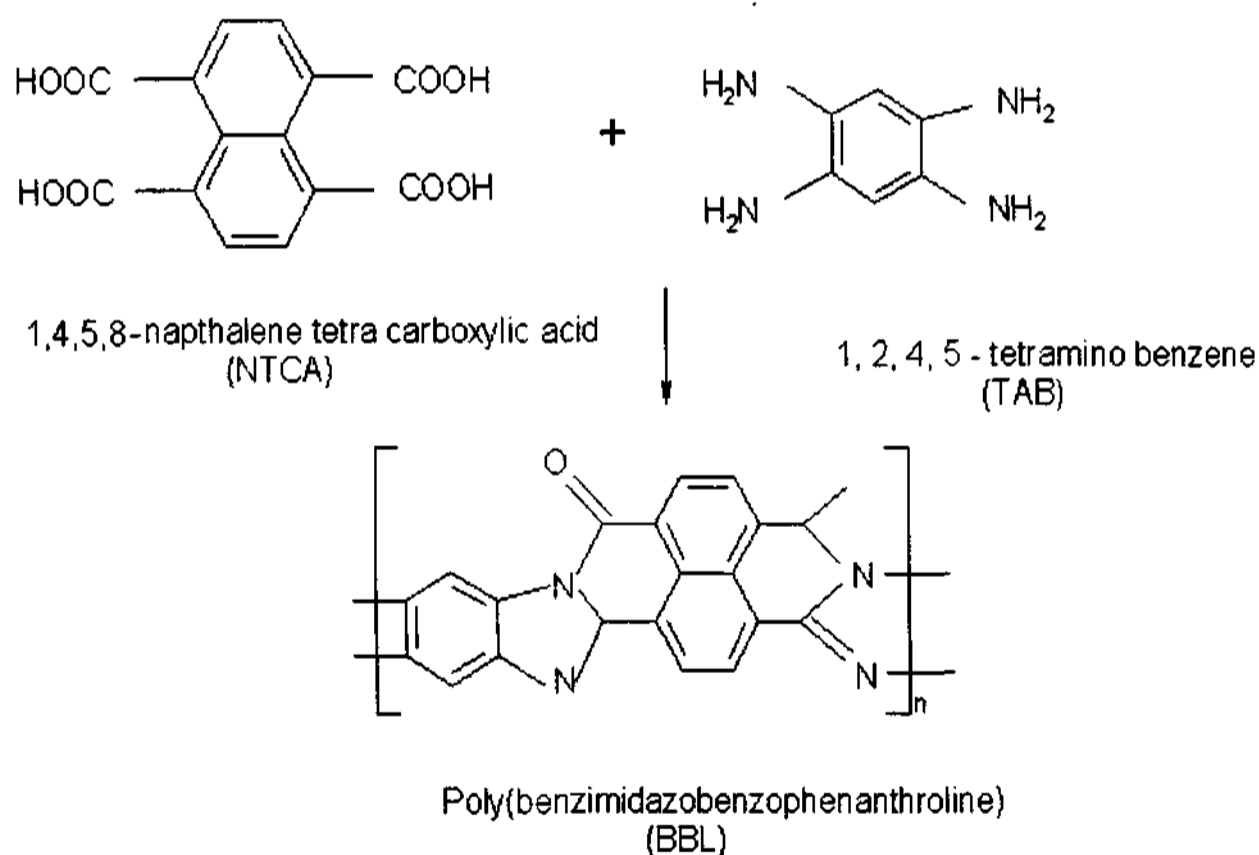


Fig. 4.1 Chemical synthesis of BBL through polycondensation reaction

The chemical structures of these polymers are shown in the figure. BBL consists of naphthalenic and benzenoid units condensed with N-imino amide units. The theoretical calculations on BBL relates π bandwidth of the highest occupied molecular orbitals (HOMO) is quite narrow, 0.61 eV, indicating the poor hole delocalization along the polymer backbone [147]. BBL is a semiconductor with a band gap of 2 eV and it is mainly arising from the aromatic form of the naphthalenic unit and the bond alternation of C-N bonds at the imine site. Characterization using TGA, DSC, IR, NMR, UV-Vis, X-ray, tensile profile, viscosity measurements were carried out at different laboratories to ascertain the integrity and the nature of the polymer prior to using the samples for the electronic studies.

Ladder-type polymers can be chemically as well as electrochemically doped to achieve higher dark conductivity. They exhibit high thermal stability (>400-600°C) and excellent mechanical strength and stiffness [146]. These materials have potential applications not only as electrophotographic receptors but also in all-polymer light emitting diodes (LEDs), large area flat panel displays, and photonic devices. However, owing to their very stiff chains and strong intermolecular interactions (primarily Van der Waals in nature), they are insoluble in organic solvents from which thin films could be prepared for characterization of solid-state properties or for device applications. We have adapted a novel approach to the preparation of thin films of conjugated polymers containing heteroatom (S, O, N etc) such as BBL, BBB, PPI, PBZT, and PSPQ. By forming their Lewis acid (e.g. AlCl_3 , GaCl_3) coordination complexes, the conjugated polymers become soluble in organic solvents, giving viscous solutions that can be processed into thin films or coatings (either spin cast or dip coating) by conventional techniques [146]. After processing, the complexation is reversed by washing the films or coatings in water, alcohol or similar Lewis base, returning the conjugated polymers to their pristine form as films or coatings [146]. It is interesting that the soluble polymer complexes retain the rodlike conformation of the pristine materials as

evidenced by their formation of liquid crystalline solutions in organic solvents. Processing from isotropic and lyotropic liquid crystalline phases allows control of morphology (order/disorder) of the materials [146]. This makes the possibility of producing highly aligned transparent films with anisotropic optical, electrical properties in particular the generation of spatially selective conductive patterns in such aligned transparent polymers opens up the new perspectives for applications in lithography, microelectronics, optics and molecular electronics.

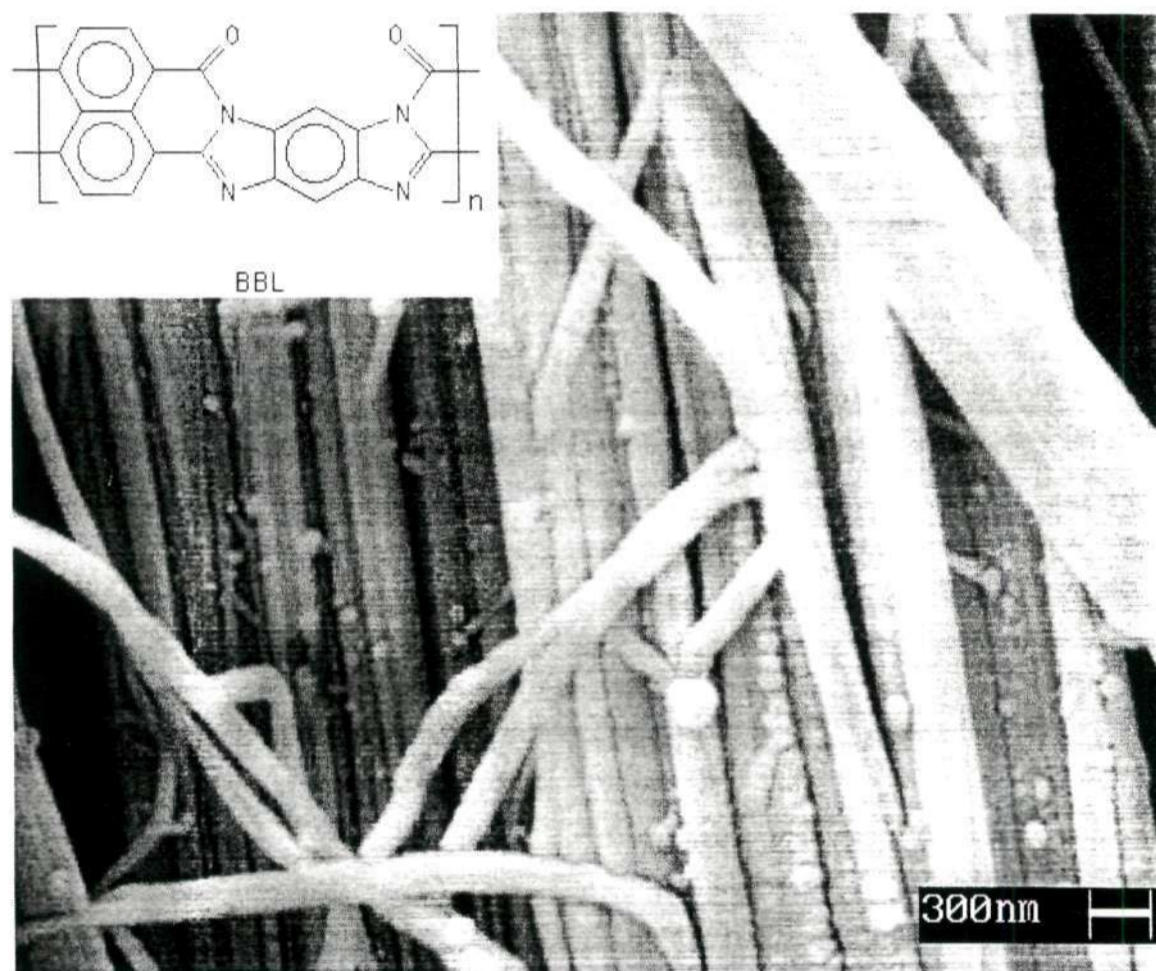


Fig. 4.2 SEM picture of BBL fiber (15 μm diameter)

The polymer in form of films, fiber and powder was obtained from the US Air force Research laboratory, Polymer Branch.

Pristine, un doped BBL, 10^{-12} S/cm with an optical λ_{max} at about 2-2.2 eV. The large accessible temperature range (10 K - 600 K) makes this polymer a suitable candidate for such thermal probes, encompassing a wide energy (trap depth) range. BBL is also one of the rare known n type polymers with the electron as the predominant carrier. The cast films of 20 μm thickness and oriented fibers of 15 μm in diameter were used for the studies presented in this report. Fig. 4.2 shows the scanning electron microscopic picture of oriented fiber. Films were obtained from the polymer solution with methane sulfonic acid (MSA) as the solvent.

4.1 Processing of thin BBL films

Thin films of $\simeq 200$ nm thickness were obtained from a reversible electron donor-acceptor complex formation between heterocyclic polymer and Lewis acids (GaCl_3 , AlCl_3 , FeCl_3 , SbCl_5 , SbCl_3) in appropriate organic solvents (nitroalkanes, acetonitrile, dimethyl sulfoxide, trifluoroacetic acid etc) [146]. Lewis acid complexes formed with AlCl_3 which were soluble in common solvents such as $\text{C}_6\text{H}_5\text{NO}_2$ used for experiments, were spun-cast on the conducting aluminium substrate electrodes in an inert atmosphere. The samples were obtained by spun-cast from the Lewis acid complex AlCl_3 and as a solvent. The films were washed with methanol and distilled water and dried in an inert atmosphere in order to remove the traces of residual solvent. The thin BBL films were coated either on conducting substrates or other polymeric materials to study the interfacial effects and the role of localized states. It will be discussed in detail on forthcoming chapters.

4.2 BBL characterization

The various properties of the BBL which describe the non-electronic aspect is briefly described in this section. Some of these properties are further elaborated in the

following chapters.

4.2.1 UV-VIS absorption spectra

Fig. 4.3 shows the electronic absorption edge for the ladder-type polymer BBL. Electronic absorption spectra of thin films were obtained by using a UV-vis-near-IR spectrophotometer. Pristine, un doped BBL film, with thickness of about 200 nm shows an optical λ_{max} at 555 - 560 nm, that can be attributed to $\pi - \pi^*$ transitions [$\simeq 2.2$ eV [151]] The optical absorption edge in this spectra is at $\simeq 700$ nm, which corresponds to the semiconductor band gap of $\simeq 1.77$ eV.

The calculated value of the absorption coefficient is in the range of 10^5 in the absorption

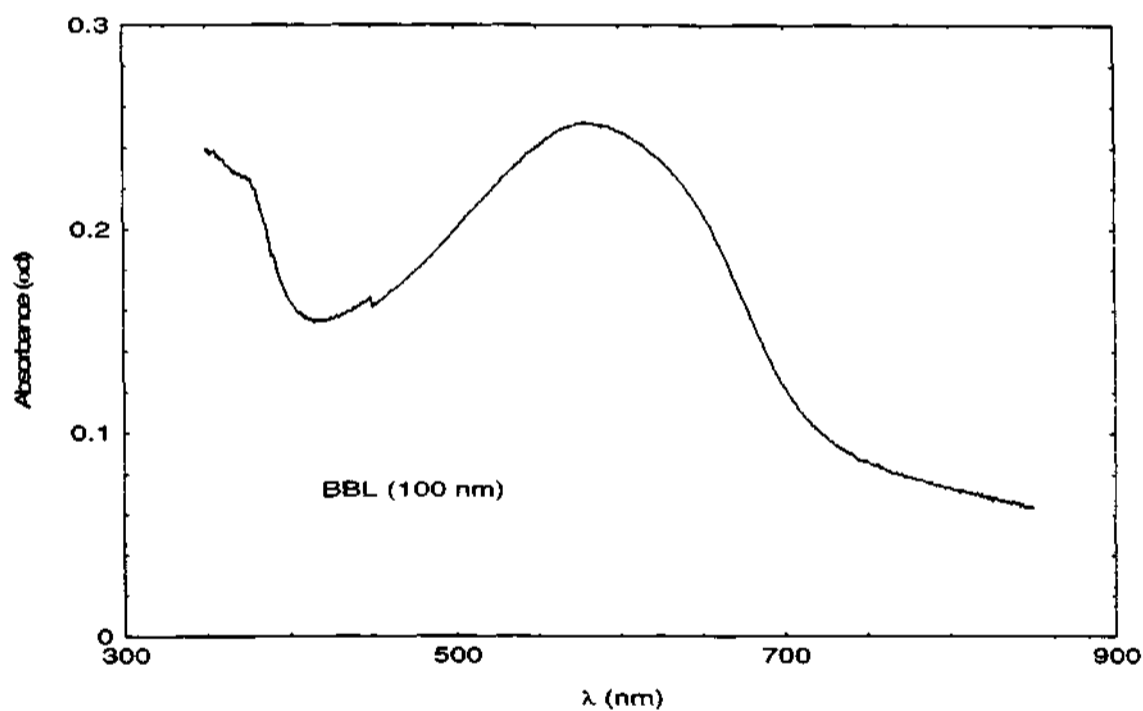


Fig. 4.3 UV-Vis absorption spectra of BBL spun-cast film.

region and is on the higher side compared the conventional conjugated polymers such as PPV and PTH. The intrinsic viscosity $[\eta]$ of BBL in the different solvents was

measured in AFRL, WPAFB by using Cannon-Ubbelohde capillary viscometers and a constant temperature bath. BBL polymers of 8.9 to 30 $\frac{dl}{gm}$ were used to make the thin films. Ladder polymers such as BBL, PBT, PBO exhibit rod-like properties in dilute form, whereas BBB show flexible coil-like in dilute concentrations [146]. The molecular weight of the polymer is around $\simeq 1000000$.

4.2.2 Thermogravimetric analysis (TGA)

TGA was used to verify the moisture sensitivity of BBL thin films. The sample was thoroughly washed prior to any measurement process and the experiments were done under air as well as in inert atmospheres such as argon and nitrogen. The sample starts to decompose above 700⁰C, indicative of its high thermal stability compared to other rigid-rod polymers. The pristine sample does not show any appreciable amount of weight loss both in the temperature range 25 - 300⁰C.

4.2.3 X-ray analysis (X-ray)

The Xray of cast unoriented films BBL was done by using Rigaku diffractometer at JNCASR. The X-ray data were taken at different temperatures ranging from 80 - 600 K. BBL sample, the X-ray data taken at room temperature, shows there is a peak at 4.23⁰, and a sharp peak at 6.53⁰ corresponding to the interplanar distances of 5.223Å and 3.412 Å. The sample shows there is a clear distinct peak at 11.15⁰ corresponds to the interplanar distance of 2.037 Å. This implies that the sample has structurally well ordered than that of sample prior to heat treatment. The conductivity results also reveal that after heat-treatment to above 550 K, there is a drastic change in the conductivity measured either in parallel and perpendicular directions.

The results of X-ray were compared with those of previously obtained [151]. BBL forms a two dimensional lattice of nematic liquid crystalline structure. An orthorhombic cell with cell parameters of $a = 7.87\text{Å}$, $b = 3.37\text{Å}$ and $c = 11.97\text{Å}$. In this film, the rigid chains are expected to form a layered structure across the film thickness, but in a very unusual manner, i.e., the very large molecular plane is stand-

ing perpendicularly to the film surface plane. The reports of BBL, reveal that the molecular planes are standing perpendicular on the film surface and the chain axis is lying parallel to the film surface, resulting in an anisotropic layered structure in the polymer thin films. High degree of anisotropy is expected from the crystal structure (orthorhombic) and morphology [151].

4.2.4 Photoluminescence Spectra (PL)

Fig.shows the PL of BBL cast thin films. The data was taken at room temperature and 100K. In this figure, PL is observed at energies below the band gap of the material when the excitation occurs at band gap energies. The singlet intrachain exciton decay is quite small, indicative of low PL yield. At low temperatures, the peak position shift towards to the lower energy side, indication of the enhancement of excitonic features. The PL yield is quite low < 1 % and implies the large presence of non-radiative transitions.

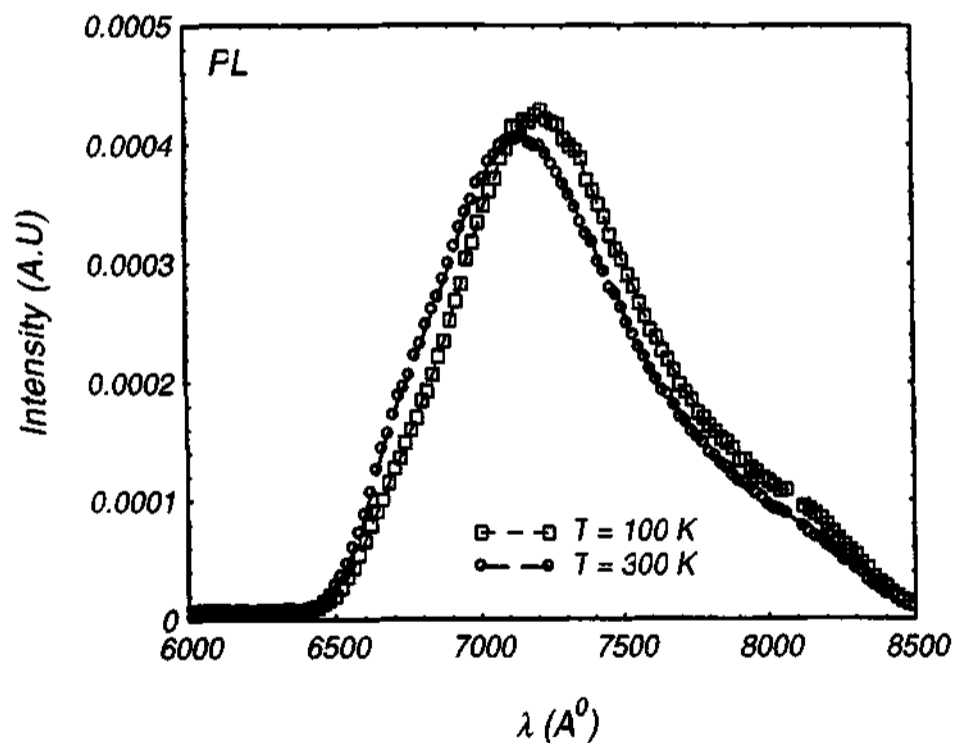


Fig. 4.4 Photoluminescence spectra of BBL at 100K and 300 K.

The spectra is broad, also indicating the local density of electron or hole density of localized states or impurity states. The electroluminescence (EL) in BBL devices is not observed at all due to the existence of non-radiative centers which would quench the luminescence and is consistent with the PL measurements. The traps or localized states may act as non-radiative centers and is discussed in detail in subsequent chapters.

4.2.5 Photo thermal spectroscopy (PDS)

Photo thermal spectroscopy is a group of sensitivity methods used to measure optical absorption (especially around the band tails) and thermal characteristics of a sample. The basis of photo thermal spectroscopy is a photo-induced change in the thermal state of the sample. Light energy absorbed and not lost by subsequent emission results in sample heating. This heating results in a temperature change as well as changes in thermodynamic parameters of the sample which are related to temperature. Measurement of the temperature, pressure or density changes that occur due to optical absorption are ultimately the basis for the photo thermal spectroscopic methods.

Ingle and Crouch classify PDS as one of several indirect methods for optical absorption analysis. Indirect methods do not measure the transmission of light used to excite a sample directly, but rather measure an effect that the optical absorption has on the sample. The term indirect applies to the light measurement, not to the optical absorbance. This is method, in a sense, a more direct measure of optical absorption than optical transmission based spectroscopic signals are directly dependent on light absorption. Scattering and reflection losses do not produce photo thermal signals. Subsequently, PDS more accurately measures optical absorption in scattering solutions, in solids, and at interfaces. This aspect makes it particularly attractive for application to surface and solid absorption studies, and studies in scattering media.

Fig. 4.4 shows the PDS of BBL at room temperature, carried out in Prof. K. L. Narasimhan's laboratory at TIFR, Mumbai. The absorption coefficient is plotted

as a function of wavelength ranging from 600 to 2000 nm. The sample absorbs range from far infra-red region(1900 nm) to visible region 600 nm. This could be due to the existence of localized states located below the band gap of the material. The onset of BBL in PDS around 1000 - 1200 nm does not coincide with the UV visible spectra.

(i) Basic Processes in Photo thermal Spectroscopy

The basic processes is responsible for PDS is shown in the figure. Optical radiation, usually laser, is used to excite the sample [152,153]. The sample absorbs some of this radiation resulting in an increase in the internal energy. The internal energy is dispersed in two different modes of hydrodynamic relaxation.

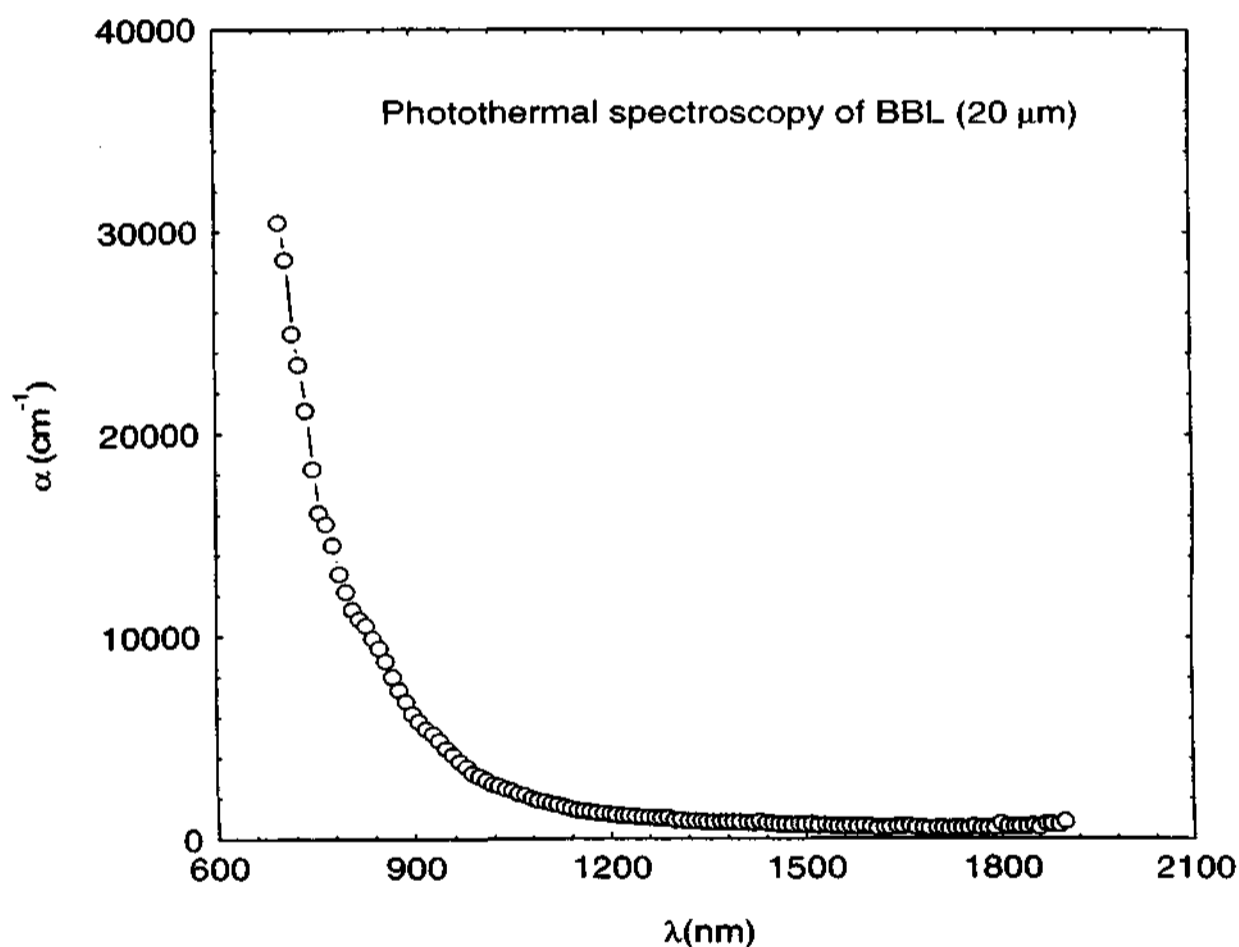


Fig. 4.5 PDS of cast film (15 μm)

The increased internal energy results in a temperature change in the sample or coupling

fluid density. In particular, the sensitive PDS is based on measurement of the refractive index change that occurs with changes in temperature and density of the sample. After the absorption, the molecules are in an excited state. Excited state relaxation transfers energy to the solvent or sample matrix. Radiative relaxation does not result in complete loss of the absorbed energy to the sample. Some of the energy is lost in the form of radiated light. Thermal relaxation transfers the energy to the sample and results in sample heating. Excited species may also form long lived metastable states that trap energy and prevent further optical absorption [153]. This will result in a delayed heating of the sample. The excited state species may also participate in photochemical reactions. This produce heat but also produce new kind of chemical species which alter the thermal and optical characteristics of the sample. The signal is monitored as a function of wavelength. The results of BBL would be discussed in detail in the forthcoming chapters.

The quantitative information can also be deduced from the optical absorption data. The sub-bandgap region ($E < E_g$) is of special interest in quantifying the shallow and deep gap states in the case of amorphous semiconducting materials. Sub-bandgap spectroscopies such as photo thermal Deflection spectroscopy[1, 6] and CPM or SSP have been extensively studied over the past decades. The important reason is the fact that both the techniques are easy to implement and suitable tool for process optimization and characterization of device quality. In certain respects, both the techniques are considered as complementary techniques. PDS is sensitive to surface/interface and bulk states and CPM leads to information primarily on bulk properties. However in combination of these techniques in principle allows one to determine both the surface/interface and bulk contributions. The main objective of this thesis is

- ¶ to determine the individual contribution of the surface/interface and of the bulk to the joint DOS (shallow and deep states)
- ¶ to address the problem of inhomogeneities, i.e., the variation of material parame-

ters of this polymeric system.

(ii) Theoretical and experimental aspects

PDs has been applied to study the absorption behavior of solids, liquids and gases. This technique is highly sensitive and the low sensitivity on scattering effects. Absorbance values as low as possible could be measurable in the range of $\alpha d \simeq 10^{-7}$. This technique probes the gradient of refractive index and it can be expressed in the form:

$$\Delta\phi \propto n^{-1} \left(\frac{\partial n}{\partial T} \right) P_{inc} [1 - \exp(-\alpha d)] \quad (135)$$

In other words it can be rewritten in the form of $\Delta\phi = K \cdot [1 - \exp(-\alpha d)]$ where n is the index of refraction of medium, P_{inc} is the incident power of the pumb beam at a given wavelength λ , $\alpha = \alpha(\lambda)$ denotes the absorption function and d is the film thickness. The thermo deflection signal $\Delta\phi$ is proportional to the rate of optical transitions from all initially occupied states N_i to all possible unoccupied final states N_f separated by an energy $E = h\nu$. $\Delta\phi$ is related to the absorption function [152].

4.3 Essentials of polymer stability

The following are the basic features as important for high thermal stability:

- § Maximum influence of the poly bonding effect.
- § Minimum of low-energy paths allowing rearrangement processes.
- § Maximum bond strength via resonance stabilization.

Ideally fused ring/ladder-type polymers are more stable than the ring chain compounds, since with multiple bonding, chain disruption, etc. However, the stability of ladder-type polymeric systems reaches an optimum.

The rigid, planar, 'double stranded', quasi-two-dimensional structure of BBL suggests that the maximum π electron delocalization, leads to a large third-order optical susceptibility χ as found in picosecond degenerate four-wave -mixing and picosecond

third-harmonic-generation experiments. It has been suggested that the existence of multiple conjugation paths would also result in higher conductivities because carriers could bypass a defect on one of the chains. Due to its coplanar structure this polymer is expected to show an anisotropy, but less than that of graphite. This implies that the conductivity is not only due to intra chain interaction also due to inter chain interactions. The inter chain interactions can be modified and controlled by the external thermodynamical variables such as pressure, temperature etc.

Differences can be observed for BBB and BBL polymer systems in dilute solutions; the former exhibits flexible coil behaviour while the latter demonstrates a rigid rod-like configuration. For the semi-ladder system the introduction of flexible groups[e.g: -O- and -C(CF₃)₂ - mid chain has resulted in an increased solubility and tractability. Ladder(double strand systems) in which two molecular strands are often linked together via complex ring systems."Perfect" ladder polymers require the rupture of at least two bonds within the same ring before major reduction in molecular weight can occur [146].

It involves the chemical modification of main-chain backbone and/or side groups of the macromolecule. The process requires rupture of primary valence bonds and results in reduced molecular weight, cross linking, or cyclization. As a general criterion, degradation adversely affects those polymer properties critical for commercially viable plastics, fibers, or rubbers.

Chapter 5

Experimental Techniques

5.1 Basics of DC conductivity measurements

An accurate measurement of $\sigma(\text{dc})$ of these polymer systems is necessary, since the results are used to predict the transport mechanisms and to derive certain intrinsic material properties.

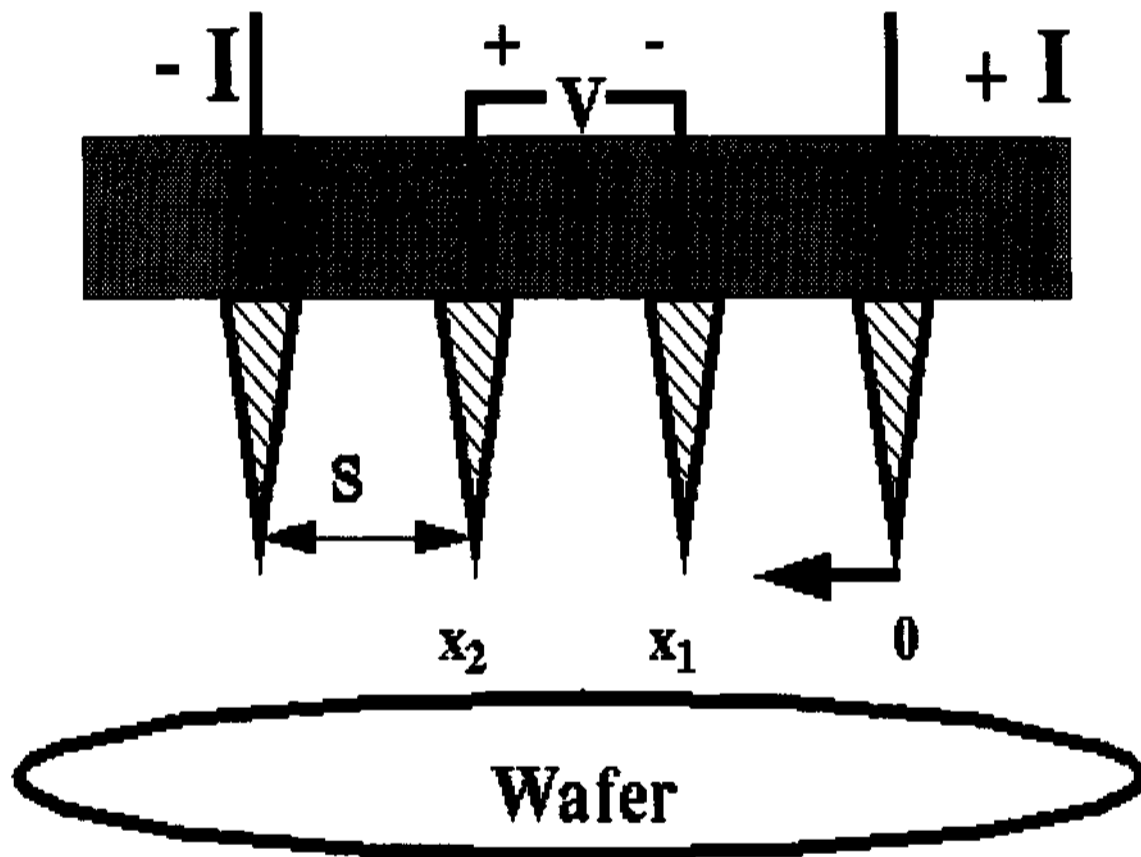


Fig. 5.1 Four probe conductivity measurements in different configurations

An overview of σ measurement principles is presented in this section. Differences measurement methods are adopted depending upon whether the sample is metallic or insulating, regular or irregular shape and other such factors [154–157].

5.2 Four-point probe technique

Resistivity, ρ , is a particularly important semiconductor parameter because it can be related directly to the impurity content of a sample: A standard technique for the measurement of the resistivity of a semiconductor is the four-point probe technique. The four point probe is the apparatus typically used to determine bulk resistivity. It can measure either bulk or thin film specimen, each of which consists of a different expression. This technique is illustrated in the figure. Sample geometries for van der Pauw resistivity and Hall effect measurements. The cloverleaf design will have the lowest error due to its smaller effective contact size, but it is more difficult to fabricate than a square or rectangle [154-156] .

A collinear row of four sharpened gold electrodes are placed in contact with the surface of the semiconductor. The probes are equally spaced by a distance s . A constant current is introduced through the two outer probes and the voltage drop across the two inner probes is measured. In general, the flow of current through the semiconductor is non-uniformly distributed over the cross-section of the semiconductor and is not parallel.

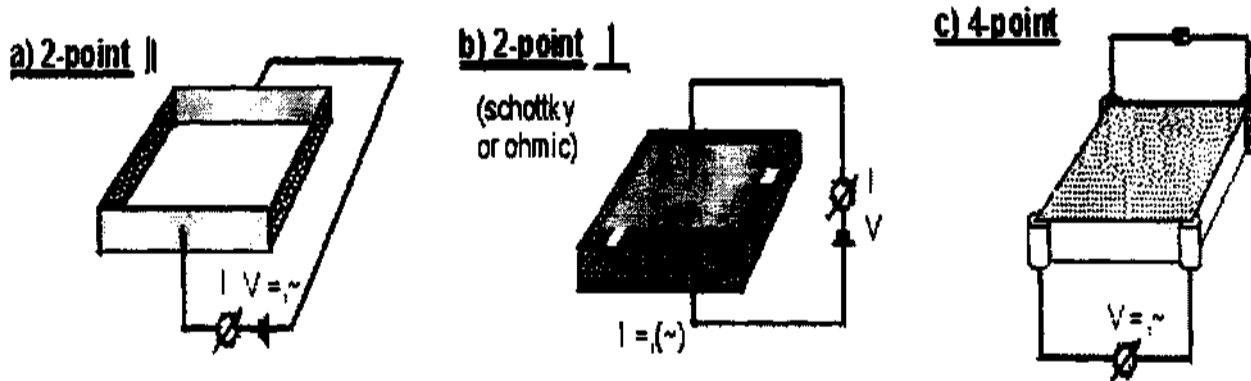


Fig. 5.2 Schematic picture of DC conductivity measurements

The four point-probe technique thus effectively measures an average resistivity across the cross-section of the semiconductor.

Consider an infinite conducting sheet of resistivity ρ_s . If one of the probes carries a current I , the potential at a distance r from it can be written

$$V - V_0 = -\frac{I\rho_s}{2\pi} \ln(r) \quad (136)$$

In this technique, we have the dipole current source with current flow I in opposite directions, so that the potential is

$$V - V_0 = -\frac{I\rho_s}{2\pi} \ln\left(\frac{r_1}{r_2}\right) \quad (137)$$

where r_1 and r_2 represent the distance from each current probe to some point on the sheet. The potential difference between the two (usually) inner voltage measuring electrodes is thus

$$V = -\frac{I\rho_s}{\pi} \ln(2) \quad (138)$$

giving the sheet resistivity of

$$\rho_s = \frac{V}{I} \frac{\pi}{\ln(2)} \quad (139)$$

This analysis is applicable to an infinite sheet. For a finite sheet, the method of images needs to be applied. The formula for the sheet resistivity can be then written $\rho_s = \frac{V}{I} \pi C$ where C is a correction factor which depends on the geometry of the sample [154].

It is usually assumed that the semiconductor sheet is infinitely thin in many cases and the equation is slightly modified due to correction factors. If the slice has a finite thickness w , then the four-point probe will introduce voltage gradients perpendicular to the surface [156,157]. Again correction factors have to be introduced to account for this thickness and it can be written as

$$\rho = \rho_s w = \frac{V}{I} w \frac{\pi}{\ln(2)} F\left(\frac{w}{s}\right) \quad (140)$$

where $F\left(\frac{w}{s}\right)$ is the correction factor which approaches unity as the quantity $\frac{w}{s}$ approaches zero. The four point probe resistance on the top surface of a semiconductor

structure having a vertically non-uniform structure can be obtained by solving the Laplace equation. This complicates the equation furthermore and this can be modeled by assuming that the non-uniformity layer can be considered as a series of distinct layers, each having the uniform resistivity. The result is complicated, but, for the case of a finite layer thickness x on an insulating substrate

$$\frac{V}{I} = \frac{\rho x}{\pi x} \ln \left[\frac{\sinh(\frac{1}{x}s)}{\sinh(\frac{1}{x}s)} \right] \quad (141)$$

If we now have a uniform thin layer of resistivity ρ such that $x \ll S$, that is, the separation of the probes is very much greater than the thickness of the layer, then this expression reduces to

$$\frac{V}{I} = \frac{\rho \ln(2)}{\pi x} \quad (142)$$

The sheet resistance of the layer is

$$\rho_s = \frac{\rho}{x} = \frac{\pi}{\ln(2)} \frac{V}{I} \quad (143)$$

as similarly obtained. The precision of the technique can be improved by making two measurements for each data point. The first is taken with the current flowing through the two outer probes(1 and 4) and the voltage measured across the two inner probes(2 and 3). The second measurement is taken with the current flowing through probes 1 and 3 and the voltage measured across the probes 2 and 4.

5.3 Two-point probe technique

In the case of probes, two probes are placed in contact with the surface of the semiconductor. A small voltage is applied across them and the resistance measured. The measured resistance consists of three parts: the resistance of the probe-semiconductor contact R_c ; the resistance of the semiconductor between the probes R_s ; and the spreading resistance R_{sp} [157]. The spreading resistance is the resistance due to the semiconductor immediately below the contact. For an ideal circular metal

contact of radius r on a semiconductor of local resistivity ρ , the spreading resistance is $R_{sp} = \frac{\rho}{4r}$.

Consider a semiconducting material with resistivity $1000 \Omega\text{cm}$, a probe radius of $10 \mu\text{m}$, and a probe separation of $20 \mu\text{m}$. The spreading resistance is of the order of $10^5 \Omega$, which may be dominant factor in measuring the resistance of the specimen, where the metal-semiconductor resistance is relatively low. It is practically difficult to measure the spreading resistance since a real probe has a poorly defined contact area. It is a complicated function of the resistivity, the probe radius, the conductivity type of the semiconductor and surface conditions. The samples of known resistivity are used for calibration purposes in avoiding the complications involved during the measurement process.

Four probe technique is used to measure the dc conductivity of the samples. The contact resistance is eliminated by this technique and is illustrated in the figure. Four thin gold wires are attached onto the sample surfaces either by mechanical contact or by silver paste to ensure the better contact. the resistance of the sample can be measured by applying either current source or voltage source. In addition to the contact resistance problems, a small random fluctuations exists at the contact joints due to the local temperature gradient. This effect could be eliminated by changing the current direction ($I \rightarrow -I$) and measuring the resistance of the sample as $R = \frac{V_+ + V_-}{2I}$. The conductivity, σ , is given by

$$\sigma = \frac{1}{R} \frac{l}{tw} \quad (144)$$

where l , t , w are the sample length, thickness and width respectively.

The resistivity of a material is its fundamental property which gives an idea about the concentration and mobility of the charge carriers in the material. The resistivity measurement system uses four probe method, both in collinear and van der Pauw geometry. The current through the two probes is sent using Keithley's 220

current source and the resultant voltage across the other two probes is measured using Keithley's 2001 digital multimeter. The temperature of the sample is controlled using Lakeshore temperature controller and is stable within 100 mK. The resistivity can also be measured in the temperature range of 15 to 600 K.

Polymer-metal interactions play an important role in determining the electrical and opto-electronic properties. The parameters which affect the charge transport properties are the work function of the electrode, and the Fermi level, ionization energy, and electron affinity of the conjugated polymer, and in the case of multilayer or bilayer devices, the polymer-polymer interfaces. The work function ϕ of a metal can be described as the energy required to remove an electron from the Fermi level to the state of rest outside the surface of the metal (vacuum level). However, the work function consists of two parts (i) the volume contribution (the energy of an electron due to the periodic potential of the crystal and the interaction of the electron with other electrons) and a surface contribution (due to the possible existence of a dipole layer at the surface). Thus workfunction is typically very sensitive to the surface dipole layer. Any modification in the surface layer will change the surface charge distribution and hence there is a change in the dipole moment due to the oriented or unoriented dipoles present in the surface layers. This features lead to a considerable amount of changes in ϕ_m . It is important to note that the workfunction is a statistical concept and represents the weighted average of the energies necessary to remove an electron from the valence and conduction bands, respectively. In particular polymer-polymer interactions play a major role in making the devices such as blend systems. The thickness of the interfacial can be viewed as the degree of immiscibility of the polymeric systems. Higher the degree large the thickness of the interfacial layers. Similarly the workfunction is also comprised of bulk and surface contributions. The ionization energy (I) of a semiconductor or insulator is the energy required to ionize an electron from the highest occupied molecular orbital level (i.e., top of the valence band)

to vacuum level. The term electron affinity χ_s can be defined as the energy difference between the vacuum level and the bottom of the conduction band just inside the surface. χ_s is also sensitive to the surface dipoles. The differences between I and χ_s gives the bandgap of the semiconductor. In the conjugated polymers, the Fermi level E_F , is not an intrinsic property of the material. It depends on the nature and the concentration of the localized states. As a consequence, it is practically to determine for intrinsic (undoped) conjugated polymer, although electrochemical methods have been applied to measure doped polymers. In principle, I can be determined from the photoemission threshold. However, only limited number of conjugated polymers have been measured in this way. χ_s is even more difficult to determine directly. It can be generally inferred from the relationship $\chi_s = I - E_g$, or electrochemical measurements.

Basically there are three types of contact may form between the metal electrode and the polymer depending on the relative positions of the Fermi level (workfunction) of the electrode and the ionization potential and electron affinity :

(i): Neutral contact: It is defined as the contact in which both the work functions of the electrode and the sample are the same, whereas the electrons or holes don't pile up at the region of the contact.

(ii) Ohmic contact: An ohmic contact on a semiconductor is defined as the contact impedance or resistance is negligible when compared to the total impedance or resistance of the sample (p-type) and it is expected that the bulk properties does not vary much. In other words, an ohmic contact can supply the necessary amount of the current for which it obeys Ohm's law and does not prevent the carriers from leaving the material. This can be assumed that the interfacial layer or interfacial states are formed, the condition for forming an ohmic contact is $I - \phi_m \leq 0$ for hole injection and $\phi_m - \chi_s \leq 0$ for electron injection. The typical range of I for conjugated polymers is between 4.8 to 5.4 eV and χ_s is from around 2.5 eV. Thus to form an ohmic contact, a high workfunction metal ($\phi_m > 4.8$ eV) is need for hole injection and a low workfunc-

tion metal ($\phi_m < 2.5$ eV) is required for electron injection. Few examples of high work function and low work function metals are Pt, Au, ITO... and Cu, Mg, Ca...etc (Al). The problems encountered with the low work function metals are highly reactive and in fact that the injection properties into the semiconductor are not only affected also they are modified by an appreciable amount. The energy band curves of the sample the sample bend upward near the surface, and as a result, holes are piled up near to the surface providing a reservoir of the charges. The current will flow through the recombination process, and the contact is ohmic.

(iii)Blocking or rectifying contact: It is defined as the contact impedance or resistance is larger when compared to the total impedance or resistance of the sample (p-type) device and the bulk properties are strongly affected by this type of contact. The energy band curves bend toward the contact, leaving very few holes near the contact. The application of an external bias can either flatten the bands near the contact or sharpen the curvature by changing the direction of the applied voltage. This is similar to a p - n junction where the current increases with the electric field exponentially in the forward bias and almost zero in the reverse direction. Similarly the same concept can be applied to an n -type sample, workfunction of the samples is greater than the electrodes and smaller for blocking contact. If $I - \phi_m$ or $\phi_m - \chi$ is large a barrier is formed between the metal and the semiconductor. This type of contact is called a rectifying contact. In semiconductor physics, this kind of barrier is often referred to as a Schottky barrier. A Schottky barrier is often described by two parameters: the barrier height and the thickness of the depletion region. for holes, the barrier height is $\phi_b = I - \phi_m$ on the metal side and $V_D = \phi_m - \phi_p$ on the polymer side when no external bias is applied to the barrier, where ϕ_p is the workfunction of the polymer and the term V_D is the diffusion potential. It represents the built-in-potential in the absence of any current flow through the polymer. However, this quantity cannot be measured directly simply by means of an electrometer or voltmeter to the system (A

voltmeter simply measures only the relative difference between the two Fermi levels).

5.4 Photoconduction mechanism

Absorption of light by a semiconductor will result in the production of electrons and holes. Initially, the free carriers produced in this way have larger kinetic energy in their respective bands. Then they would relax towards the band edge, initially by the emission of longitudinal optical (LO) phonons until they are within one LO phonon energy of the band edge. The time scale for this to happen is within 10^{-14} to 10^{-12} [158]. Following this, energy relaxation occurs by acoustic phonon emission. This is a much slower process, occurring in times of the order of 10^{-9} . During this time, the carriers may be captured by the impurities or recombine with another carrier. There is an increase in number of the carriers on the application of light and hence there is a change in the electrical conductivity of the semiconductors. This is known as photoconductivity. Second, the excess photogenerated carriers will recombine radiatively (electrons and holes) and may generate light is known as photoluminescence. This is one of the powerful tools in the characterization of semiconductors. they may also dissipate heat in the phonons due to nonradiative process, which can be detected by thermal wave spectroscopy. The increase in the conductivity of a semiconductor following the absorption of light (photoconductivity) can be measured by applying voltage across the sample. In general, the optical illumination will increase the electron and hole concentration by Δn and Δp , respectively. This will result in a change in the conductivity of

$$\Delta\sigma = e\mu_e\Delta n + e\mu_h\Delta p \quad (145)$$

where μ is the mobility of the charge carriers.

It is be noted that the diffusion currents will also be set up due to the non-equilibrium generation of the charge carriers. This will be ignored by assuming a uniform generation of carriers and application of high electric fields. In the case of extrinsic n-type

semiconductor, the minority carrier excess concentration is given by

$$\frac{d}{dt}(\Delta p) = g_{opt} - \frac{\Delta p}{\tau_{p0}} \quad (146)$$

where τ_{p0} is the minority carrier lifetime. The excess majority carrier concentration is obtained from the charge neutrality condition is $\Delta n = \Delta p$.

Consider light of intensity I on a semiconductor of thickness d and optical absorption coefficient α . After travelling a distance d in the crystal, the intensity of the light will be $(1-R)I\exp(-\alpha d)$, where R is the intensity of the reflection coefficient at the front face of the crystal. Ignoring reflection from the back face of the solid, the optical power absorbed per unit surface area is given by $(1-R)[1-\exp(-\alpha d)]\frac{I}{\hbar\omega}$, where, $\hbar\omega$ is the photon energy. If the product αd is small, then we have uniform light absorption in the semiconductor and the carriers generated per second per unit volume is

$$(1-R)[1-\exp(-\alpha d)]\frac{I\eta}{\hbar\omega d} = (1-R)\frac{\alpha\eta I}{\hbar\omega} = g_{opt} \quad (147)$$

where η is the quantum efficiency, the probability of the absorbed photon will produce a free carrier. In equilibrium, $\frac{d}{dt}\Delta p = 0$, so that $\Delta p = g_{opt}\tau_{p0}$ and

$$\frac{\Delta\sigma}{\sigma} = g_{opt}\tau_{p0}\frac{\mu_e + \mu_h}{n_0\mu_e + p_0\mu_h} \quad (148)$$

so that the ratio of

$$\frac{\Delta\sigma}{\sigma} = \frac{\Delta p(1 + \frac{\mu_e}{\mu_h})}{p_0 + \frac{n_0\mu_e}{\mu_h}} \quad (149)$$

The minority carrier lifetime can be observing the rise or fall of the photoconductivity when light is switched on or off. For example, suppose we irradiate the semiconductor with light and steady-state conditions have been achieved, once the light is switched off at the time $t = 0$. Then

$$\frac{d}{dt}(\Delta p) = -\frac{\Delta p}{\tau_{p0}} \quad (150)$$

and

$$\Delta p = \Delta p_0 \exp\left[-\frac{t}{\tau_{p0}}\right] \quad (151)$$

so that the photoconductivity decays exponentially.

The phenomenon photoconductivity may arise from the impurity states (extrinsic photoconductivity). It is not necessary to produce a transition from the ground state of the bound impurity electron directly into the conduction band or valence band. If the absorption produces a transition to an excited bound state, then thermal energy may be sufficient to ionize the bound charge carrier into the relevant band and the process is known as photothermal ionization spectroscopy [153]. It is one of the sensitive techniques for to find out the unknown parameters of the shallow levels with excellent accuracy. The phenomenon is usually observed when the concentration of charge carriers is large upon photoirradiation than in the normal thermal equilibrium states. If the light of weak intensity is irradiated, a recombination process of charge carriers is negligible and hence the photostationary concentration of charge carriers, $n(\text{cm}^{-3})$ is given by $n = n_0\tau$, where n_0 is the number of charge carriers generated by the photoirradiation per second per unit volume

$$J_{ph} = n_0\tau e\mu E \quad (152)$$

If the intensity of light be I_0 (photons/cm²s), the photoabsorption coefficient of the sample be α cm⁻¹, the quantum yield for the photogeneration of charge carriers be η , the thickness of sample (distance between the electrodes) be l cm⁻¹

$$n_0\tau Sl = SI_0[1 - \exp(-\alpha l)]\eta\tau J_{ph} = \frac{1}{l}I_0[1 - \exp(-\alpha l)]\eta\tau e\mu E \quad (153)$$

when the light is absorbed on the surface of the sample(α),

$$J_{ph} = \frac{1}{l}I_0\eta\tau e\mu E \quad (154)$$

the distance across that the charge carriers drift during their lifetime is termed the range (Schubweg). Both the concentration of charge carriers and the drift mobility of charge carriers can be quantitatively evaluated by means of transient measurement using a pulse light. Either the electric charge induced on the electric current that flows the external circuit is measured.

5.4.1 Monomolecular recombination

In the case of monomolecular recombination is proportional to the excess of charge carriers and therefore the rate equation for the rise process is given by $\frac{dn}{dt} = g_n - \frac{n}{\tau_n}$, where g_n is the generation rate of charge carriers. It is assumed to be constant during the process and is equal to $\alpha I_0 \eta$, where I_0 is the intensity of radiation generation ($\frac{W}{cm^2}$). The rate equation for the holes also obtained based on the same approach. If $g_0 = 0$, the equation represents the decay curve. Assuming that τ_n is independent of n , the solution of these equations can be written as

$$n = n_0[1 - \exp(-\frac{t}{\tau_n})] \text{ --- ---risen} = n_0 \exp(-\frac{t}{\tau_n}) \text{ --- ---decay} \quad (155)$$

where n_0 is the steady state value of excess electrons created by optical excitation and its value can be easily obtained by putting $\frac{dn}{dt} = 0$; that is $g_n \tau_n = n_0$. Thus in the trap-free case and when the diffusion currents are negligible, the rise and fall can be represented by an exponential expression. In this case, the time constant τ_n represent the average mean lifetime of the electrons. This means that it is a freetime that electrons spend in the conduction band taking part in the conduction process. Obviously it is a time between two successive collisions with holes and it is given by $\tau_n = [S_r \langle v \rangle p]^{-1}$, where $\langle v \rangle$ is the average relative motion of electrons with respect to holes, p is the hole density, S_r is the recombination cross section is a function of temperature. The large variation in the capture cross section helps to explain the variation in the time constants. In a wide band-gap semiconductors, the density of optically active traps is considerably high and frequently recombination is dominated by flaws or defects. The concept of carrier capture was developed. It has been shown

that the continuity equation can also be applied in this situation. The major difference in this case is that the lifetime than band-to-band transitions. there is no other competing mechanism, the mean lifetime of the electrons is given by

$$\frac{1}{\tau_n} = R_n = [N_t - n_c] \langle c_n \rangle \quad (156)$$

where $N_t - n_c$ is the number of flaws and $\langle c_n \rangle$ is the mean capture cross section by where N_e is the density of states function for the conduction band and it is defined as $N_e(E) = 4\pi \frac{(2m_e)^{3/2}}{h^3} (E')^{1/2}$, where E' is the energy measured with respect to the bottom of the conduction band, $C_1(E)$ is the probability of capturing an electron from the conduction band, and P_c is the probability of the state is occupied by an electron. A considerable variation in two parameters, namely the density of states of recombination centers and their capture cross sections is observed. the recombination center density varies from 10^{12}cm^{-3} (even for purity and good quality materials) to 10^{18}cm^{-3} . Similarly cross section also varies from 10^{-12}cm^{-2} to 10^{-18}cm^{-2} . Naturally the lifetime is also a function of temperature.

5.4.2 Bimolecular recombination

In this case the recombination rate is proportional to the square of the excess of charge carriers instead of directly proportional to it. This is very familiar Auger process for band-to-band transitions in heavily doped semiconductors. There are extensive calculations of Landsberg. On this type of recombination, Even in a pure direct but narrow-band-gap semiconductor, this process was found to be dominant. In this case, the rate equations for rise and decay parts are given by the expressions

$$\frac{dn}{dt} = g_n - R_{BM}n^2 \quad (157)$$

$$\frac{dn}{dt} = -R_{BM}n^2 \quad (158)$$

solving these and taking into account the initial conditions, equations for the rise and decay curves are given by

$$n = n_0 \tanh r(g_n R_{BM}) n = n_0(1 + n_0 R_{BM} n^2) \quad (159)$$

The value of n_0 is obtained by putting the rate equation equal to zero, $n = (\frac{g_n}{R_{BM}})^{\frac{1}{2}}$.

It is clear from these equations that,

- the rise and decay curves are assymterical
- the intensity of the equilibrium value of photocurrent is proportionla to the square root of the incident radiation.
- The initial part of the rise curve is directly proportional to time.

None of the above mentioned properties are considered to be characterestic of the bimolecular process; but the three processes together can be used to identify the presence of bimolecular processes. It is possible only a fraction, f , of the total electrons are recombined in a linear process and the remaining, $1-f$, are recombined in bimolecular process. Then the rate equation becomes,

$$\frac{dn}{dt} = g_n - fR_n n - R_{BM}(1-f)n^2 \quad (160)$$

and the solution for rise part will be given as

$$n = \frac{n_0[a_1 + (a_1^2 + 4b_1g_n)]^2}{a_1 + (a_1^2 + 4b_1g_n)^{\frac{1}{2}} \coth[\frac{t}{2}(a_1^2 + 4b_1g_n)^{\frac{1}{2}}]} \quad (161)$$

and for decay part

$$n = \frac{n_0 \exp(a_1 t)}{1 + (n_0 b_1 a_1)(1 - \exp(-a_1 t))} \text{decay} \quad (162)$$

where $n_0 = \frac{2g_n}{[a_1^2 + 4b_1g_n]^{\frac{1}{2}} + a_1}$, $a_1 = fR_n$, $b_1 = (1-f)R_{BM}$. In fact there exists several other complicated mechanisms such as phonon-assisted band-to-band recombination.

5.4.3 Higher-order reombination processes

A typical example is the Auger process when the density of photoexcited charge carriers is very high as when the sample is irradiated by a laser beam (photon density is

approximately 10^{16} . Junanrkar and Alfana [159,160] observed a recombination rate given by

$$\frac{dn}{dt} = -cn^3 - n \quad (163)$$

It has also been observed that in some cases the recombination rate is proportional to an odd fractional power of n , recombination even band-to-band, is a complicated process, because of variety of phenomena [e.g. radiative and non-radiative] are involved [160]. The mechanism could include emission or absorption of one or more phonons (in the case of indirect band gap semiconductors), or recombination could take place via excitons either free or bound to donor (acceptors) as the case may be. Frequently, recombination can also be activated through the traps, dislocations or defects.

5.4.4 Role of traps

The presence of traps not only makes the photoresponse slow and causes the relaxation curves to deviate from an exponential nature but also photocurrent varies with non-linear behavior. In this case one has to consider the effects of a single set of recombination centers trapping levels, independently, both under low and high level injection of photocarriers. In this model the number of excited electrons and holes is either higher or lower than the number of electrons trapped in the recombination centers. However this model is not frequently valide because of no direct verification through the experimental results. This chapter reveals that the traps significantly affect the photoresponse of the carriers which are generated. A large variety of informations are available that the materials show the photocurrents have been insensitive to temperature or at least in certain specied ranges and in others they have been found to increase or even decrease with temperature.

5.5 Steady State Photocurrent Measurements

I_{ph} measurements were carried out in vacuum conditions using sandwich type devices of ITO/Polymer/Al with the light incident on the ITO side, using sensitive lock-in techniques as well as dc methods. In the planar (surface) geometry, the polymer was deposited on quartz substrates. After processing it to the base form, metal

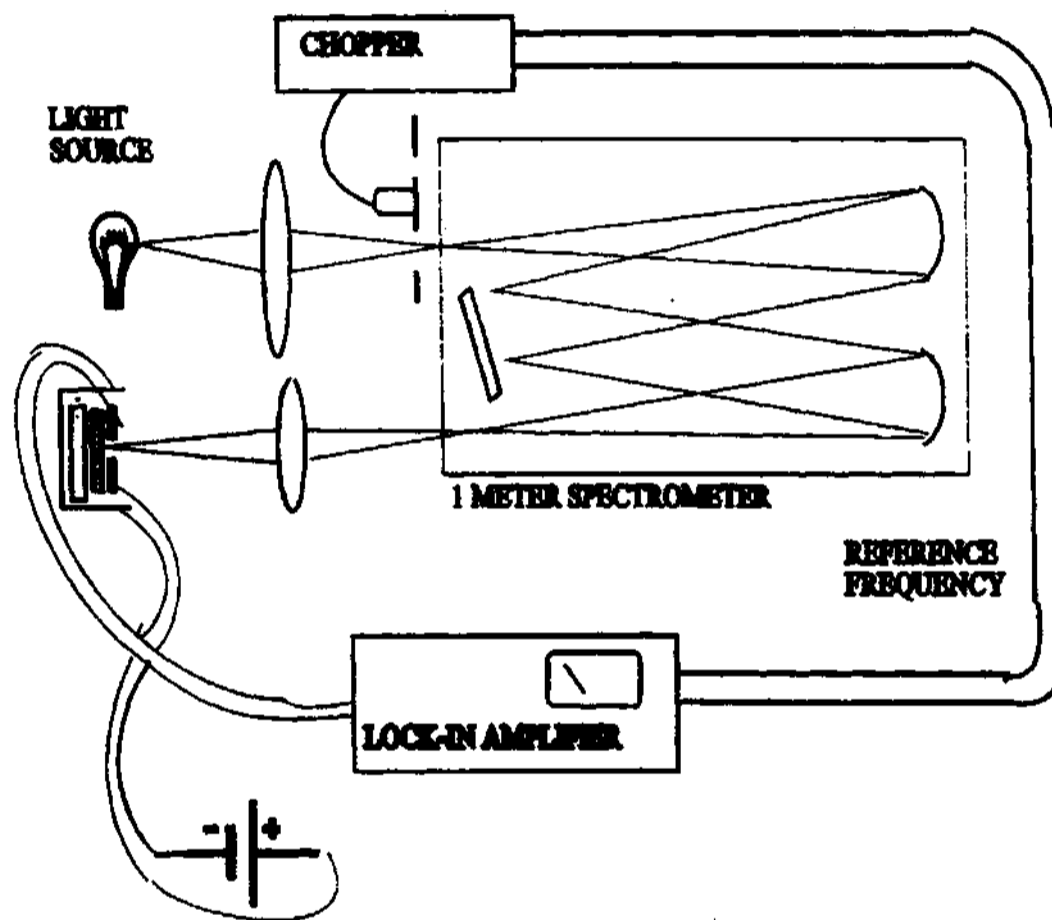


Fig. 5.3 Experimental set up for steady state photocurrent measurements

electrodes, 0.1 mm apart, were deposited on the surface. Spectral response of the photocurrent was carried out using a 150 W xenon lamp along with a monochromator using the lock-in technique. Temperature dependent measurements $I_{ph}(T)$ were carried using a closed cycle refrigerator offering a wide temperature range capability

of 10 K - 500 K, with the sample mounted alongside a calibrated thermometer, on the cold head of the cryostat fitted with quartz windows. 5 mW diode lasers at 532 nm and 473 nm were used as the light source for the $I_{ph}(T)$ measurements.

5.6 Transient photocurrent measurements

The transient response essentially represents the photo-induced current decay due to a single laser pulse. For a single relaxation process the decay is largely exponential. However, the presence of traps and defect states results in a deviation from a simple exponential.

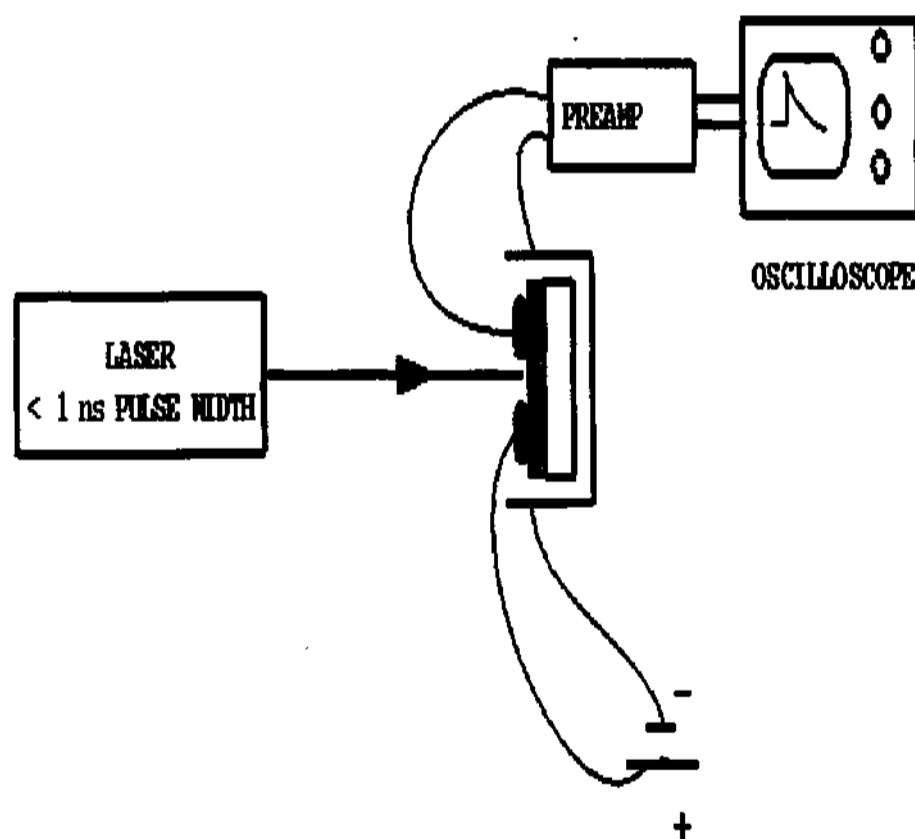


Fig. 5.4 Experimental set up for transient photocurrent measurements

Several parameters which are difficult to evaluate by other independent methods (density and distribution of optically active traps, their cross section, etc) are involved in

the kinetics of the carriers. These parameters can vary from sample to sample and are very sensitive to the external factors such as temperature, level of radiation, effects of contacts, and surface conditions. The transient curve is seriously influenced by the contact properties and most often is ignored. when the injecting contacts are present, then the properties of the semiconductor under them are modified because, carrier concentrations are changed, Space charges are created, Diffusion currents are set up. The kinetics of the charge carriers leads to a set of non-linear different equations, and it is known that there is no closed solution for such a system. Charge carriers are trapped in the centres and re-ejected to either conduction band or valence band. This kind of delayed contribution in the relaxation process is expected, however, mathematical analysis of the delayed equation is not at such a level that it can be used directly for the present problem.

Transient decay measurements were performed on BBL samples in the planar auston-strip configuration using 10 ns pulse laser at 532 nm, 10 Hz repetition rate and a 54520A HP digitaloscilloscope. The temporal resolution for the transient measurements was around 20 ns.

Chapter 6

Experimental results: DC conductivity of BBL

The results and analysis of dc conductivity σ (T) measurements of BBL is presented in this chapter [161]. σ (T) of Oriented and isotropic BBL films and fibers were studied in different geometries to ascertain anisotropic features. These measurements carried out in different forms of BBL and are necessary to develop an understanding of the processes controlling bulk properties such as conductivity in ladder polymers.

An added aspect which is involved in the sigma studies of BBL is the effect of heat treatment. The polymer is basically thermally stable upto 700 K as far as the chemical and mechanical properties. However, large changes in electronic properties are observed upon thermal excitation. The sigma properties in relatively high temperature regime hitherto has not been closely studied for a conducting polymer, primarily due to lack of thermal stability. The fully conjugated ladder polymer poly (benzimidazobenzophenanthroline) BBL provides a model system to study the electronic properties in the high temperature because of its stability at temperatures up to 600°C in air and 700°C in nitrogen and the processability by which thin films and fibers of micron sized diameter can be obtained [144,145]. These polymers, in the form of films or fibers, due to their high molecular weight, display good mechanical properties (high tensile strength, high modulus) and exceptional solvent chemical resistance and high intrinsic viscosity ($8.9 \frac{dl}{gm}$) [144–146]. The polymer has a repeat unit which possesses a double-stranded chemical structure consisting of aromatic naphthalenic and benzenoid units and alternating bond lengths of imines in the neutral ground state. Recently wide angle x-ray measurements of BBL films have revealed scattering patterns suggesting that molecular chains are arranged in a layered configuration with

their molecular planes almost perpendicular to the film surface.⁶ It is expected that the ladder-like BBL polymer chains form a layered structure across the film thickness like other stiff polymers [58,?]. The high degree of coplanarity is reflected in the anisotropy of conductivity even for samples with film thickness ranging up to 15 μm with the in-plane conductivity greater than three orders of magnitude than the out of plane conductivity.^{7, 8} The absorption spectrum shows the onset of π - π^* transition at around 1.68 eV with a broad absorption maxima at about 1.9 eV. [151] The broad transition spanning over a range of 0.22 eV was attributed to the wide distribution of length scales of the conjugated system and other broadening mechanisms arising from the disorder in the system. The photocurrent studies also revealed the band edge observed in the absorption spectra but show subtle differences with respect to the photon energy when the measurements are carried in the surface and sandwich configurations.

It is also been observed that dc conductivity in pristine BBL films depends on ambient conditions and varies from $10^{-11} \frac{\text{S}}{\text{cm}}$ to $10^{-14} \frac{\text{S}}{\text{cm}}$. Some of the methods to enhance the conductivity in BBL have been through chemical doping, ion implantation, pressure treatment, pyrolysis, and heat treatment. Humidity dependent studies reveal surface effects which dominate the transport process. However, the thermally induced processes are more pronounced with conductivity changing by nearly seven orders in magnitude at room temperature when heated to 625 K. In this paper we study the thermally induced electronic conductivity closely and speculate on the mechanism leading to this enhancement. The temperature dependence of the conductivity and the stability of the electronic properties depend on the sample history and morphological aspects. Polymer samples in film and fiber forms are studied to resolve these unique features. The anisotropy in conductivity and the dependence on ambient conditions of the enhanced conductivity are also studied.

The cast films of 20 μm thickness and oriented fibers of 15 μm in diameter were

used for the present studies. Films were obtained from the polymer solution with methane sulfonic acid as the solvent. The dc conductivity of the films as well as fibers were measured by the standard four probe and two probe methods. The conductivity cell consists of four electrodes with spring loaded arrangement specially designed for reliable high temperature measurements under high vacuum. The contact region on the samples were coated with gold for uniformity and measurements for resistance were done in the ohmic region from the current-voltage curves. The temperature was monitored by the suitable thermocouples and RTDs along with a digital Keithley multimeter (model 2001) and current was measured using a Keithley 6512 electrometer. Fig. shows the experimental set up for DC conductivity measurements. The measurements were carried out for a wide range of temperature as possible with the sample resistance of $10^{12}\Omega$ as the limit of measurements.

6.1 RESULTS AND DISCUSSION

The room temperature conductivity of the BBL as measured by four probe conductivity of cast films with equidistant electrodes on the plane of the film, $\sigma_{\parallel} \simeq 10^{-8} \frac{S}{cm}$. The conductivity perpendicular to the film, $\sigma_{\perp} \simeq 10^{-12} \frac{S}{cm}$ and that of the fiber, with the electrodes placed along the fiber axis, $\sigma_{fib} \simeq 5 \times 10^{-7} \frac{S}{cm}$. The values of the conductivity in different configurations reveal the anisotropy present in cast films. The source of anisotropy could arise from extrinsic effects leading to modification of surface states or can be intrinsic in origin. The importance of these extrinsic effects can be studied by the temperature dependence of the anisotropy. The conductivity σ of the film and fiber in different configurations as a function of temperature, T is shown in Fig. 6.1. Fig. 6.1 shows that the plot of $\sigma_{\perp}(T)$ and the arrow traces the thermal cycle in the measurement process. The predominant features accompanying the cycle of measurement is the presence of large hysteresis in $\sigma(T)$ between the initial heating process and the subsequent cooling and warming process. There was no discernible hysteresis in $\sigma_{\perp}(T)$ upon repeated heating and cooling after the initial first round.

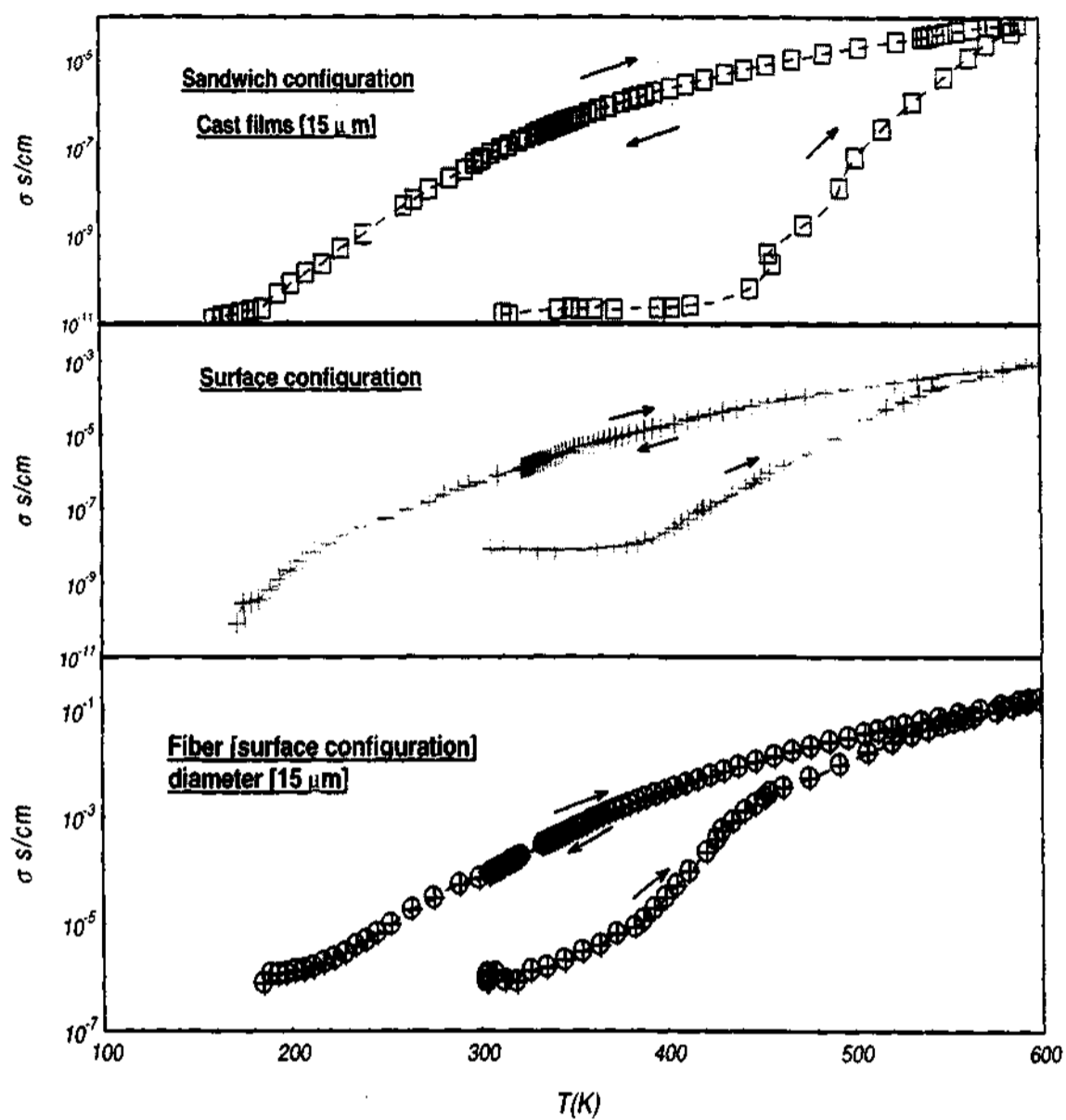


Fig. 6.1 $\sigma(T)$ as a function of temperature for fiber (A), parallel (B), and perpendicular (C) configurations. The arrow indicates the thermal cycle, "I" indicates first round of heating and cooling, and "II" indicates second round of heating and cooling. The chemical structure of BBL is also depicted in the inset.

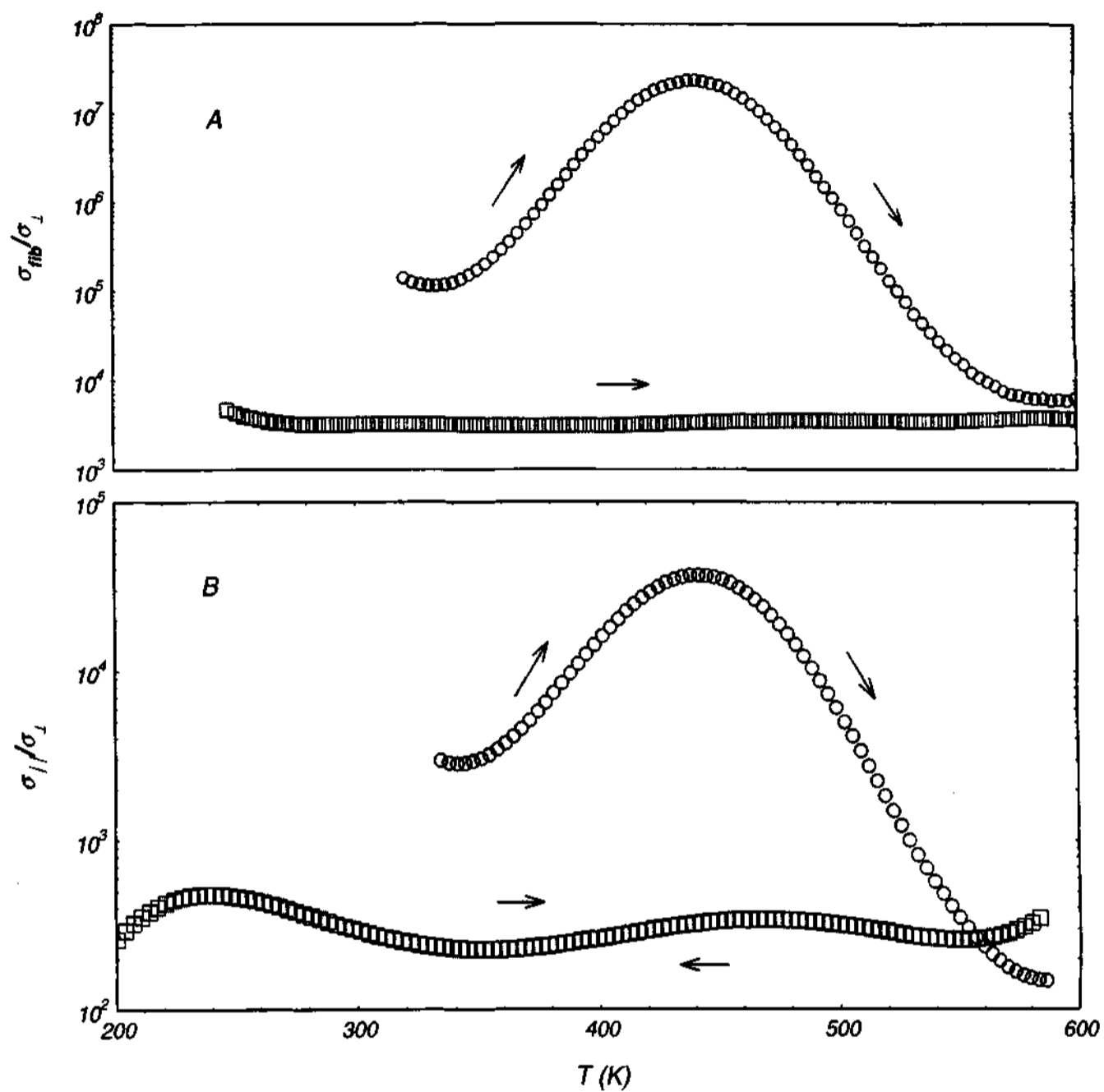


Fig. 6.2 Anisotropy in conductivity as a function of temperature for the entire thermal cycle (A) $(\sigma_{\parallel}/\sigma_{\perp})$ vs T , (B) $(\sigma_{\perp}/\sigma_{\parallel})$ vs T ; The arrow indicates the thermal cycle, "1" indicates first round of heating and cooling, and "2" indicates second round of heating and cooling.

However, if the sample is heated in the first round to a T_{max} lower than 600 K, appreciable hysteresis is obtained for $\sigma_{\perp}(T)$ during the subsequent cooling and warming cycles. The $T_{max} \simeq 625$ K, the temperature corresponding to a minimum in the area of the hysteresis between the first round cooling and second round heating, can be assigned to the maximum value of an energy barrier which is thermally accessible for increasing the conductivity. Preliminary thermally stimulated current measurements also reveal peaks indicative of well defined trap energy levels.

The conductivity measurement of the sample with the probes along the surface, i.e., $\sigma_{\parallel}(T)$ showed similar behavior as shown in Fig. 6.2(A). However, the subtle differences become more obvious in the anisotropy, $\frac{\sigma_{\parallel}}{\sigma_{\perp}}$ as a function of temperature. The anisotropy profile as a function of temperature is shown in Fig. 6.2(B) and shows a broad maximum centered around 430 K. $\sigma_{\parallel}(T)$ increases more rapidly than $\sigma_{\perp}(T)$ for $T > 430$ K and the ratio $\frac{\sigma_{\parallel}}{\sigma_{\perp}}$ settles down to 400 as the temperature is increased. The ratio is fairly independent of temperature subsequently on cooling and re-heating. The anisotropy decreases by three orders in magnitude after the thermal treatment at room temperature.

Measurements done on fiber also qualitatively reveal similar $\sigma_{fib}(T)$ behavior as depicted in Fig. 6.1. The magnitudes of the conductivity, however are shifted by three to four orders in magnitude with $\sigma_{fib} \simeq 1 \frac{S}{cm}$ at $T = 600$ K. The high conductivity value is expected due to an increased degree of crystallinity, order and chain orientation. The anisotropy profile as a function of temperature is shown in Fig. 6.2(A). The $\frac{\sigma_{fib}}{\sigma_{\perp}}$ shows a broad maximum centered around 430 K. $\sigma_{\perp}(T)$ increases more rapidly than $\sigma_{fib}(T)$ for $T > 430$ K and the ratios settle down to 3500 as the temperature is increased.

The conductivity mechanism changes prior to sample getting exposed to $T \simeq 600$ K and thereafter as evidenced from Fig. 6.1 and Fig. 6.3. The mechanism crossover can also be bench marked in terms of the temperature dependence of the anisotropy. As the sample is heated the crossover temperature can correspond to the point where the

anisotropy ratio $\frac{\sigma_{\parallel b}}{\sigma_{\perp}}$ decreases to a constant value of ≈ 3500 and is nearly temperature independent.

The anisotropy present prior to heating can be considered to arise from extrinsic

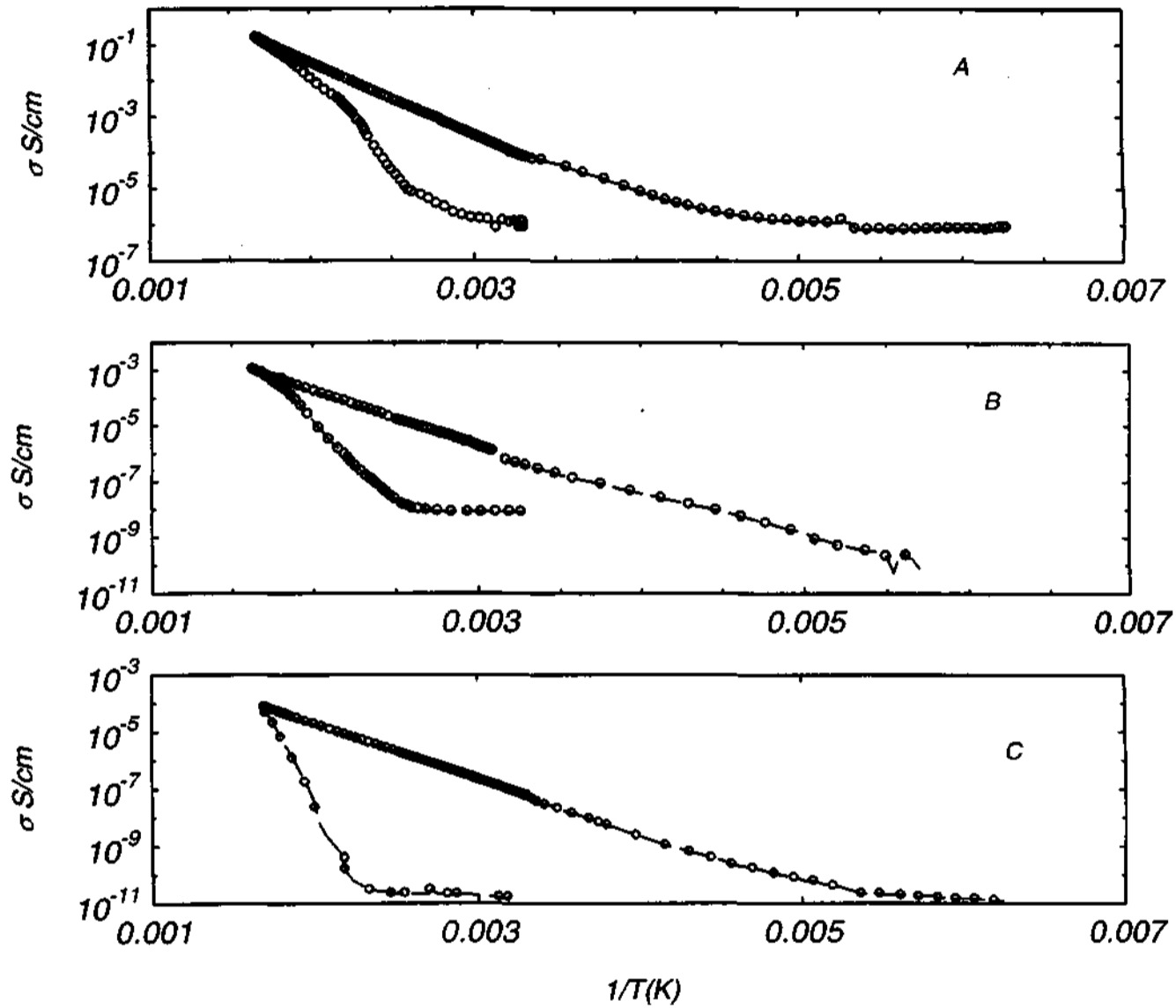


Fig. 6.3 $\sigma(T)$ for the entire thermal cycle in log scale as a function of reciprocal of temperature for different configurations fiber (A), parallel (B), and perpendicular (C) respectively and arrow indicates the thermal cycle. The dashed and solid lines indicate fits to a simple activation behavior model.

ambient sources which preferentially modifies the surface compared to the bulk and

gives rise to the peculiar temperature dependence with a rounded maximum around 430 K. The anisotropy after the sample is heated to 625 K and maintained in vacuum conditions can correspond to some sort of intrinsic anisotropy of the system as indicated by the lack of temperature dependence.

The time dependence of conductivity mentioned above also supports the view of different mechanisms for the charge transport process. The conductivity value for all the systems at room temperature, in vacuum conditions after heating, is fairly constant, however the value gradually drops over a period of hours when exposed to air and converges to its original value as shown in Fig. 6.4. Earlier reports on the humidity dependence of BBL were explained on the basis of H₂O adsorption where the sites close to the surface are significantly affected.¹⁰ The samples studied, were however, in the highly insulating regime. The fiber conductivity was more stable with respect to ambient conditions. The high conductivity of the fiber at room temperature obtained by heating persisted longer. These results suggest that the fiber is less sensitive to moisture indicating that the diffusion rates are small when compared to films and they have not altered the electronic properties. Also thermogravimetric analysis (TGA) studies indicate there is a marginal weight loss below the degradation temperature of BBL at 675 K which can be attributed due to the moisture content in the samples.

The difference in the energetics of the mechanisms can be gauged by fits to the simple activated models. The fits are not crude as expected and the barrier energies obtained can be used to highlight the differences. The initial heating process of the three configurations can be modeled in terms of an activated behavior and conductivity via barrier hopping as the leading mechanism. There is a gradual increase in $\sigma_{\perp}(T)$ up to 440 K which can be approximately fitted to a simple activated model: $\sigma = \sigma_0 \exp[-\frac{\Delta}{kT}]$ with $\Delta \simeq 0.045$ eV. $\sigma_{\perp}(T)$ increases more rapidly for $T > 440$ K and is indicated in the fit to the activated model with the value of Δ of $\simeq 2.308$ eV. $\sigma_{\perp}(T)$ for $T = 600$ K is in the order of $10^{-5} \frac{S}{cm}$. For the surface measurement, $\sigma_{\parallel}(T)$ of BBL films,

the initial heating process can be modeled in terms of a simple activated behavior with two different regimes; $\Delta \simeq 0.011$ eV for $T < 390$ K and $\Delta \simeq 1.12$ eV for $600 \text{ K} > T > 350$ K, and $\sigma_{fib} \simeq 10^{-3} \frac{\text{S}}{\text{cm}}$ at $T = 600$ K. For the fiber measurement, $\sigma_{fib}(T)$, the initial

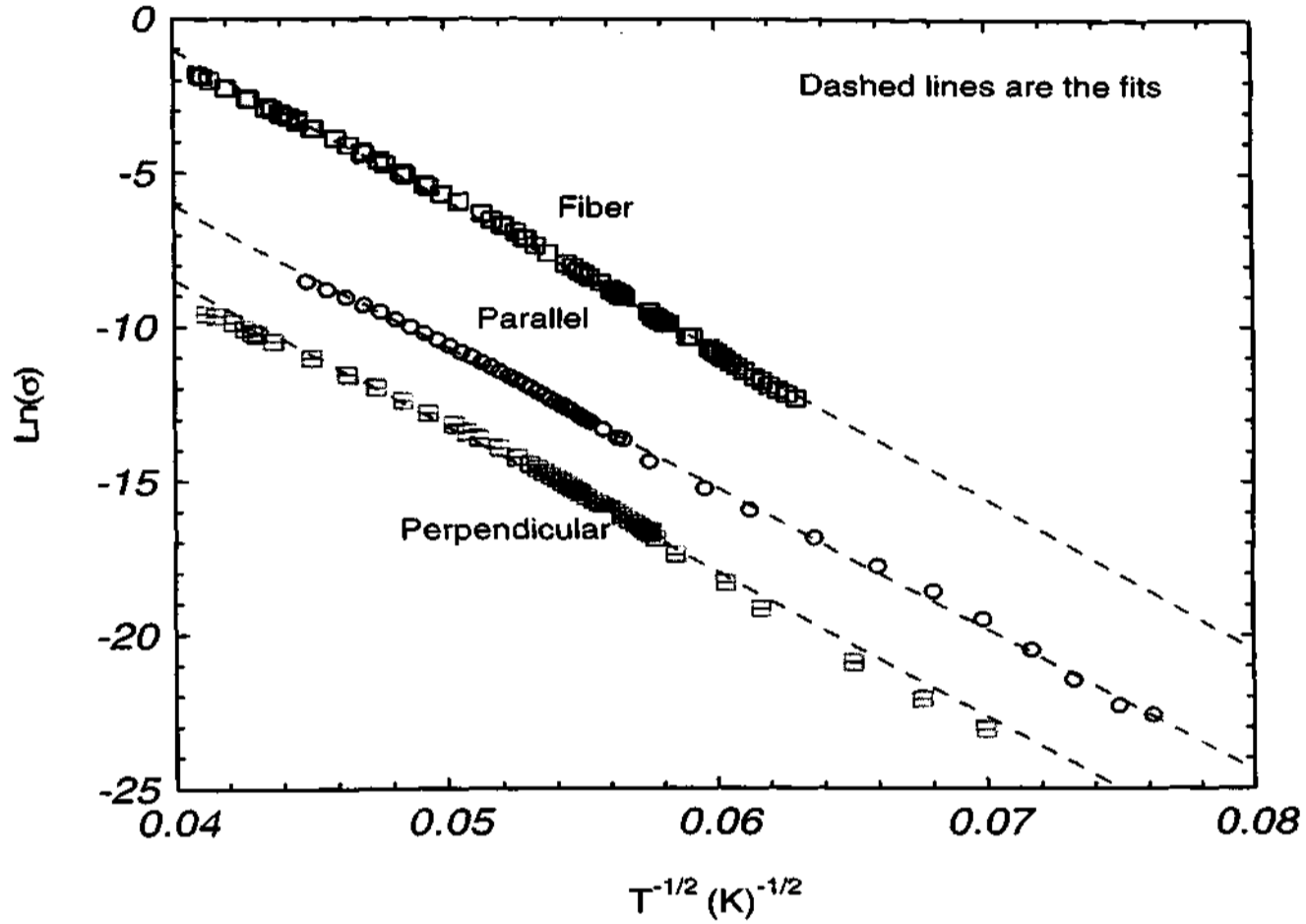


Fig. 6.4 $\ln(\sigma)$ Vs $1/T^{1/2}$ for the heated samples fiber (A), parallel (B), and perpendicular (C) configurations. The dashed lines (---) are fits to the 1-d variable range hopping model

heating process can also be modeled in terms of a simple activated behavior with two different regimes; $\Delta \simeq 0.098$ eV for $T < 350$ K and $\Delta \simeq 0.878$ eV for $600 \text{ K} > T > 350$ K, and $\sigma_{fib} \simeq 0.1 \frac{\text{S}}{\text{cm}}$ at $T = 600$ K .

Upon cooling from 600 K, $\sigma(T)$ for the different film geometries and fiber can also be approximately fitted to a single activated process. $\sigma_{\perp}(T)$ gradually decreases

uniformly on cooling with $\Delta \simeq 0.35$ eV and reaches $\simeq 10^{-8} \frac{S}{cm}$ at room temperature. $\sigma_{\parallel}(T)$ gradually decreases uniformly on cooling with $\Delta \simeq 0.364$ eV reaching $\simeq 10^{-6} \frac{S}{cm}$ at room temperature. $\sigma_{fib}(T)$ gradually decreases uniformly on cooling with $\Delta \simeq 0.377$ eV approaching $\simeq 10^{-4} \frac{S}{cm}$ at room temperature. The notable feature is that the activation energy values for all configurations and fibers are almost similar.

The results obtained after the initial heating process ($T_{max} \simeq 625$ K) can be considered to be a better representative of the system for studying the electronic transport process because of the insensitivity to subsequent heating cycles yielding consistent results. 3-D Mott variable range hopping models¹⁵ have been previously used to describe the $\sigma(T)$ behavior with

$$\sigma(T) = \sigma_0 \exp\left[-\frac{T_0}{T}\right]^\gamma \quad (164)$$

where $(\frac{1}{\gamma} - 1)$ is the dimensionality and for isotropic system $\sigma_{\parallel} = \sigma_{\perp}$, the parameter $T_0 = \frac{A}{k_B N_D(E_F)} \epsilon^D$ where ϵ is the localization length, N_D is the density of localized states near the Fermi level in D dimensions and A is a numerical factor of order unity. For anisotropic neighboring chains 3-D system the effective ϵ is equivalent to a geometrically averaged $(\epsilon_{\parallel}^2 \epsilon_{\perp})^{\frac{1}{3}}$ where ϵ_{\parallel} and ϵ_{\perp} are intra plain and inter plain localization lengths.⁷ The conductivity anisotropy i.e., $\frac{\sigma_{\parallel}}{\sigma_{\perp}}$ in the model¹⁶ is found to be $\simeq (\frac{\epsilon_{\parallel}}{\epsilon_{\perp}})^2$. The ratio of the localization lengths $\frac{\epsilon_{\parallel}}{\epsilon_{\perp}}$ have been estimated to be $\simeq 30$. The present value of $\frac{\sigma_{\parallel}}{\sigma_{\perp}} \simeq 400$ which is in the same order of magnitude as $(\frac{\epsilon_{\parallel}}{\epsilon_{\perp}})$ can be then argued to arise from the anisotropy in localization length. However, in the present case $\sigma_{\parallel}(T)$, $\sigma_{\perp}(T)$ and $\sigma_{fib}(T)$ yields better fits to a quasi 1-D models than 2-D, 3-D VRH or a simple activated model. The deviation from a 3-D model which was used to describe the transport properties in BBL can be attributed to differences in factors such as orientation, impurity concentration, and processing conditions. The low dimensional picture is more plausible for the micron sized, drawn fibers which can be considered to be packed with fibrillar structures as observed in scanning electron microscopy images and these structures are present in the films as well.

Another crucial feature in the present case is lack of temperature dependence of $\frac{\sigma_{\parallel}}{\sigma_{\perp}}$ for surface and bulk configurations and $\frac{\sigma_{fb}}{\sigma_{\perp}}$ for fiber and bulk configurations which is also revealed by the similar values of T_0 obtained in the 1-D model fits, with values of $kT_0 \simeq 0.0407$ eV, 0.0414 eV, and 0.0419 eV for bulk, surface and fiber configurations respectively as show in Fig. 5. The system can be modeled in terms of a quasi 1-D system with a strong intrachain hopping and a weak interchain hopping component. For the component of inter-chain hopping conductivity parallel to the chain,

$$\sigma_{\parallel}(T) = \left[\frac{e^2 \nu_{ph} (2\pi t_{\perp} \tau_i \hbar)^2}{\alpha k_B T z A} \right] \exp\left[-\left(\frac{T_0}{T}\right)^{\frac{1}{2}}\right] \quad (165)$$

and the component of interchain hopping perpendicular to the chain,

$$\sigma_{inter}(T) = \left[\frac{2e^2 g(E_F) b^2 \nu_{ph}}{A (2\pi t_{\perp} \tau_i \hbar)^2} \right] \exp\left[-\left(\frac{T_0}{T}\right)^{\frac{1}{2}}\right] \quad (166)$$

, where $T_0 = \frac{8\alpha}{g(E_F) z k_B}$, ν_{ph} is the characteristic phonon frequency, t_{\perp} is the interchain exchange integral, τ_i is the interchain mean free time, α is the inverse of longitudinal localization length, b is the inverse of transverse localization length, z is the number of nearest ains. A is the average cross-sectional area of each chain, $g(E_F)$ is the density of states with one sign of spin.^{17, 18} A detailed structural information on the arrangement of the polymer chains in the bulk is needed to know how the quasi-1d models can be adopted for $\sigma_{\perp}(T)$. However it must be mentioned that several other models also result in this kind of temperature dependence such as charge energy limited tunneling for granular metal and 3d variable range hopping model with a coulomb gap.¹⁸ It is not possible with the present experimental information to have a complete understanding of the physical process involved in the conduction mechanism, but, what is established is the identical nature of the temperature dependence of the conductivity in different geometries and morphology after thermal treatment.

The X-ray studies done on uniaxially oriented films revealed Bragg peaks at $\theta \simeq 13.24^\circ$ and 19.01° with d values corresponding to 3.3626 Å and 2.3648 Å respectively and are consistent with the earlier observations.

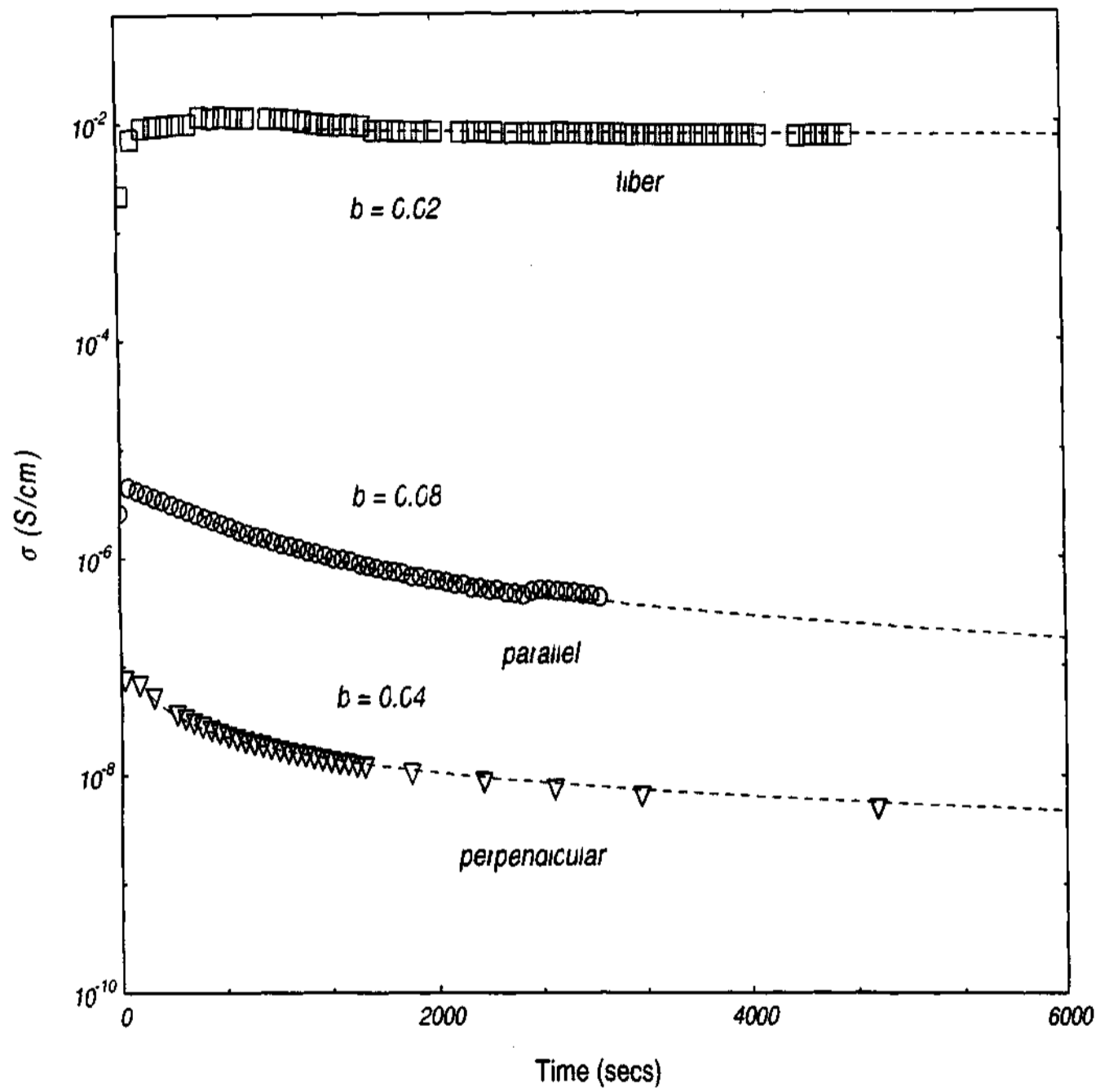


Fig. 6.5 $\sigma(t)$ as a function of time for heated samples at room temperature and exposed to air for different configurations, $t = 0$ sec. corresponds to vacuum conditions. dashed lines are fits to the data.

Preliminary observations in the X-ray studies also reveal additional features which are dependent on the sample history. Fibers are expected to show a microstructure similar to the uniaxially grown films. Efforts are being pursued to study these features in detail as a function of temperature and correlate the results with the transport results.

The samples when exposed to air vary significantly with respect to time after heat treatments. Upon exposing the sample $\sigma_{\parallel}(t)$ and $\sigma_{fib}(t)$ initially increases marginally and subsequently ($t > 100$ secs) the conductivity in all configurations progressively decreases with time as shown in Fig. 6.5. The decrease in $\sigma(t)$ can be fitted to $\ln(\sigma) = at^b$ where a and b are constants. The rate of decrease in conductivity for the different geometries can be evaluated in terms of magnitude of the constant b , since $\frac{d\sigma}{dt} = b\sigma \frac{\ln(\sigma)}{t}$. The fiber conductivity decreases at a much slower rate compared to $\sigma_{\parallel}(t)$ and $\sigma_{\perp}(t)$ with $b \simeq 0.04, 0.08,$ and 0.02 for bulk, surface, and fiber configurations respectively. This process is irreversible and the sample regains the higher conductivity, ($t = 0$ value) only upon thermal treatment. These features indicate the sensitivity of the electronic properties on the physio-chemical interactions at the surface. The results also clearly demonstrate that these changes brought about extrinsically can be overcome by thermal treatment.

Earlier studies on the pressure dependence of the electronic transport of the thermally treated polymer in ambient conditions also show the anisotropic behavior. The resistance in the transverse configuration, R_{tr} , and in the planar surface configuration, R_{sur} show drastically different behavior as a function of pressure. The R_{tr} of the sample gradually decreases with an increasing pressure with the process being reversible. The surface resistance on the other hand increases with increasing pressure initially and then decreases for $P > 25$ Kbar with an appearance of a rounded peak at $P \simeq 20$ Kbar and this process was irreversible. A possible explanation for the results was given in terms of occurrence of an initial physio-chemical process such as removal of

water from the surface for $P < 20$ Kbar, and subsequently physical processes such as packing, and orientational changes taking over for $P > 25$ Kbar as the major factors influencing the dc conductivity.

Previous results on photocurrent studies on heated samples in ambient conditions reveal a small but significant presence of photocurrent in the surface cell configuration, well below the absorption edge (< 1.68 eV). [162] In contrast to the surface cell configuration photocurrent the sandwich cell configuration photocurrent follows the absorption spectra closely around the edge.⁹ A possible source for this effect was thought to arise from the presence of extrinsic impurities which can cause tails in the density of states by perturbing the band edge via deformation potential, via coulomb interaction or by forming a band of impurity states. The present results may explain the origin of the features observed in the pressure dependence and photoconductivity results and stress the importance of geometrical effects in the experimental studies due to the surface processes in this material.

6.2 Summary

The present results add further insight into the electronic structure of BBL and the sensitivity of electronic properties to ambient conditions and thermal treatment. The ambiguous manner in which the conductivity of BBL enhances due to thermal treatment and the decrease upon exposure to moisture is completely traced and the results are consistent with previous experimental observations. The energy barriers and the time constants involved in these process are also estimated. The anisotropy in the electronic conductivity studied as a function of these parameters also highlights the importance of structural and morphological aspects in the ladder type polymer.

Chapter 7

Results and Analysis: Active defects in BBL

Results of defect-induced thermally stimulated current (TSC), transient photocurrent measurements (I_{tr}), steady state photocurrent measurements (I_{ph}) and photo thermal deflection spectroscopy (PDS) in BBL are reported in this section [163]. These are complementary experiments and provide considerable insight in understanding the barrier limiting processes of charge transport. Stimulated current in combination with photocurrent measurements gives out the valuable information about the gap state distribution in the upper half of the band gap, i.e., in a range between the Fermi level and the conduction band edge. Measurements such as steady state photoconductivity is widely used to give a rapid assessment of optical and electronic properties of density of photogenerated carriers and mobility lifetime product. I_{tr} measurements can reveal the information on n_t , Δ_t and τ . However, detailed information on the individual values of mobilities and lifetimes of both the species of carrier, and measurement conditions are the factors. The results based on these experimental techniques would identify the nature and the energetics of the trap levels in this polymer. Variations in the results as a function of the initial trap-filling parameters and the thermal history are reported. The long-lived component in the photo-induced current decay, an indicator of defect states is also studied in this context. The barrier limiting processes of the photocurrent are correlated with the results obtained from TSC measurements and we speculate on the origin of these defects.

It is well known that the luminescence is strongly affected by carrier traps, which exists as localized states within the bandgap. The traps also have their bearing on the switching response in these polymer-based photocurrent and light emitting devices.

TPC measurements have shown that the photo generated charge carriers are generally trap limited and result in a decay profile which is long-lived and indicative of low mobilities in these systems. There are very few quantitative estimates of the densities and the energetics of these trap states in spite of their profound impact on the optical and electronic properties of these polymeric systems [?,?]. The nature of traps prevalent in these polymers can be discussed in terms of their location (interfacial and bulk), depth (deep and shallow) and origin (extrinsic and intrinsic).

In this chapter, we evaluate the trap concentration and energetics on the basis of TSC and TPC measurements. The nature of these trap states and their role in the charge transport along with quantitative estimates specifically in a ladder type polymer system are probed in this chapter. The large accessible temperature range makes this polymer a suitable candidate for such thermal probes, encompassing a wide energy (trap depth) range.

Another specific motivation for studying the trap levels in BBL is the unusual electrical conductivity behavior upon heat treatment and the large persistent photoconductivity [144,164]. The room temperature electrical conductivity of BBL significantly increases when heated to 600 K by more than six orders of magnitude as discussed in the previous chapter. The conductivity prior to exposure to the high temperature was compared with post-heated samples and analyzed in terms of activated and hopping models. The enhanced conductivity subsequently decays to its initial value after a prolonged exposure to ambient moisture conditions and is indicative of accessible trap levels [164].

It was concluded that it was not just a plain case of "volatiles" being driven off as clearly indicated by weight loss and calorimetry measurements. The microscopic origin of $\sigma(T)$ is due to a moisture driven physio-chemical adsorption at ambient conditions and is accompanied by a slow diffusion (several days) into the bulk, which finally results in a modification of electronic structure leading to a defect mediated transport with

a lower $\sigma(T)$. The electronic transport mechanism gets abruptly modified only at temperatures exceeding 500 K. The effect is extremely subtle and is not picked up by structural probes. Consequently TSC measurements prior to exposing it to 600 K is extremely informative.

7.1 TSC Procedure

For the TSC measurements, the samples were mounted on the sample holder with the proper radiation shield in order to avoid temperature gradients across the sample during the measurements. These measurements were carried out in different geometries with samples sandwiched between the two electrodes and also in the planar geometry where the metal electrodes were deposited on the surface with a gap of $\simeq 1$ mm. The TSC measurements were carried out by filling up the traps using constant current voltage source at different temperatures, following which the TSC was measured upon heating the sample at a constant rate under short-circuit conditions. All the TSC measurements done on different samples were heated to 400 K (to drive away any volatiles) under high vacuum conditions for several hours prior to measurements.

A typical scan was as follows: the sample was heated initially to $T_P \simeq 375$ K and maintained for 45 min. and voltage was applied (time of field polarization, $t_P \simeq 30$ min.) to sweep the residual trap charges. The samples were subsequently cooled to 15 K in the presence of this voltage bias. The sample electrodes are shorted prior to any measurement for $t_s \simeq 30$ min. duration enough in order to remove the residual or stray charges present in the polymeric samples. The linear heating rate (β) typically was 2.5 K/min. Fresh samples from the same batch i.e. not exposed to high temperature and field, were also used to verify the absence of the history dependent long-lived effects entering into the measurement process.

7.2 Results and Discussions

The initial poling temperature, T_P , of 375 K - 400 K is chosen to study the TSC

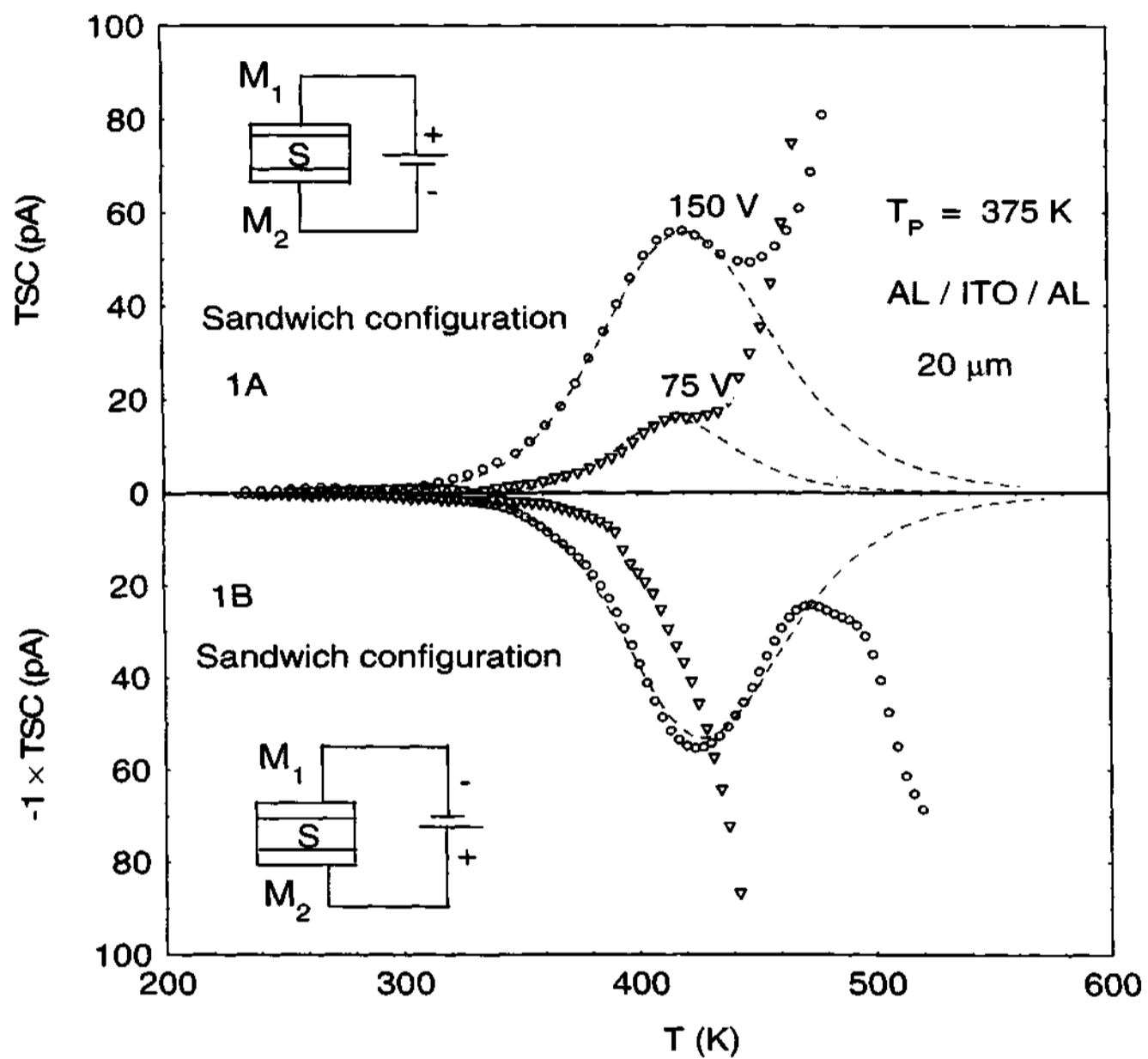


Fig. 7.1: TSC spectra obtained for oriented BBL films with different polarities. M_1 and M_2 represent the metallic electrodes and S is the sample. Dashed lines are the fits based on general order kinetic model.

in the pre-annealed phase of the material. Fig. 7.1 shows the TSC of the oriented BBL film after poling at 375 K at different bias voltages in sandwich geometry. I_{TSC} (T) as shown in this figure consists of a single, broad, local peak which is positioned at $T_{max} \simeq 419$ K with the corresponding $I_{max} \simeq 56$ pA for initial poling voltage, V_P , of 150 V. Similarly the TSC also is obtained upon changing the polarity of the poling fields, F_P is shown in the Fig. 7.1. The TSC measured in sandwich configuration for different polarities are nearly symmetrical and scales with the initial poling fields. This feature reveals the absence of any leakage or any other source for the spurious current. The symmetrical response is indicative of electric field driven TSC process. The small variations for different polarities for TSC could be attributed due to the differences in the polymeric (morphological) interfacial areas of different electrodes and slight thermal gradient due to heating rates. The value of T_{max} is nearly independent of the initial F_P . However for the temperature regime $T > 450$ K, where the conductivity of the sample is significantly high along with factors such as small thermal gradient result in the sharp increase of the current which eclipses the TSC component. The magnitude of the stimulated current changes with the initial V_P as indicated is as shown.

Fig. 7.2 shows the TSC curve obtained on a heat-treated sample ($\simeq 550$ K) and indicates a large shift in the $T_{max} \simeq 60$ K. This clearly indicates that the samples are highly sensitive to initial poling conditions. The results highlight the sensitivity of TSC to the trap-filling parameters, such as the magnitude of V_P and T_P . The experimental results are analyzed and incorporated in terms of various models such as initial rise method and first and general order kinetics methods. The trapping parameters are obtained by fitting the experimental curves in Fig. 7.2 around the local maxima, $200 < T < 450$ K to the general order kinetics TSC model eqn.

The fits yield effective activation energy or trap depth $E_t \simeq 0.7$ and 0.47 ± 0.02 eV for the TSC curves with initial poling voltage of 75 and 150 V. The uniqueness of

the value obtained was ascertained by using elaborate fitting procedures.

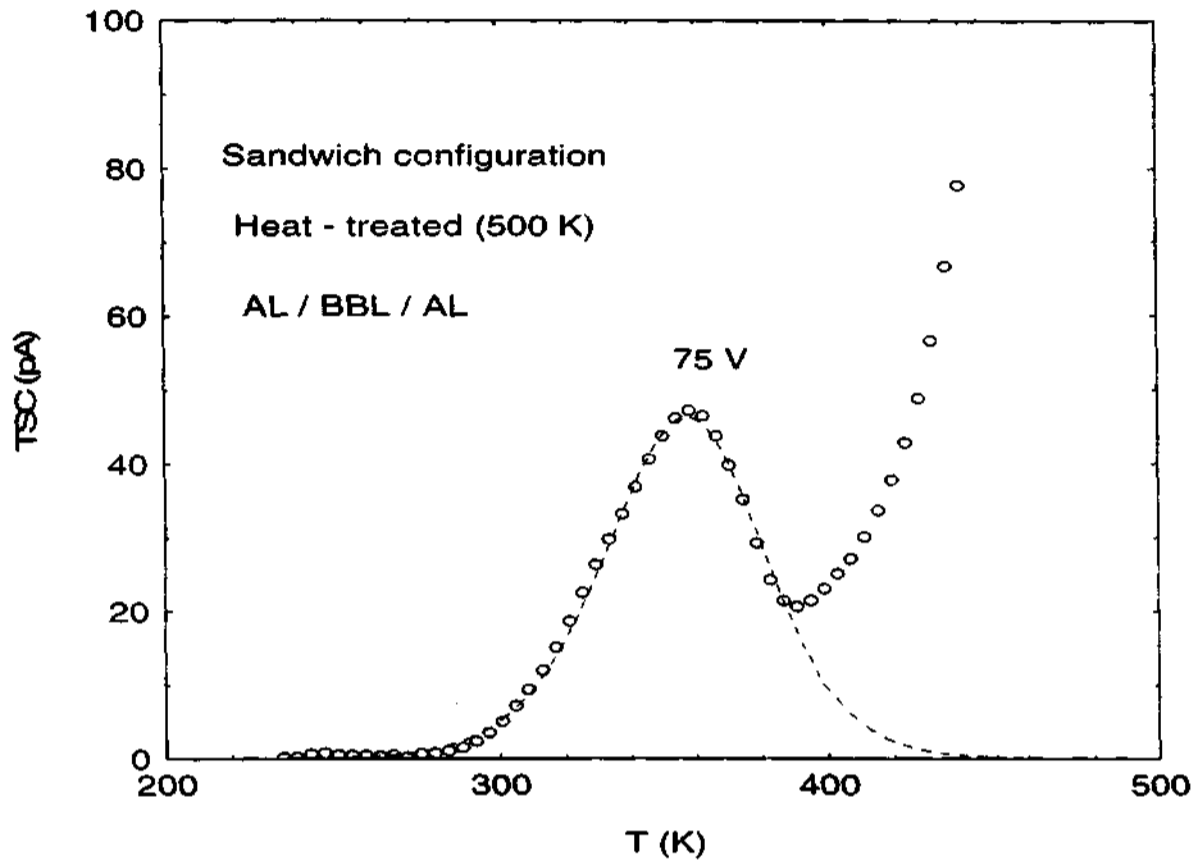


Fig. 7.2: TSC spectra of heat-treated oriented BBL films. Dashed lines are the fits based on general order kinetic model.

The permissible range of values for $l(1 < l < 2)$, $d(-2 < d < 2)$, $E_t(0 < E_t < 0.8 \text{ eV})$ in eqn. 4 also restricts the fits to yield a unique value with a realistic magnitude for the parameters. The total charge Q released in this process can also be evaluated from the integral ($Q = \int I_{TSC} dt$, $dt = \frac{dT}{\dot{T}}$). The total charge released from the trap states is ≈ 58 and $140 \pm 3 \text{ nC}$ for the integrated TSC curves 75 and 150 V respectively. It is to be noted that the integral of the TSC around the peak does not reveal the total stored charge but only a fraction of the charges which can be released. The lower limit for the trapped carrier densities $\approx 7.0 \times 10^{14}$ and $2.0 \times 10^{15} \text{ cm}^{-3}$ respectively are estimated by

assuming a uniform field across the film and knowing the sample geometry. The field distribution across the sample has to be taken into account to determine the releasable carrier trap density more accurately. The values of released charges obtained from the area integral value is an indicative of true measurement of the TSC measurements and is slightly higher than that of values are obtained from the theoretical models. It is more appropriate and approach when only mono-energetic peak exists in the polymeric samples.

The experimental results are analysed and incorporated in terms of various models such as initial rise method and first and general order kinetics methods. This marked differences highlights the variations in those values, which is an indicative of the trapping parameters are significantly temperature dependent. The models such as initial rise method, Grossweiner's method etc. depend mainly on the initial rising portion and independent of kinetics and insignificant to the trapping parameters are sensitive to temperature. The methods such as Chen's peak width analysis is based on the peak shape and it is practically difficult to identify the position of T_{max} and it more valid for undistorted peaks. Each and every method has its own constraints, in the limit of certain range. The models based on fitting procedures could cover the whole area of the curve(rising and trailing part of the curve)and it is significant to he parameters which are T dependent.

The TSC curves yield good fits to eqn. 4 with value of l in the fits approaching that for a second order. l close to one did not yield any good fits. The closeness of the fit to eqn. 4 is representative of second order kinetics and signifies the dominant re-trapping processes and verified by the Chen's peak width and Grosswiener's models.^{11,12} The second order kinetics has been recently observed for the organic molecular solid AlQ₃ where a wide distribution with energies ranging form 0.06 eV to 0.5 eV.³ The nature of the traps can also be identified by the estimates obtained for the trapping cross section. The values of cross-section reported in the literature span the

range from 10^{-15} to 10^{-12} cm^2 for coulombic attractive centres, 10^{-17} to 10^{-15} cm^2 for neutral centres and down to 10^{-22} cm^2 for coulombic-repulsive centres¹². An estimate for the trapping cross section, $S(T) \simeq 10^{-19}$ cm^2 was obtained from fits to the results in Fig. 7.1 and Fig. 7.2.

Fig. 7.2 represents the TSC for the sample after heat-treatment (550 K and after an elapsed time of 12 hours at 300 K). Experiments carried out immediately after the heat treatment do not show any features because of the large thermally induced dc conductivity, which persists for certain duration. The effect of heat treatment is reflected in the decrease of T_{max} in the marginally heat-treated sample. The fit yields an effective activation energy or trap depth of $E_t \simeq 0.51 \pm 0.03$ eV. The total charge released from the trap states is $\simeq 110 \pm 2$ nC and the corresponding trapped carrier density is $\simeq 1.4 \times 10^{15}$ cm^{-3} .

The trapping parameters obtained from the fits are also closely compared with Chen's peak width and Grosswiener's models. However, models such as the initial rise method which has been used previously for related systems is largely valid for dielectrics with mono-energetic electrically active defects over a limited temperature range. An alternative, simplistic approach for analyzing the peaks in the TSC spectra, which is valid in certain cases, is in terms of the initial rise method [?]. The drawback of this method is apparent in systems where several activated trapping levels are present.

Fig. 7.3 shows the TSC (similar procedure as for Fig. 7.1) for cast films. There is a marked difference in TSC profile as compared to that for the oriented film in the lower temperature regime $T < 400$ K and this highlights the importance of morphology in these systems. The TSC curve for 75 V has a rounded peak current at $T_{max} \simeq 135$ K. The experiment was repeated by reversing the polarity yielding a symmetrical response with a reversal in the current direction. The fit to a first order kinetics yields a trap depth value of $\simeq 16 \pm 0.5$ meV for both cases. From the initial rise method, we obtain a trap depth of $\simeq 19$ meV and trapping cross section, $S(T) \leq 10^{-20}$ cm^2 . The total

charge released in the process of heating is $\approx 50 \pm 0.2$ nC which corresponds to

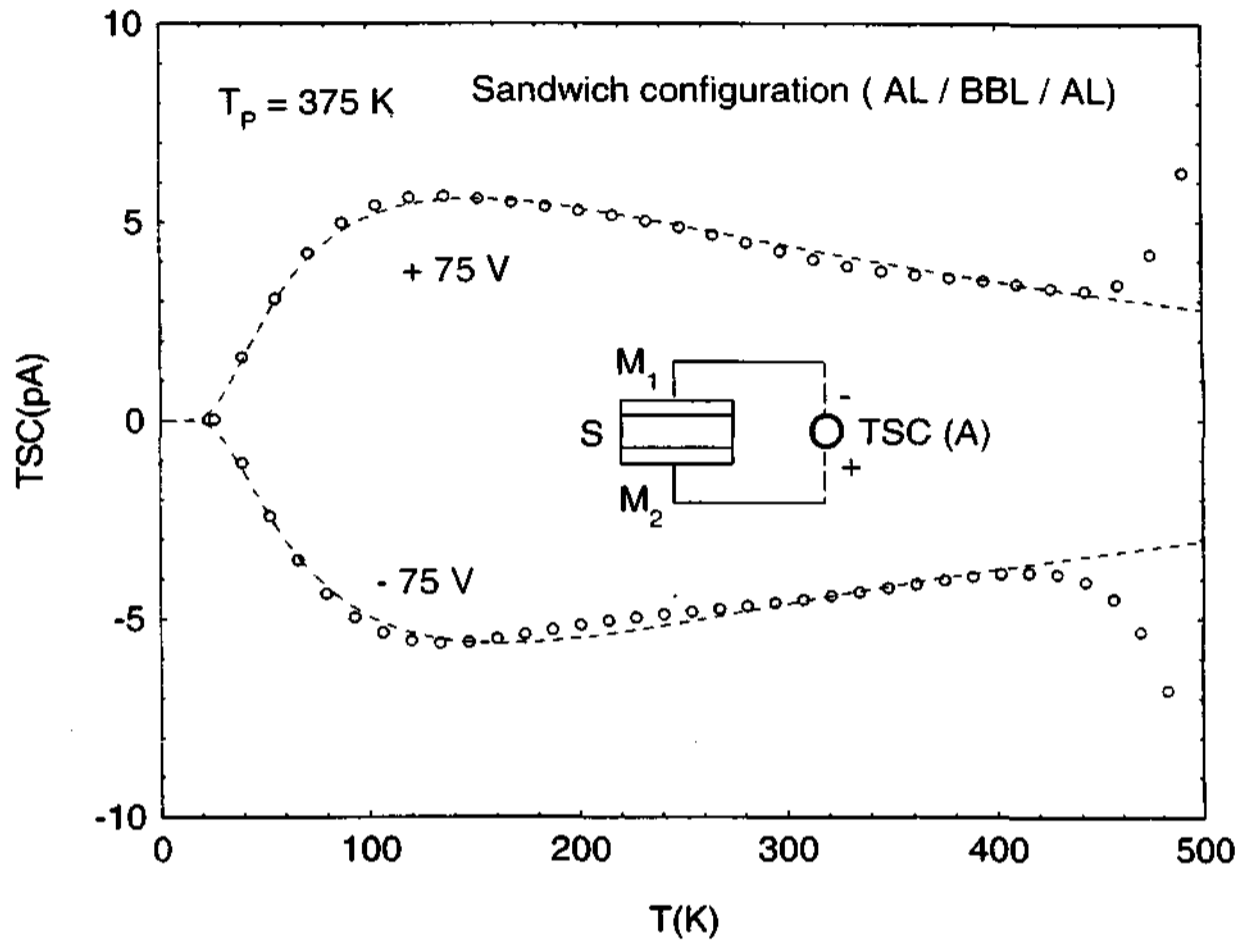


Fig. 7.3 TSC spectra of cast films ($20 \mu\text{m}$) measured in sandwich geometry. Dashed lines are the fits based on first order fits

a releasable trap carrier density of $\approx 9 \pm 0.5 \times 10^{14} \text{ cm}^{-3}$. The lower cross sections indicate the higher release probabilities for the traps and fewer retrapping effects.

Fig. 7.4 shows the TSC of thin cast films measured in sandwich geometry. The results there is a slight deviation of the spectra obtained for different polarities. From the initial rise method $E_t \approx 12 \pm 2$ meV. From the first order fits, $E_t \approx 20$ meV. TSC spectra of the thin films does not show the symmetrical response (for polling conditions of different polarity) which was observed for the thick films. This indicates that trapping parameters also depend on thickness variations.

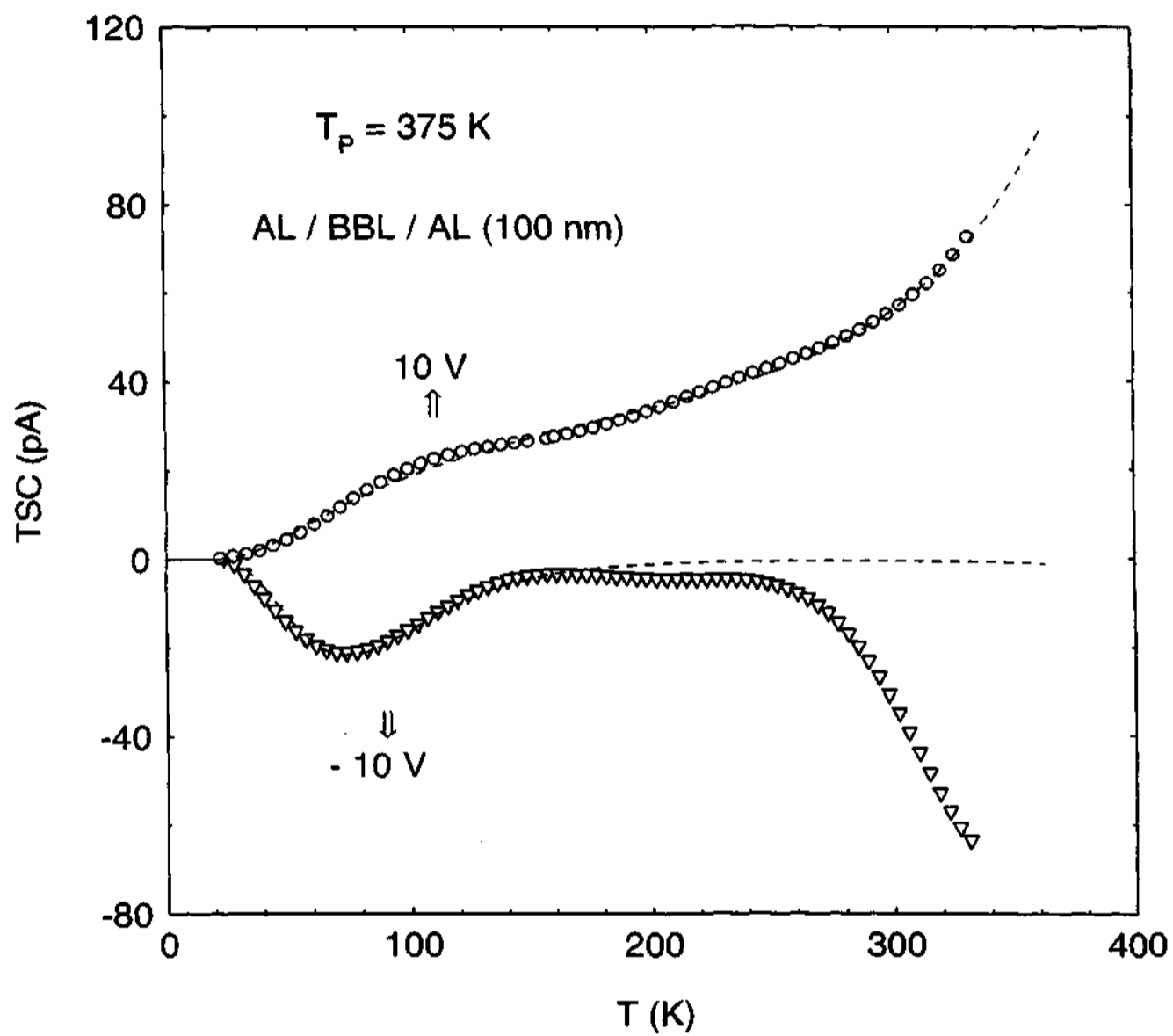


Fig. 7.4 TSC spectra of cast films (100 nm) measured in sandwich geometry. Dashed lines are the fits based on first order fits

The released charges from the trap states is $1.25 \mu\text{C}$ which corresponds to trap concentration of $\approx 3 \times 10^{18} \text{ cm}^{-3}$. The results of TSC on cast BBL films reveals an insignificant variation in thickness dependent stimulated measurements.

Fig. 7.5 shows the TSC spectrum obtained for a cast film in the surface configuration. The effect of the apparent gradient in the trap distribution across the sample thickness, with a higher density close to the surface, can be observed in measurements in this configuration. The TSC in this case essentially reveals the current carrying processes mediated by surface defects which are prevalent in these unannealed samples.¹⁷

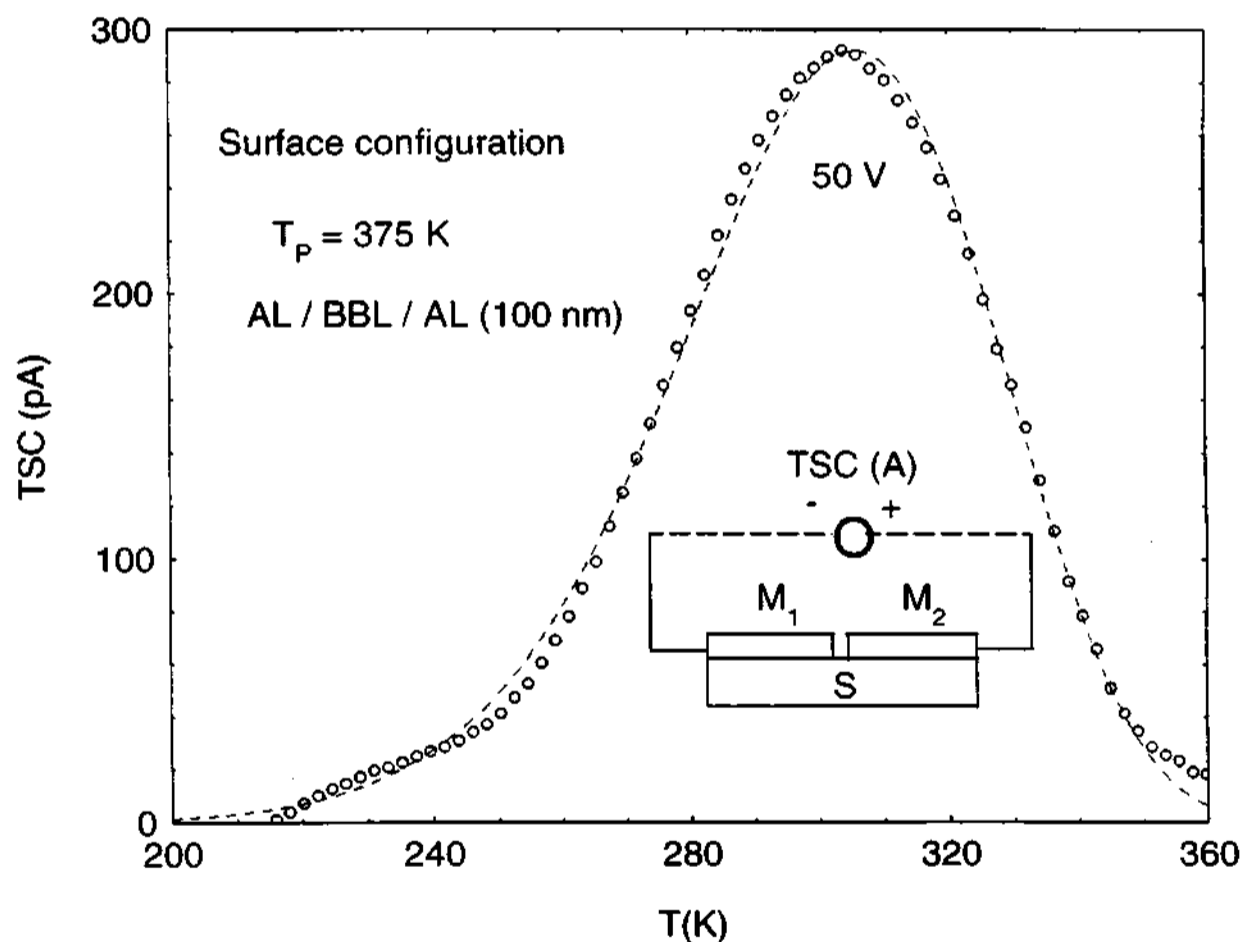


Fig. 7.5: TSC spectrum of a unoriented cast BBL film (200 nm) measured in the planar configuration, dashed lines are the first order fits

Since the results from TSC do not convey any spatial information on the origin of traps, we probe the samples in various geometries, and also carry out the thickness

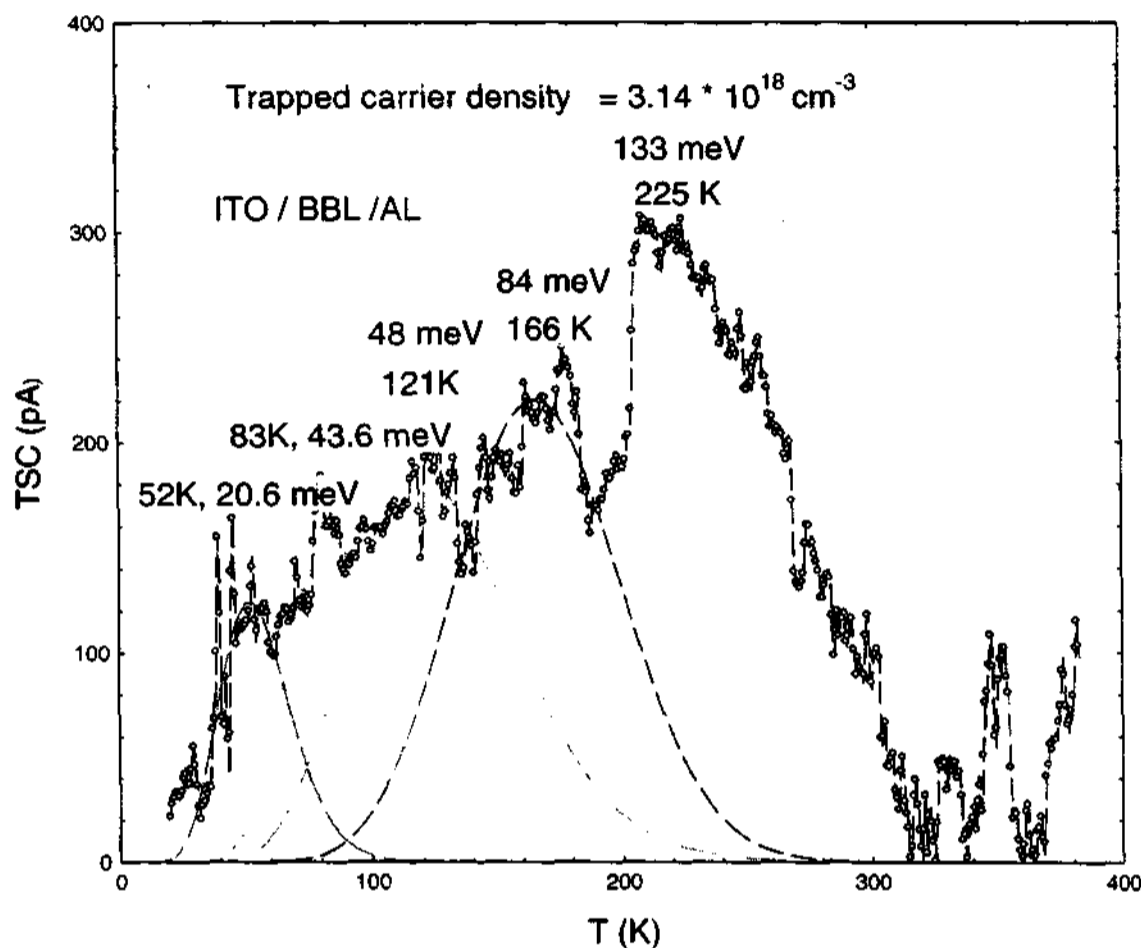


Fig. 7.6 TSC spectra of cast BBL films. Dashed lines are the fits based on first order kinetic model.

dependent studies. The TSC curves shown in the above figure was obtained for a poling voltage of 50 V at 375 K. A distinct maximum is observed at $T_{max} \simeq 305$ K with a linear heating rate of 2.5 K/min. The T_{max} value is nearly independent of the poling voltage but the I_{max} value increases non-linearly with increasing voltage in the range 0 - 100 V. From the fits, the TSC yields a barrier of 0.35 eV with better fits to first order kinetics. The total charge released in the process of heating is $\simeq 4.4 \times 10^{-7}$ C corresponding to a trapped carrier density of $\simeq 6 \pm 2 \times 10^{17} \text{ cm}^{-3}$ and $S(T) \simeq 5 \times$

10^{-18} cm^2 .

Fig. 7.6 shows the TSC of cast thin films, measured in sandwich configuration. In the temperature regime $T < 350 \text{ K}$, there exists several multiple overlapped peaks and the origin of this mechanism is due to extrinsic in nature. The trapping parameters are obtained from the first order kinetics fits. The trap depths corresponding for the traps located at several T_{max} are $\simeq 21 \text{ meV}$ (52K), 44 meV (83K), 48 meV (121K), 84 meV (166K) and 133 meV (225K) respectively. The total amount of charges released during this experiment is given by $Q \simeq 1.2 \mu\text{C}$ and the corresponding releasable trap concentration is $\simeq 3 \times 10^{18}$. The results based on TSC measurements of sample (ITO/BBL/AL) show slight differences when compared with the samples (AL/BBL/AL) in various configurations. In this section, we highlight the differences in this TSC spectra and probably could be due to the polymer-electrode (ITO) interface.

7.3 Photo-Induced Current Measurements

TSC results from BBL indicate the existence of a variety of trap states, which depend on the morphology and thermal history. The TSC measurements of oriented films in the sandwich configuration reveal deep trap states in the range of $\simeq 0.4 - 0.5 \text{ eV}$ which may have their origin at the intrachain level. Un-oriented cast films reveal a TSC contribution, which is essentially from shallower states. The sources for the extrinsic defect states could be interfacial in origin or from environmentally induced processes. Previous results on BBL films showed that the polymer samples are highly sensitive to the relative humidity. It is experimentally observed that the physisorbed molecules, which are close to the surface of the films, show barrier limited transport processes, which are different from the bulk of the films. In the recent studies of PPV based LED devices, deep traps have been assigned to the influence of the environment, while shallow ones have been assigned to a doping process by

the substrate such as the indium tin oxide used for fabrication [?]. An analogous situation may be also applicable in the present case of BBL films. The switching response of photocurrent and the temperature dependence also reveal trap-mediated mechanisms. The difference in the barrier estimates from the TSC process(0.3 eV) and the photocurrent process(0.12 eV) in the same geometry highlights the slower, rate-limiting diffusion process of the photo generated carriers in the bulk to the surface, similar to the mechanism used to explain the persistent photocurrent in PPV. [?].

BBL exhibits appreciable photocurrent response over a wide spectral range, and the spectral response almost matches the absorption spectra as shown in Fig. 7.7

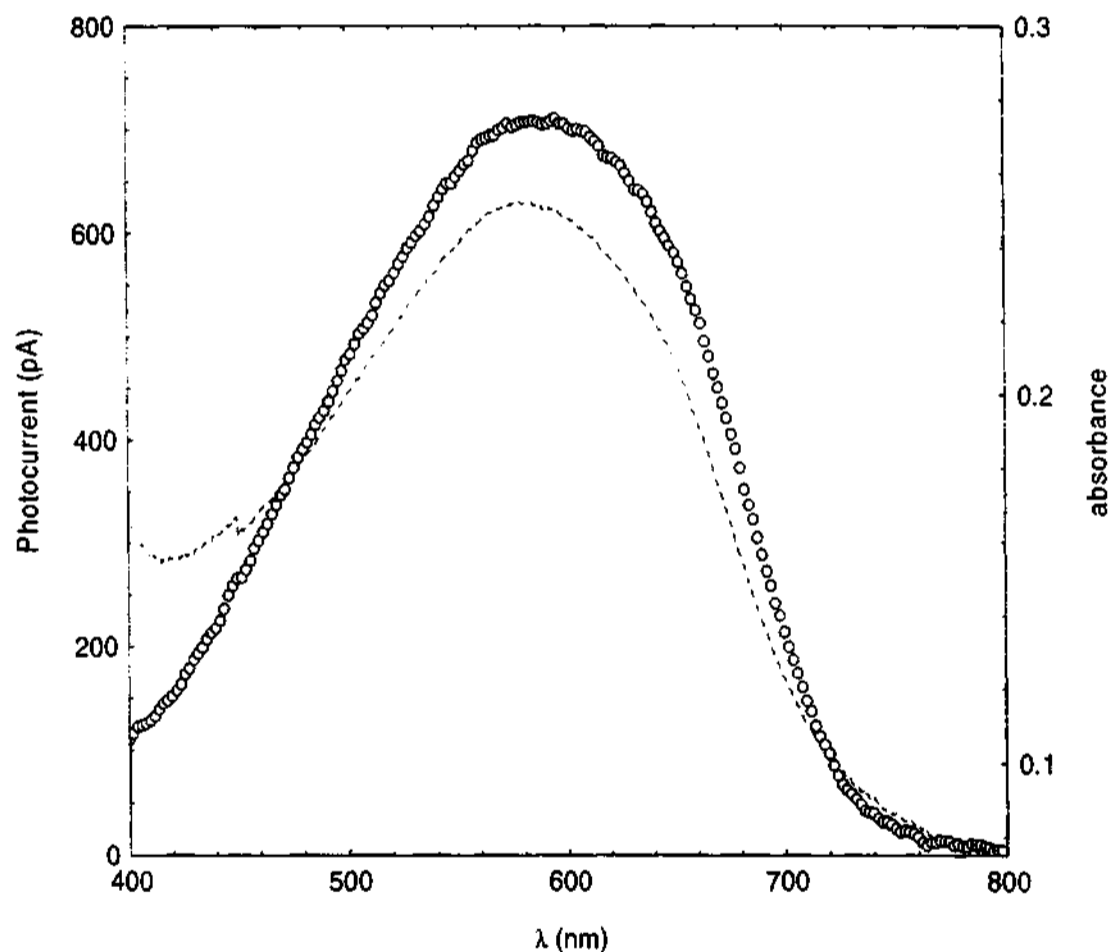


Fig. 7.7 Spectral response and absorption spectra of BBL cast films.

The problem of extracting the trap parameters from transient photocurrent data usu-

ally referred to as spectroscopic analysis. Transient photocurrent measurements in amorphous and crystalline materials and insulators contain a large amount of information on the nature of the carriers, their lifetime and mobility, and the distribution of traps in the gap.

The phenomena of early processes ($< 1 \mu\text{sec}$) leading to photocurrent in conjugated polymers is not completely understood due to the possibility of different routes to generate the free carriers upon photoexcitation. For example; Based on the coincidence of the onsets of the photoconductivity and absorption in MEH-PPV, it was concluded that photoexcitation of PPV leads to a direct generation of mobile charges through an interband π - π^* transition.^{8, 9} On the other hand, based on a variety of complementary experiments, it is argued that the photocurrent (I_{ph}) originates from secondary processes, where the initial intrachain excitons dissociate to free charges.

We do not emphasise on the photocarrier generating mechanisms in BBL, but study the extrinsic/defect processes in I_{ph} . Long-lived current (few msec) upon switching off the excitation source is a classic signature of defect induced processes. The evolution of I_{ph} upon photoexcitation and the subsequent decay is a valuable tool to explore various processes and develop a deeper understanding of phenomena such as electroluminescence in these systems.

7.4 Transient photoconductivity measurements

The response of a BBL in a coplanar geometry with a 30 V bias to a chopped beam of light observed on the oscilloscope is shown in Fig. 7.8. It is clearly obvious that from the response that both the build-up and the decay processes are not instantaneous ($\geq \text{ns}$). The long-lived decay signals can also be studied by frequency dependent steady state photoconductivity measurements using a lock-in technique or by studying the decay profile of the current when the light is switched off. The response of the sample (during the off cycle) in the planar geometry with a bias field to a chopped laser

source(70 Hz), recorded by the oscilloscope, at different T is shown in Fig. 7.8.

The trap dominated mechanism for transport in BBL is also observed in the photocurrent measurements.

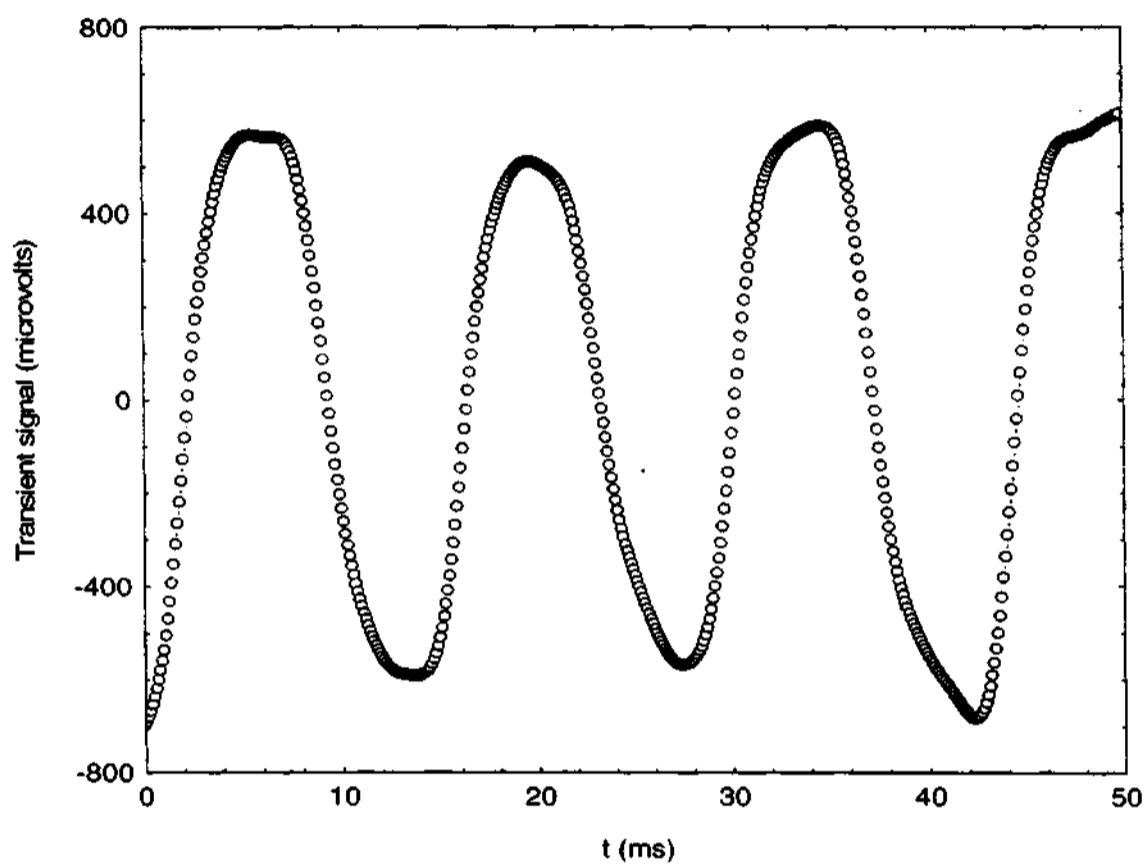


Fig. 7.8 Pulse response of BBL cast film at 300 K

The photo-induced current, I_{tr} of the sample after an exposure to a 10 nanosecond laser pulse, shown in Fig. 7.9. has a sizeable long-lived dispersive component.

The long-lived decay which is temperature dependent is a signature of the trap-limited transport mechanism. This long-lived decay of the TPC I_{tr} is typical of multiple relaxation processes, and fits better over a large range to a stretched exponential behaviour(Kohlrausch law)²⁰.

$$I(t) = I_0 \exp \left[-\frac{t}{\tau_r} \right]^\beta, \quad (167)$$

where β is the dispersion parameter and $0 < \beta < 1$. The values of $\beta \simeq 0.37$ and $\tau_r \simeq 0.2$ ms are obtained from the stretched exponential fits. The pulse shape of the response is mainly

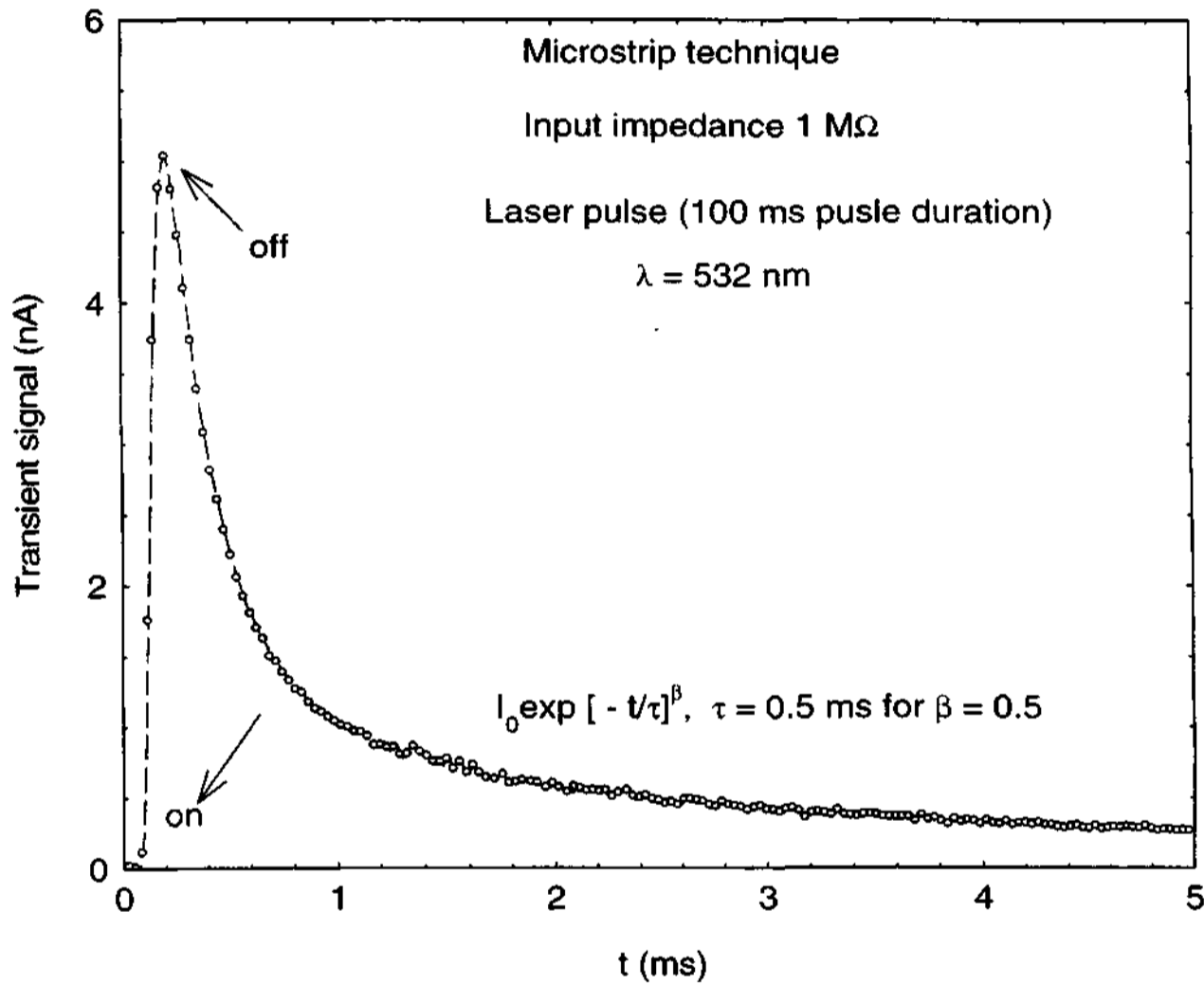


Fig. 7.9 The TPC decay measurements of cast films (10 ns laser pulse, on - pulse rise, off - starting of the decay response).

determined both by the carrier trapping and release rates and the recombination lifetimes.

The decay curves on this time scale can be fitted to a single lifetime decay process, for the range $1 \text{ ms} < t < 10 \text{ ms}$, for comparison purposes; $I(t) = I_0 \exp\left[-\frac{t}{\tau_r}\right]$ where I_0 is the maximum signal and τ_r is a recombination lifetime of the carriers. It is to be noted that a single time constant does not describe the decay profile over the entire range, especially at low T.

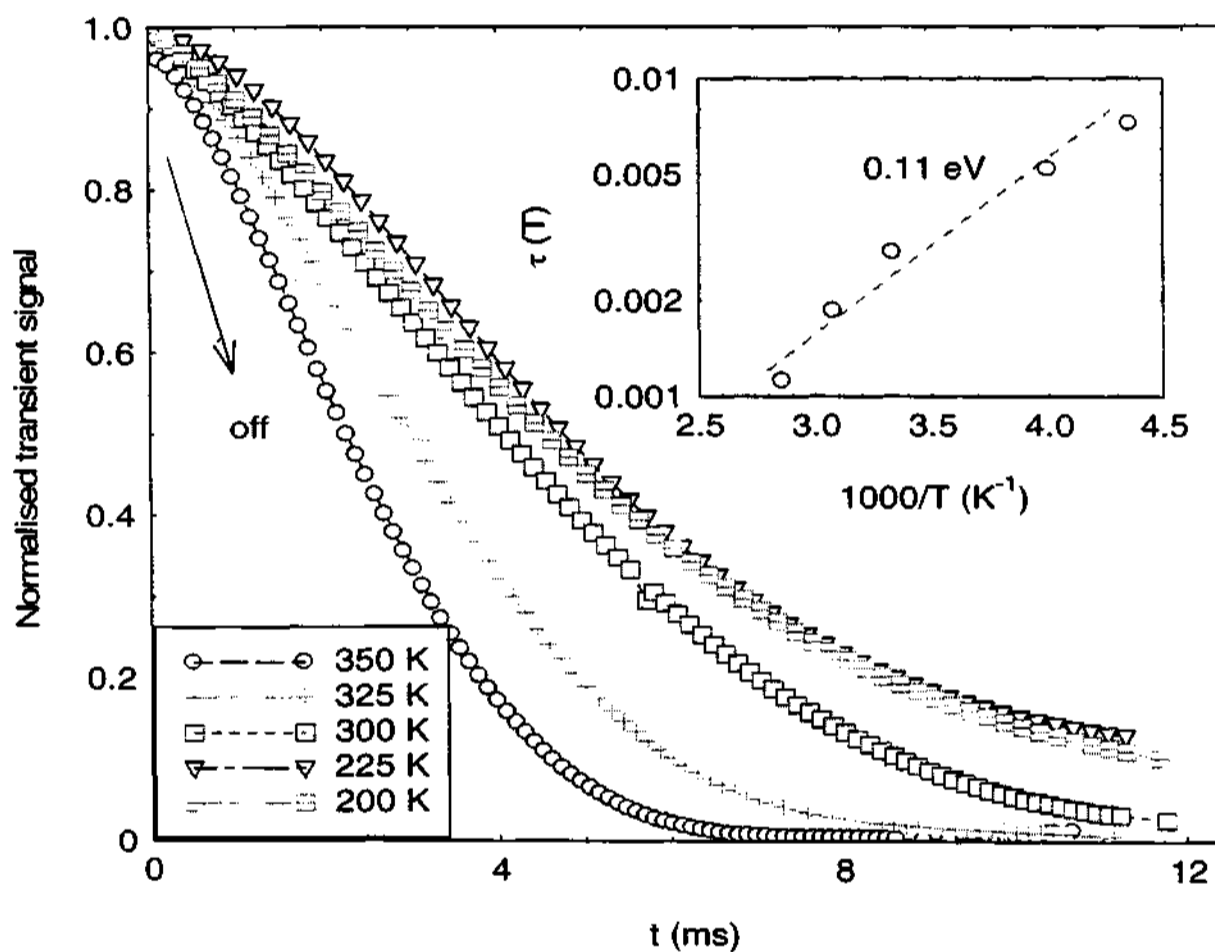


Fig. 7.10 Transient photocurrent response ($t = 0$ represents initiation of off cycle) carried out with a chopped light pulse at different temperatures. The dotted line represents the fit to the data.

For the photo-induced current measurements, the gold electrodes were deposited with an inter-electrode gap of $\approx 0.2 \text{ mm}$ on the surface of the cast films. Steady state

photoconductivity was measured with He-Ne laser source chopped nominally at 10-20 Hz range and the photocurrent was detected by a lock-in amplifier. The transient measurement was done with a 10 nsec pulsed source at 532 nm. The transient signal was recorded and stored using a 500 MHz digital oscilloscope with a 1 M Ω input impedance. The long-lived characteristics were measured by studying the response using a chopped laser beam which was incident on the polymer in presence of a bias ($0 < V < 200$ V) using the oscilloscope in an averaging mode.

Each experiment was performed on three to four different samples from different batch and was also repeated couple of times to ensure reproducibility. The experiments were also done with different electrodes to verify absence of any contact effects.

The decay kinetics in polymers such as PPV has been explained in terms of a fast intrinsic component which is weakly temperature dependent, and a slow extrinsic defect induced component which has an activated functional form for the temperature dependence²¹. The temperature dependence of the decay in this case largely represents the slow component features as shown in Fig. 7.10. A general trend of increase in $\tau(T)$ with decrease in T is observed. The $\tau(T)$ dependence, shown in the can be fitted to an activated behavior with a barrier height of $\simeq 0.11$ eV. There is a considerable deviation from a simple activated behavior at low T. The barrier estimated for $T > 150$ K is $\simeq 0.13$ eV. The pulse shape and magnitude is mainly determined by the trapping and release rate along with the recombination lifetime of the carriers.

Fig. 7.11 shows the T dependence of dark and steady state photocurrents over the range 10 - 350 K. For a simplistic model, the photocurrent can be viewed to arise from a distinct charge generation component time the charge transport component. In the extreme case of high purity samples with large mobility, the photocurrent is normally not dependent on temperature. In the present case, however, I_{ph} and I_d are strongly dependent on temperature and show similar dependence. This can be indicative of barriers in the transport process. The temperature dependence of steady

state photoconductivity primarily in the range $T > 200$ K is reflective of the kinetics of the long-lived component.

Fig. 7.12 shows the plot of I_d and I_{ph} in log scales and T in reciprocal scale.

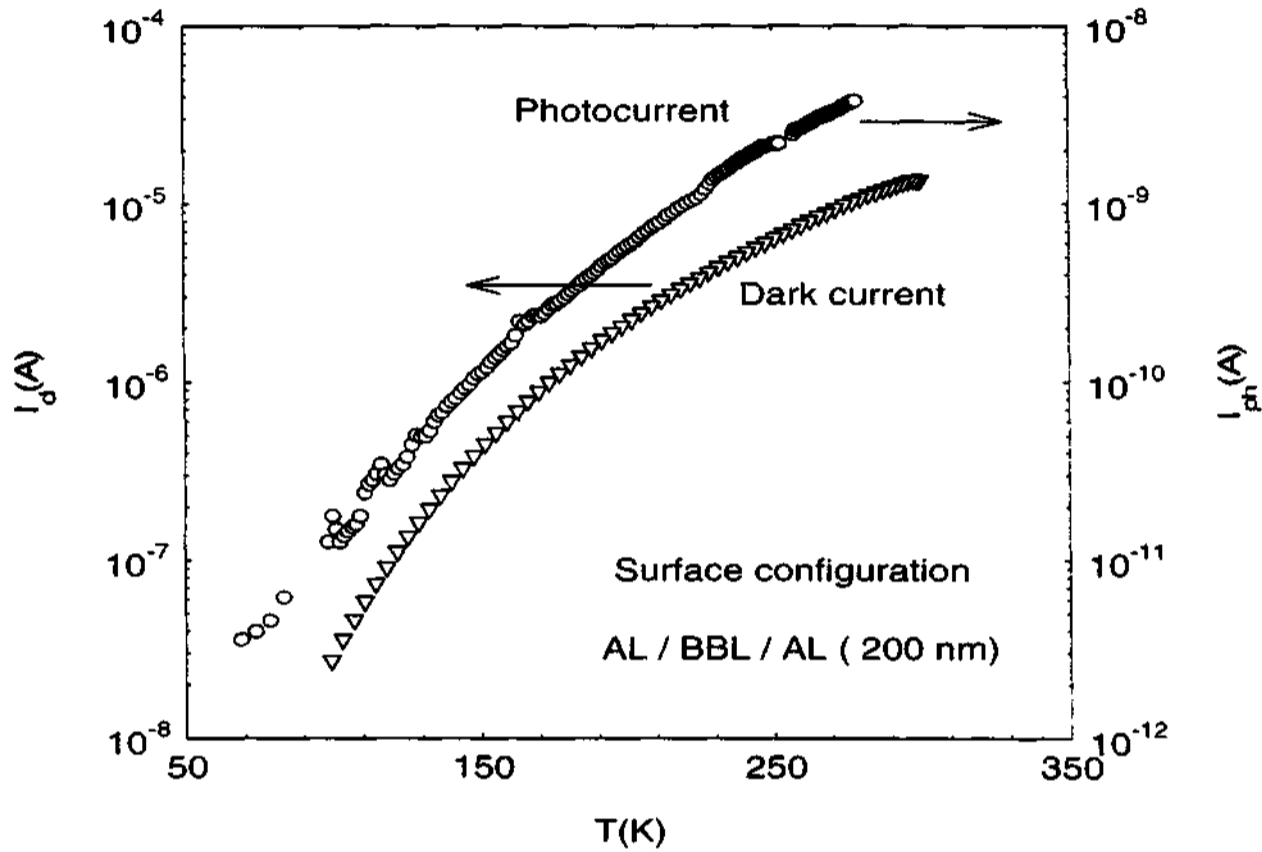


Fig. 7.11 Temperature dependent dark ∇ and photocurrent \circ spectra of BBL in surface configuration.

There is a deviation from a single activated model for $I_{ph}(T)$, especially at low temperature $T < 250$ K. The similarity in $I_{dark}(T)$ and $I_{ph}(T)$ for $T > 250$ K indicates that $I_{ph}(T)$ is primarily governed by the transport limiting factors rather than carrier generating mechanisms. The differences in $I_{dark}(T)$ and $I_{ph}(T)$ for $T < 250$ K are significant and indicate the processes which are exclusive to the photo-generated charge carrier species. $I_{ph}(T)$ in the high temperature region yields barrier energy value $\simeq 0.1$ eV when fitted to a simple Arrhenius behaviour. The barrier value obtained from

$I_{ph}(T)$ closely matches that obtained for $\tau(T)$ and is indicative of a recombination limited transport processes.

Qualitatively, the long-lived current-decay measurements after an initial photoexcitation yield information which can be analogous to the TSC measurements carried out after trap filling.

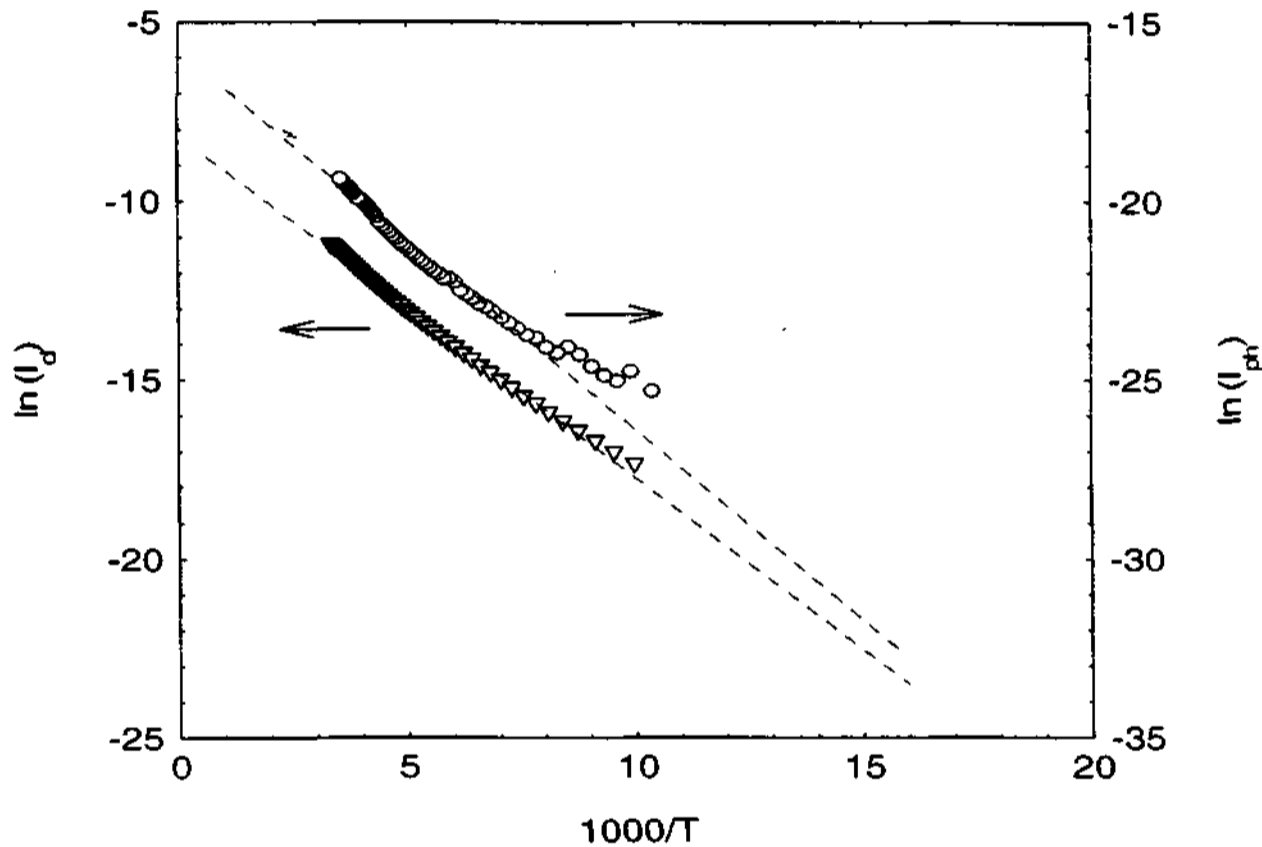


Fig. 7.12 shows the fits of an activated model for I_d and I_{ph} . The dotted lines are the fits to an activated model.

In both cases, the integral of $I(t)$ can estimate the trap carrier density, but crucial differences can exist due to differences in the initial conditions of trap filling. The excess charge which persists in the sample upon photo-excitation is $Q = \int I dt$, the trap carrier density is then estimated by using this expression, $N_t \leq \frac{Q\alpha}{eWL}$, where e is the charge of the trapped carrier, α the absorption coefficient determining the depth up to which

the charge carriers are located. W and L the electrode and inter-electrode dimensions. Trapped charge carrier densities in cast films of BBL from TSC measurements were $\simeq 10^{16} \text{ cm}^{-3}$ while the photo-induced long-lived $I_{ph}(T)$ measurements yielded $\simeq 10^{17} \text{ cm}^{-3}$. The differences in the electric field and the initial trap filling parameters used for the two measurements can account for the discrepancy in the estimates. The activation energy obtained from the photoinduced transport measurements involving $I_{ph}(T)$ and $\tau(T) \simeq 0.1 \text{ eV}$ can be regarded as an effective barrier estimate, comprising of all the trap states as observed from TSC measurements and processes which are exclusive to photo generated charge carriers.

In summary, two experimentally different approaches were used to study the trap distribution and energetics of BBL. TSC measurements indicate a feasible approach to study the various defect characteristics in ladder type polymers with an estimate of trap states of $\simeq 0.7 \text{ eV}$, 0.3 eV , and 16 meV in BBL. An effective activation barrier of 0.1 eV from $I_{ph}(T)$ measurements was obtained. The trapped charge carrier densities were also evaluated from these measurements indicating the magnitude of the various types of defects present in this system.

Chapter 8

8.1 Light emitting, electro luminescent materials.

In this chapter we explore the presence of traps in organic LED devices. The active layers of MEHPPV and P3OT are studied in a typical LED configuration. The single layered LED devices constructed are not efficient as far as brightness/output is concerned, but they provide a relatively less complex structure for trap characterization studies [166]. Luminescence, i.e., the de-excitation of excited atoms or molecules by the re-emission of absorbed energy as photons, provides information about the nature and dynamics of excited states of atoms or molecules in a solid. In molecular systems, the covalent binding of atoms within a molecule is much stronger than the van der Waals binding between molecules. For this reason, excitations are usually localized on a molecule. Charging and discharging of these trap levels or localized states can play an important role in the operation and performance of the devices, made of organic materials, such as the organic light emitting diodes (OLED's). The origin of the traps, in terms of interface or bulk, is important to understand to control the device efficiency.

A simplistic picture of processes at the metal/semiconductor interface is that a large part of the injected carriers will be trapped and are crowded near the electrodes. This process is known as trap-charge limited process which can be considered as a special case of the general space charge limited (SCL) regime. The trap energy level distribution is generally described by one of the following ways:

- § an exponential distribution,
- § a set of discrete levels.
- § and a Gaussian distribution.

Typically the highest filled electronic level, corresponding to the photoemission threshold, is $I_c = 5.1 \pm 0.3$ eV for the conjugated polymers.

The highest I_c is for PPP $\simeq 5.4$ eV, which has been measured directly. Several potential electrode materials (e.g., gold) have work functions comparable to the values above, so they should form an ohmic contact to any CP. The HOMO and LUMO levels

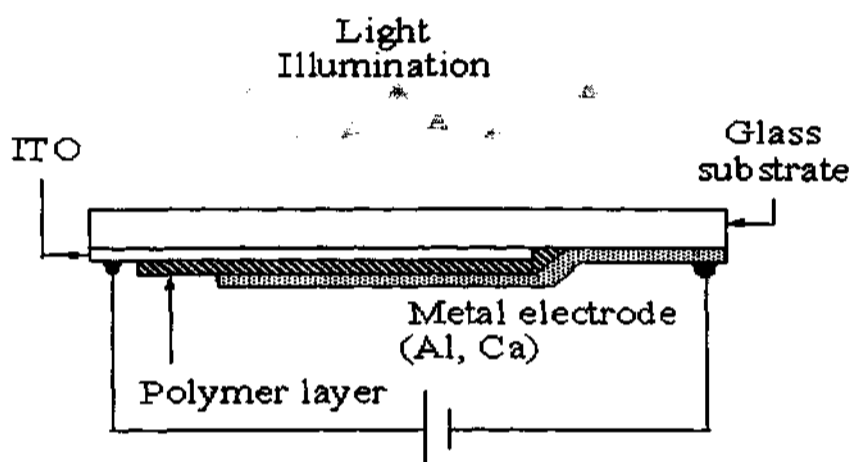


Fig. 8.1 Single layer LED device with asymmetric electrodes.

for P3OT, and PVK are 5.8 eV, 2.4 eV ($E_g = 2.6$ eV), MEH-PPV 4.9eV, 2.8 eV($E_g = 2.1$ eV) and for PVK 5.8 eV, 2.2 eV ($E_g = 2.6$ eV), respectively [?, ?, ?]. Similarly the workfunctions for metals are given: Ca (2.87 - 3.00 eV), In (4.12 - 4.20 eV), Ag (4.26 - 4.74 eV), Al (4.06 - 4.41 eV), Cu (4.65 - 4.70 eV), Cr (4.3 - 4.5 eV), ITO (4.6 - 4.9 eV), Au 5.1 - 5.47 eV) [?]. But interface states may greatly modify interface barrier shapes, so the choice of the value applicable to a real interface may be a problem. A particularly promising anode material is ITO conducting glass since, being transparent throughout the visible, it transmits the emitted light out from the diode. The importance of the chemical nature of the interfaces, and especially how it can modify the charge transport properties of the polymeric system has been theoretically and experimentally studied

for various aspects. However the interface layer is active when the interface gap lies in the forbidden gap of the bilayer or multilayer systems.

In this case, both holes and electrons can be trapped by the resulting interface wells. The interface layer can act as a quantum well for electrons or holes. Of course this happens only when the bandgap associated with the interface is small enough (otherwise the interface well will not be deep enough to trap the carriers). The localization in interface wells always lowers the effective gap.

In the case of metals with low workfunctions such as Li, Cs, Ca, etc are highly reactive to the surface with any oxygen available at the polymer surface, even in ultrahigh vacuum. Thus forms a thin, wide-bandgap barrier layer, plays a major role in

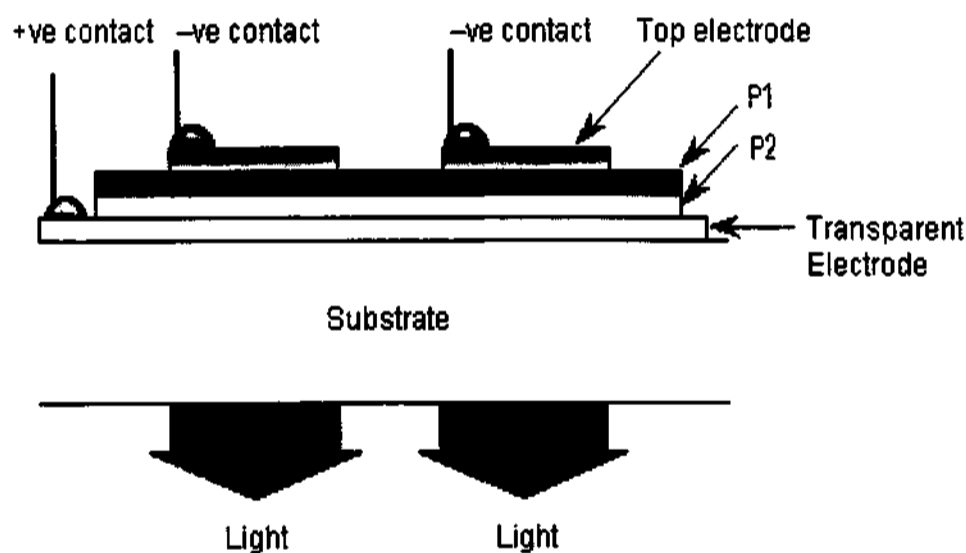


Fig. 8.2 Bilayer LED device with different metallic electrodes. P_1 and P_2 are the different CP's.

controlling the efficiency of the device. This problem can be encountered by choosing much larger workfunction metals (> 3 eV) such as Mg or Mg/Ag alloy (3.7 eV) or Al (4.3 eV), are able to inject enough electrons to generate intense EL. A sizable voltage drop occurs through the Al_2O_3 layer. This feature implies that the hole injection is rather easy than electron injection in CP's. This will result in imbalance in producing EL because most of the majority carriers will reach their respective electrodes without recombination. In order to achieve better EL efficiency, the insulating interface layer can be inserted may inhibit or even slow down, this hole extraction, depending on the relative positions of the bands. All CP's used in EL are non-degenerate ground-state polymers. In this case the carriers are not so free as in conventional inorganic semiconductors, the type of carriers such as polarons and bipolarons are involved. The characteristic times and relative binding energies are different from conventional inorganic materials.

8.2 Role of traps in EL devices

An existence of the trap can modify both transport and recombination of charge carriers is discussed in the chapter 3. Trap can bind and therefore immobilize an electron or a hole or the corresponding polarons. In three dimensions, trapping is expected that is independent of electric field up to very large fields, but diffusion and therefore the kinetics in trapping in quasi-one dimensional solids are peculiar. The carrier will spend most of the time in traps, its effective transit time being lengthened accordingly. Moreover the trapped charges does not contribute current, but it does to the recombination process, through the interaction with a free charge of the opposite sign, generally yield an emission spectrum and yield characteristic property of the traps. On the other hand, this may provide an alternate route of adjusting the emission color, or even of obtaining multicolor emission by balancing the emissions of several traps. In the case of molecular crystals with small μ , trap capture cross sections S_n (T) are usually very close to the geometric dimensions of the impurity, typically 10

given by $\tau_t = (N_t S_n v_{th})^{-1}$, where v_{th} is the average thermal velocity, assumed large compared to the drift velocity $\mu_0 E$. With $N_t \simeq 10^{16} \text{ cm}^{-3}$, $\tau_t \simeq 1 \mu\text{s}$. On the other hand detrapping or releasing time $\tau_{dt} = \nu \exp[-\frac{E_t}{kT}]$ where ν is a frequency factor (typically $10^{11 \pm 2} \text{ s}^{-1}$). This chapter completely emphasizes on the role of traps in single and bilayer organic devices. A key difference between the organic and inorganic LED's is the carrier transport properties. The carriers are directly injected in the former device and in the latter device, carriers originate from the dopants (donors and acceptors). As a result of this difference, the potential and charge distribution profiles in the devices are quite different for the two cases. Usually, the carrier distributions nearly a constant in the quasi neutral regions outside of the depleted $p - n$ junction in the inorganic devices, carriers are often crowded nearer to their respective electrodes, and their concentration drops rapidly away from the electrodes, hence the name the name space charge limited conduction.

In the electroluminescence device an electron and hole must recombine radiatively. This will depend on the nature of the electrodes and the transport properties of the charge carriers. Most of the cases in conjugated polymers, the hole mobility is high so that the controlled of electrons is necessarily adequate. In order to produce high efficient EL process, one must encounter the following cases:

- ¶ The carrier move as a delocalized wave pattern in a broad range with a relatively large mobility and high mean free path. This type of motion is considered as band type motion. In this case, the mobility $\mu \gg 1 \text{ cm}^2 \text{ V}^{-1} \text{ s}^{-1}$ with the temperature dependence as $\mu \propto T^{-n}$, where $n > 1$.
- ¶ Secondly the carriers are localized in a regime and moves by hopping from one site to site, with relatively small mobility and mean free path. Each type of motion is characterized by the magnitude and temperature dependence of the mobility.

In this case, for a strongly localized carrier, mobility $\mu \ll 1 \text{ cm}^2 \text{ V}^{-1} \text{ s}^{-1}$ and $\mu \propto \exp[-\frac{E}{kT}]$ which is thermally activated process. Most of the undoped conjugated polymers fall

in the category of hopping motion because of disorder (physical or chemical defects), large density of traps and less mobility.

8.3 Experiments and Results:

We demonstrate the applicability of this approach to characterize the trap states in other conjugated polymer systems such as poly-3-octylthiophene P3OT and poly-2-methoxy-5-(2'-ethyl-hexyloxy)-1, 4 paraphenylenevinylene MEHPPV.

8.3.1 Introduction

There is very little quantitative estimates of the densities and the energetics of these trap states in spite of their profound impact on the optical and electronic properties in these polymeric systems [7.167]. The nature of traps is usually discussed in terms of their location (interfacial and bulk), depth (deep and shallow), origin (extrinsic or intrinsic). We employ TSC measurements to estimate the magnitude and the type of kinetics in these polymeric systems. The interpretation of the results is based on fitting the experimental results to expression from different models for the kinetic processes. The existence of wide variety of traps in these systems is observed unambiguously. We probe the nature of these trap states and their role in charge transport. The choice of the conjugated polymers P3OT. and MEHPPV used for the present studies have been based upon the strong evidence of traps in these systems from previous experimental results. The availability of regioregular head to tail (H-T) polyoctylthiophene was an important criteria. The H-T regiospecific polymers have improved conductivity and NLO properties over regiorandom polymer. In other words the regioregular polymers have lesser defects due to unhindered linkages compared to regio random polymers. On the other hand MEHPPV has been the most studied light emitting polymer in the last decade, especially in terms of device properties and photophysical excitations.

8.3.2 Experimental

High purity regioregular P3OT and MEHPPV were obtained from different

sources. Solutions of P3OT and MEHPPV were prepared by dissolving the pristine polymers in *p*-Xylene. Experiments on free standing oriented films were also studied. Thin films were obtained from the solution using spin coating and casting techniques

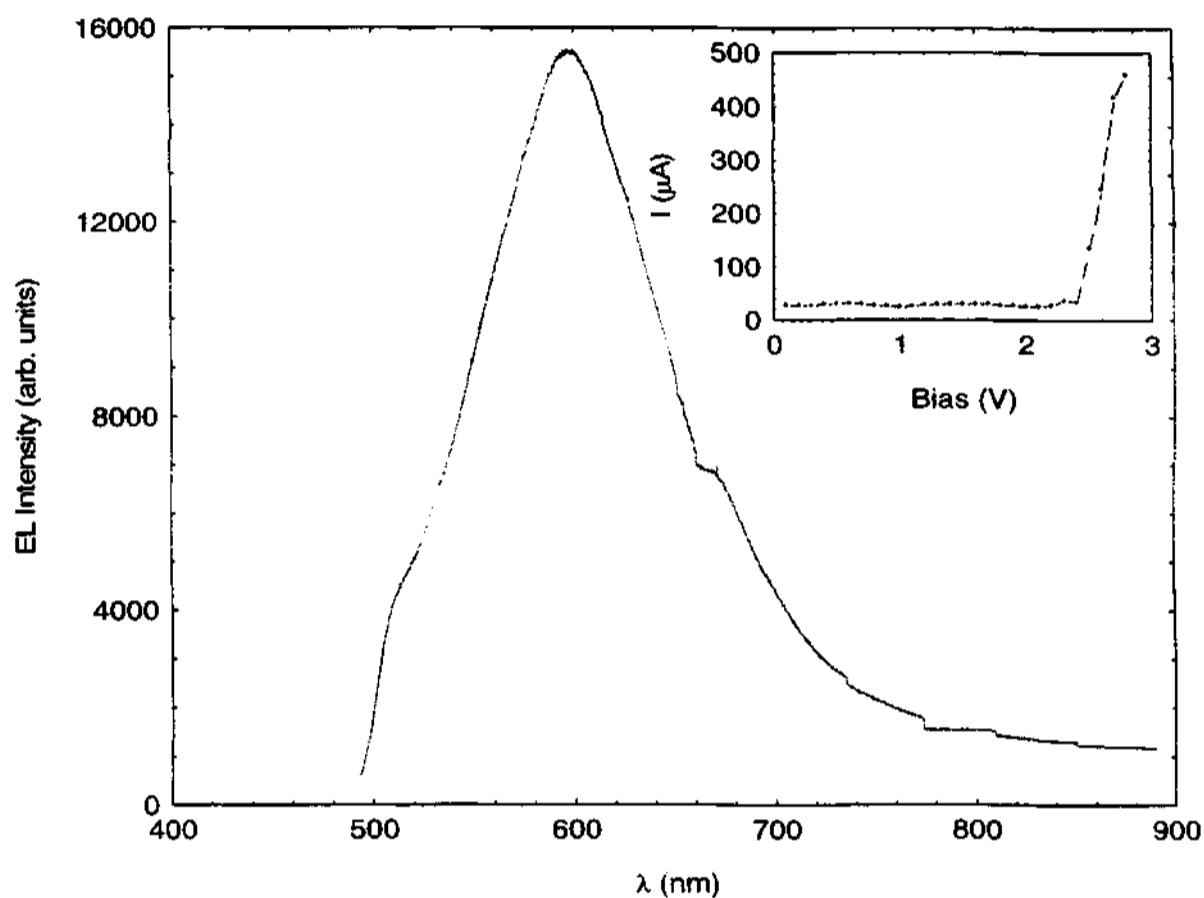


Fig. 8.3 I-V characteristics (inset) and spectral response of ITO/MEHPPV/Al single layer LED device.

on different electrodes. Measurements were done on samples with symmetric electrode configuration with aluminium or gold as the top and bottom electrode. For MEHPPV based devices asymmetric configuration with ITO and aluminium was also fabricated. The thickness of the spin coated P3OT and MEHPPV films used for measurements in this report were in the range of 100 - 200 nm. The thickness of these films were measured using a multiple interference technique developed in our laboratory [?]. The

technique involves in relating the thickness of the polymer film to the difference in the interference pattern obtained from the top and bottom layer of the film. Fig. 8.3 shows the schematic picture of single layer polymer device. Inset shows a typical I-V curve and a spectral response of ITO/MEHPPV/AL device obtained in our laboratory.

TSC measurements were carried out by filling up the traps using constant voltage/current source at different temperatures, following which the TSC was measured up on heating the sample at constant rate under short-circuit conditions.

8.3.4 Results and Discussion

Fig. 8.4 shows the TSC results of thin P3OT films with different initial current injection values. A peak at $\simeq 50$ K was consistently observed for all samples. In this case the fits to an initial rise method requires a correction in the offset term corresponding to the starting temperature which varies with the initial trap filling parameters. Initial estimates of E_t indicate trap depth of $\simeq 50$ meV using the initial rise method. Efforts are on in our laboratory to relate this value obtained for the trap depth to other feature observed in P3OT in other experiments. Regioregular P3OT has one of the highest measured mobility amongst conjugated polymers with recent field effect mobility values of 10^{-2} cm²/Volt-sec. The low activation depth of 50 meV of the hole traps in P3OT is indicative of such high mobility values. From the first order fits, the trap depths for the peaks at $T_{max} \simeq 50$ K and 225 K are 13 meV and 53 meV. The total releasable charges from the trap states obtained from the area under the integration is $\simeq 19$ μ C and its corresponding releasable charge density is given by $\simeq 5 \simeq 10^{19}$ cm⁻³, respectively. P3OT also exhibits features such as thermochromism where a mild thermal treatment causes changes in optical absorption due to possible subtle changes in the electronic structure. This phenomenon has been attributed to the twisting of the thiophene chain with a subsequent decrease of conjugation length. The thermal processes which leads to these changes are of the same order as the trap

depth values.

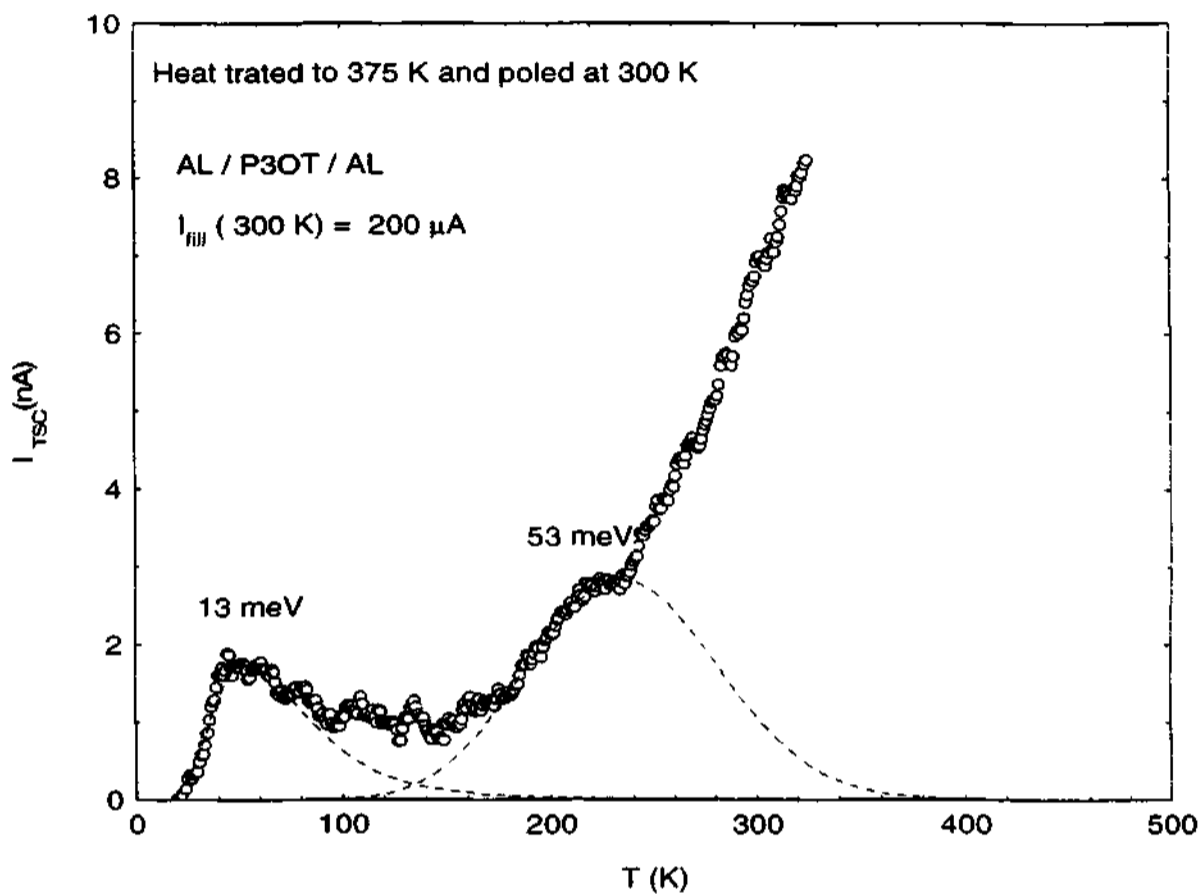


Fig. 8.4 TSC obtained after trap filling current ($200 \mu\text{A}$) for AL/P3OT/AL sample. Dashed lines are the first order fits.

The origin of these traps can then be speculated to arise from intrinsic processes such as subtle structural distortion/conformations, which upon thermal excitation can lead to effective changes in conjugation parameters.

Fig. 8.5 shows the TSC results of a standard ITO/MEHPPV/AL device. The initial parameters for trap filling was carried out by applying a voltage bias of 1 V, at $I = 15 \text{ mA}$ (linear I-V range of the device). The total releasable charges from the trap states is $\simeq 38 \pm 2 \text{ nC}$ and its trap density is $\simeq 10^{18} \text{ cm}^{-3}$. A distinct maxima is

observed at 225 K corresponding to a trap level of 0.1 eV based on a fit to an initial rise model, accompanied by local peaks. The trap depths are obtained for several maxima (from the second order fits, it fits better better than the first order fits) is given by 71, 88 and 128 ± 3 meV, respectively. The TSC results are sensitive to the time duration between successive temperature scans due to a long-lived persistence effect.

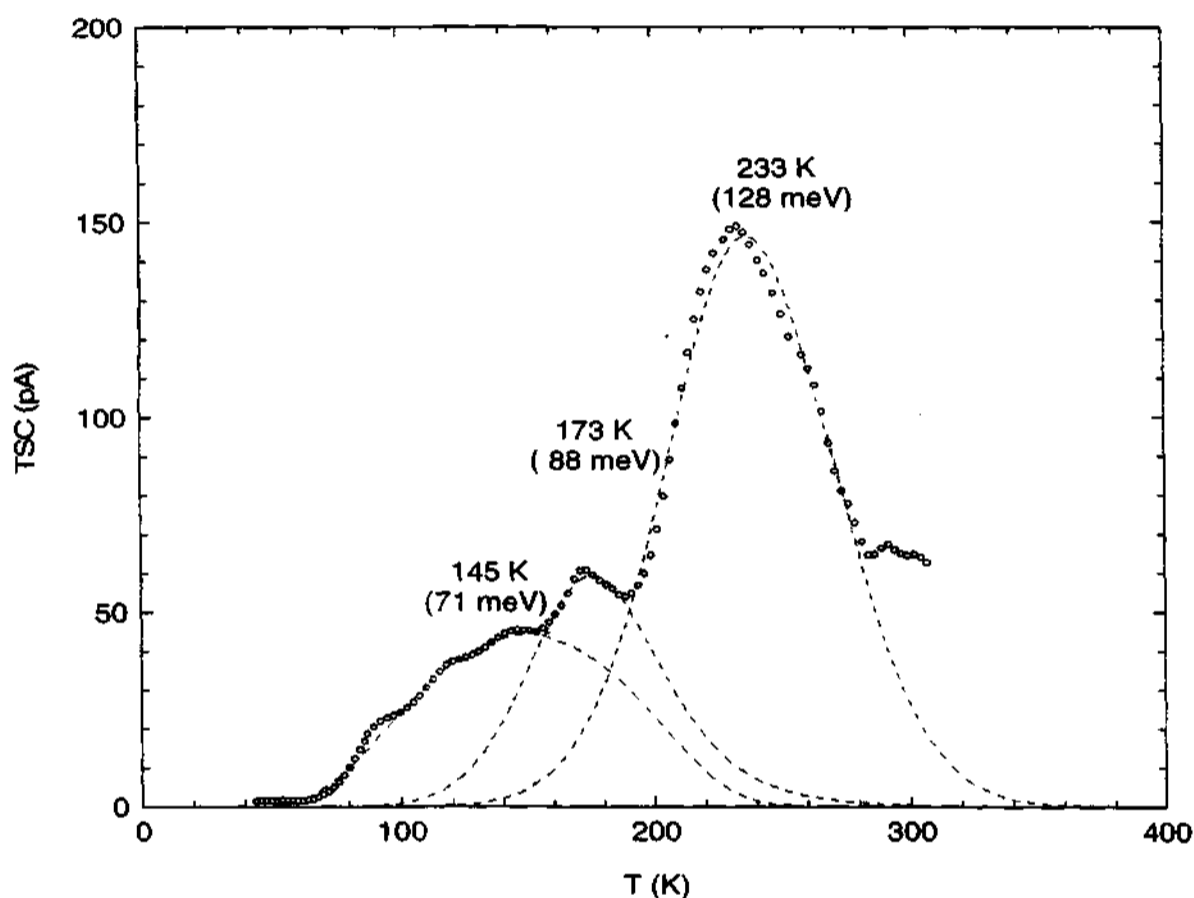


Fig. 8.5: TSC of ITO/MEHPPV/AL device after initial trapping current of 15 mA. Dashed lines are the second order fits.

Previous studies on MEHPPV using transient capacitance spectroscopy technique showed the presence of a majority-carrier trap at 1.0 eV and two minority traps at 0.7 and 1.3 eV, respectively which were comparable to TSC results on PPV. In the recent studies of underivatized PPV based LED devices, two TSC peaks were observed at

100 K and 150 K. The two peaks were analyzed in terms of different types of traps. Deep traps were assigned to the influence of the environment, while the shallow ones were assigned to a doping process by the ITO substrate. The results on MEHPPV based devices can also be expected to have similar qualitative features in their TSC responses.

In summary, we demonstrate the use of TSC measurement techniques as an effective tool to estimate the magnitude of the trap levels and their densities. We have determined the existence the trap levels of 50 meV, and 0.1 eV for P3OT and MEHPPV respectively. The studies of TSC on the dependence on initial trap-filling conditions are expected to throw considerable insight in the nature of the traps in these systems.

Chapter 9

Interfacial effects in bilayer devices

9.1 Introduction

In this chapter, interfacial effects in bilayer devices are probed. Bilayers are constituted with the intrinsically *n*-type BBL and a *p*-type polymer such as P3OT or PVK [168–181,204]. The interface formed in this case are however, quite different from that of inorganic junctions. This section explores the results of photocurrent and TSC properties of these bilayer systems.

Charge transfer upon contact between two dissimilar materials is inevitable. Contact charging can be defined as the spontaneous redistribution of charge across the interface between the two materials brought in contact with one another [131,130]. Primarily the study contact charging is made more complex even for simpler systems because of the higher concentrations of impurities and defects usually prevalent at surfaces. It is still not possible to get an accurate measurement of the contact charge density, quantity of chief interest, because the actual area of contact between the materials is indeterminate. All surfaces are rough or irregular or at least on a microscopic scale, and the actual contact area is always less than the apparent area of contact. In addition to that the material is viscoelastic, as are polymers, the contact area can change during the period of contact under deformation conditions [131].

A tremendous advantage in CP based devices is the possibility of multilayered structure similar to the heterostructures in conventional inorganic semiconducting materials, but without the constraints of factors such as lattice matching epitaxial growth encountered inorganic semiconductor devices. An important criteria for the bilayered

polymer structures is the necessity of different solvents for each polymer. The post-processing of the polymer layer which are grown also need to be compatible. Bilayer devices of CPs have shown much improved LED efficiencies, due to the following reasons:

- ¶ Reduction of barrier at the electrodes,
- ¶ Possibility of matching electron and hole injection rates, and
- ¶ Control of the recombination zone.

However, the multiple steps also introduce defects which are detrimental to the device emission efficiency. Fig. 9.1 (a) and 9(b) show the configuration of single layer, bilayer and three layer LED devices and the charge distribution in different devices. In this section we discuss the results of the photocurrent enhancement in bilayer devices and explore the possibility of evaluating the traps in a bilayer CP system using TSC measurements.

The specific motivation for these studies as far as BBL is concerned is from the perspective of the photovoltaic properties. The *n*-type nature of BBL was recently established using photo induced discharge curve PIDC (xerographic discharge experiments) [?].

It was found that the negative charge acceptance (surface charge density) on BBL films/fibers was much higher than positive charge acceptance. It was also observed that the derivative of initial decay of PIDC is higher when the surface was charged negative indicating electrons as the predominant charge carriers in BBL. It has also been recently observed in our laboratory that BBL in a bilayer form with polythiophene and PPV derivatives have large quantum efficiency for short-circuit photocurrent generation with nearly three orders in magnitude more than in the single layer of BBL, and greater than a factor of 100 to P3OT single layers.

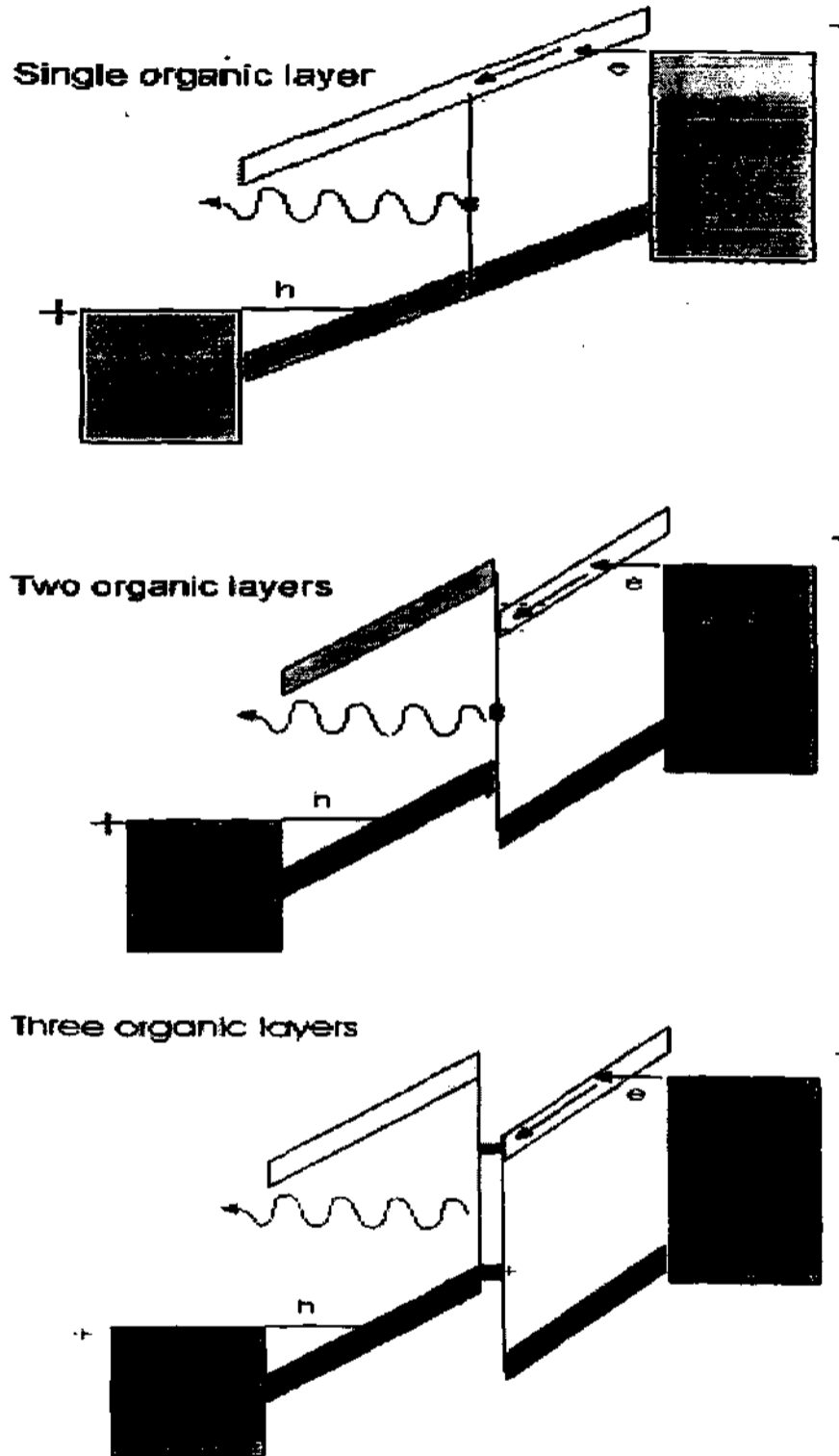


Fig. 9.1 (a) Different layer LED devices

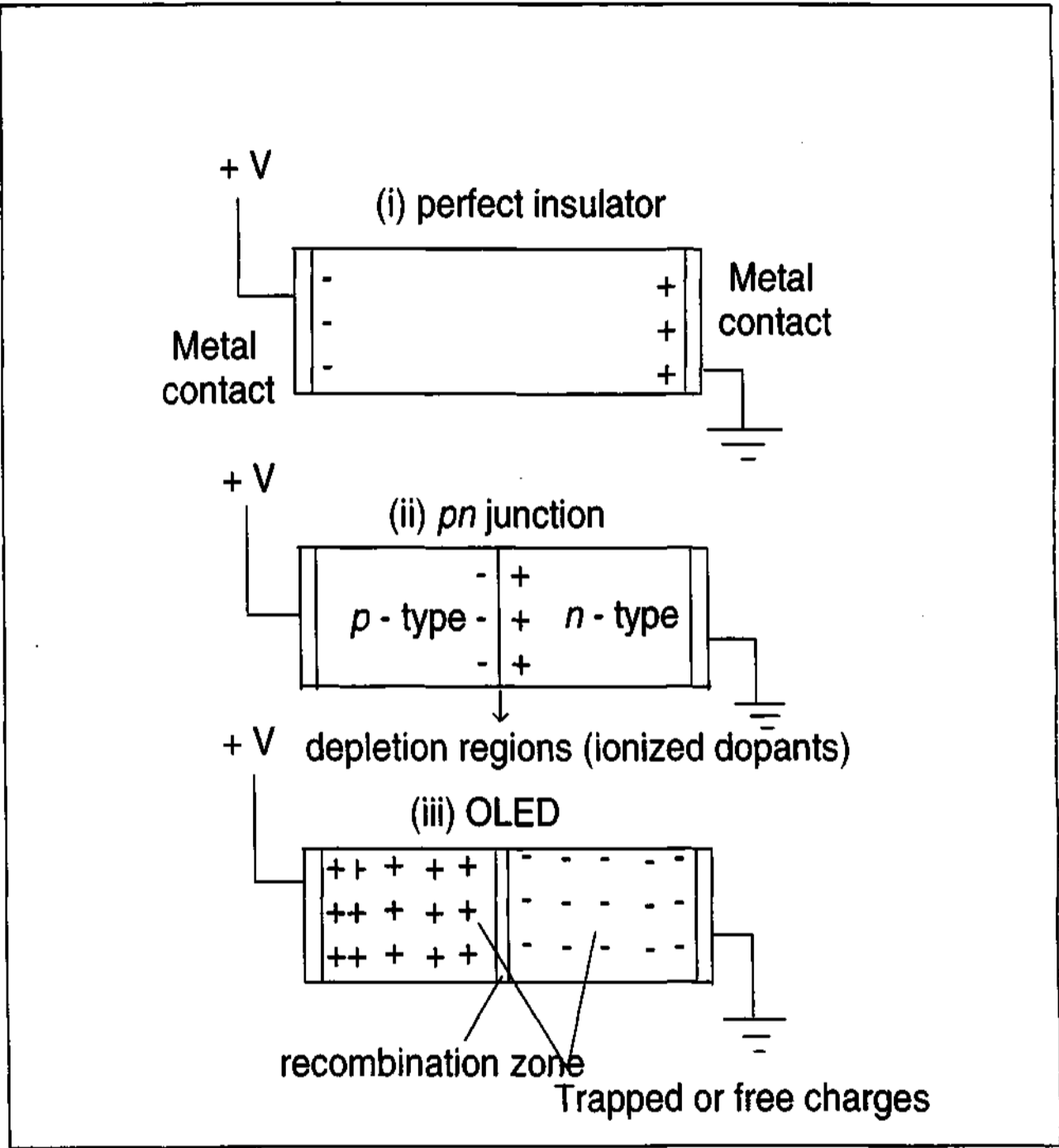


Fig. 9.1 (b) Illustration of charge distribution in insulator, p - n device and OLED.

A simple band model of M1/BBL/PVK (or P3OT)/ITO as shown below can explain this picture. The bilayer system is different from a conventional heterostructure p - n junction. The band picture reveals the possibility of the various barriers existing in this device; at the electrode interfaces and at the polymer-polymer interface. The choice of the electrodes for photovoltaic properties is governed by minimizing the barrier for the electron transfer across the BBL/M1 junction and the hole transfer across the PVK (or P3OT) ITO junction. The right combination of HOMO and LUMO levels of the two polymer layers are then chosen to assist this photogenerated transport property. In this case, BBL/P3OT satisfy this basic criteria for enhanced photogenerated transport. However, the polymer-polymer interface forms the crucial region where the charge-separation enhancement (in reverse bias) takes place. TSC and photovoltaic measurements were carried out in these BBL/P3OT and BBL/PVK samples to probe the effect of the interfaces.

9.2 Bilayer structure

Thin cast BBL films ($\simeq 100$ nm thick) are obtained from the Lewis acid complexation routes. The cast films of BBL are coated on P3OT ($\simeq 100$ nm) and PVK ($\simeq 100$ nm) and vice versa. Photovoltaic measurements were carried with light incident on the ITO side, and the zero bias photocurrent was measured in the steady state and transient mode also. TSC measurements on bilayer devices such as ITO/P3OT/BBL/AL, ITO/PVK/BBL/AL, ITO/BBL/P3OT/AL and ITO/BBL/PVK/AL were carried out in sandwich geometry. The metal electrode Al ($\simeq 50$ nm) was coated on both sides of surfaces of the samples. The TSC measurements were carried out for different bilayer samples by filling out of the traps using constant current source (10μ A). All the samples were poled at $T_P \simeq 350$ K, following which the TSC was measured upon heating the sample at a constant rate under short-circuited conditions. The linear heating rate (β) typically was 2.5 K/min for all the bilayer systems and all the experiments were

performed in vacuum.

9.3 Results and Discussions

9.3.1 Short circuit photocurrent (I_{ph}^{sc}) measurements)

Fig. 9.2 shows the zero bias photoinduced transient currents measured as a function of time of different bilayers. The key features of the results from these bilayers are as follows:

- ¶ I_{ph}^{sc} photocurrent efficiency (Photocurrent per unit incident photon) in bilayer devices are higher than single layer devices, as shown in Fig.
- ¶ Charge accumulation effects are observed in bilayers, with a decay of I_{ph}^{sc} after an initial built-up with the light on, upon prolonged exposure (> 10 msec). Charge accumulation effects can be minimized with pulsed sources with a control of the pulse width and pulse repetition rate. This procedure was adopted with LED sources driven by function generator [205]
- ¶ The direction of short-circuit photocurrent indicated hole transfer to ITO and electron transfer to Al electrode as shown in Fig. 9.2 in ITO/P3OT/BBL/Al devices. This observation along with the first point implies a light induced hole transfer from BBL layer to P3OT layer or/and an electron transfer from P3OT to BBL. Recent experiments examining this processes, with light incident from both sides simultaneously, have indicated that hole transfer from BBL to P3OT

seems to be a likely event.

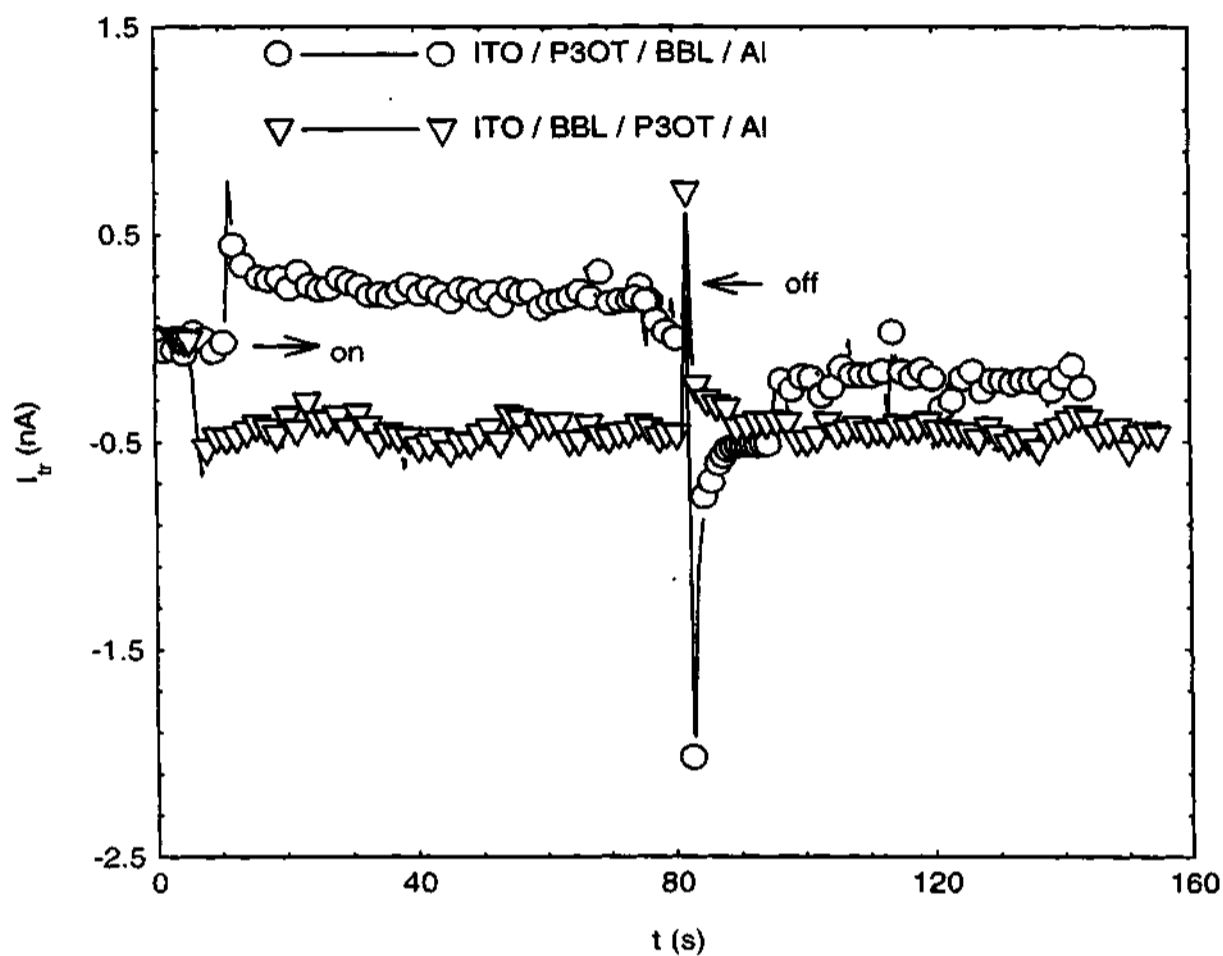


Fig 9.2 I_{ph}^c of ITO/P3OT/BBL/AL and ITO/BBL/P3OT/AL bilayer systems.
i.e.; the on and off cycle.

- ¶ It was also observed that Au forms a more stable electrode than Al, with reduced space charge effects.
- ¶ Studies done on devices with barrier at the electrode devices such as ITO/BBL/P3OT/AL and ITO/BBL/PVK/AL also indicate that the polymer/polymer interface is the dominant factor for the photocurrent with the electrode barriers playing a secondary role, as shown in Fig.

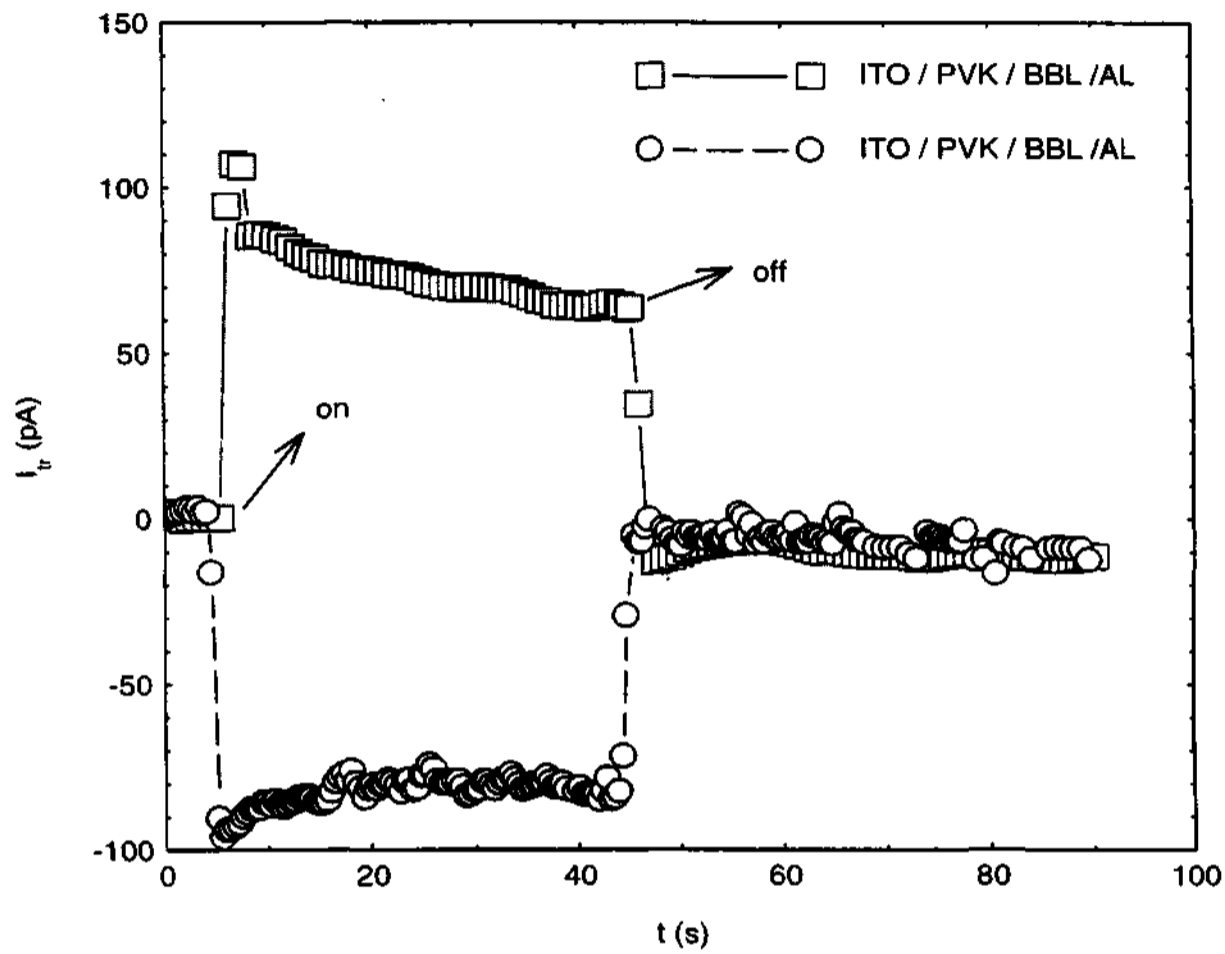


Fig. 9.3 I_{ph}^{sc} of ITO/PVK/BBL/AL and ITO/BBL/PVK/AL bilayer systems.
i.e.; the on and off cycle.

The spectral response of the single (ITO/BBL/AL and ITO/P3OT/AL) and

bilayer devices

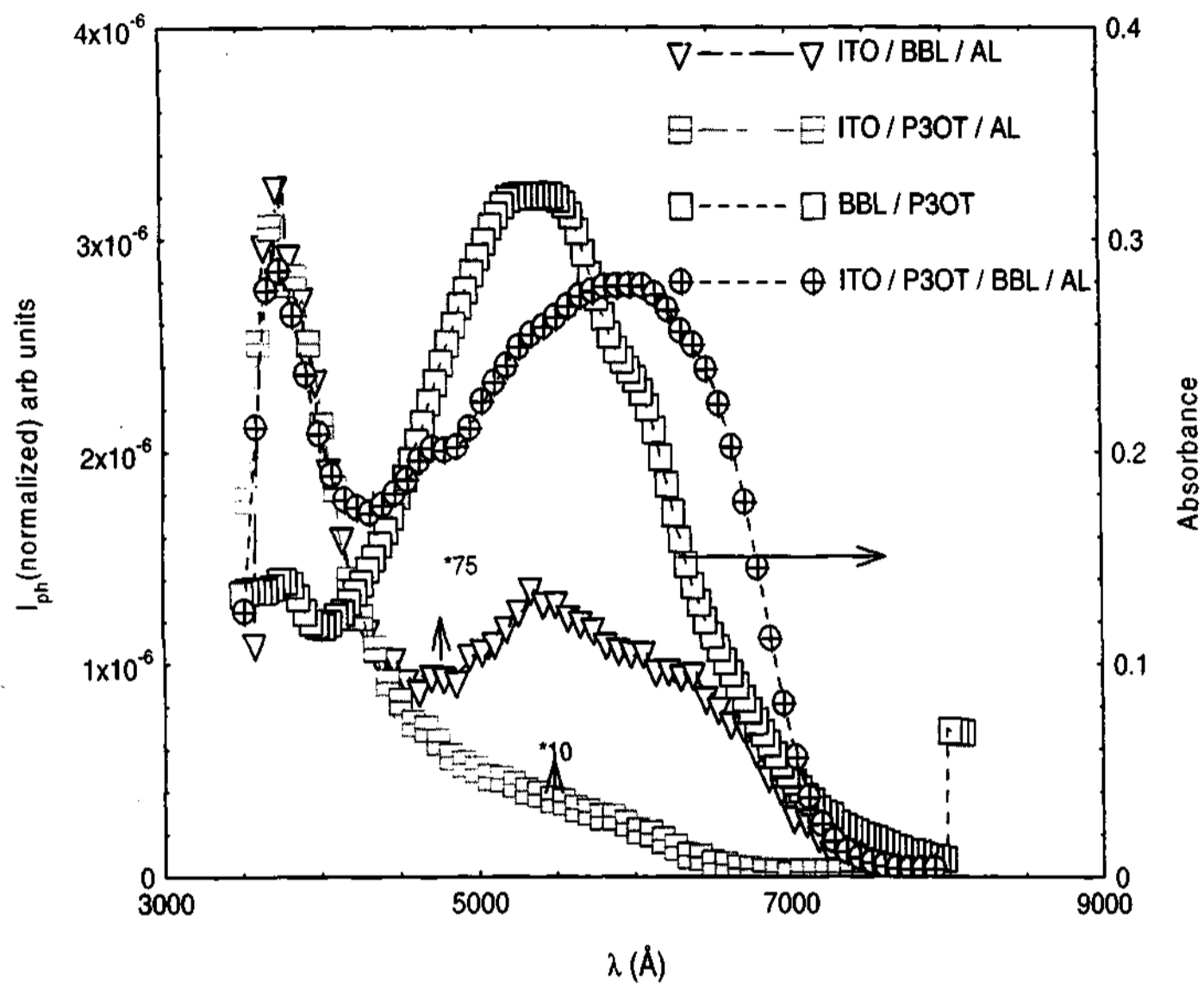


Fig. 9.3 Spectral response of single and bilayer devices

of ITO/P3OT/BBL/AL are shown in Fig. 9.4. The spectral range covers the entire visible region and is wider than single layered BBL device (due to an enhancement near the absorption edge).

9.4 Thermally stimulated current (TSC) measurements

The added effect of the interface in a bilayer sample is studied using TSC. The initial poling temperature, $T_P < 350$ K is chosen to study the TSC in the pre-annealed phase of the material.

Fig. 9.3 shows the TSC of the ITO/PVK/BBL/AL film after poling at 350 K at constant current source $I_{sour} = 10 \mu\text{A}$ in sandwich geometry. $I_{TSC}(T)$ as shown in this

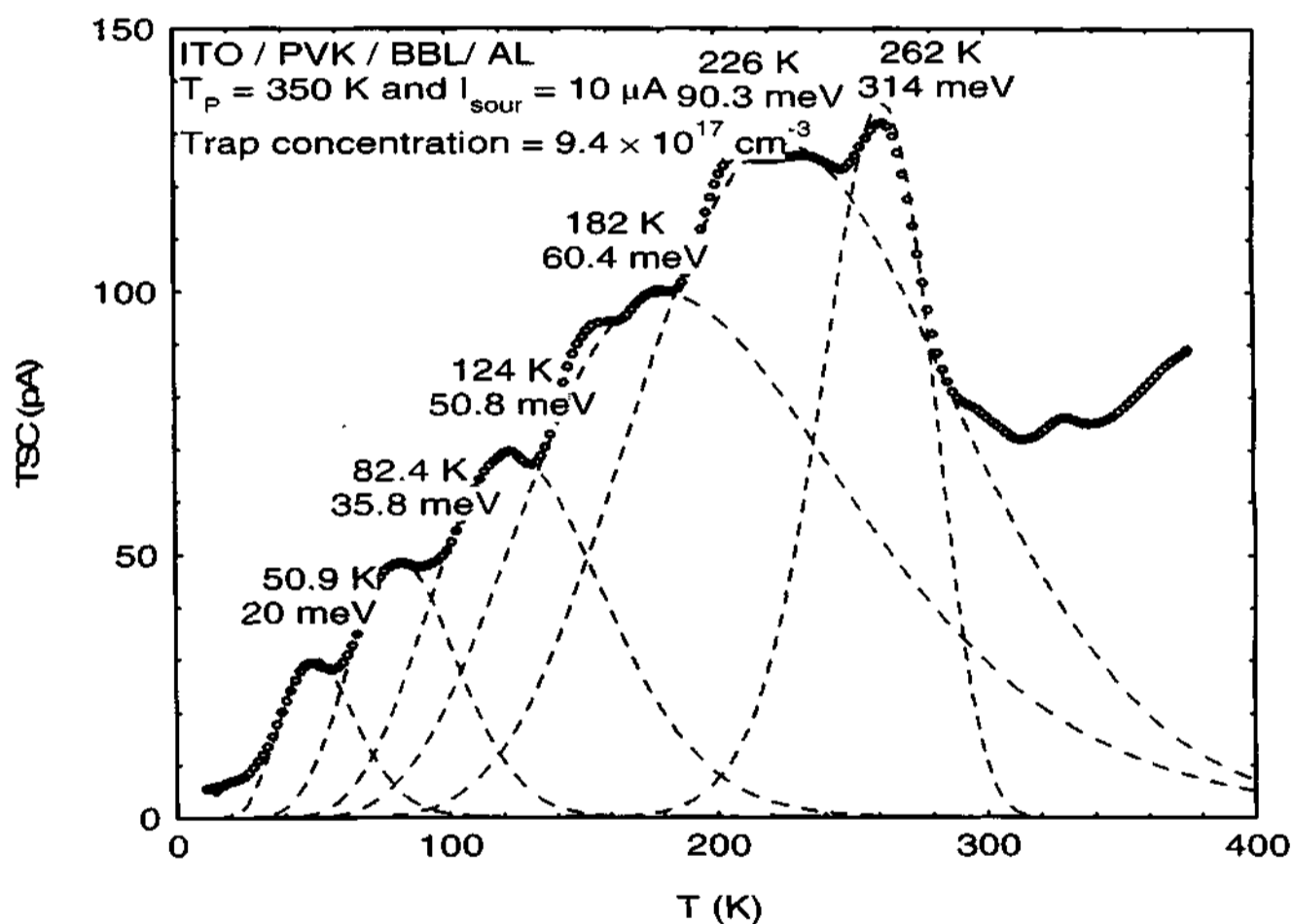


Fig. 9.3 TSC spectra obtained for ITO/PVK/BBL/AL film. Dashed lines are the fits based on first order kinetic model.

figure consists of several peaks positioned at $T_{max} \simeq 51$ K (20 meV), 82 K (36 meV), 124 K (51 meV), 182 K (60 meV), 226 K (90 meV) and 262 K (0.31 eV) respectively. The trapping parameters are obtained from the first order fits. The total number of released charges during this experiment is $\simeq 68$ nC which corresponds to the releasable trap density is $\simeq 10^{18} \text{cm}^{-3}$.

Fig. 9.4 shows the TSC of the ITO/P3OT/BBL/AL film after poling at 350 K at constant current source $I_{sour} = 10 \mu\text{A}$ in sandwich geometry. $I_{TSC}(T)$ as shown in this

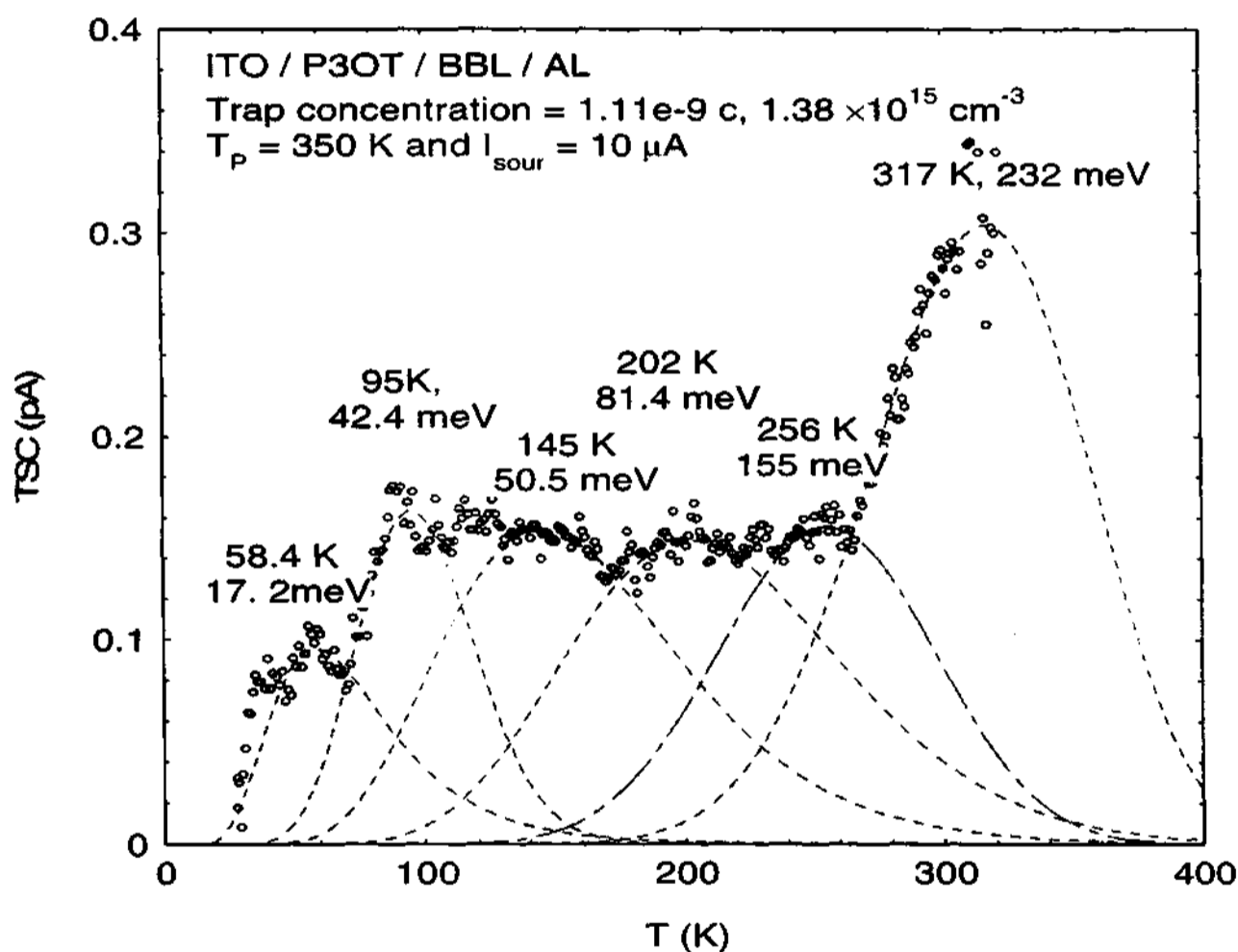


Fig. 9.4 TSC spectra obtained for ITO/P3OT/BBL/AL film. Dashed lines are the fits based on first order kinetic model.

figure consists of several peaks positioned at $T_{max} \simeq 58$ K, 95 K, 145 K, 202 k, 256 K and 317 K. From the first order fits, the trap depths corresponding to T_{max} are 17 meV, 42 meV, 51 meV, 81 meV, 155 meV and 232 meV respectively. The total number of released charges during this experiment is 1.19 nC which corresponds to the releasable trap density is $\simeq 1.4 \times 10^{15} cm^{-3}$. The lower value of releasable trap density could indicate the interfacial effects are drastically reduced by three to four orders of magnitude when compared with the other bilayer devices.

When the polymer films are sandwiched between the two metal electrodes, there is presumably a spontaneous charge transfer takes place at the polymer-polymer and metal-polymer interfaces, which in turn produces a current in the system under short-circuit conditions. As the temperature rises, the charge trans-

fer takes place across the interfaces,

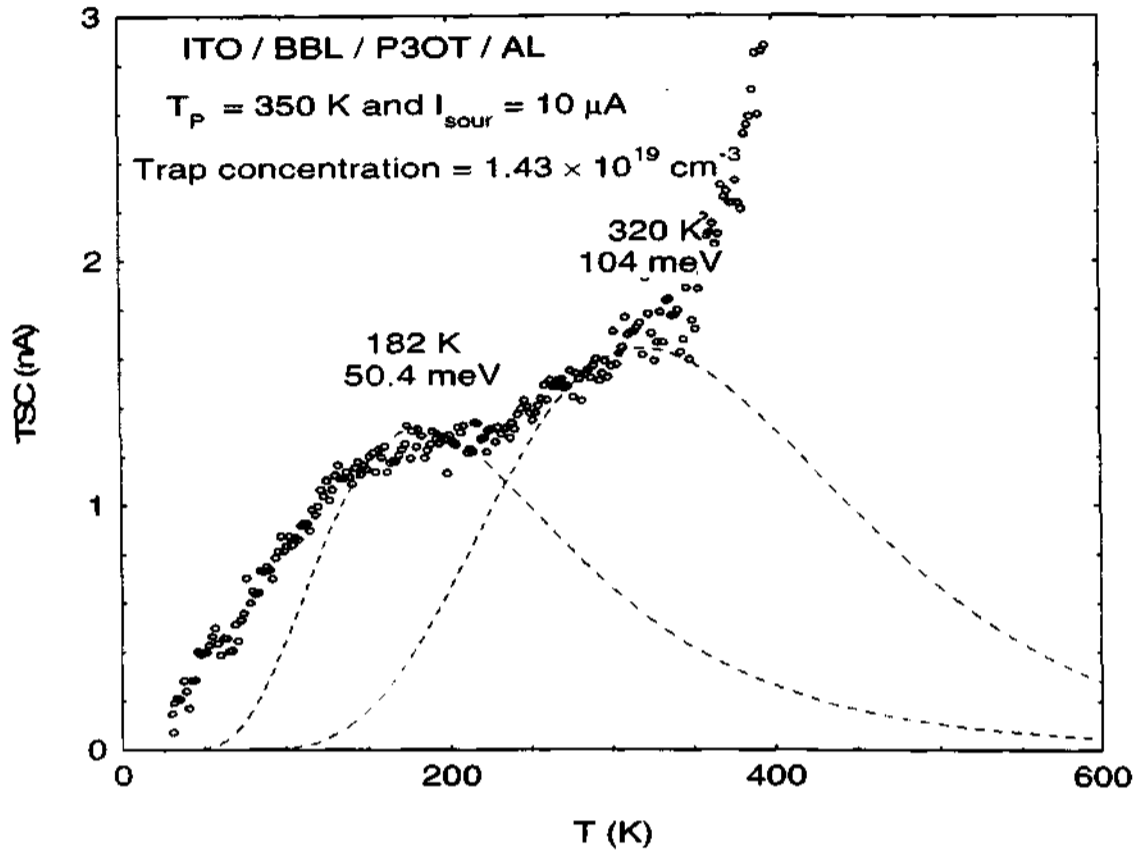


Fig. 9.5 TSC spectra obtained for ITO/BBL/P3OT/AL film. Dashed lines are the fits based on first order kinetic model.

reflected as a change in the current with temperature, which is probably due to the relative temperature dependence of the relative work functions of the individual materials. In addition to that inherent conductivity of the polymers can also contribute TSC partially. Furthermore, the increase in TSC is due to the disorientation of the frozen-dipoles or released trapped space charges within the polymers. The direction of TSC is similar to I_{ph}^{sc} in these bilayer devices in all the combinations.

Fig. 9.5 shows the TSC of the ITO/BBL/P3OT/AL film after poling at 350 K at constant current source $I_{sour} = 10 \mu A$ in sandwich geometry. I_{TSC}

(T) as shown in this figure consists of several peaks positioned at $T_{max} \simeq 182$ K (50 meV) and 320 K (0.1 eV) respectively. The total number of released charges during this experiment is $\simeq 11 \mu\text{C}$ which corresponds to the releasable trap density is $\simeq 10^{19} \text{cm}^{-3}$.

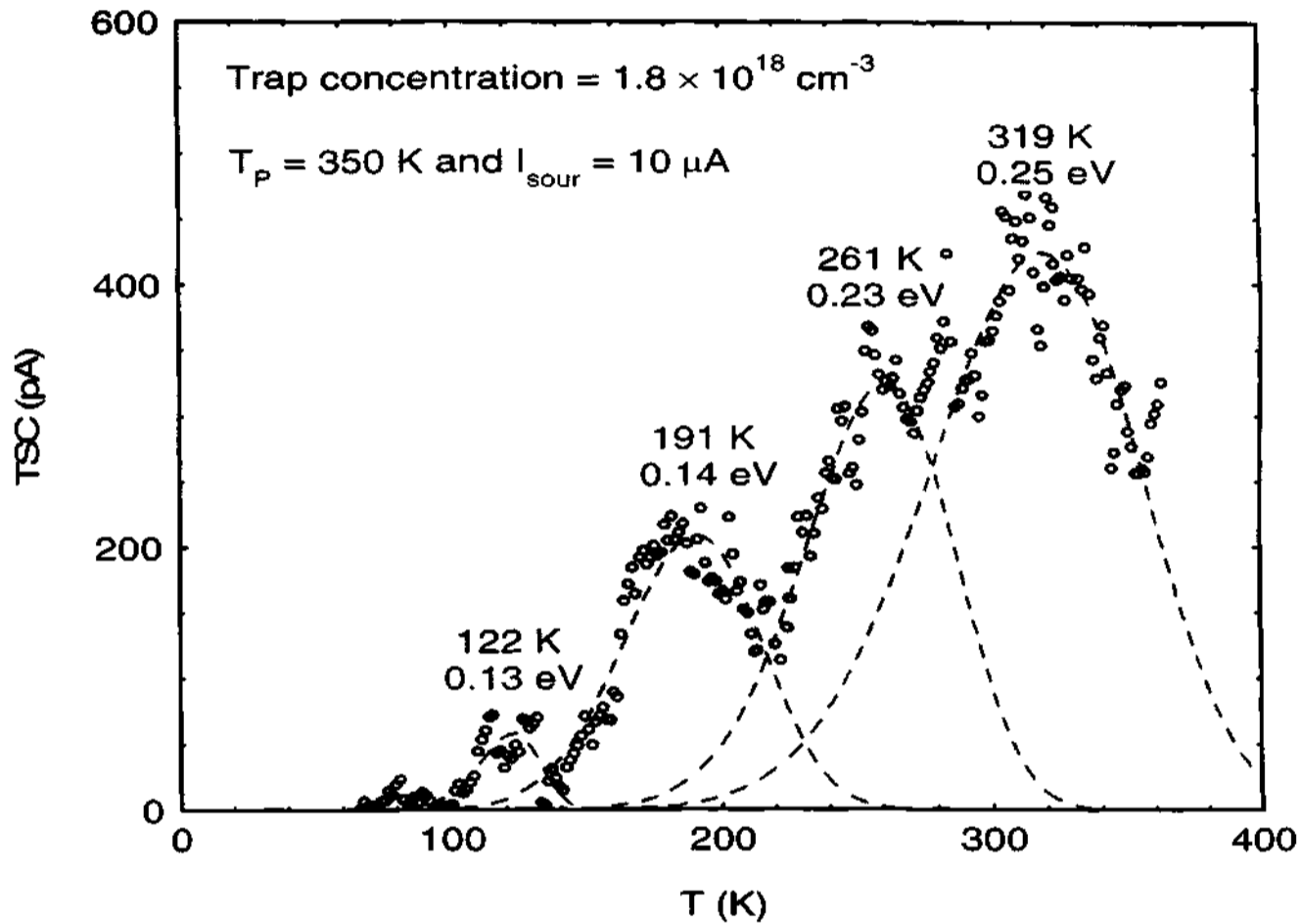


Fig. 9.6 TSC spectra obtained for ITO/BBL/PVK/AL film. Dashed lines are the fits based on first order kinetic model.

The relatively large difference in the trap concentration obtained for this configuration could be due to largely presence of barriers involved in this system.

Fig. 9.6 shows the TSC spectra of the ITO/BBL/PVK/AL film after poling at 350 K at constant current source $I_{\text{sour}} = 10 \mu\text{A}$ in sandwich geometry. $I_{\text{TSC}}(T)$ as shown in this figure consists of several peaks positioned at $T_{max} \simeq 122$

K (0.13 eV), 191 K (0.14 eV), 261 K (0.23 eV) and 319 K (0.5 eV) respectively. The total number of released charges during this experiment is $\simeq 1 \mu\text{C}$ which corresponds to the releasable trap density is $\simeq 10^{18} \text{cm}^{-3}$.

The measurements of bilayer systems seem to indicate that the trap distribution is more discrete in distribution when Schottky-type electrodes are used. In the case of symmetric (nearly ohmic) metal contacts a single broad TSC peak is the main feature. It is difficult to ascertain the exclusive contribution from the defects at the polymer-polymer interface. The defect densities obtained from the integral of the TSC curves indicate a much lower (nearly three order) defect densities in ITO/P3OT/BBL/AL ($\simeq 10^{15} \text{cm}^{-3}$) compared to single layer ITO/BBL/AL ($\simeq 10^{18} \text{cm}^{-3}$) device. This feature qualitatively implies a defect ridden ITO/BBL interface. The defect densities obtained for the bilayer devices such as ITO/PVK/BBL/AL and ITO/BBL/AL do not vary significantly. However, with a systematic study (appropriate electrodes and thickness) it may be possible to pick up features in TSC arising from space charge relaxation processes which are evident in the photocurrent experiments. It is evident that the concentration of released trapped charges obtained for bilayer devices are distinctly different than those for the single layer devices. The difference is, in all probability, the effect of the polymer-polymer interfaces.

Chapter 10

I-V Characteristics and Relaxation processes in Kapton

This chapter focusses on electronic defects in the non-conjugated polymer Kapton [206]. Poly-4, 4'-oxydiphenylene-pyromellitimide (Kapton) is an aromatic polyimide with a rigid chain structure, is a high resistant insulating material. It is an organic solid with no melting point, but it has a glass transition temperature at $T_g \simeq 385^\circ\text{C}$. electrical and mechanical properties such as low dielectric constant $\simeq 3.5$ (1kHz), breakdown strength of $\simeq 4 \times 10^6$ V/cm, and specific resistivity of 10^{17} $\Omega\text{-cm}$ at room temperature Kapton^(R) is a high performance polymer which is typically orange and transparent in appearance. It has got excellent electrical and mechanical properties such as low dielectric constant $\simeq 3.5$ (1kHz), breakdown strength of $\simeq 4$ MV/cm, and specific resistivity of $\simeq 10^{17}$ $\Omega\text{-cm}$ at room temperature¹. It is commercially available as Dupont Kapton^R and was gifted by Prof. Govindaraju, University of Windsor, Canada.

Kapton is typically used as a dielectric insulator. Polyimides are a group of thermally stable materials that exhibit excellent chemical resistance and good mechanical properties [207–215,217–223,?]. Known for its outstanding thermal, mechanical, chemical and electrical properties, Kapton^(R) is an advanced electrical insulation material used in the electrical industries, which

- ¶ maintains its mechanical stability at very high and very low temperatures ranging from 4 K to 675 K,
- ¶ resists high mechanical stress during assembly operations,
- ¶ has excellent electrical insulation and thermal properties.
- ¶ has outstanding resistance to most chemicals, solvents, lubricants and fuels,
- ¶ allows space and weight savings.

It is highly used in microelectronic devices, in aircraft and space applications, mainly owing to their thermal stability upto $\approx 500^\circ\text{C}$.

Fig. 10.1 shows the synthesis of polyimide from PPA precursor. It is manufactured

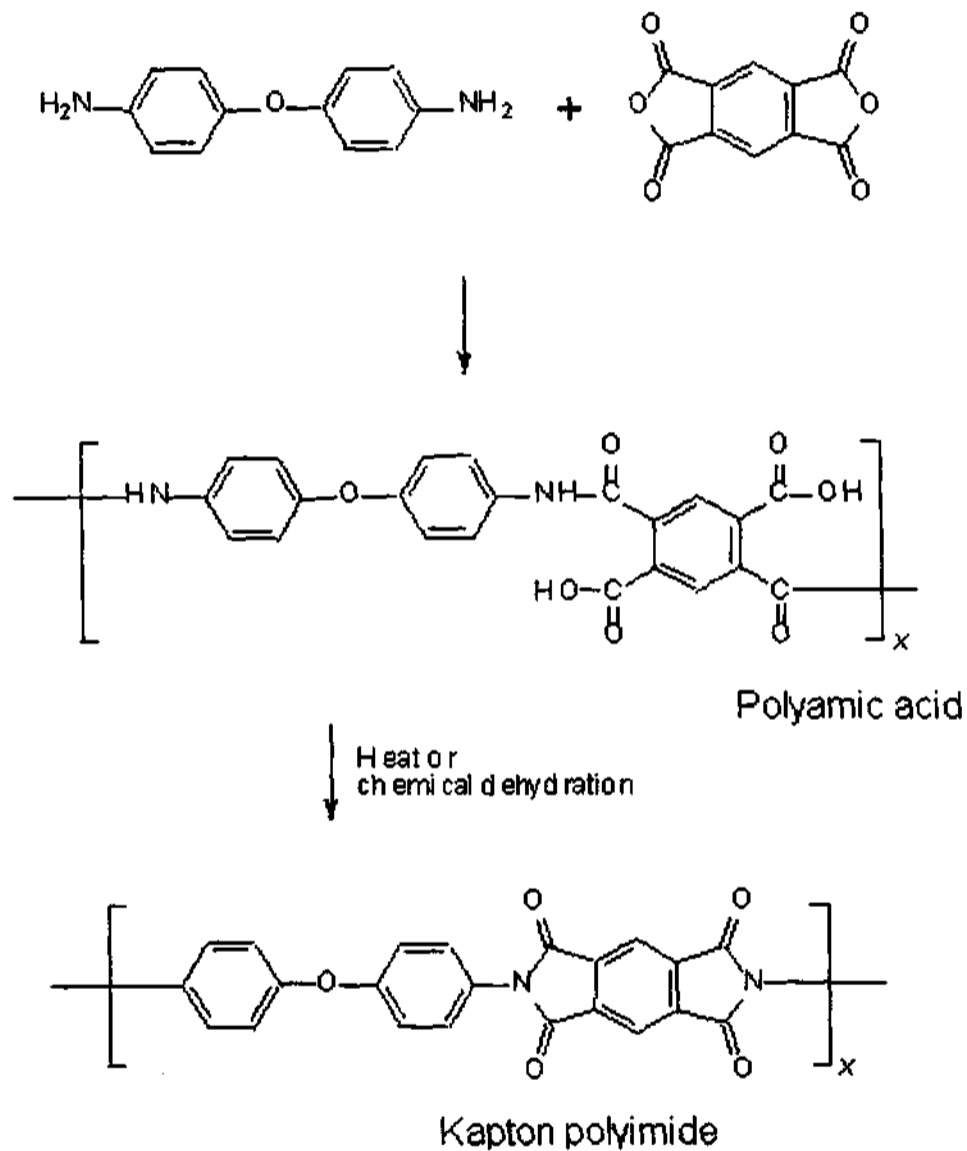


Fig. 10.1 Synthesis of polyimide Kapton through PPA precursor

through the dehydration and cyclization of its polyamic acid (PPA) precursor. This produces a largely amorphous film, having an as-received crystallinity of

5%. Since annealing at 515 K for more than 24 hours only raises the crystallinity to 9.5 % with the remarkable stability. PPA precursor was prepared by dissolving diamindiphenyl ether (DDE) in *N*-dimethylacetamide (DMAc) or *N*-methyl-2-pyrrolidone (NMP). Despite of their attractiveness for many applications, the conduction mechanisms in polyimide Kapton are presently not well understood. In these kind of materials, charge transport is mainly due to defects along with an ionic component. Several workers have reported the results of their investigations for various commercial grades of kapton. Yet to now, there is no reasonable agreement among them on the type of conduction mechanism in kapton, especially at high electric fields. Structural relaxation which occurs during the physical ageing in these glassy materials or amorphous materials is strongly temperature dependent. One of the important factors which controls the electrical and mechanical properties in these systems is that of morphology. The important factor anisotropy of molecular orientation in polyimide is known to cause anisotropy of electrical and optical properties, dielectric relaxation and mechanical properties. The commercial polyimide film has a two-phase structure consisting of ordered and less-ordered (amorphous) phases. We report the results of kapton and the transport mechanisms from various experimental techniques over the wide accessible temperature (15 K to 500 K). The transport and injection mechanism in this material is not understood completely, due to the presence of sizable defects or trap states. In this report, we present results covering a wide range of T and F , to study the applicability of the different models to study electrical transport in Kapton.

Thermal analysis(TA), Differential scanning calorimetry(DSC), Differential thermal analysis(DTA), Relaxation map analysis(RMA), thermally stimulated relaxation phenomena are the powerful tools to study the relaxation phenomena associated with these materials. [207–209,213–215,207,217–221] In high-resistivity

materials, an alteration of the external voltage may cause very time-consuming electric relaxation processes which are, e.g., due to an accumulation or redistribution of excess charges at or from electrode or interface regions. Here the signals to be measured are very often superimposed by slowly changing (creeping) background signals of comparable magnitude. Stationary conditions often are not attained even if the measuring time is extended to several hours. The slow electric relaxation currents are undesirable and sometimes it can be misinterpreted [207]. The electric relaxation current (ERC) measurements which we have used for the semiconducting polymers is a useful technique to study these insulating polymers also. but with the implications in final properties such as dielectric breakdown, high voltage stresses etc [207-209,215,207.217-219].

10.2 I-V Characteristics:

The following models are used to discuss the Current-Voltage relationships in Kapton: 1. Ionic hopping

$$J = J_0(T) \exp\left[\frac{eaF}{2kT}\right] \quad (168)$$

2. Poole - Frenkel effect [223]

$$J_{P-F} = B(T)E \exp\left[-\frac{\phi_F - \beta_F E^{\frac{1}{2}}}{kT}\right] \quad (169)$$

3. Schottky effect [223]

$$J_S = A(T)T^2 \exp\left[-\frac{\phi_s - \beta_s E^{\frac{1}{2}}}{kT}\right] \quad (170)$$

4. Thermally assisted tunneling [223]

$$J_T = G(T) \exp\left[-\frac{\phi + DE^{\frac{1}{2}}}{kT}\right] \exp[CE^{\frac{1}{2}}] \quad (171)$$

5. Space charge limited current [222]

$$J_{SCL} = \frac{9\epsilon\epsilon_0\mu\theta}{8x_i^3} V_{appl}^2 \quad (172)$$

where μ is the mobility of the free carriers, ϕ_F is the zero-field ionization energy of the donor, $\beta_F [= 2\beta_s]$ where $\beta_s [= \frac{e^3}{4\pi\epsilon\epsilon_0}]^{\frac{1}{2}}$ are the Poole-Frenkel and Schottky coefficients of reduction of ionization energy due to the applied electric field, V_{appl} is the applied voltage, ϕ_s is the effective work function between the Fermi level of the metal and the conduction band of the insulator or semiconductor, ϵ is the specific permittivity of the material ($\simeq 3.5$), θ is the fraction of free carrier concentration to trapped carrier concentration, A, B, C, D, G are constants appearing in the corresponding mechanisms. In this section, we present results covering a wide range of T and F, to study the applicability of the different models to study electrical transport in Kapton.

10.3 Procedures for studying Electric Relaxation Currents in insulators

(a) Isothermal relaxation process, the system is perturbed at constant temperature, the signal is monitored as a function of time. This method is useful in finding the defect or trapping parameters without the knowledge of kinetic orders.

(b) In non-isothermal process, the system is perturbed at a sufficiently low temperature to reduce the probability to establish a new statistical equilibrium. Subsequently, the temperature is raised according to a well-controlled heating program $T(t)$, thus increasing the reaction rates and the relaxation of the system can be monitored as a function of temperature and time. The term relaxation refers to the process of the retarded motion of a system to an external action or to an alternation of the external conditions. In the case of electrical phenomena the reaction usually corresponds to a charge displacement caused by an alteration of the acting electric field.

An electric relaxation process may have quite different reasons, e.g., a shift of the electrons relative to the centers of molecules (ionic polarization), an ori-

entation of dipoles (orientational polarization), and in non homogeneous systems the movement of free charges.

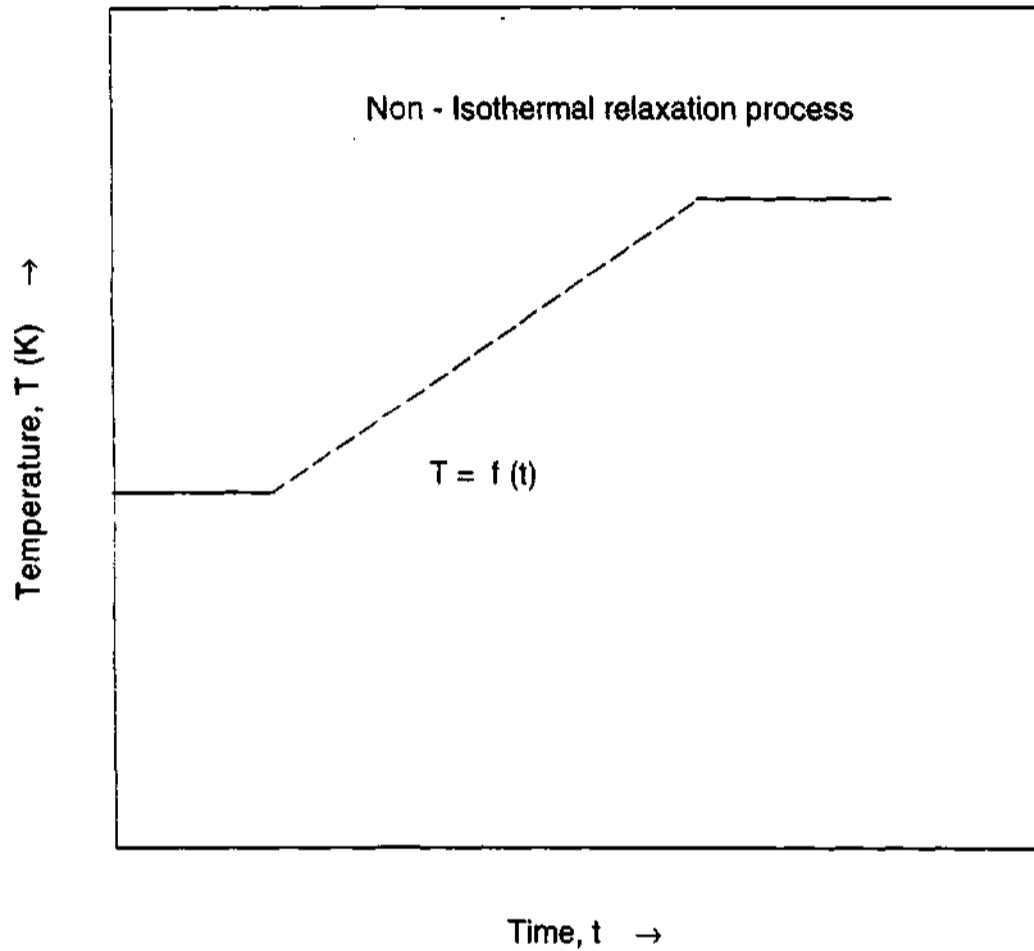


Fig. 10.2 Schematic picture of non-isothermal relaxation process

Background

Considering the relaxation processes, there are three different situations arise

- ¶ If the external action corresponds only to a single short perturbation of the considered system (single pulse) this system will return to the old equilibrium state after some time.
- ¶ If the external conditions are changed but then again are kept constant (single step) the system does not react instantly but adapts gradually to the

corresponding new equilibrium state

- ¶ If the external conditions vary permanently, e.g., as periodic function of time, the adjustment of the corresponding equilibrium states will always lag behind the time regime of the external action.

The basic conditions have to be fulfilled for the occurrence of thermally stimulated relaxation processes (TSR).

- § The system must be removed faraway from statistical thermodynamic equilibrium and exists in a state, which requires a free energy in order to move towards the reestablishment of equilibrium.
- § The system must be in contact with the temperature reservoir that provides sufficient thermal energy necessary to activate the relaxation processes.
- § The equilibrium of the system may be perturbed by changing the concentration of the reactants, temperature, pressure, electric or magnetic field.

The establishment of a new thermal equilibrium condition during and after the perturbation may be monitored by the measurement of the concentration of the involved species and the results can be utilized for the study of the involved chemical or physical reactions. The two basic types of relaxation processes involve either isothermal or non-isothermal relaxation techniques. There is a strong correlation between the mechanical and electrical ageing and the micro dielectric behavior of insulating materials. The isothermal relaxation current from a polymeric volume correlates with the intensity and the duration of the stress applied to the samples. Therefore the method of Isothermal Relaxation current-analysis (IRC-Analysis) offers a destruction free possibility to investigate the degradation processes of insulators including polymeric materials.

The IRC-Analysis is the first destruction free method, which could be able to quantify the remaining mechanical strength of the insulating materials. The time characteristic of the isothermal relaxation current varies significantly with

the residual strength of polymeric specimens. According to the theory of Simmons and Tam any relaxation process leads to an external relaxation current, discharging the polarized polymeric materials. This current represents a superposition of several physical phenomena of different components depending on discernible mechanisms of charge trapping, distributed over the complete energy band. equation shows the probability e_N per unit time of a trapped electron being emitted to the conduction band from a trap level located at a energy level W_H [208,207].

$$e_N = \nu_{ph} \exp\left\{-\frac{W_H - W_C}{kT}\right\} \quad (173)$$

The general current-time characteristic describes the integration of the "trapped carrier currents" in the external measuring circuit at constant temperatures.

$$W(t) = W_C - W_H = kT \ln(\nu t) \quad (174)$$

The product of the instantaneous current and time is linearly proportional to the number of the occupied traps with the energy $W = W_H$ which is proportional to $\ln(\nu t)$, as shown in the equation 2. With W_c for low edge conduction band energy, k_B is the Boltzmann's constant and T be the absolute temperature. It is postulated that the depolarization processes from discernible traps and the destruction free detection of the ageing is determined by the dynamics of the relaxation current components. The time constants and the weighted components can be calculated from the external current. The parameters have also got a direct relation to the discrete trap levels of the investigated materials and to the TSC-temperature of the maximum current at the measurement of Thermally stimulated depolarization currents (TSDC) [7]. with the calculated time constants it is accordingly possible to get quantitative information about the solid-state physical properties.

10.4 Relaxation mechanisms in Kapton

Electric polarization and depolarization mechanisms are the dynamic

processes that depend on the structure and molecular properties of the material. The main polarization mechanisms that occur in the materials are as follows: Figure shows the various types of relaxation mechanism exist in a polymer or dielectric material:

10.4.1 Dipolar orientation

The dipolar relaxation mechanisms [result from dipoles created by the attraction of the positive and negative charges existing in a dielectric. Different kind of dipoles are created due to the distance between the impurity and cation vacancy. When the impurity

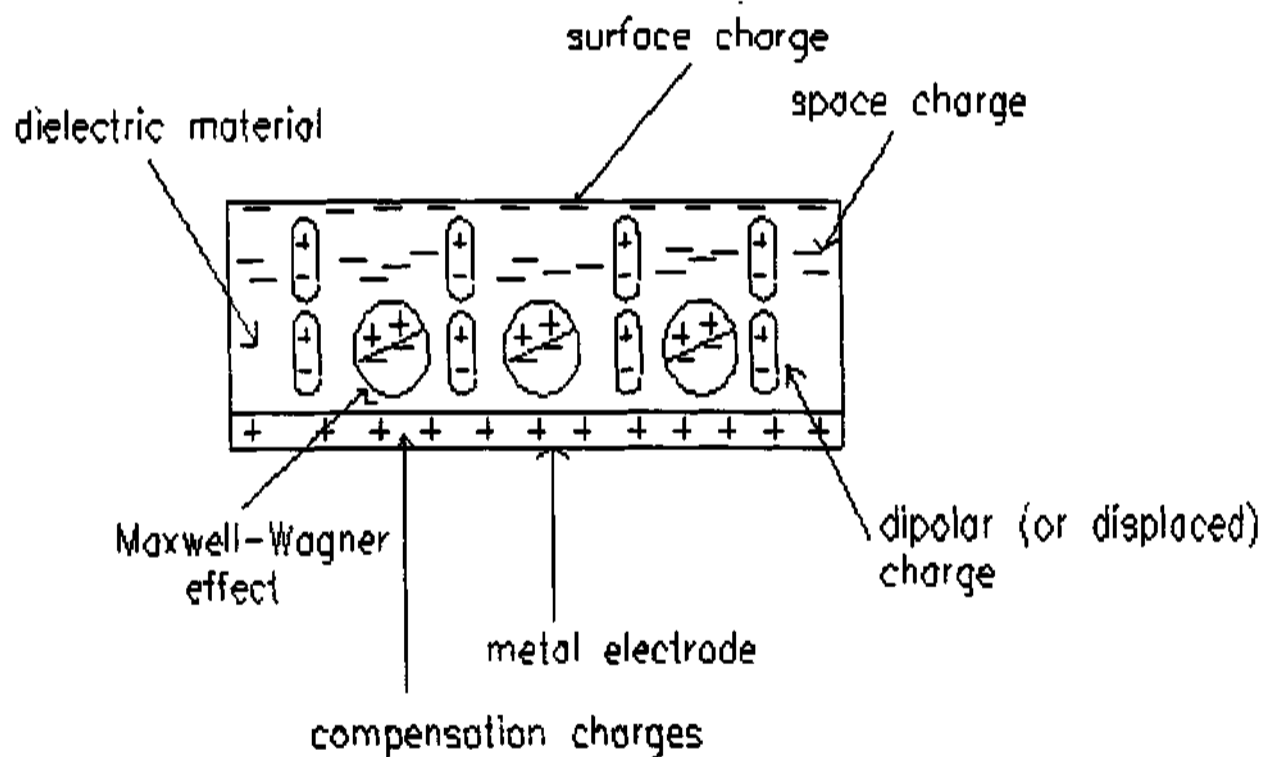


Fig. 10.3 Different polarization mechanisms in insulators.

concentration is high, then the dipole clusters may be formed, such as dimers,

trimers and so on. It is also known as orientation polarization which results from the alignment of permanent dipoles (e.g. water) in the direction of applied electric field. Dipole relaxation processes in polymers are characterized by a broad distribution of several relaxation times, with a strong temperature-dependent mean relaxation time τ (T). The isothermal dipole relaxation processes can be described by the stretched exponential or Kohlrausch-Williams-Watts (KWW) function which reveals the deviation from an exponential decay or hyperbolic decay. In combination with non-isothermal techniques, such as TSC or TSDC (which yields product of the stretching parameter and the activation energy of the dipole relaxation process) a complete characterization of the dipolar-relaxation process is possible [V. Halpern, J. Phys. D, **26** 307 (1993)].

10.4.2 Space charge or interfacial mechanism

Space charge relaxation, is caused by both intrinsic and extrinsic free carriers (i.e. ions or electrons). The polarization of these charges is attributed to the macroscopic movement of the charge carriers towards the electrodes and their accumulation at the interfaces within the material. During the movement of the carriers, several processes may proceed simultaneously. Their parameters vary not only with time and space but they depend also on many variable atypical of the material. A special case of the polarization is known as charge migration polarization that originates from the ionic migration or hopping of charge carriers (e.g. electron, proton) between localized sites.

Finally, the interfacial or Maxwell-Wagner (MW) relaxation mechanism, [9-11] usually appears in heterogeneous structures. It is the result of

- ¶ Formation of charge layers at the interfaces, due to the different conductivity currents within the various phases, or
- ¶ the migration of the carriers over microscopic distances and the subsequent

trapping.

These relaxation mechanisms depend not only on electric field, also it strongly depends on temperature too. However the various material show there is a transition of one mechanism to other type depending upon the temperature range.

10.5 Theory of thermally stimulated relaxation processes for insulating systems

The thermally stimulated depolarization currents (TSDC) or ionic thermo currents (ITC) method is a high-resolution technique for electrical characterization of dielectrics [216]. The method is as follows: The sample is polarized by an external applied electric field E_P , at a temperature T_P , for a duration time t_P much longer than the relaxation time at the polarizing temperature. in order to orient the vast majority of the polarizing specimens existing in the sample. This polarization is subsequently frozen in by cooling (under the existence of the applied electric field) the sample to a temperature T_0 such that the frozen-in polarization remains unchanged even if the external field is switched off. This happens because at such a low temperature the relaxation time of the polarization processes is very big compared to that at room temperature. By heating up the sample by a constant heating rate β , the depolarization current, as the polarizing specimens relaxes, is detected by the high sensitive electrometer. In the case of a single relaxation process obeying the Debye type relaxation processes, the relaxation time, $\tau(T)$ must the usual Arrhenius relation, $\tau(T) = \tau_0 \exp[\frac{E}{k_B T}]$, where τ_0 is the pre-exponential factor, E is the activation energy, the depolarization current is expressed as

$$i(T) = \frac{AP_0}{\tau_0} \exp[-\frac{E}{k_B T}] \exp[\frac{1}{\beta \tau_0} \int_{T_0}^T \exp[-\frac{E}{k_B T'}] dT'] \quad (175)$$

where A is the surface area of the sample and P_0 is the initial polarization. It may be proved that the depolarization current is maximized at $T = T_{max}$ whenever

the general condition [14]

$$\left[\frac{d\tau}{dt}\right]_{T=T_{max}} = -1 \quad (176)$$

is fulfilled. The above conditions leads to the well-known equation for noninteracting dipoles:

$$T_m^2 = \frac{\beta E \tau_0}{k_B} \exp\left[\frac{E}{k_B T}\right] \quad (177)$$

For a single curve, the relaxation time $\tau(T)$ calculated according to the so-called area method is given by the formula [12, 15]

$$\tau(T) = \frac{\int_{T_i}^{T_f} i(T) dT}{\beta i(T)} \quad (178)$$

where T_i is the temperature that the current appears and T_f is the temperature that the current vanishes. An Arrhenius plot ($\ln\tau$ versus T^{-1}) permits the evaluation of E and τ_0 . The initial rise current for temperatures much smaller than the temperature T_m (i.e., when $i_m = \frac{i_m}{10}$, where i_m is the maximum current) is given by

$$i(T) \simeq \frac{AP_0}{\tau_0} \exp\left[-\frac{E}{k_B T}\right] \quad (179)$$

From the logarithmic plot $\ln i(T)$ versus T^{-1} the activation energy E is directly obtained.

This method is sensitive since it can measure dipole concentrations up to 0.1 ppm. The existence of a single peak in most cases is rather unrealistic even in ionic single crystals. Usually, many overlapping peaks may appear making the distinction and the calculation of the parameters very difficult. The TSDC method offers alternative experimental techniques in order to dissociate the different kinds of polarization mechanisms or to distinguish several relaxation times. Finally the TSDC thermogram comprises several distinct mechanisms collectively

and practically difficult to interpret the data.

10.6 Isothermal transient current measurements (ITC)

Upon application of a step voltage to an insulating material, the current flows in an external circuit decays with time and this current has been termed variously as charging, conduction, desorption or poling current depending upon the duration of applied voltage stress. It is well known and accepted that the transient current flowing through a dielectric or polymeric material, after the application or removal of step voltage decays generally, at least in some decays of time, following the Curie-Von Schweidler law

$$i(t) = \frac{Ae^2 E \lambda^2 N_t^2 (2\nu_{ph})^{1-n}}{3k_B T} t^{-n} \quad (180)$$

The variation in the fast and slow decay can be characterized by the index "n" in the power law expression, where A is a constant with the dimension of m³, N_t the number density of traps and n(T) is the index of current decay, [223] and ν_{ph} is the phonon frequency [223]. The index is found to follow the relation, being a temperature dependent, so that $n(T) = a - bT$ where a and b are constants. The mechanisms responsible for the generation of absorption currents have been variously identified [?][D. K. Das Gupta and K. Joyner, J. Phys. D: Appl. Phys., 9, 824 (1976) as

- * electrode polarization,
- * dipolar orientation,
- * charge injection leading to space charge effects,
- * hopping of charge carriers between trapping sites and
- * tunnelling of charge carriers from the electrodes into the traps.

The origin of these dielectric absorption and desorption currents is still a controversy and number of mechanisms have been proposed, the most important of

which are dipolar relaxation, tunneling to empty traps, hopping of charge carriers, and electrode polarization.[1-7]. When an electric field is applied to a dielectric material at high temperature, and subsequently the material is cooled, it becomes a thermo electret. the electret is a dielectric material that produces a permanent external electric field which results from permanent ordering of molecular dipoles(bounded charge), and/or surface or volume free-charge mechanism activation. The formation of electret consists of simultaneous electrical and thermal treatments. In the thermal treatment two steps can be differentiated:

- ¶ the sample is kept at a constant temperature. T_p (polarization temperature) for a time t_p (isothermal polarization time) and
- ¶ the sample is cooled down to a temperature T_f (final temperature) that may be the room temperature (or any temperature at al. 10.)

Conveniently, the simultaneous electrical treatment is an electrical field, E_p (polarization field), applied during both steps so that during the first step the temperature dependent mechanisms are activated, and during the second step they are activated by the polarizing field and "frozen" because of the cooling. The trapping and relaxation processes of the charge are intimately related to the physical and chemical properties of the material. At room temperature, the decay time of the activated charge relaxation process is much longer than the duration of the studies made on them, and because of this, thermal stimulation of these relaxation processes is a very adequate technique for studying these materials. A classical TSDC of an electret is formed in a sandwich configuration (electrode-dielectric-electrode), and it is heated at a constant rate while it is short circuited through an ammeter. The intensity is recorded as a function of the temperature, and the relaxation processes can be seen as intensity peaks in the thermogram that reflects the TSDC spectrum. The interpretation of TSDC is not easy, for two reasons. One reason is that the charge activated during the polarization may be

due to several microscopic processes[5] (induced dipole polarization, alignment of permanent dipoles, ions or ionic vacancies migration and subsequent trapping, drift of electrons or holes and their trapping, excess charges injection from electrodes). The other reason is that the relaxation processes are elementary, as they can not be generally described by a single relaxation time and/or by a single activation energy; they have to be described in terms of natural frequencies and the activation energy distributions. One can say that to study a material by TSDC, two aspects may be considered: the origin of the peaks that appears in the spectrum and the determination of the kinetic parameters of the processes. In order to elucidate the origin of a peak in the TSDC spectrum, some methods have been developed which are mainly related to the behavior of the peak as a function of the polarization parameters[7] and the electrode nature[8, 9]. To resolve the complex TSDC spectrum into elementary spectra, well approximated by a single relaxation time and a single activation energy, the windowing polarization technique (WP) can also be applied to resolve the multiple relaxation mechanisms. The peak area evaluated by over the whole discharge is given by

$$Area = \int I dt = \frac{1}{\beta} \int I dT \quad (181)$$

where β is the linear heating rate. The peak area obtained is proportional to the total released charge, and it can be expressed in units of charge using the relation: $Q_{rel} = \frac{Area}{\beta}$. The peak area is plotted as a function of n_t , linear correlation whose slope is found to be 1 and an indication of the fitting process goodness as both magnitudes and released charges. In this report, the correlation of TSDC and IRC is discussed.

Injection of charge carriers and transport phenomena in metal/organic interfaces and electronic transport in organic solids is a subject of considerable interest. The presence of defects alters the electrical, optical and optoelectronic properties, especially in insulating amorphous materials, the study of electrical transport in

these materials has been studied extensive in low and high field regimes [1]. A general trend of non-linear increase in currents at high F is observed in these materials. At very low T , tunneling mechanism is one of the operative mechanisms and $I(T)$ is weakly T dependent while phonon-assisted hopping model is more valid at high temperature regimes. Schottky and Poole-Frenkel mechanisms are other possibilities depending on the nature of the electrodes, work function of the materials and other factors such as interfacial and space charge polarization.

Kapton^(R) film of thickness $\simeq 125 \mu\text{m}$ was used for all experimental purposes. Al electrodes ($\simeq 1000 \text{ \AA}$) were used for the contacts to form the guarded sandwich geometry. The sample was always short-circuited prior to measurements to avoid any spurious currents which results in measurement errors. It was then verified that the remaining background currents could be neglected or subtracted from the background with respect to the transient currents observed after voltage application. On the other hand, the series of measurements related to a given material were carried out with different samples in order to avoid a possible influence electrical and thermal history. A voltage of 200 V in steps of 5V was applied to the film upto 200 V at each T setting, ranging from 10 - 500 K. Prior to making measurements, the sample temperature was held constant typically $\simeq 30$ min to avoid erroneous results. The TSDC measurements were also performed over the different poling fields, F_P (8, 12 and 16 KV/cm) and at different poling temperatures, T_P (300, 400 and 500 K). The samples were poled for 45 minutes and heated at a linear rate (3.0 K/min) over the whole range. The IDC were measured at various T_P (15, 150, 300, 400 and 500 K) at 1.6 MV/m. The measurements were carried out by using digital source meter (2000), Keithley electrometer (6512) and Lakeshore temperature controller (330). $I(V)$ were done with the samples and results were verified to ensure reproducibility. All the experiments were performed in vacuum (10–4 torr) over the entire range.

Fig. 10.4 (A) and (B) show the plot of current density, $J(T)$ as a function of F at different T ranging from 15 - 250 K and 300 - 500 K. $J(F)$ does not vary significantly with T , in the range $T < 300$ K, as indicated by small variations in the scaling factors for the current in Fig.10 A. $J(F)$ is more sensitive to T for $T > 300$ K as shown in Fig.10 B. Analysis of results published previously on conduction mechanism shows that there is no reasonable agreement on the mechanism, especially at high T and F . $J(F)$ at different T in the present

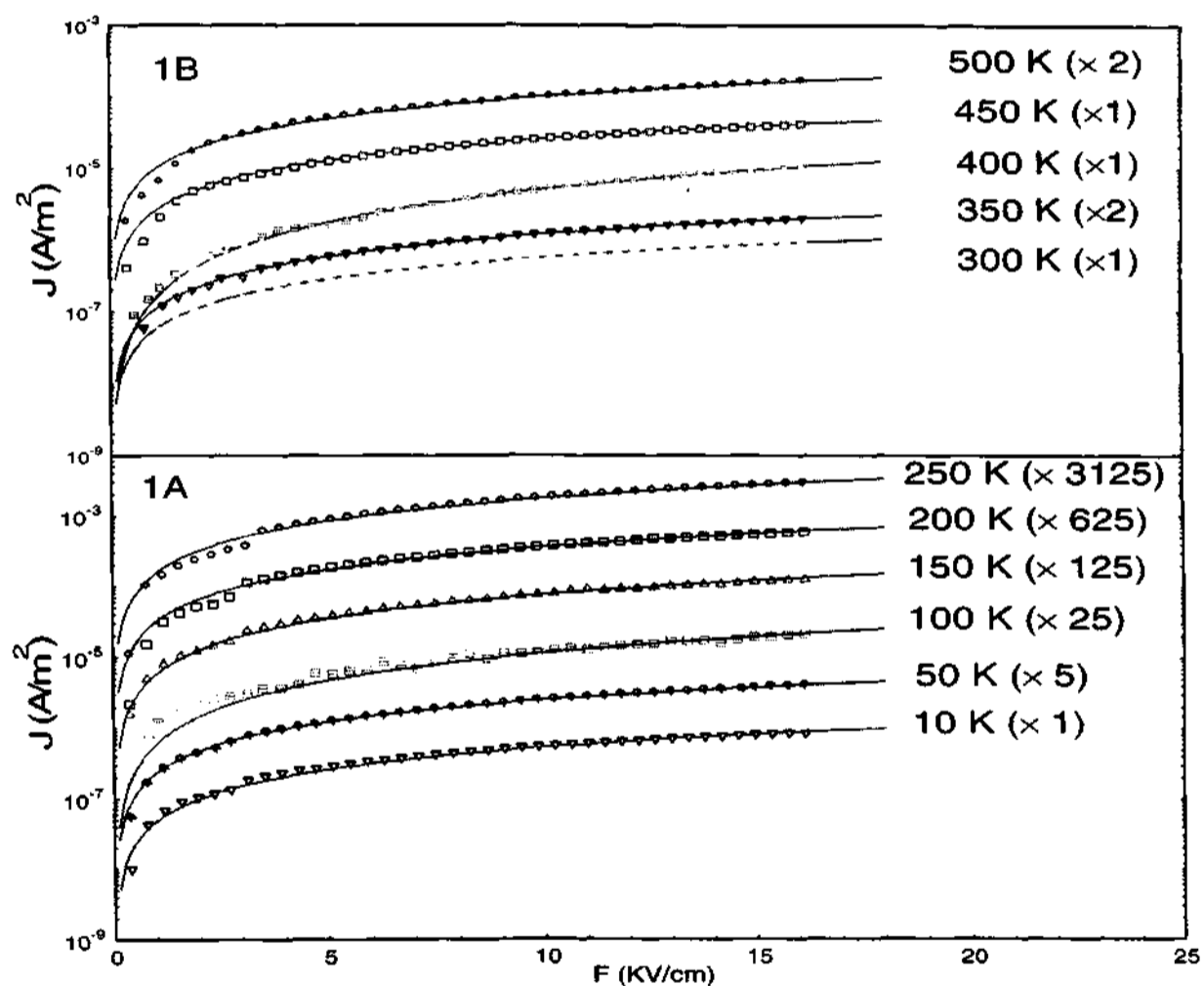


Fig. 10.4 Current density $J(T)$ as a function of electric field (F) at different temperature $T < 300$ K, (A) and $T > 300$ K, (B). Note that the current is scaled by factors and the fits represented by solid lines.

case is analyzed in terms of phonon-assisted hopping model, which fits better, compared to other models. The observed current density may be expressed as:
[4]

$$J \simeq 2e\lambda N_t \nu_{ph} \sinh\left[\frac{e\lambda F}{2kT}\right] \exp\left[-\frac{\Delta}{kT} + \frac{e^2\lambda^2 F^2}{16\Delta kT}\right] \quad (182)$$

where Δ is the difference in energy between the two successive traps, ν_{ph} the attempt to escape frequency, λ the hopping distance between successive traps, N_t the density of trap states, F the field applied, T the absolute temperature.

Fig. 10.5 shows the plot of I as a function of $1/T$ at different F (12 and 16 KV/cm). $J(T)$ shows a drastic variation in its response with respect to T for T

< 300 K.

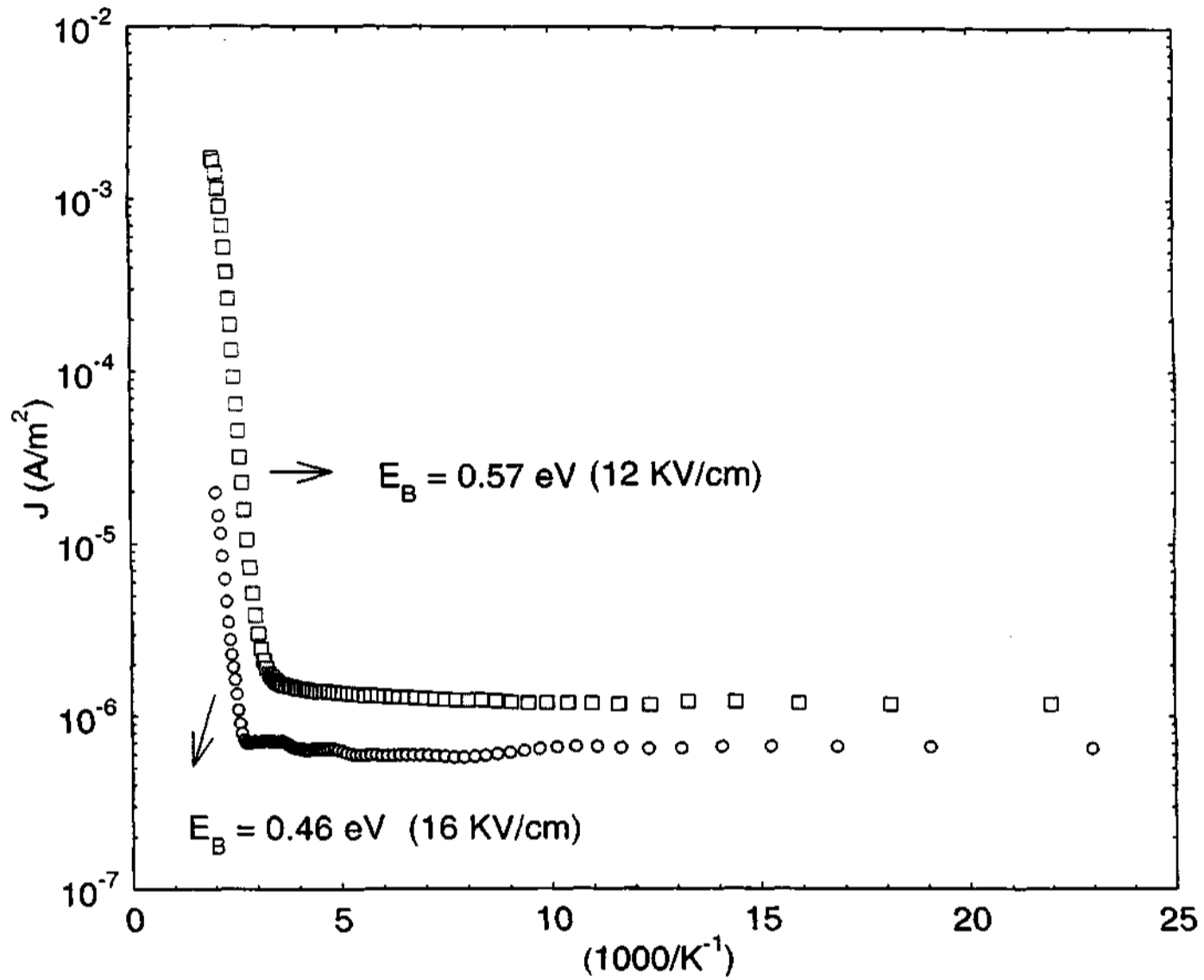


Fig. 10.5 J as a function of $1000/T$ at different F and inset is the estimated λ and Δ as a function of T . The symbols \circ and \diamond represent for $F = 12$ and 16 KV/cm respectively.

The experimental data does not fit to models such as 3-D variable range hopping and stretched exponential fits over the entire T range with a single parameter. The estimate for the barrier energy E_B involved can be analyzed in terms of simple

activated models for the two distinct regimes. The E_B , involved for transport at $T > 300$ K is greater than that for $T < 300$ K region as shown in Fig. 10.5. The results have to be analyzed in terms of a distribution of defect levels corresponding to multiple barrier energies for accurately modeling the results. It is also observed that E_B varies marginally with F . A more consistent picture emerges upon fitting the $J(T)$ in the two regimes to PAH (eqn. 7) and in the process yielding values of barrier energy similar to the ones obtained from fits to Fig. 10.4.

Fig. 10.6 shows the isothermal discharge current which was measured at constant poling field, F_P (1.2 MV/m) and at different poling temperatures, T_P (10 K, 150 K, 300 K, 400 K and 500 K). The discharge current can be described in terms of a power law with two components for decay, a fast component at times $t \leq 300$ s and a slow component for $t > 300$ s as shown in the log - log plot in Fig. 10.6 and is in consistent with previous observations on this sample¹¹. The variation in the fast and slow decay can be characterized by the index n in the power law expression $J(t) = Ct^{-n}$. The variation of $n(T)$ for the slower and faster components as a function of T over the range 15 - 500 K is shown in Fig. 10.7. The IDC has less pronounced at $t > 300$ s. The index $n(T)$ of the faster component decreases more rapidly than the slower component as T goes up is shown in the Fig. 10.7. This study allows us to study to what degree the steady-state currents are limited by bulk phenomena and by electrode effects, respectively. A systematic shift in the temperature that corresponds to the crossover from the slow component to the fast component is also observed in the context of the power law analysis and is depicted in the Fig. 10.7.

Most of the polymers exhibit this behavior after application of a step voltage and removal of the voltage. The desorption current generally consists of two slopes: A depolarization component with a slope in the range of - 0.5 to - 1.1 followed by a nearly constant transport component at longer durations. The

initial slope may also be followed by a current decay having slope of $\simeq -2$ which suggests a negligible transport current and a Debye type of relaxation. For short times and low temperatures ($< 100\text{C}$) the polarization component predominates while at higher temperatures and longer durations the transport current is the dominant component. The faster component has the variation of $n(T) = 1.26 - 2.5 \times 10^{-3} T$.

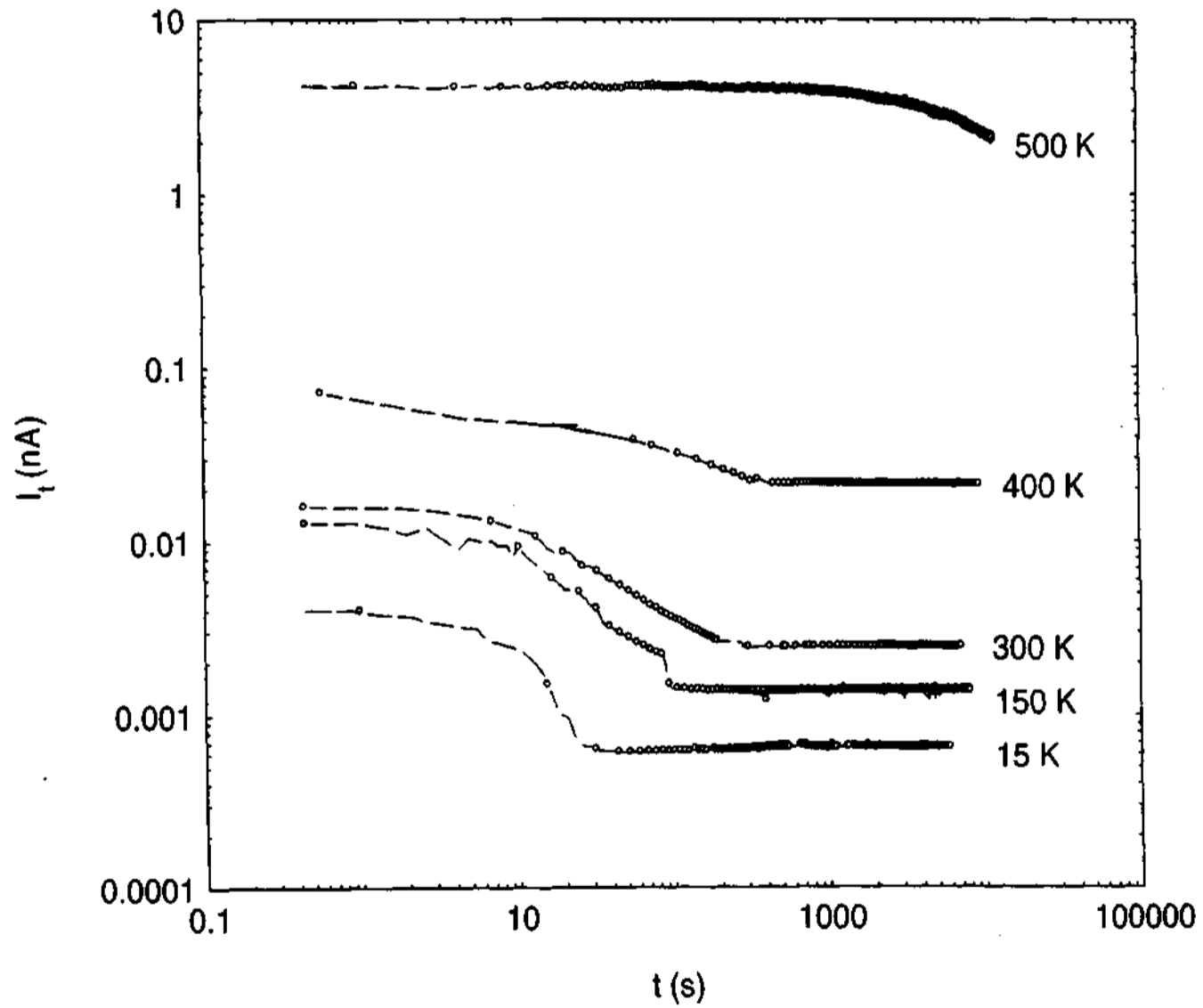


Fig. 10.6 Current density $J(T)$ as a function of time $t(s)$, poled at different temperatures.

The slower component is small at low T and increases nonlinearly with T. The slower component fits to an activated behavior (0.37 eV) rather than a linear fit. This feature clearly indicates the electrical relaxation mechanism here consists of two components, a depolarization component and a residual conduction component. At low T, depolarization mechanism predominates and at high T, the transport or conduction mechanism dominates.

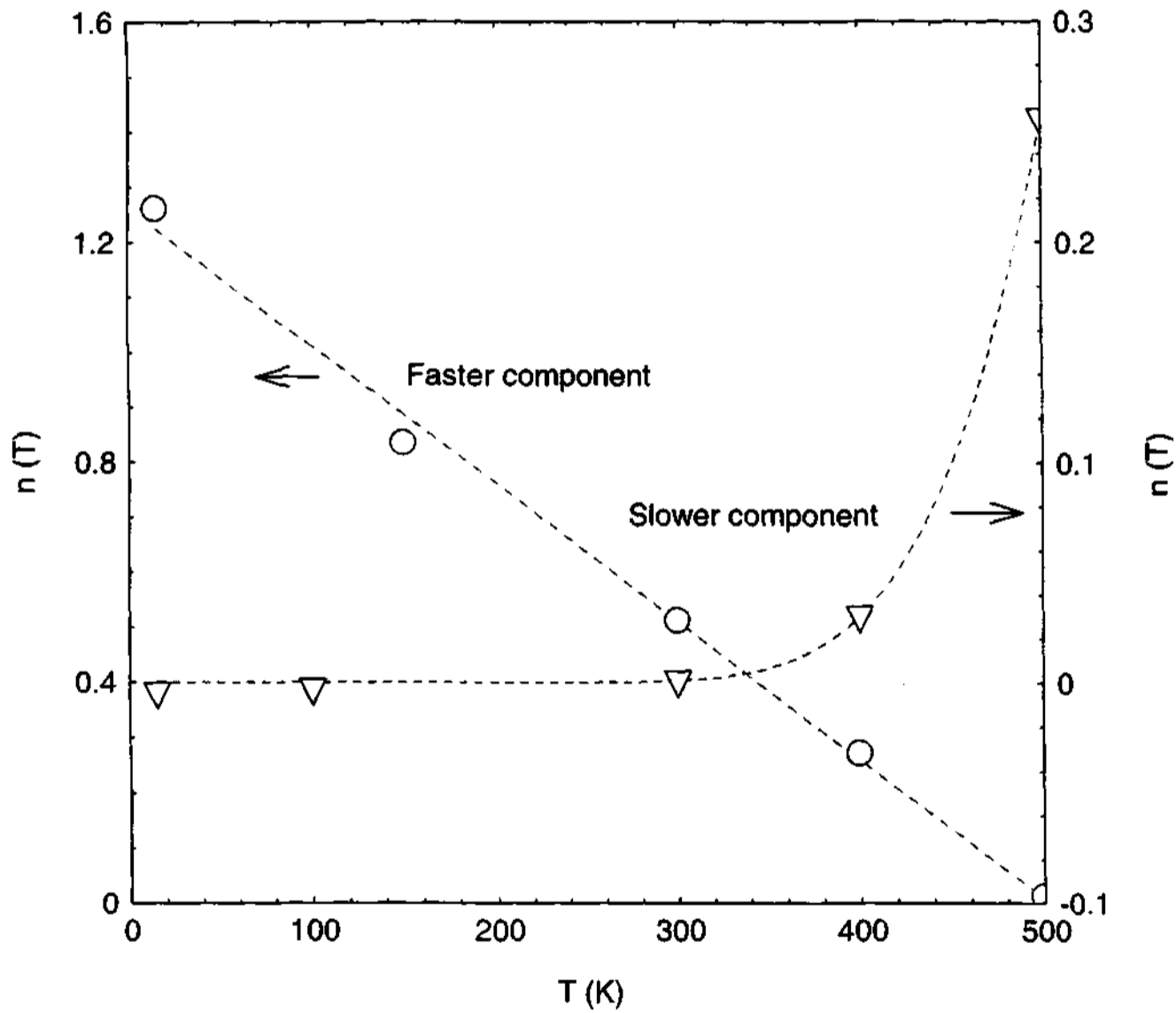


Fig. 10.7 Plot of index "n" as a function of T for slower and faster relaxation components

In device grade polyimide Smith observed $0.6 < n < 0.8$ in the time range of 1 - 16, 000 s and temperature range of 300 - 400 K [223]. In contrast Hanscomb and Calderwood (1973) obtained $0.2 < n < 0.6$ at short times in the range $80 \text{ ms} < t < 2 \text{ ms}$ and temperature range of 425 - 450 K. In this section, we observe $0.01 < n < 1.26$ in the time range of 1 - 15000 s and the temperature range of 15 K - 500 K [224]. The variations could be due to method of sample preparation conditions, amount of time in which electric stress is applied to the sample, experimental (environmental) conditions etc. We have also attempted to fit the experimental data to WWW or stretched exponential decay for Kapton. From the stretched exponential fits, the factor β is close to 1 at low T and 10^{-4} at high T for the faster component. This signature indicates that the single dipolar relaxation processes is possible at low T and non-activation behavior at high T. It is not reasonably agreeable for insulating systems such as kapton. From the I-V, TSDC, DC conductivity measurements, the experimental results suggests that the conduction mechanism is dominant at high T and dipolar type of mechanism dominant at low T.

The IDC results also suggest a possible crossover at $T > 350 \text{ K}$ from dipolar processes to space charge mechanism. This conjecture is also consistent with results from IV, DC conductivity measurements. The results also illustrate the dependence of thermal and field history.

Fig. 10.8 shows the TSDC spectra of the sample obtained at T_P (300 K), with the constant F_P (16 KV/cm). The sample was poled for 60 minutes, prior to the sample temperature was held constant for 30 minutes. The samples were heated at a linear rate, $\beta = 2.5 \text{ K/min}$. The spectra consists of several peaks located at $T_m \simeq 180, 390$ and 475 K with F_P (16 KV/cm). The highest temperature peak is generally recognized as the α peak and occurs due to micro-brownian motion of main chains. The TSDC process is expected to arise due to

the following reasons [208,215]

§ dipole orientation polarization,

§ polarization due to trapped carriers and

§ polarization due to the migration of charge carriers in bulk over microscopic distances.

It may be due to the mechanical and dielectric relaxations of the polymers. The peak at the next two lower temperatures are β and γ transitions. They originate as a result of side group motion, possible partial rotation of side groups.

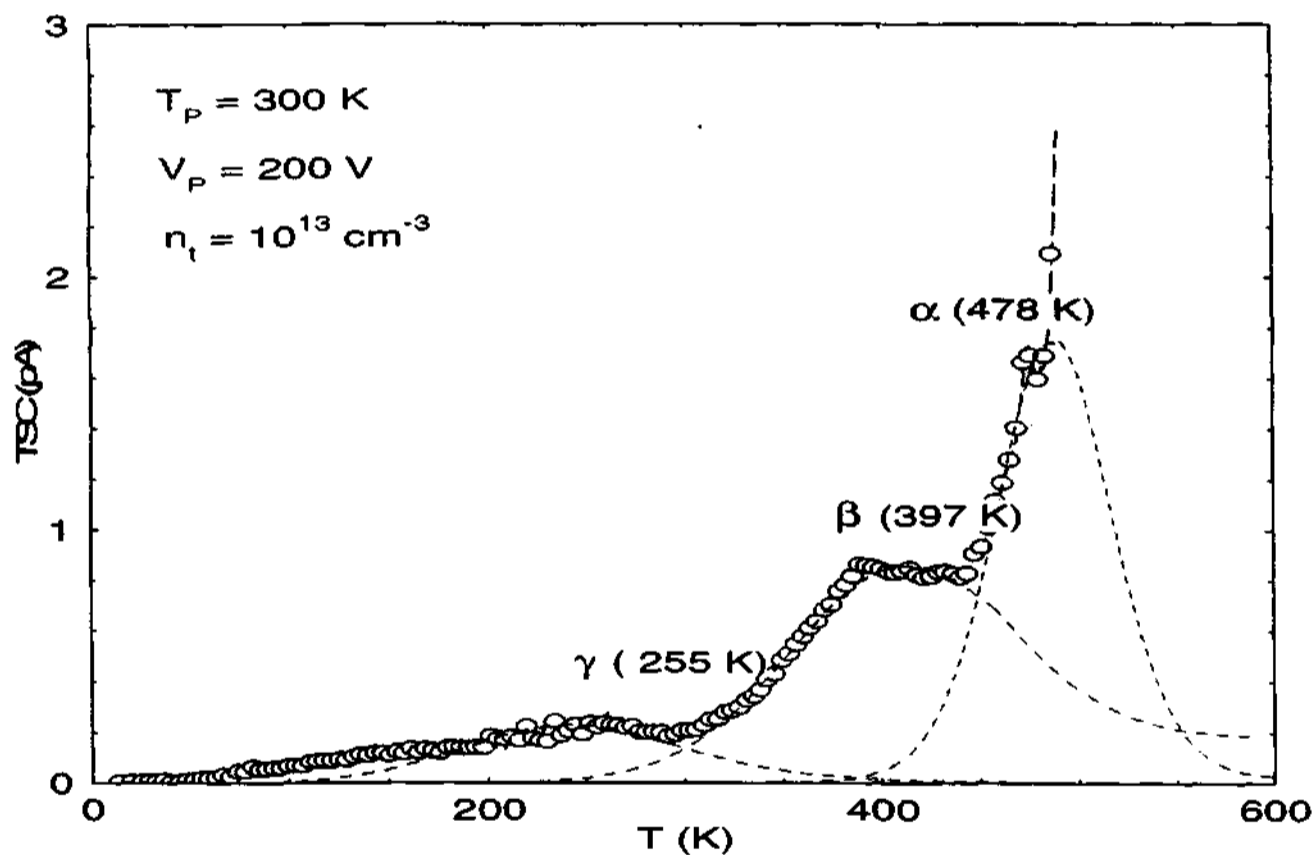


Fig. 10.8 TSDC spectra for Kapton poled at 300 K (16 KV/cm).

The peak at lower T corresponds to the same peak that occurs at higher frequency. Therefore γ relaxation occurs at a higher frequency than β relaxation. The lowest temperature peak is possibly due to the motion of a smaller dipolar unit if the side

chain has more than one dipolar group, O - H bond or C = O bond. Alternatively it may be electronic in nature. This clearly illustrates the γ relaxation must be a smaller dipolar group than the side chain. The peaks at high and low T may be due to space charge polarization and dipole orientation polarization processes. The overlapping of several peaks is an indication that the polarization mechanism is not due to single relaxation, but from a distribution of several relaxation times. The activation

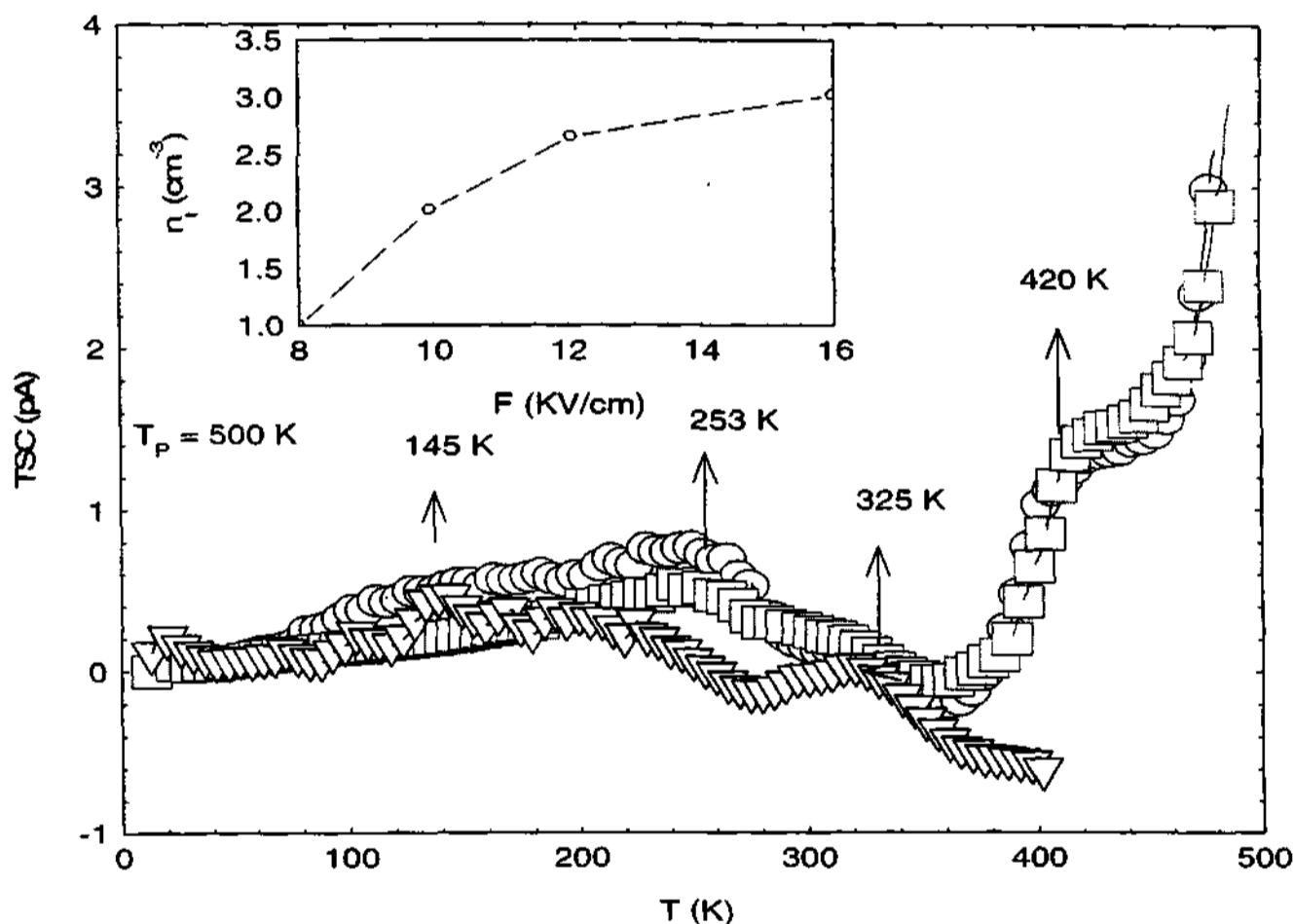


Fig. 10.9 TSDC spectra (T_P 500 K) for different fields say at F_P 8, 12 and 16 KV/cm. Inset shows η_i Vs F_P .

energy can be obtained from the slope of the straight line of the $\ln(TSC) - (1/T)$

relation. From the plot, the activation energies for the peaks located at $T_{max} \simeq 180$ (16 meV), 390 (0.19 eV) and 475 (0.4 eV). Higher the T_{max} , greater the activation energy. The total charge released during this process could be found out by using this expression $Q_T = \int_{T_0}^T \frac{I(T)}{\beta} dT$. By knowing the sample geometry, the total trapped carrier density can be obtained from the total charge released during this process. The parameters obtained from the above equation are $Q_T \simeq 0.17$ nC and the corresponding $N_t \simeq 8.6 \times 10^{12} \text{ cm}^{-3}$. The values were obtained agree with the previous reports. The increase of TSC currents at such high T could be due to dipolar mechanism. The total released charges tend to saturate at higher poling fields F_P at high temperatures T_P is shown in the figure. This feature indicates that all the trapped charges are released from the active traps do contribute TSDC and thermally disconnected ones do not contribute significantly.

Fig. 10.9 shows the TSDC of the samples were poled at T_P (500 K), and F_P (16 KV/cm). The TSDC spectra consist of several peaks that are located at $T_{max} \simeq 145, 250, 325$ and 420 K. Similarly the activation energies are obtained from the initial rise portion of the TSDC. From the integral values, $Q_T \simeq 18.3, 160$ and 205 pC and their corresponding N_t are $10^{11}, 8 \times 10^{12}$ and 10^{13} cm^{-3} . The samples poled at different T_P show that the charges released are nearly the same and Q_T increases as F rises. Initially there is a drastic change and becomes saturation is an indication of space charge polarization and if varies linearly, it may be due to dipolar orientation polarization processes.

10.7 Summary

Electrical conduction in Kapton films was studied in a sandwich geometry as a function of temperature, T (10 K - 500K) and electric field (0 - 16 KV/cm). The time dependent isothermal discharge currents (IDC) were studied at different temperatures (10 K < T < 500 K). Thermally stimulated discharge current (TSDC) studies were carried out as function of initial poling conditions. A dis-

tinct change in conduction mechanism as a function of T was observed at $T \geq 300$ K from I-V, DC conductivity, ITC and TSDC measurements. The origin of this behavior is discussed in terms of a crossover from dipolar to a space charge mechanism. The effective barrier energy, Δ , for transport and hopping parameters are estimated for Kapton on the basis of these studies. The results obtained for kapton suggests that, at lower than T_g and in low or moderate fields, the transient currents are essentially governed by dipolar relaxation mechanisms.

Chapter 11

Summary and Future Directions

The presence of defect-contributing electronic processes in conjugated polymers is clearly observed. These defects significantly affect the electronic, optical and opto-electronic properties. It is observed that the understanding the role of defects and quantifying their densities, energetics is a crucial step to raise the performance levels of the polymer based devices and prevent the aging/degradation processes.

The electronic properties of the ladder type polymer BBL was rigorously studied. The thermally induced processes are more pronounced with conductivity changing by nearly seven orders in magnitude at room temperature when heated to 625 K. The unusual manner in which the conductivity of BBL increases upon thermal treatment and the subsequent decrease upon exposure to moisture is completely traced. The anisotropy in conductivity and the dependence on ambient conditions of the enhanced conductivity are also studied. The energy barriers and the time constants involved in these process are also estimated. In BBL, σ_{\parallel} (T), σ_{\perp} (T) and σ_{fib} (T) yields better fits to a quasi 1-D models than 2-D, 3-D VRH or a simple activated model. The deviation from a 3-D model which was used to describe the transport properties in BBL was attributed to differences in factors such as orientation, impurity concentration, and processing conditions.

A variety of experimentally different approaches were used to study the trap distribution and energetics of BBL. A substantial magnitude of TSC is observed in poled BBL samples in the pre - annealed phase. TSC measurements indicated a feasible approach to study the various defect characteristics in ladder type polymers. Trap states of $\simeq 0.5$ eV, 0.3 eV, and 20 meV in BBL was estimated.

Another clear feature of trap-related processes was the long-lived transient photocurrents in these systems. An effective activation barrier of 0.1 eV from I_{ph} (T) measurements was obtained. The trapped charge carrier densities were also evaluated from these measurements indicating the magnitude of the various types of defects present in this system.

TSC of MEHPPV and P3OT were also studied in a device structure. The use of TSC measurement techniques as an effective tool to estimate the magnitude of the trap levels and their densities was demonstrated. The existence of the trap levels of 50 meV, and 0.1 eV for P3OT and MEHPPV respectively was determined.

Interfacial effects in bilayer devices are discussed in detail. Bilayers are constituted with the intrinsically n - type BBL and a p - type polymer such as P3OT or PVK. The polymer-polymer interface forms the crucial region where the charge-separation enhancement (in reverse bias) takes place. Photocurrent enhancement in these bilayers were observed. The TSC from these devices were dependent on the type of electrode contacts. TSC results obtained from devices with Schottky type electrode contacts were different from that of devices with symmetric ohmic electrodes.

Electrical conduction in non-conjugated insulating polymers such as Kapton films was also studied as a function of temperature, T (10 K - 500K) and electric field (0 - 16 KV/cm). The time dependent isothermal discharge currents (IDC) were studied at different temperatures (10 K < T < 500 K). Thermally stimulated discharge current (TSDC) studies were carried out as function of initial poling conditions. A distinct change in conduction mechanism as a function of T was observed at $T \geq 300$ K from IV, DC conductivity, IDC and TSDC measurements. The origin of this behavior was discussed in terms of transition of dipolar to space charge mechanism which can be attributed to carrier trapping

and release of charge carriers from the trap states. The effective barrier energy, Δ , for transport and hopping parameters were estimated for Kapton on the basis of these studies. The results obtained for kapton suggests that, at lower than T_g and in low or moderate fields, the transient currents are essentially governed by dipolar relaxation mechanisms.

Future Directions

Procedures for extracting the trap density of states from TSC, photoconductivity, optical charging spectroscopy, and capacitance transient spectroscopy (CTS) measurements which have been applied for amorphous semiconductors, needs to be developed for these conjugated polymer systems. The thermal relaxation probes can also be correlated with other direct probes such as photoinduced infrared (PIR) absorption, photoluminescence-detected magnetic-resonance (PLDMR) techniques used to investigate the states in the gap. The importance of defects has become crucial especially in polymers where field effect transistor action has been observed. The factors leading to the restriction of mobility of carriers in these semiconductors needs to be determined. Relationship between these different traps and mobility needs to be established. Another issue of concern is the lack of n -type polymers (there are few polymers which have $\mu_n > \mu_h$). The knowledge and understanding of the origin of defects and their effects are essential for the success of polymer based electronics.

REFERENCES

- [1] J. Mort, *Polymers. Elec. properties*, Encyclopedia of Phy. Sci. and Tech., Vol. 11, 48 - 60 (1987).
- [2] <http://www.nobel.se/announcement/2000/chemen.html>.
- [3] <http://www.ems.psu.edu/MATSE/polymerintro.html>.
- [4] <http://www.halycon.com/nanojbl/NanoConProc/nanocon4.html>.
- [5] <http://www.research.philips.com>
- [6] M. Schott and M. Nechtschein, Introduction to Conjugated and Conducting Polymers, 495 - 538. Ed: J. Farges, Marcel Dekker, Inc., New York (1994).
- [7] H. G. Elias, *New Commercial Polymers*, New York (1969 - 1975).
- [8] A. J. Epstein, "Electrically Conducting Polymers: Science and Technology", MRS Bulletin, pp. 16 - 23 (1997).
- [9] D. Baeriswyl, Conjugated Conducting Polymers, Ed: by H. Kiess. Springer Series in Solid-State Sciences 102, Heidelberg: Springer Verlag, p. 7 (1992).
- [10] L. Salem, *The Molecular Orbital Theory of Conjugated Systems*. London: Benjamin (1966).
- [11] S. Roth, "One - Dimensional Metals", Weinheim VCH (1995).
- [12] J. M. Andre and J. Ladik, eds., "Electronic structure of Polymers and Molecular Crystals", Plenum Press, Newyork (1975).
- [13] A. A. Askadskii and G. L. Slonimskii., *Russ. Chem. Rev.*, 44, 767 (1975).
- [14] W. R. Salaneck, I. Lundstrom, and Ranby, Ed's., Oxford Sci., Oxford (1993).
- [15] H. Meier, *Organic Semiconductors*, Verlag-Chemie, Weinheim (1974)

- [16] J. L. Bredas, R. R. Chance and R. Silbey, *Phys. Rev. B*, **26**, 5843 (1982) and J. L. Bredas, J. C. Schott, K. Yakushi, and J. B. Street. *Phys. Rev. B*, **30**, 1023 (1984).
- [17] C. W. Tang, *Appl. Phys. Lett.*, **48**, 183 (1986).
- [18] J. Simon, J. J. Andre, *Molecular Semiconductors*, Springer, Berlin (1985).
- [19] C. J. Brabec, N. S. Sariciftci, *Semiconducting Polymers* (Eds: G. Hadziioannou, P. F. Van Hutten), WILEY-VCH, Weinheim, Ch. **15**, pp. 515 ± 560 (1999).
- [20] J. Kanicki, *Handbook of Conducting Polymers*, Vol. **1** (Ed: T. A. Skotheim), Marcel Dekker, New York, pp. 543 ± 660 (1986).
- [21] M. Kaneko, *Handbook of Organic Conducting Molecules and Polymers*, Vol. **4** (Ed: H. S. Nalwa), Wiley, New York, 661 (1997).
- [22] R. S. Kohlman, J. Joo and A. J. Epstein, Ch. **34**, *Handbook of the Physical Properties of Polymers*, (Ed: J. Mark (AIP press)) (1995).
- [23] M. S. Bashir and E. W. Gary, Ch. **3**, (Ed: L. V. Interrante and M. J. Hampden-Smith), Wiley-VCH (1998).
- [24] J. Mort and G. Pfister " *Electronic properties of Polymers*" Wiley: Newyork (1982).
- [25] G. Grem, G. Ledditzky, Buldrich, GLeising, *Adv. Mater* **4**, 36 (1992).
- [26] P. L. Burn, A. B. Holmes, A. Kraft, D. D. C. Bradley, A. R. Braun, R. H. Friend, *J. Chem. Soc. Chem Commun* **34** (1992).
- [27] H. C. Longuet-Higgins, L. Salem, *Pro.Roy.Soc.London*, **A251**, 172 (1959).
- [28] H. Kuhn, *J.Chem.Phys*, **16**, 840 (1948) and **17**, 1198 (1949).

- [29] G. Konig, G. Stollhoff, *Phys. Rev. Lett* **65**, 1239 (1990).
- [30] M. J. Rice, *Phys. Lett.* **71A**, 152 (1979).
- [31] S. A. Brazovski, *Sov. Phys. JETP* **51**, 342 (1980).
- [32] Y. Lu *Ed. Solitons and Polarons in Conducting Polymers*, Singapore World Scientific (1988).
- [33] S. M. Bishop, *Composite Struct.*, **3**, 295 (1985).
- [34] P. E. Cassidy, "Thermally stable polymers synthesis and properties", Marcel Dekker, Newyork (1980).
- [35] J. L. Cotter, *Rev. Of High Temp. Materials*, **3**, 277 (1978)
- [36] J. P. Critchley, *Angew. Macromol Chem. Int. Ed*, **109 – 110** 41 1982)
- [37] H. Domininghaus. High temperature resistant engineering plastics-properties, processing and applications, **69**, 1 (1979); J. P. Critchley, Royal Aircraft Establishment, page 143 - 170, Polymers, thermally stable, Encyclopedia of Phy. Sci. and Tech. Vol **11** (1987); H. G. Elias, An Introduction to Plastics, Ch. 8, Electrical properties, p. 185 - 193 (1998); O. K. Kim, *J. Polymer Sci. Polym. Let.*, Ed. **23**, 137 (1985) and (b)O. K. Kim, *ibid*, **20** 63 (1982); Z. H. Kafafi, J. R. Lindle, C. S. Weisbecker, F. J. Baroli, J. S. Shirk, T. H. Yoon, O. K. Kim, *Chem. Phys. Let.*, **179** 979 (1991); L. R. Dalton, *Polymer*, **29** 543 (1987); I. Belaish, D. Davidov, H. Selig, M. R. McLean, L. R. Dalton, *Angew. Chem. Int.*, Ed. Engl. **28** 1569 (1989).
- [38] U. Scherf, *J. Mater. Chem.*, **9**, 1853 - 1864 (1999); U. Scherf and K. Mullen, *The Synthesis of Ladder polymers*, in *Adv. Polym. Sci.*, Vol. **123**, p. 1 (1995); C. S. Wang. *Trends Polym. Sci. (TRIP)*, **5**, 138 (1997); A. D. Schluter, *Adv. Mater.*, **3**, 282 (1991).

- [39] R. Peierls, *Quantum Theory of Solids*; Oxford University Press: London, p 108 (1955).
- [40] H. C. L. Higgins and L. Salem, *Proc. Roy. Soc. A*, **25**, 172 (1959).
- [41] W. P. Su, J. R. Schrieffer and A. J. Heeger, *Phys. Rev. Lett.*, **42** 1698 (1979) and W. P. Su, J. R. Schrieffer and A. J. Heeger, *Phys. Rev. B*, **22** 2095 (1980).
- [42] S. Roth and H. Bleier, *Advances in Phys.*, **36**, 385 - 462 (1987).
- [43] C. S. Yannoni and T. C. Clarke, *Phys. Rev. Lett.*, **51**, 1191 (1993).
- [44] J. A. Pople and S. H. Walmsley, *Mol. Phys.*, **5**, 15 - 20 (1962).
- [45] H. Kalhert, O. Lertner and G. Leising, *Syn. Met.*, **17**, 467 (1987)
- [46] S. Capponi, N. Guilhery, J. Malrieu, b. Miguel, D. Poilblane, *chem. Phys. Lett.*, **255**, 238 (1996).
- [47] D. Emin and T. Holstein, *Phys. Rev. Lett.*, **36**, 323 (1976).
- [48] J. Chen and A. J. Heeger, *Solid State Comm.*, **58** 251 (1986).
- [49] M. Pope and C. E. Swenberg, *Electronic Processes in Organic Crystals*, Oxford Univ. Press, London (1982).
- [50] D. P. Craig and S. H. Walmsley, *Excitons in Molecular Crystals*, W. A. Benjamin, New York (1968).
- [51] H. Shirakawa, E. J. Louis, A. G. MacDiarmid, C. K. Chiang, and A. J. Heeger, *J. Chem. Soc. Commun.*, **577** (1977).
- [52] Shirakawa, H., Louis, E. J., MacDiarmid, A. G., Chiang, C. K., and Heeger, A. J., *Chem. Commun.*, **578**, 578, (1977).
- [53] Chiang, C. K., Fincher, C. R. Jr., Park, Y. W., Heeger, A. J., Shirakawa, H.,

- Louis, E.J. and others, *Phys. Rev. Lett.*, **39**, 1098, (1977)
- [54] H. Naarman, N. Theophilou, *Syn. Met.*, **22**, 1 (1987) and H. Naarman, *Syn., Met.*, **17**, 233 (1987).
- [55] J. Tsukamoto, A. Takahashi, *Syn. Met.*, **41 - 43**, 7 (1991)
- [56] A. J. Heeger, S. Kivelson, J. R. Schrieffer, W. P. Su. *Rev. Mod. Phys.* **60**, 781 (1988).
- [57] H. Kuzmany, M. Mehring and S. Roth, Electronic Properties of Conjugated Polymers, *Solid State Sciences*, **76**, 38 (1987).
- [58] Y. Wang, Dissertation (1996).
- [59] J. C. W. Chien, "Polyacetylene: Chemistry, Physics, and Material Science", Academic Press (1984).
- [60] 22 E. Huckel, *Z. Phys.* **70** (1931) 204] method in 1959 and H. C. Longuet-Higgins, L. Salem, *Proc. Roy. Soc. A* **251** 172 (1959).
- [61] E. Heilbronner, H. Bock, *Das HMO - Modell und seine Anwendungen*, Verlag Chemie (1968).
- [62] J. J. Andre, A. Bieber and F. Gautier, "Physical Properties of Highly Anisotropic Systems: Radical-ion Salts and Charge Transfer Complexes." *Ann. Phys.*, **I**, 145 - 256 (1976).
- [63] I. F. Shchegolev, "Electric and Magnetic Properties of Linear Conducting chains", *Phys. Stat. Solidii.*, (a) **12**, 9 - 45 (1972).
- [64] J. H. Burroughes, D. D. C. Bradley, A. R. Brown, R. N. Marks, K. Mackay, R. H. Friend, P. L. Burns, A. B. Holmes, *Nature.* ,**347**, 539.(1990)
- [65] D. Braun, A. J. Heeger, *Appl. Phys. Lett.* **58**, 1982.(1991)

- [66] D. Braun, A. J. Heeger, H. Kroemer, *J. Electron. Mater.* **20**, 945. (1991).
- [67] N. C. Greenham, S. C. Moratti, D. D. C. Bradley, R. H. Friend, A. B. Holmes, *Nature.* , **365**, 628. (1993)
- [68] I. D. Parker, *J. Appl. Phys.* **75**, 1656.(1994)
- [69] J. H. Schon, Ch. Kloc, A. Dodabalapur, B. Batlogg, *Science.* **287**, 599 (2000)
- [70] J.H. Schon, A. Dodabalapur, Ch. Kloc, B. Batlogg. *Science.* **290**, 963. (2000)
- [71] J.H.Schon, S.Berg, Ch. Kloc, B.Batlogg. *Science.* **1022**, (2000).
- [72] J.H.Schon, A.Dodabalapur, Ch.Kloc, B.Batlogg. *Science.* **290**, 963. (2000)
- [73] Horowitz. G., *Adv. Mater.*, **10**, 365 (1998).
- [74] H. Sirringhaus, T. Kawase, R.H. Friend, T. Shimoda, M. Inbasekaran, W. Wu, and E.P. Woo, *Science* **290**, 5499 (2000).
- [75] K. S. Narayan and B. Singh *Appl. Phys. Lett.*, **74**, 345 (1999).
- [76] K. S. Narayan, A. G. Manoj, J. Nanda and D. D. Sarma (*App. Phys. Lett.* **74**, 871 (1999).
- [77] K. S. Narayan, A. G. Manoj, J. Nanda and D. D. Sarma (*App. Phys. Lett.* **74**, 871 1999)
- [78] K.S. Narayan, K.S. Gautam, *J. Appl. Phys.*, **79**, 1935-1938 (1996)
- [79] H. Antoniadis, Abkowitz M A, and Hsieh B R 1994 *Appl. Phys. Lett.* **65** 203.
- [80] Hertel D, Bässler H, Scherf U, Horhold H H 1999 *J. Chem. Phys* **110** 9214.
- [81] Francis Garnier, Ryad Hajlaoui, Abderrahim Yassar, Pratima Srivastava. *Science.* **265**, 1684. (1994).

- [82] S. Stafstrom, R. Riklund and K. A. Chao, *Phys. Rev. B*, **26**, 4691 (1982).
- [83] P. W. Anderson, *Phys. Rev.*, **109**, 1442 (1958).
- [84] N. F. Mott and E. Davis, *Elec. Proc. Non – Cryst. Mat.*, Clarendon Press, Oxford (1979).
- [85] Y. A. Firsov, in *Localization and Metal Insulator Transition*, Ed. H. Fritzche and D. Adler (Plenum Press) p. 471 (1985) and W. Apel and T. M. Rice, *J. Phys. C*, **16**, L 1151 (1983).
- [86] P. A. Lee and T. V. Ramakrishnan, *Rev. Mod. Phys.*, **57**, 287 (1985).
- [87] A. L. Efros and B. I. Shkloviskii, *J. Phys. C*, **8**, L49 (1975) and in: *Electron – Electron Interactions in Disordered System* Ed: A. L. Efros and M. Pollak (North-Holland, Amsterdam, 1985).
- [88] Y. Wang, *Dissertation* (1996).
- [89] P. Sheng, E. K. Sichel and J. I. Gittleman, *Phys. Rev. Lett.*, **18**, 1197 (1978).
- [90] B. Abeles, P. Sheng, M. D. Coutts and Y. Arie, *Adv. in Phys.*, **24**, 407 (1975) and P. Sheng, B. Abeles and Y. Arie, *Phys. Rev. Lett.*, **31**, 44 (1973).
- [91] N. F. Mott, *Philos. Mag.*, **24**, 911 (1971).
- [92] M. H. Cohen and J. Jortner, *Phys. Rev. Lett.*, **15**, 699 (1973).
- [93] E. P. Nakhmedov, V. N. Prigodin and A. N. Samukhin, *Sov. Phys. Solid State*, **31**, 368 (1989).
- [94] A. Miller and E. Abrahams, *Phys. Rev.*, **120**, 745 (1960).
- [95] V. K. S. Shante, C. M. Varma, A. N. Block, *Phys. Rev. B*, **8**, 4885 (1973).

- [96] Z. H. Wang, A. Ray, A.G. MacDiarmid, and A.J. Epstein, *Phys. Rev. B* **43** p. 4373 (1991) and J. Joo, V. N. Prigodin, Y. G. Min, A. G. MacDiarmid, and A. J. Epstein, *Phys. Rev. B* **50** p. 12226 (1994).
- [97] R. S. Kohlman, J. Joo, Y. Z. Wang, J. P. Pouget, H. Kaneko, T. Ishiguro, and A.J. Epstein, *Phys. Rev. Lett.* **74** p. 773 (1995) and R. S. Kohlman, J. Joo, Y. G. Min, A. G. MacDiarmid, and A. J. Epstein, *Phys. Rev. Lett.* **77** p. 2766 (1996).
- [98] A. B. Kaiser, *Phys. Rev. B* **40**, 2086 (1989).
- [99] J. T. Randall and M. H. F. Wilkins, *Proc. R. Soc. London, Ser. A* **184**, 366 and 390 (1945); (b) G. F. S. Garlick and A. F. Gibson, *Proc. Phys. Soc. London* **60**, 574 (1948).
- [100] J. Slowik *J. Appl. Phys.* **47**, 2982 (1976); (b) R. Eiermann, W. Hofberger, and H. Bässler, *J. Non-Cryst. Solids* **28**, 415 (1978); (c) I. Glowacki and J. Ulanski, *J. Appl. Phys.* **78**, 1995 (1995)
- [101] L. I. Grossweiner, *J. Appl. Phys.* **24**, 1306 (1953); (b) W. Fuhs and M. Milleville, *Phys. Status Solidi B K* **29**, 98 (1980); (c) L. Viex-Rochaz and A. Chenevas-Paule, *J. Non-Cryst. Solids* **35-36**, 737 (1980).
- [102] J. Dijon, *Solid State Commun.* **48**, 79 (1983); (b) M. Yamaguchi, *J. Non - Cryst. Solids* **59-60**, 425 (1983).
- [103] H. Fritzsche and N. Ibaraki, *Philos. Mag. B* **52**, 299 (1985); (b) D. S. Misra, A. Kumar, and S. C. Agarwal, *Phys. Rev. B* **31**, 1047 (1985); (c) M. Zhu and H. Fritzsche, *Philos. Mag. B* **53**, 41 (1986).
- [104] R. Haering and E. N. Adams, *Phys. Rev.* **117**, 451 (1960) and T. Cowell and J. Woods, *Br. J. Appl. Phys.* **18**, 1045 (1967).

- [105] P. Braunlich, *Thermally Stimulated Relaxations in Solids*, Topics in Applied Physics, (Edited by P. Braunlich), Springer, Berlin, **37** (1979) and (b) P. Braunlich and P. Kelly, *Phys. Rev. B*, **1**, 1596 (1970).
- [106] A. Halperin and A. A. Braner, *Phys. Rev.* **117**, 408 (1960).
- [107] G. A. Dussel and R. H. Hulse, *Phys. Rev.* **155**, 764 (1967).
- [108] I. Chen, *J. Appl. Phys.*, **47** 2988 (1976).
- [109] T. Cowell and J. Woods, *Br. J. Appl. Phys.*, **18** 1045 (1967).
- [110] J. Slowik, *J. Appl. Phys.*, **47**, 2982 (1976).
- [111] A. G. Lewandowski and S. W. S. McKeever, *Phys. Rev. B*, **43**, 8163 (1991).
- [112] A. Mandowski and J. Swiatek, *J. Phys. D Appl. Phys.*, **25**, 1485 (1992).
- [113] P. Saunders, *J. Phys. C* **2**, 2181 (1969), A. Opanowicz, *Phys. Status. Solidii A* **101** 589 (1987) and P. Kivits and H. Hagebeuk, *J. Lumin.* **15** 1 (1977).
- [114] F. Urbach, *Storage and Release of Light by Phosphors*, Cornell Symposium (New York: Wiley) P. 115 (1948).
- [115] R. Chen, Glow curves with general order kinetics by *J. ElectroChem. Soc.*, **106** 1254 - 1259 (1979).
- [116] L. I. Grossweiner, A note on the analysis first order glow curves, *J. Appl. Phys.*, **24**, 1306 - 1307 (1953).
- [117] Ch. B. Lushchik, The investigation of trapping centers in crystals by the method of thermal bleaching. *Sov. Phys. - JETP*, **3**, 390 -399 (1956).
- [118] R. Chen, On the calculation of activation energies and frequency factors from glow curves, *J. Appl. Phys.*, **46**, 570 - 585 (1969).
- [119] C. Muntoni, A. Ricci and A. Sergi, *Ric. Sci.* **9**, 762 (1968).

- [120] E. B. Podgrosak, *Proc. 3rd Int. Conf. on Luminesc. Dosim.*, **249**, 1 - 7 (1971).
- [121] Y. S. Horowitz, *Nucl. Instrum. Methods Phys Res.* **243**, 207 - 214 (1986).
- [122] K. H. Nicholas and J. Woods, *Brit. J. Appl. Phys.* **15** 783 (1964).
- [123] G. Micocci, A. Serra, A. Tepore, *J. Appl. Phys.*, **81**, 9 (1997).
- [124] D. R. Vij, V. K. Mathur, *Brit. J. Appl. Phys. (J. Phys. D)* **2**, 624 (1969).
- [125] H. M. Gupta, *J. Appl. Phys.*, **48**, 3448 (1977).
- [126] A. Rizzo, G. Micocci, A. Tepore. *J. Appl. Phys.*, **48**, 3415 (1977).
- [127] R. Chen, *Chem. Phys. Lett.* **6**, 125 (1970).
- [128] K. Kuriyama, *Phys. Rev. B.* **47**, 12415 (1993).
- [129] S. L. Sharma, T. Pai, H. N. Acharya, *J. Appl. Phys.*, **75**, 7884 (1994).
- [130] M. Mudarra and J. Belana *J. Poly. Sci. B. Poly. Phys.*, **36**, 1971 (1998).
- [131] M. Rajan and S. Elison, *J. Poly. Sci. B*, **35**, 2901 (1997).
- [132] W. Brutting, E. Buchwaid, G. Egerer, M. Meir, K. Zuleeg, M. Schwoerer, *Synth. Metals*, **84**, 677 (1997).
- [133] Inan. Chen, *J. Appl. Phys.* **47**, 2988 (1976).
- [134] P. Braunlich, P. Kelly. *Phys. Rev. B.*, **1**, 1596 (1970).
- [135] P. Braunlich, P. Kelly, *Phys. Rev. B.*, **1** 1586 (1970).
- [136] S. D. Singh, R. K. Gartia, N. C. Deb, *J. Phys. D. Appl. Phys.*, **31** 231 (1998).
- [137] S. Guissi, R. Bindi, P. Lacconi, D. Jeambrun, D. Lapraz, *J.Phys.D.Appl.Phys.* **31**, 137 (1998).

- [138] C. M. Sunta, R. N. Kulkarni, T. M. Pipers, W. E. Feria Ayta, S. Watanabe
J. Phys. D. Appl. Phys. **31** 2074 (1998)
- [139] I Glowaki, J. Ulanski *J. Appl. Phys.* **78**, 1019 (1995).
- [140] M. N. Bussac, D. Michoud, L. Zuppiroli. *Phys. Rev. Lett.* **81**, 1678 (1998).
- [141] S. Ikeda, K. Matsuda. *J. Appl. Phys.*, **50** 6475 (1979).
- [142] M. Meier, S. Karg. K. Zuleeg, W. Brutting, and M. Schwoerer, *J. Appl. Phys.*, **84**, 87 (1998) and S. Karg, J. Steiger, H. von Seggern, *Synt. Met.*, **111-112**, 277 (2000).
- [143] G. Leditzky and G. Leising, *J. Phys. D: Appl. Phys.* **27**, 2185 (1994): (b) M. Onoda, D. H. Park, and K. Yoshino, *J. Phys. Condens. Matter* **1**, 113 (1989).
- [144] F. E. Arnold and R. L. Van Deusen, *Macromolecules* **2**, 497 (1969); (b) F. E. Arnold and R. L. Van Deusen, *J. Appl. Polym. Sci.* **15**, 2035 (1971).
- [145] S. A. Jenekhe, L. R. dePaor, X. L. Chen, and R. M. Tarakka, *Chem. Mater.* **8**, 2401 (1996); (b) C. S. Wang, C. Y. C. Lee, and F. E. Arnold, in *Electrical, Optical, and Magnetic Properties of Organic Solid State Materials*, edited by L. V. Chiang, A. F. Gartio, and D. J. Sandman, No. **247** of MRS Symposia Proceedings (Materials Research Society, Pittsburgh, p. 747, 1992).
- [146] R. L. Van Deusen, *J. Polym. Sci., Polym. Lett. Ed.* **4**, 211 (1966): (b) S. A. Jenekhe and S. J. Tibbetts, *J. Polym. Sci., Part b: Polym. Phys.* **26**, 201 (1988); (c) S. A. Jenekhe and P. O. Johnson, *Macromolecules* **23**, 4419 (1990).
- [147] S. Y. Hong, M. Kertesz, Y. S. Lee, and O. K. Kim, *Macromolecules*, (1994).
- [148] H. Mizes and E. Conwell, *Phys. Rev. B* **44**, 3963 (1991).

- [149] J. W. Blatchford and A. J. Epstein, *Am. J. Phys.*, **64**, 120 (1996).
- [150] H. Antoniadis, M. A. Abkowitz, J. A. Osaheni, S. A. Jenekhe M. Stolka, *Chem. Mater.*, **61**, 6 (1994); (b) S. A. Jenekhe and P. Johnson, *Macromolecules*, **23**, 4419 (1990).
- [151] H. H. Song, A. V. Fratini, M. Chabinyk, G. E. Price, A. K. Agrawal, C. S. Wang, J. Burkette. D. S. Dudis, and F. E. Arnold, *Synth. Met.* **69**, 533-535 (1995).
- [152] H. Curtins and M. Favre, *Advances. in Semiconductors*. Vol. **1and2**, Ed., H. Fritzsche (1989).
- [153] E. E. Haller, W. L. Hanson, *Adv. in Phys.*, **30**, 93 - 138 (1981) and references therein
- [154] Jr. A. Uhler *Bell Systems Technical Journal* **34**, 105 (1955).
- [155] P. M. Smits *Bell Systems Technical Journal* **37**, 711 (1958).
- [156] P. A. Schumann and E. E. Gardner, *J. Electrochem. Soc.* **116**, 87 (1969).
- [157] C. G. Wiegenstein and K. H. Schulz, *Rev. Sci. Instrum.*, **68**, 1812 (1997)
- [158] T. E. Jenkins, *Semiconductor Science*, p. 290 (1995).
- [159] P. W. Baumeister, *Phys. Rev.* **121**, 359 (1961)
- [160] K. W. Boer and H. Gutzjednr, *Z. Phys.*, **152**, 203 (1958).
- [161] K. S. Narayan, A. A. Alagiriswamy, and R. J. Spry (Bull. of Amer. Phys. Soc.), (41) 756 (1998).
- [162] K. S. Narayan, A. K. Singh, and S. K. Ramasesha, *J. Phys. D: Appl. Phys.* **30**, L16 - L18 (1997)
- [163] A. A. Alagiriswamy and K. S. Narayan (submitted).

- [164] Narayan K S, Taylor B E, Spry R J and Ferguson J B *J. Appl. Phys.* **77** 3938 (1995).
- [165] Dulieu B, Wery Lefrant J S and Bullot J 1998 *Phys. Rev. B* **57** 9118 and Lee C H, Yu G and Heeger A J 1993 *Phys. Rev. B* **47** 15543.
- [166] R. H. Friend, R. W. Gymer, A. B. Holmes, J. H. Burroughes, R. N. Marks, C. Taliani, D. D. C. Bradley, D. A. Dos Santos, J. L. Bredas, M. Lögdlund, and W. R. Salaneck. *Nature*, **397**, 121 (1999).
- [167] Harrison, R. H. Friend, *Appl. Phys. Lett.*, **74** 1144 (1999)
- [168] J. H. Burroughes, D. D. C. Bradley, A. R. Brown, R. N. Marks, K. Mackay, R. H. Friend, P. L. Burns, A. B. Holmes, *Nature*, **347**, 539. (1990)
- [169] D. Braun, A. J. Heeger, *Appl. Phys. Lett.* **58**, 1982. (1991)
- [170] D. Braun, A. J. Heeger, H. Kroemer, *J. Electron. Mater.* **20**, 945. (1991).
- [171] N. C. Greenham, S. C. Moratti, D. D. C. Bradley, R. H. Friend, A. B. Holmes, *Nature*, **365**, 628. (1993)
- [172] I. D. Parker, *J. Appl. Phys.* **75**, 1656. (1994)
- [173] G. Yu, K. Pakbaz, A. J. Heeger, *Appl. Phys. Lett.* **64**, 3422. (1994)
- [174] H. Antoniadis, B. R. Hsieh, M. A. Abkowitz, M. Stolka, S. A. Jenekhe, *Polym. Prepr.* **34**, 490. (1993)
- [175] H. Antoniadis, B. R. Hsieh, M. A. Abkowitz, S. A. Jenekhe, M. Stolka, *Synth. Met.* **62**, 265. (1994)
- [176] W. Rie, S. Karg, V. Dyakonov, M. Meier, M. Schworer, *J. Lumin.* **60**, 906. (1994)
- [177] N. S. Sariciftci, L. Smilowitz, A. J. Heeger, F. Wudl, *Science* **258**,

- 1474.(1992)
- [178] N. S. Sariciftci, D. Braun, C. Zhang, V. Srdanov, A. J. Heeger, G. Stucky, F. Wudl, *Appl. Phys. Lett.* **62**, 585. (1993)
- [179] G. Yu, J. Gao, J. C. Hummelen, F. Wudl, A. J. Heeger, *Science*. **270**, 1789.(1995)
- [180] J. J. M. Halls, C. A. Walsh, N. C. Greenham, E. A. Marseglia, R. H. Friend, S. C. Moratti, A. B. Holmes, *Nature*. **376**, 498.(1995)
- [181] L. Smilowitz, N. S. Sariciftci, R. Wu, C. Gettinger, A. J. Heeger, F. Wudl, *Phys. Rev. B*. **47**, 13 835.(1993)
- [182] B. Kraabel, J. C. Hummelen, D. Vacar, D. Moses, N. S. Sariciftci, A. J. Heeger, F. Wudl, *J. Chem. Phys.* **104**, 4267.(1996)
- [183] N. S. Sariciftci, A. J. Heeger, *Int. J. Mod. Phys. B*. **8**, 237.(1994)
- [184] N. S. Sariciftci, *Prog. Quantum Electron.* **19**, 131.(1995)
- [185] X. Wei, Z. V. Vardeny, N. S. Sariciftci, A. J. Heeger, *Phys. Rev. B*. **53**, 2187 (1996).
- [186] S. Morita, A. A. Zakhidov, K. Yoshino, *Solid State Commun.* **82**, 249.(1992)
- [187] K. Yoshino et. al *Solid State Commun.*, **85**, 85.(1993)
- [188] S. Morita, A. A. Zakhidov, K. Yoshino, *Jpn. J. Appl. Phys.* **32**, L873(1993).
- [189] K. Yoshino et. al *Solid State Commun.* **90**, 41(1994).
- [190] J. J. M. Halls, R. H. Friend, *Synth. Met.* **85**, 1307. (1997)
- [191] G. Yu, A. J. Heeger, *J. Appl. Phys.* **78**, 4510.(1995)
- [192] N. S. Sariciftci and A. J. Heeger *Handbook of Organic –*

- Conductive Molecules and Polymers*, Vol. 1 (Ed: H. S. Nalwa), Wiley, New York pp. 414 (1996).
- [193] B. Kraabel, C. H. Lee, D. McBranch, D. Moses, N. S. Sariciftci, A. J. Heeger, *Chem. Phys. Lett.* **213**, 389.(1993)
- [194] B. Kraabel, D. McBranch, N. S. Sariciftci, D. Moses, A. J. Heeger, *Phys. Rev. B.* **50**, 18 543.(1994)
- [195] C. H. Lee, G. Yu, N. S. Sariciftci, D. Moses, K. Pakbaz, C. Zhang, A. J. Heeger, F. Wudl, *Phys. Rev. B.* **48**, 15 425.(1993)
- [196] P. M. Allemand, G. Srdanov, A. Koch, K. Khemani, F. Wudl, Y. Rubin, F. N. Diederich, M. M. Alvarez, S. J. Anz, R. L. Whetten, *J. Am. Chem. Soc.* **113**, 2780.(1991)
- [197] V. Dyakonov, G. Zorinians, M. C. Scharber, C. J. Brabec, R. A. J. Janssen, J. C. Hummelen, N. S. Sariciftci, *Phys. Rev. B.* **59**, 8019 (1999).
- [198] H. Meier, *Organic Semiconductors*, Verlag-Chemie, Weinheim (1974).
- [199] C. W. Tang, *Appl. Phys. Lett.* **48**, 183 (1986).
- [200] J. Simon, J.-J. Andre, *Molecular Semiconductors*, Springer, Berlin (1985)
- [201] C. J. Brabec, N. S. Sariciftci, in *Semiconducting Polymers* (Eds: G. Hadziioannou, P. F. van Hutten), WILEY-VCH, Weinheim, Ch. 15, pp. 515 - 560 (1999).
- [202] J. Kanicki, *Handbook of Conducting Polymers*, Vol. 1 (Ed: T. A. Skotheim), Marcel Dekker, New York pp. 543 - 660 (1986).
- [203] M. Kaneko, *Handbook of Organic Conductive Molecules and Polymers*, Vol. 4 (Ed: H. S. Nalwa), Wiley, New York, p. 661 (1997)

- [204] B. O'Regan, M. A. Grtzel, *Nature*, **353**, 737 (1991).
- [205] A.G. Manoj, Mol. Elec. Lab., JNCASR, Bangalore. bibitemKumar N. Kumar and K. S. Narayan, *Appl. Phys. Lett.*, **78**, 1556 (2001).
- [206] A. A. Alagiriswamy, K. S. Narayan and R. Govindaraju (submitted)
- [207] P. Muller, *Phys. Stat. Sol.*, **67** 11 (1981).
- [208] N. Borgis, J. Grammatikkas and A. N. Papathannassiou, *Phys. Rev. B*, **58**, 10319 (1998).
- [209] C. Bucci and R. Fieschi, *Phys. Rev. Lett.*, **12**, 16 (1964) and C. Bucci and R. Fieschi, *Phys. Rev. Lett.* **148**, 816 (1966).
- [210] J. Rybicki, M. Chybicki, S. Feliziani, G. Mancini, *J. Phys. Con. Matter*, **2**, 3547 (1990) and J. Rybicki, M. Chybicki, S. Feliziani, G. Mancini, "Non - Isothermal Dispersive Transient Currents in Non - Homogeneous Insulating Layers", Proceedings of the 21st Europhysics Conference on Macromolecular Physics "Electrical and Optical Active Polymers", Sulejow (PL) (1989).
- [211] H. Wang and N. G. Geok-Ing, Current Transient in Polyimide-Passivated InP/InGaAs Heterojunction Bipolar Transistors: Systematic Experiments and Physical Model, *IEEE Trans. Electron Devices*, Vol. **47**, no. 12 (2000).
- [212] L. H. Dao, X. F. Zhong, A. Menikh, R. Paymter, F. Martim, Annu. Tech. conf. SPE **49**, 783 (1991).
- [213] B. Tieke, W. Gabriel, *Polymer* **31**, 20 (1990).
- [214] M. B. Meador, D. H. Green, J. V. auping, J. R. Gaier, L. A. Ferrara, D. S. Paradopoulos, J. W. Smith, D. J. Keller, *J. Appl. Polym. Sci.* **63**, 821 (1997).

- [215] J. Vanderschueren, M. Ladang, J. Niezkette and M. Corapci, *J. Appl Phys.*,
, 58, 15 (1985).
- [216] T. Tanaka, S. Hirabayashi and K. Shibayama, *J. Appl. Phys*, 49, 784 (1978)
- [217] S. L. Kaplanan, H. Hirish, *Polyimides : Chemistry, processing, properties*,
"New industrial polymers" (D.Deanin.ed). Ch 8, p 100. Marcel Dekker. New
York (1975).
- [218] K. L. Mittal, "Polyamides synthesis, Chacterization and application " Vol
1 and 2 Plenum Press New York (1984).
- [219] "Degradation and stabilization of Polymers" (G. Gueskens, ed.)p.43, Ap-
pled science publishers, London (1975).
- [220] F. Gutman and L. E. Lyons., "OrganicSemiconductors" Wiley. New York
(1967).
- [221] F. P. Darmory, *Procesable Polyamides*, In "New Industrial Poly-
mers" (D.Deanin.ed). Ch. 10, 124 Marcel Dekker. New York (1975).
- [222] Sessler G M, Hahn B and Yoon D Y 1986 J Phys. D: Appl. Phys. 60 318
- [223] H. J. Wintle, *J. Non-Cryst. solids*, 15, 471 (1974). D. K. Das Gupta and K.
Joyner, *J. Phys. D: Appl. Phys.*, 9, 2041 (1976), F. W. Smith, H. J. Neuhaus,
S. D. Senturia, Z. Fen, D. R. Day and T. J. Lewis. *J. Electronic Materials*,
15, 93 (1987).
- [224] Smith F. W, Neuhaus H. J. Senturia S. D, Feit Z. Day D. R and Lewis T.J,
1987, *J. Electronic Materials*, Vol. 16, 93 (1987) and G. Williams and D.
C. Watts, *Trans. Faraday. soc.* 66 80 (1970).

228
12
240

620.192 a12 972
p01

228

